Translational pharmacokinetics-pharmacodynamics in zebrafish: integration of experimental and computational methods

Wijk, R.C. van

Translational pharmacokinetics-pharmacodynamics in zebrafish: integration of experimental and computational methods

It takes two to translate

Rob Christiaan van Wijk

Cover design and printing: GVO Printers and Designers B.V., Ede, The Netherlands

ISBN: 978-94-6332-594-3

The research described in this thesis was performed at the Systems Biomedicine and Pharmacology division of the Leiden Academic Centre for Drug Research (LACDR), Leiden University (Leiden, The Netherlands), and at the Animal Sciences and Health division of the Institute of Biology Leiden (IBL), Leiden University (Leiden, The Netherlands).

Translational pharmacokinetics-pharmacodynamics in zebrafish: integration of experimental and computational methods

It takes two to translate

Proefschrift

ter verkrijging van
de graad van Doctor aan de Universiteit Leiden,
op gezag van Rector Magnificus prof. mr. C.J.J.M. Stolker,
volgens besluit van het College voor Promoties
te verdedigen op donderdag 6 februari 2020
klokke 16:15 uur

door

Rob Christiaan van Wijk

geboren te Zevenaar, Nederland

op 30 juni 1991

Promotores:	Prof. dr. P.H. van der Graaf
	Prof. dr. H.P. Spaink
Copromotor:	Dr. E.H.J. Krekels

Promotiecommissie:	Prof. dr. H. Irth, voorzitter
	Prof. dr. J.A. Bouwstra, secretaris
	Prof. dr. U.S.H. Simonsson
	Uppsala University
	Prof. dr. J. Gabrielsson
	Swedish University of Agricultural Sciences
	Prof. dr. J. den Hertog
	Hubrecht Institute, KNAW
	Prof. dr. ir. F.J. Verbeek
	Dr. J.G.C. van Hasselt

Table of content

Section I. Introduction to high-throughput experimentation in whole vertebrates

Chapter 1

Introduction and scope

1.1 Systems pharmacology in drug development

Drug discovery and development integrates biomedical and pharmacological research at all scales; from elucidation of molecular pathways, through the identification of new chemical entities with the potential of becoming drug compounds, to testing those compounds *in vitro* and *in vivo*, and finally reaching clinical application[1]. Within this process, translation from one experimental context or species to another is important, yet challenging. Reliable translation requires quantitative understanding of underlying pharmacological and (patho)physiological processes.

Quantitative, (semi-)mechanistic pharmacometric modelling is advancing and developed models describe (patho)physiological and pharmacological mechanisms with increasing detail[2]. Quantitatively describing all relevant elements and interactions of a biological system (systems biology) and its interactions with the drug(s) perturbing it (systems pharmacology), improves prediction of drug effects in previously unstudied individuals, (sub)populations, or species. The systems-based approach characterizes the molecular profile of a dimension higher than the reductionistic one of a single molecule and a single target[3]. With that, systems pharmacology contributes to the paradigm shift from chemistry- and biology-based medicine to pathology-directed medicine or systems therapeutics[4].

The increased predictive power of systems pharmacology models comes at a cost of both increased model complexity and the requirement of larger and smarter datasets. It is unlikely that it is possible to gather all required data in these datasets from clinical practice or even mammalian studies as this is often too invasive, cumbersome, or costly. More resource efficient preclinical experiments are therefore necessary to capture all the necessary information on the relevant mechanisms in experimental data to allow for the development of mathematical systems-models that form the basis for the translation to early clinical trials[5]. Known differences in pharmacological or (patho)physiological processes between species can be incorporated to improve the interspecies translation. Starting this learn and confirm cycle with early preclinical data might improve the efficiency and adequacy of the whole developmental process[6]. Therefore, there is a strong need for experimental data and computational methods dedicated to systems pharmacology[7,8].

1.2 Zebrafish larva as vertebrate model organism with high-throughput potential

The zebrafish (*Danio rerio*), especially the zebrafish larva, is increasingly used in drug discovery and early drug development[9]. It forms a link between *in vitro* experiments and *in vivo* studies in mammalian species. The zebrafish is readily genetically modified to develop disease models because of its external fertilization[10], has large litter size, and its embryos and larvae are small and develop rapidly[11], which is ideal for high-throughput experiments. The suitability of this species for high-throughput experiments, with the potential for 1,000-10,000 assays per day[12], allows for the generation of a wealth of relevant data, in a relatively short time and at relatively low costs. But in contrast to *in vitro* or invertebrate experiments at similar rates, the zebrafish larva is a whole vertebrate organism and shows 70% genetic homology with humans[13]. The zebrafish larva is therefore a data and resource efficient model organism in pharmaceutical research[14]. Additionally, it is ethically preferable to perform *in vivo* experiments in the least developed organism, and no ethical approval is necessary for experiments before the larvae start independent feeding[15]. Moreover, zebrafish embryos and larvae in their early life stages are transparent which enables optical imaging of for example fluorescently labelled cells, tissues, or organs[16], or drugs[17]. Because of the non-invasiveness of this technique, repeated longitudinal measurements can be taken, following disease dynamics within an individual. The transparency of the larvae is lost after start of pigmentation, but a transparent adult zebrafish line has been developed to benefit from the possibilities of imaging at later life-stages[18]. Thus, by combining experimental efficiency with the translational potential of a whole vertebrate, the zebrafish larva is a unique model organism for systems pharmacology (Figure 1.1).

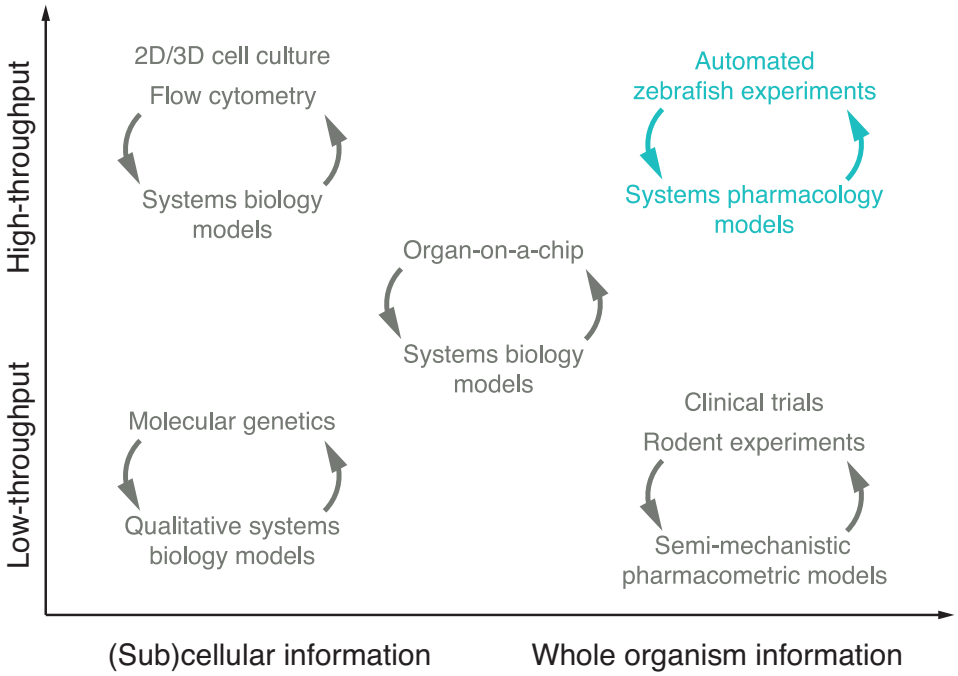

Figure 1.1 Overview of experimental and computational methods relevant for drug development. The horizontal axis specifies the level at which information is gathered, while the vertical axis specifies the speed at which data is collected. From Chapter 3.

1.3 Scope of this thesis

The zebrafish and zebrafish larvae thus bring many advantages to early drug development, which are further described in **Section I**. However, pharmacological experiments with zebrafish and zebrafish larvae are commonly performed by dissolving the drug of interest in the water surrounding the zebrafish. Quantification of the internal drug exposure is often neglected, thereby assuming that the internal and external drug concentrations are the same when interpreting data on the drug efficacy and/or toxicity. This assumption ignores the changes of internal exposure over time, which is driven by pharmacokinetic processes of absorption, distribution, metabolism, and excretion, and this may lead to unreliable interpretation of pharmacological findings (Figure 1.2).

This thesis covers three important elements within the understanding, quantification and subsequent translation of pharmacological findings, that are required for implementation of the zebrafish and zebrafish larva as full member of the preclinical drug development pipeline. It is the scope of our work to develop and integrate experimental and computational methods to quantify these three elements:

1. The internal exposure over time of drugs tested in zebrafish larvae needs to be quantified (**Section II**). Internal exposure is commonly not measured in zebrafish larvae, while it is the concentration at the target site that drives pharmacological effect[19].
2. The internal exposure needs to be linked to disease dynamics (**Section III**). When internal exposure is quantified, it can be related to the observed disease dynamics and changes therein. This will elucidate the onset, intensity, and duration of the drug response on the disease.
3. Differences between species in disease mechanisms need to be quantified, as these are essential for inter-species translation of drug response thereon (**Section IV**). To translate pharmacological findings from zebrafish larvae to higher vertebrates, the differences in pharmacological and (patho) physiological processes between the different species need to be taken into account.

1.4 Introduction to high-throughput experimentation in whole vertebrates

In this introductory Section I, the advantages of zebrafish larvae in drug development are described in detail. In **Chapter 2**, the genetic homology with humans is reviewed with a focus on hepatic metabolism. Using paracetamol (acetaminophen) as paradigm compound, the enzymes responsible for drug oxidation, sulfation, and glucuronidation are identified in the zebrafish. This makes the case that hepatic metabolism studied within the zebrafish, can translate to higher vertebrates. **Chapter 3** gives our perspective on the position of the zebrafish larva within drug development using automation and high-throughput experimentation. Innovative computational methods like outside-in model identification can analyse these large amounts of data obtained in high-throughput experiments in early drug discovery and development to identify the relevant features in a (patho)physiological network upon perturbation thereof. **Chapter 4** gives an example of an experimental set-up that has the potential of high-throughput biomedical data gathering in zebrafish larvae; the Vertebrate Automated Screening Technology (VAST). This bioimager can be used to quantify the volume and surface area of the full zebrafish larva or from fluorescently marked cell-types, tissues, or organs.

1.5 Quantification of internal exposure over time

Quantification of internal exposure over time in zebrafish larvae is challenging because of small sample volumes and low drug amounts in these samples. It requires sensitive bioanalytical techniques in combination with experimental innovations and model-based analysis. In Section II, paracetamol is used as paradigm compound to study internal drug exposure in zebrafish larvae. **Chapter 5** introduces the first pharmacokinetic analysis in zebrafish larvae of 3 days post fertilization after waterborne paracetamol treatment. Two experiments are performed, a constant waterborne treatment experiment and a wash-out experiment. Using internal exposure data gathered from these two experiments, a pharmacokinetic model is developed, which results in a clearance estimate relative to the total volume of the larvae, which is compared to clearance in higher vertebrates. **Chapter 6** expands this line of experimentation to answer the question what the impact of larval age is on pharmacokinetic parameters. In this fast developing organism, a single day can make a difference. Based on this analysis, it is explored at what age pharmacokinetic experiments can be performed best. In **Chapter 7**, the elimination of paracetamol is studied in mechanistic detail. Paracetamol and its two major metabolites are measured, to confirm functionally that metabolism is similar between species, in addition to the genetic homology of metabolising enzymes from Chapter 2. A method to draw nanoscale blood samples is developed resulting in data on blood concentrations, necessary for the pharmacokinetic metabolite model to estimate volume of distribution and absolute clearance, both of which are compared to higher vertebrates.

1.6 Linking internal exposure to disease dynamics

Section III focusses on linking internal exposure to disease dynamics. Repeated measurements of

Figure 1.2 Internal drug exposure over time inside the zebrafish or zebrafish larva needs to be quantified in pharmacological or toxicological studies. It is commonly assumed that internal drug concentration in zebrafish or zebrafish larvae is similar to the external concentration of the waterborne treatment and constant over time (middle). It is however more likely that the concentration inside the zebrafish is lower than outside because of slow absorption or fast elimination (left). Another possibility is drug accumulation inside the zebrafish, where the internal concentration is higher than the external one (right). Quantification of the internal exposure is of importance, because that drives the effect.

biomarkers reflecting a disease during the full time course of treatment improve understanding of the drug response on that disease. The resulting information on the disease dynamics can be used to characterize onset, intensity, and duration of the response of the drug. In **Chapter 8**, tumour size is repeatedly quantified in the neuroblastoma disease model in zebrafish[20] upon waterborne treatment with isotretinoin (13-cis-retinoic acid). The internal exposure over time of this photo-sensitive compound, and of its photo-isomers 9-cis-retinoic acid and all-trans-retinoic acid, is quantified as well. These pharmacodynamic and pharmacokinetic experiments are necessary to link internal exposure to response.

1.7 Mechanistic and quantitative translation of exposure-response from zebrafish to higher vertebrates

Translation of pharmacological findings to higher vertebrates needs to take into account the differences between the different species regarding disease mechanisms and response to pharmacological perturbations. A quantitative understanding of these differences will improve translation of findings for new drugs for a disease. Section IV focusses on that quantitative translation based on tuberculosis, a disease studied extensively in zebrafish[21]. In **Chapter 9**, the natural growth of two strains of *Mycobacterium marinum* are studied over an extensive period of time. The established multistate tuberculosis pharmacometric model[22], developed to quantify natural growth of *Mycobacterium tuberculosis* and drug effect thereon in humans and higher vertebrates, is utilized to quantify the *M. marinum* natural growth data. **Chapter 10** uses one of the *M. marinum* strains to infect zebrafish embryos and subsequently treat them with waterborne isoniazid at increasing doses. Infection is quantified by repeated fluorescence imaging and a quantitative, internal exposure-response relationship is developed. This quantitative relationship is subsequently translated to humans, utilizing translational factors to account for differences in disease mechanisms.

1.8 Discussion, perspectives, and conclusion

The results of the previous sections are discussed in **Chapter 11**, including our recommendations for the inclusion of zebrafish and zebrafish larvae in the drug development pipeline. There is large potential for this model organism to answer pharmacological questions at an early stage in drug development. We envision future perspectives and application in this context, including further extension and improvement of the experimental and computational methodologies that we have developed in this thesis with state-of-the-art methods under development at this point.

1.9 References

1. Lesko LJ, Rowland M, Peck CC, et al. Optimizing the science of drug development: opportunities for better candidate selection and accelerated evaluation in humans. J Clin Pharmacol. 2000;40(8):803-814.
2. Vicini P, Van der Graaf PH. Systems pharmacology for drug discovery and development: paradigm shift or flash in the pan? Clin Pharmacol Ther. 2013;93(5):379-381.
3. Van der Greef J, McBurney RN. Rescuing drug discovery: In vivo systems pathology and systems pharmacology. Nat Rev Drug Discov. 2005;4(12):961-967.
4. Danhof M, Klein K, Stolk P, et al. The future of drug development: The paradigm shift towards systems therapeutics. Drug Discov Today. 2018;23(12):1990-1995.
5. Musuamba F, Manolis E, Holford N, et al. Advanced methods for dose and regimen finding during drug development: summary of the EMA/EFPIA workshop on dose finding (London 4-5 December 2014). CPT Pharmacometrics Syst Pharmacol. 2017;6:418-429.
6. Sheiner LB. Learning versus confirming in clinical drug development. Clin Pharmacol Ther.

1997;61(3):275-291.
7. Nijsen MJ, Wu F, Bansal L, et al. Preclinical QSP modeling in the pharmaceutical industry: an IQ consortium survey examining the current landscape. CPT Pharmacometrics Syst Pharmacol. 2018:Accepted article.
8. Van der Graaf PH. Pharmacometrics and/or systems pharmacology. CPT Pharmacometrics Syst Pharmacol. 2019;8(6):331-332.
9. Rennekamp AJ, Peterson RT. 15 years of zebrafish chemical screening. Curr Opin Chem Biol. 2015;24:58-70.
10. Howe DG, Bradford YM, Eagle A, et al. The zebrafish model organism database: New support for human disease models, mutation details, gene expression phenotypes and searching. Nucleic Acids Res. 2017;45(D1):D758-D768.
11. Kimmel CB, Ballard WW, Kimmel SR, et al. Stages of embryonic development of the zebrafish. Dev Dyn. 1995;203:253-310.
12. Ali S, Champagne DL, Spaink HP, Richardson MK. Zebrafish embryos and larvae: A new generation of disease models and drug screens. Birth Defect Res (Part C). 2011;93:115-133.
13. Howe K, Clark MD, Torroja CF, et al. The zebrafish reference genome sequence and its relationship to the human genome. Nature. 2013;496:498-503.
14. Zon LI, Peterson RT. In vivo drug discovery in the zebrafish. Nat Rev Drug Discov. 2005;4(1):35-44.
15. Strähle U, Scholz S, Geisler R, et al. Zebrafish embryos as an alternative to animal experiments — A commentary on the definition of the onset of protected life stages in animal welfare regulations. Reprod Toxicol. 2012;33:128-132.
16. Pulak R. Tools for automating the imaging of zebrafish larvae. Methods. 2016;96:118-126.
17. Li Y, Chen T, Miao X, et al. Zebrafish: A promising in vivo model for assessing the delivery of natural products, fluorescence dyes and drugs across the blood-brain barrier. Pharmacol Res. 2017;125(Part B):246-257.
18. White RM, Sessa A, Burke C, et al. Transparent adult zebrafish as a tool for in vivo transplantation analysis. Cell Stem Cell. 2008;2(2):183-189.
19. Morgan P, Van der Graaf PH, Arrowsmith J, et al. Can the flow of medicines be improved? Fundamental pharmacokinetic and pharmacological principles toward improving Phase II survival. Drug Discov Today. 2012;17(9/10):419-424.
20. He S, Mansour MR, Zimmerman MW, et al. Synergy between loss of NF1 and overexpression of MYCN in neuroblastoma is mediated by the GAP-related domain. eLife. 2016;5:e14713.
21. Meijer AH, Spaink HP. Host-pathogen interactions made transparent with the zebrafish model. Curr Drug Targets. 2011;12(7):1000-1017.
22. Clewe O, Aulin L, Hu Y, et al. A multistate tuberculosis pharmacometric model: A framework for studying anti-tubercular drug effects in vitro. J Antimicrob Chemother. 2016;71(4):964-974.CHapter Chapter

Chapter 2

Systems pharmacology of hepatic metabolism in zebrafish larvae

Rob C. van Wijk, Elke H.J. Krekels, T. Hankemeier,
Herman P. Spaink, Piet H. van der Graaf

Drug Discovery Today: Disease Models 22: 27-34 (2016)

2.1 Abstract

Interspecies translation of pharmacological processes needs to improve to reduce attrition in drug development. Systems pharmacology integrates systems biology and pharmacometrics to characterize and quantify system-specific behaviour upon exposure to drugs in different species. The zebrafish is a suitable vertebrate model organism for systems pharmacology, combining high-throughput potential with high genetic homology to higher vertebrates. Zebrafish larvae have been increasingly used for drug screens, but the influence of internal drug and metabolite exposure is hardly studied. Quantifying this internal exposure is essential for establishing both exposure-response and dose-exposure relationships, needed for translation. The zebrafish may also serve as a suitable model species for translational studies on the occurrence of hepatotoxicity and the influence of hepatic dysfunction on drug metabolism.

2.2 Introduction

Drug development is a complex and costly process with high attrition. Of the terminated drug candidates, the majority fails because of lack of efficacy and safety[1,2]. Efficacy and safety are tested in preclinical experiments, but to improve success rates, interspecies translation needs to move from an empirical to a mechanistic approach[3]. Systems pharmacology is such an approach, combining the strengths of systems biology and pharmacometrics[4]. Understanding the systems of species and their differences helps improving interspecies translation of efficacy and safety data. In this review, we will focus on systems pharmacology of hepatic function and dysfunction, and the importance of understanding the drug exposure over time in a biological system. The unique position of zebrafish larvae as vertebrate model organism for systems pharmacology with high-throughput potential will be discussed.

2.3 Systems pharmacology: integrating pharmacometrics and systems biology

Systems pharmacology is a method to contribute to translational medicine by integrating modelling and simulation with data from both preclinical and clinical experiments in a 'systems level' mechanistic way, improving interspecies translation of relevant biological processes[5]. Systems pharmacology originates from two established fields, pharmacometrics and systems biology, and aims to quantify the pharmacological perturbations of the biological system of an organism to improve our understanding of the interaction between a drug and a particular biological system.

Pharmacometrics aims to predict drug effects using mathematical models to quantify interactions between organisms and pharmaceutical compounds[6]. This results in pharmacokinetic-pharmacodynamic (PK-PD) models integrating drug pharmacokinetics, which describes drug exposure as concentration versus time, and drug pharmacodynamics, which describes effects versus drug concentration. A schematic of a PK-PD model can be seen in Figure 2.1. Observed outcome measures (i.e. concentrations and effects) are described by mathematical equations, from which the underlying primary model parameters are derived. After evaluation of the predictive performance of a model, the model can be used for predictions and to improve interspecies translation of drug pharmacokinetics and pharmacodynamics and to design treatment regimens in both preclinical and clinical studies[7].

Systems biology studies the structure and dynamics of integrated biological systems to understand processes that are too complex to intuitively comprehend by studying its isolated elements only. Like pharmacometrics, this requires quantitative data as well as advanced computational modelling[8]. Systems biology as holistic approach has the advantage of placing part of a system in the biological context of a complete organism. Characterising individual parts of the system, like gene or protein function, from *in vitro* experiments is an important first step[8]. The next step is to elucidate the interaction of these parts in the network of the whole system. This is relevant in for example disease models, as most diseases are not – as previously believed – caused by a single target, for which a single drug can be designed[9].

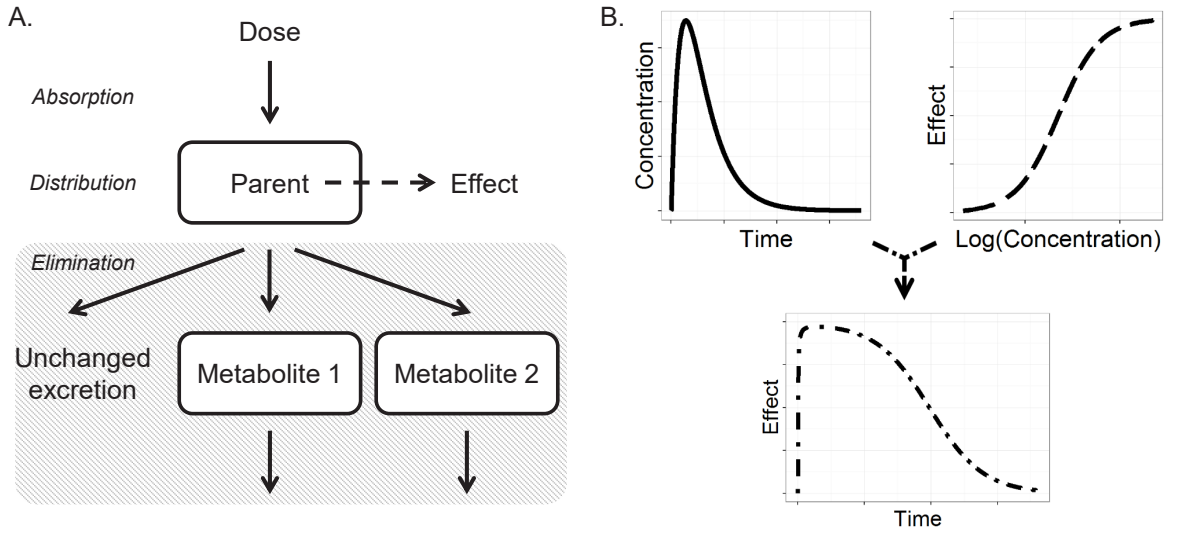

Figure 2.1 Pharmacology of a parent compound described by a compartmental pharmacokinetic model and a sigmoidal pharmacodynamic model. Panel A. Schematic representation of a compartmental model with absorption, distribution, and elimination by means of metabolism and unchanged excretion, describing the pharmacokinetics of the compound (PK, solid lines in panal B). The concentration of the parent compound drives the effect, in a sigmoidal pharmacodynamic relationship (PD, dashed line in panal B). The PK model becomes more mechanistic when including information on different elimination pathways for example metabolite formation and excretion (grey box); these system-specific properties improve translation of clearance between species. Integrating pharmacokinetics andpharmacodynamics in panel B yields the effect over time profile.

In contrast to *in vitro* experiments with human cells only, an *in vivo* whole organism experiment can identify compounds able to treat or cure such a disease[10]. Using these complementary experimental data to inform the systems biology model, the understanding of the biological processes in the organism improves, and with it the understanding of how systems differ between species. This may improve interspecies translation.

2.4 Zebrafish larvae as vertebrate model organism in drug development

Systems biology models have been developed in invertebrate organisms, such as yeast (*Saccharomyces cerevisiae*), roundworms (*Caenorhabditis elegans*) and fruit flies (*Drosophila melanogaster*)[11]. These small organisms are easily genetically modified and allow for high-throughput measurements[11]. However in pharmacological studies, a vertebrate species is believed to have improved translational potential due to its increased genetic homology to mammals. The zebrafish (*Danio rerio*) is such a vertebrate model organism that is increasingly used as a model for biomedical studies[12]. Most genes coding for essential proteins such as those in xenobiotic metabolism are evolutionary conserved. Of human and murine genes, 70% and 71% respectively have a zebrafish orthologue[13]. For comparison, 83% of human genes have a murine orthologue[13]. When considering genes for which defects can cause diseases, 82% of human genes have a zebrafish orthologue[14]. Human disease models in zebrafish larvae have been validated for hyperlipidaemia, liver steatosis, cancer, and mycobacterium infections, among others[15–17].

The use of zebrafish larvae in drug development is increasing because of its many advantages[12]. The four most relevant advantages for drug development include high fecundity, fast development, optical transparency, and easy genetic modification.

Zebrafish have a high reproduction rate. One pair of adult fish yields 100-200 fertilized eggs per mating, reaching up to 10,000 eggs per year. Adults are small (3-5 cm) and are housed in groups of on average 5 to 13 fish per litre[18]. This combination of fecundity and size results in large numbers of larvae and fish at limited costs[19].

Table 2.1 A selection of metabolising enzymes of zebrafish and their human orthologues. Enzymes involved in paracetamol metabolism are printed in italics.

Enzyme family	Zebrafish enzyme	Human enzyme	Reference
CYP1	CYP1A[a]	CYP1A1/1A2	30
	CYP1B1[b]	CYP1B1	30
	CYP1D1	CYP1D1P[c]	30
	CYP1C1,2	-	30
CYP2	CYP2AD2,3,6, CYP2N13, CYP2P1-6, CYP2V1	CYP2J2	30
	CYP2K1-8	CYP2W1	30
	CYP2R1	CYP2R1	30
	CYP2U1	CYP2U1	30
	CYP2Y3,4	*CYP2A6,13/B6/F1/S1*	30
	CYP2Y3[b], *CYP2P6*[b]	*CYP2E1*	52
	CYP2AA1-12	-	30
	CYP2AE1,2	-	30
	CYP2X1-10	-	3-
CYP3	CYP3A65	CYP3A4	30,31
	CYP3C1[d]	CYP3A4	53
	CYP3C1-4	CYP3A-se1[c],-se2[c]	30
CYP4	CYP4F43	CYP4Vs	30
	CYP4T8	-	30
SULT1	*SULT1ST2*[d]	*SULT1A1*	34
	SULT1ST5[b]	SULT1B1	54,55
	SULT1ST6[b]	SULT1E1	54,55
	SULT1ST9[b], *SULT3ST1*[d]	*SULT1A3*	36,56
SULT4	SULT4A1[b]	SULT4A1	57
UGT1	*UGT1*[e]	*UGT1*	37,58
UGT2	UGT2[e]	UGT2	37,58
	UGT5	-	37

[a] similar exon structure, [b] similar gene structure, [c] pseudogene, [d] based on function or substrate specificity, [e] paralogous relationship

After external fertilization, the embryo develops in its chorion until hatching between 48-72 hours post fertilization (hpf) and reaching the larval stage. At that time, the development of most organs is nearly complete, except for the organs in the gastro-intestinal (GI) tract[20]. After 76 hpf, the liver, pancreas, and gut are fully developed, and at 96 hpf, the GI tract is completely open[21]. Experiments are generally performed in the larval phase when the fish are largely developed but small enough (3-5 mm) to fit in multi well plates up to 384 well format.

Zebrafish are optically transparent during early embryonic and larval stages, enabling non-invasive *in vivo* optical imaging of anatomical and certain (patho)physiological developments. Because it is not required to sacrifice the fish, effects can be observed by microscopy over time in a single subject. An example is the phenotypic assay that has been developed to screen for hepatotoxicity by imaging of liver size, yolk size, and liver degeneration[22]. If automated, these assays have the potential to reach throughput rates of 1,000 to 10,000 assays per day[19].

Forward and reverse genetic modification of the zebrafish is especially easy because the external fertilization allows injections of the single cell zygote. Genetic modification enables studying gene

mutations, as well as mechanisms of action of compounds[11]. It is also possible to humanize zebrafish with human enzymes[23]. Transgenic lines have been developed, expressing fluorescent reporter proteins under control of a wide variety of promoter sequences specific for particular cell types[24]. Due to the transparency of the larvae, both gene expression and function can be examined spatially and over time using fluorescence microscopy[25].

In short, large numbers of fast developing subjects with relevant genetic modifications can be achieved with the potential of automated high-throughput screening in numbers suitable for meaningful statistical analysis[26,27]. Moreover, it is from an ethical perspective best to perform animal experiments – if at all necessary – in the available model organism that is least developed[21]. The zebrafish larvae model organism thus combines ethical and practical advantages with the increased homology to higher vertebrates, compared to invertebrates.

2.5 Drug exposure drives effects

For translation of drug effects between species it is not just systems biology and homology of drug targets that are important. The internal exposure of an organism to a drug and its metabolites over time is what drives the drug effects. Quantifying internal exposure is necessary to prevent false positives and negatives[28]. Deriving exposure-response relationships for both desired effects and adverse effects is therefore absolutely essential for interspecies translation of drug pharmacology and toxicology of the parent compound and metabolites. Unfortunately, this is almost always overlooked in pharmacological and toxicological screens with zebrafish larvae. In addition to deriving exposure-response relationships, information on the internal exposure over time in these larvae provides valuable knowledge needed for translation of drug pharmacokinetics from this small vertebrate to higher vertebrates like rodents, monkeys, and even humans, with all their physiological differences. As drug pharmacokinetics drive the dose-exposure relationship, translating it can significantly improve (pre)clinical experimental design by informing dosing rationale.

Box 2.1 Model drug paracetamol

Paracetamol, also known as acetaminophen, is a widely used analgesic[59]. Paracetamol is metabolized in the liver by both phase I and phase II enzymes, and to a limited amount excreted unchanged (<5%). Sulfation by sulfotransferases SULT1A1 and SULT1A3 and glucuronidation by urine 5'-diphospho-glucuronosyltransferase UGT1A6 are responsible for 85% of its metabolism in human adults. The remaining parent compound is oxidized, mainly by cytochrome P450 CYP2E1 to N-acetyl-p-benzoquinone imine (NAPQI), and to a lesser extent by CYP2A6 to methoxy-paracetamol. NAPQI is a toxic metabolite, which reacts with antioxidant glutathione (GSH) to form the nontoxic metabolites cysteine- and mercapturate-paracetamol, among others. At supratherapeutic doses, GSH reserves are depleted and oxidative stress results in hepatotoxicity[60].

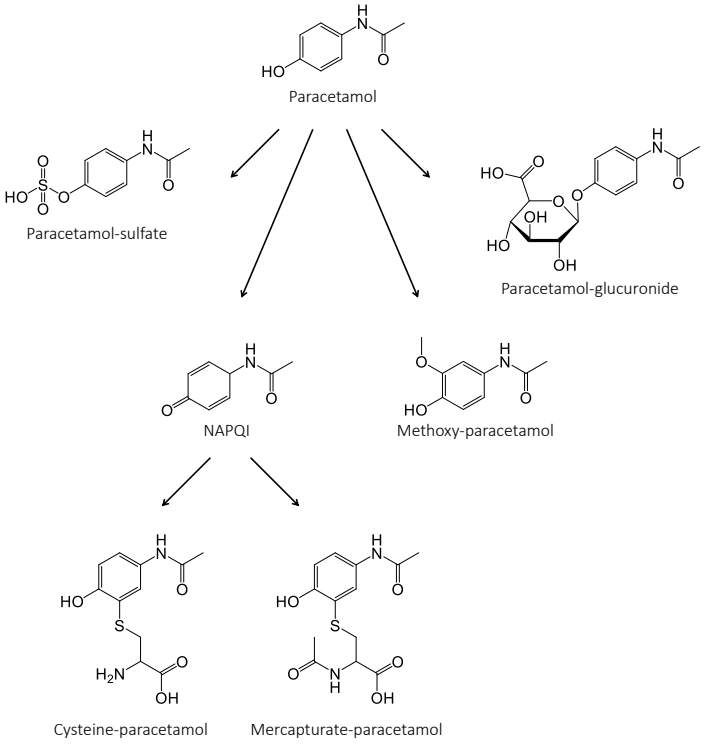

Internal exposure is quantified by describing the pharmacokinetic processes absorption, distribution, metabolism, and excretion (ADME) of drugs. Drug elimination by metabolism and excretion is quantified as clearance, which is the most important determinant of drug exposure. Metabolism of xenobiotics, including drugs, increases hydrophilicity to improve renal excretion and mostly occurs in the liver. Phase I metabolism is of catabolic nature. Xenobiotics are oxidized, reduced, or hydrolysed. Cytochrome P450 (CYP) enzymes are the most important enzymes in catalysing phase I reactions. Phase II metabolism, also known as conjugation, is anabolic and includes transfer of a hydrophilic moiety from a donor to the xenobiotic. Examples of enzymes catalysing conjugating reactions are sulfotransferases (SULTs) and UDP-glucuronosyltransferases (UGTs), amongst others. Drug metabolism can result in reactive metabolites, which may cause toxicity in the metabolising organ[29].

2.6 Hepatic metabolism in the zebrafish

A mechanistic understanding of drug metabolism by a preclinical species in relation to human metabolism requires comparison of both amino acid sequence and function of the responsible enzymes. Table 2.1 shows the relationship of a selection of metabolising enzymes in zebrafish with their corresponding enzymes in humans. These relationships are orthologous, descending from a common ancestral sequence, unless otherwise specified. Specific focus is on the enzymes responsible for paracetamol (Box 2.1) metabolism.

In humans, the most important CYP enzyme isoforms in drug metabolism are CYP3A4 and CYP2E1. CYP3A4 has at least one orthologue in zebrafish, namely CYP3A65 which is 54% identical in amino acid sequence as well as being identical in function[30,31]. Zebrafish CYP2Y3 and CYP2P6 are both 43% identical to human CYP2E1 in amino acid sequence[32].

Several human SULTs have orthologues in zebrafish, mainly from the SULT1 family[33]. Zebrafish SULT1ST2 shows similar xenobiotic sulfation as human SULT1A1, although no gene orthology has been established[34]. Human SULT1A3 is 49% identical in amino acid sequence to zebrafish SULT1ST9[35]. Although no clear homology has been found between zebrafish SULT3ST1 and human SULT1A3, this enzyme is responsible for xenobiotic sulfation similar to SULT1A3[36].

For human and zebrafish UGT enzymes, no orthologous relationships have been found. Instead, these enzymes are so called paralogues, of which the common ancestral gene has been duplicated with different genes in zebrafish and mammals as a result[37]. Despite less genetic overlap then orthologues, paralogues can still have comparable metabolic function. For paracetamol (Box 2.1) the glucuronide-metabolite that is abundantly formed in humans, has been observed in zebrafish larvae as well[38].

2.7 Quantifying metabolising function of the liver

To quantify the metabolising function of hepatic enzymes, pharmacometrics uses for instance non-linear mixed effects modelling to develop empirical compartmental models that quantify pharmacokinetics of drugs in blood, based on concentration-time data. This is the biggest challenge of the zebrafish larvae as model organism for systems pharmacology-based translation of drug pharmacology, as quantifying internal drug and metabolite exposure over time in such small organisms is difficult[12,39]. Currently the external drug concentration in the medium surrounding the larvae is most often used as predictor of the internal drug concentration. It has been tried to predict internal exposure or toxicity based on physicochemical properties of compounds such as hydrophilicity, but without success[40–42]. Only recently, our group developed a sensitive liquid chromatography-mass spectrometry (LC-MS) method to quantify internal exposure of paracetamol (Box 2.1) as a model compound, which resulted in the first pharmacokinetic model in zebrafish larvae[38]. This model quantified exposure over time of the parent

compound, which can be linked to efficacy data. The estimated parameter clearance was scaled between the zebrafish larvae and 12 higher vertebrate species, including rodents, monkeys, and humans, showing reasonable comparability. The model can be extended to include paracetamol major metabolites and their formation rates catalysed by phase I and II enzymes.

Empirical interspecies scaling of paracetamol clearance to higher vertebrates, including humans, was found to be reasonable[38]. When developing new drugs, the clearance in zebrafish might therefore also be used to scale to higher vertebrates and optimize preclinical experimental designs. An improvement over this empirical interspecies pharmacokinetic translation, is the systems approach, where mechanistic details on the metabolism can be included into the model, such as the type of enzymes involved in metabolism of a compound of interest. When the differences between the enzymes of the species of interest are known, the mechanistic model can inform the translation of the pharmacokinetics, in a systems pharmacology approach. Additionally, pharmacologically active metabolites can cause off-target (adverse) effects. It is therefore important to establish if the same metabolite species are formed in different vertebrates. If that is the case, it is essential to quantify their exposure over time to translate the exposure-response relationship of these adverse effects.

2.8 Quantifying liver dysfunction

Hepatotoxicity is an important adverse effect of drugs. One aim of drug screens in zebrafish larvae is to detect potential toxicity issues. Hepatotoxicity assays in zebrafish have been widely published[22,31,43]. This includes assessment of histopathology and transcriptome profiling in zebrafish larvae[44]. Internal drug and metabolite exposure causing this toxicity needs to be quantified for proper interpretation and translation. Moreover, hepatic dysfunction resulting from this toxicity may impact drug clearance. This impact, and its effect on the exposure-time profile, can be quantified using a similar approach as described in *2.7 Quantifying metabolising function of the liver*. The observed adverse effect is then linked to the toxic compound or metabolite (Figure 2.1). This provides mechanistic insight in the influence of hepatic dysfunction on the metabolism of both endogenous and exogenous compounds, including drugs. Informed by the relevant system-specific properties, a systems pharmacology model can translate these findings to mammalian model organisms, and humans.

The validity of a pharmaco- or toxicodynamic model increases with the use of mechanistic biomarkers that describe the disease state, in this case hepatic dysfunction[7]. Mechanistic models describe (patho) physiological processes that are important between drug administration and its intended or adverse effect. Biomarkers can be used to characterize and quantify these processes[45]. Alanine aminotransferase (ALT) and aspartate aminotransferase (AST) are for example widely used hepatotoxicity markers in the clinic. A useful biomarker is both specific and sensitive. ALT is however not liver specific, being expressed in cardiac, renal, and muscle tissue in addition to hepatic tissue[46]. Moreover, it has a delayed response to liver injury, and may not always correlate with clinical symptoms[47,48]. The novel biomarker miRNA-122 has been shown to be a more accurate and time-sensitive alternative to indicate hepatotoxicity in both preclinical and clinical settings[49]. This biomarker has also been studied in zebrafish[50].

Finally, there lies an opportunity for the objective quantification of organ size in zebrafish larvae. Transgenic zebrafish lines with fluorescent organs are available, enabling studying many organs and their development. A reproducible and automated method is the Vertebrate Automated Screening Technology (VAST). In short, complete larvae are withdrawn from a well plate or tube and flow through a capillary linked to a microscope, which captures images of the larvae from different angles in an automated manner. These images can then be processed using 3D silhouette modelling to calculate the volume of the larva[51]. Using this method, we have not only determined the volume of the zebrafish larva at different hpf, but also the volume of its liver (unpublished results). This combination of techniques can be used to observe toxic effects on organ size. Reversely, it can be used to create a database of organ properties and

their development, these system specific properties can then be linked to pharmacokinetic parameters to inform systems pharmacology or physiology-based pharmacokinetic (PBPK) models.

2.9 Conclusions

Systems pharmacology, integrating pharmacometrics with systems biology, has the potential to improve interspecies translation of pharmacological findings, and thereby drug development. The zebrafish larva is a promising pre-clinical model organism in systems pharmacology, combining high-throughput potential within a vertebrate species. Drug metabolising enzymes are comparable and metabolic rates can be derived by combining sensitive LC-MS methods and mathematical modelling. Comparable to quantifying liver function, other (patho)physiological processes, for example liver dysfunction, can also be quantified. Pivotal for proper interpretation of these experimental pharmacological findings is characterising the internal drug exposure, which can then be linked to the observed response in an exposure-response relationship needed for interspecies scaling. More emphasis on the pharmacokinetics is therefore required for this species to change the course of drug development in the future.

2.10 References

1. Kola I, Landis J. Can the pharmaceutical industry reduce attrition rates? Nat Rev Drug Discov. 2004;3:711-715.
2. Morgan P, Van der Graaf PH, Arrowsmith J, et al. Can the flow of medicines be improved? Fundamental pharmacokinetic and pharmacological principles toward improving Phase II survival. Drug Discov Today. 2012;17(9/10):419-424.
3. Van der Graaf PH, Benson N. Systems pharmacology: bridging systems biology and pharmacokinetics-pharmacodynamics (PKPD) in drug discovery and development. Pharm Res. 2011;28:1460-1464.
4. Van der Graaf PH. CPT: Pharmacometrics and systems pharmacology. CPT Pharmacometrics Syst Pharmacol. 2012;1(9):e8.
5. Sorger PK, Allerheiligen SRB, Abernethy DR, et al. Quantitative and systems pharmacology in the post-genomic era: new approaches to discovering drugs and understanding therapeutic mechanisms (white paper). NIH QSP Workshop 2011:1-48.
6. Barret JS, Fossler MJ, Cadieu KD, et al. Pharmacometric: A multidisciplinary field to facilitate critical thinking in drug development and translational research settings. J Clin Pharmacol. 2008;48:632-649.
7. Danhof M, De Lange ECM, Della Pasqua OE, et al. Mechanism-based pharmacokinetic-pharmacodynamic (PK-PD) modeling in translational drug research. Trends Pharmacol Sci. 2008;29(4):186-191.
8. Kitano H. Systems Biology: A brief overview. Science. 2002;295(5560):1662-1664.
9. Hopkins AL. Network pharmacology: the next paradigm in drug discovery. Nat Chem Biol. 2008;4(11):682-690.
10. Zon LI, Peterson RT. In vivo drug discovery in the zebrafish. Nat Rev Drug Discov. 2005;4(1):35-44.
11. Peterson RT, Macrae CA. Systematic approaches to toxicology in the zebrafish. Annu Rev Pharmacol Toxicol. 2012;52:433-453.
12. Rennekamp AJ, Peterson RT. 15 years of zebrafish chemical screening. Curr Opin Chem Biol. 2015;24:58-70.
13. Howe K, Clark MD, Torroja CF, et al. The zebrafish reference genome sequence and its relationship to the human genome. Nature. 2013;496:498-503.
14. MacRae CA, Peterson RT. Zebrafish as tools for drug discovery. Nat Rev Drug Discov. 2015;14(10):721-731.
15. Zhou J, Xu YQ, Guo SY, et al. Rapid analysis of hypolipidemic drugs in a live zebrafish assay. J Pharmacol Toxicol Methods. 2015;72:47-52.
16. Dai W, Wang K, Zheng X, et al. High fat plus high cholesterol diet lead to hepatic steatosis in zebrafish

larvae: a novel model for screening anti-hepatic steatosis drugs. Nutr Metab (Lond). 2015;12(42).
17. Meijer AH, Spaink HP. Host-pathogen interactions made transparent with the zebrafish model. Curr Drug Targets. 2011;12(7):1000-1017.
18. Lawrence C, Eisen JS, Varga ZM. Husbandry and health program survey synopsis. Zebrafish. 2016;13:S5-S7.
19. Ali S, Champagne DL, Spaink HP, et al. Zebrafish embryos and larvae: A new generation of disease models and drug screens. Birth Defect Res (Part C). 2011;93:115-133.
20. Kimmel CB, Ballard WW, Kimmel SR, et al. Stages of embryonic development of the zebrafish. Dev Dyn. 1995;203:253-310.
21. Strähle U, Scholz S, Geisler R, et al. Zebrafish embryos as an alternative to animal experiments — A commentary on the definition of the onset of protected life stages in animal welfare regulations. Reprod Toxicol. 2012;33:128-132.
22. He J, Guo S, Zhu F, et al. A zebrafish phenotypic assay for assessing drug-induced hepatotoxicity. J Pharmacol Toxicol Methods. 2013;67:25-32.
23. Poon KL, Wang X, Ng AS, et al. Humanizing the zebrafish liver shifts drug metabolic profiles and improves pharmacokinetics of CYP3A4 substrates. Arch Toxicol. 2016;91(3):1187-1197.
24. Moro E, Vettori A, Porazzi P, et al. Generation and application of signaling pathway reporter lines in zebrafish. Mol Genet Genomics. 2013;288:231-242.
25. Deo RC, MacRae CA. The zebrafish: Scalable in vivo modeling for systems biology. Wiley Interdiscip Rev Syst Biol Med. 2011;3(3):335-346.
26. Carvalho R, De Sonneville J, Stockhammer OW, et al. A high-throughput screen for tuberculosis progression. PLoS One. 2011;6(2):1-8.
27. Raterink RJ, Van der Kloet FM, Li J, et al. Rapid metabolic screening of early zebrafish embryogenesis based on direct infusion-nanoESI-FTMS. Metabolomics. 2013;9(4):864-873.
28. Diekmann H, Hill A. ADMETox in zebrafish. Drug Discov Today Dis Model. 2013;10(1):e31-e35.
29. Kramer JA, Sagartz JE, Morris DL. The application of discovery toxicology and pathology towards the design of safer pharmaceutical lead candidates. Nat Rev Drug Discov. 2007;6:636-649.
30. Goldstone J V, McArthur AG, Kubota A, et al. Identification and developmental expression of the full complement of cytochrome P450 genes in zebrafish. BMC Genomics. 2010;11(1):643.
31. McGrath P, Li C. Zebrafish: A predictive model for assessing drug-induced toxicity. Drug Discov Today. 2008;13:394-401.
32. Tsedensodnom O, Vacaru AM, Howarth DL, et al. Ethanol metabolism and oxidative stress are required for unfolded protein response activation and steatosis in zebrafish with alcoholic liver disease. Dis Model Mech. 2013;6:1213-1226.
33. Suiko M, Kurogi K, Hashiguchi T, et al. Updated perspectives on the cytosolic sulfotransferases (SULTs) and SULT-mediated sulfation. Biosci Biotechnol Biochem. 2017;81(1):63-72.
34. Yasuda S, Liu CC, Takahashi S, et al. Identification of a novel estrogen-sulfating cytosolic SULT from zebrafish: Molecular cloning, expression, characterization, and ontogeny study. Biochem Biophys Res Commun. 2005;330(1):219-225.
35. Mohammed YI, Kurogi K, Shaban A Al, et al. Identification and characterization of zebrafish SULT1 ST9, SULT3 ST4, and SULT3 ST5. Aquat Toxicol. 2012;112-113:11-18.
36. Yamamoto A, Kurogi K, Schiefer IT, et al. Human cytosolic sulfotransferase SULT1A3 mediates the sulfation of dextrorphan. Biol Pharm Bull. 2016;39(9):1432-1436.
37. Huang H, Wu Q. Cloning and comparative analyses of the zebrafish UGT repertoire reveal its evolutionary diversity. PLoS One. 2010;5(2):e9144.
38. Kantae V, Krekels EHJ, Ordas A, et al. Pharmacokinetic modeling of paracetamol uptake and clearance in zebrafish larvae: Expanding the allometric scale in vertebrates with five orders of magnitude. Zebrafish. 2016;13(6):504-510.
39. Berghmans S, Butler P, Goldsmith P, et al. Zebrafish based assays for the assessment of cardiac, visual and gut function — potential safety screens for early drug discovery. J Pharmacol Toxicol Methods. 2008;58:59-68.

40. Sachidanandan C, Yeh JJ, Peterson QP, et al. Identification of a novel retinoid by small molecule screening with zebrafish embryos. PLoS One. 2008;3(4):e1947.
41. Padilla S, Corum D, Padnos B, et al. Zebrafish developmental screening of the ToxCast TM phase I chemical library. Reprod Toxicol. 2012;33:174-187.
42. Ordas A, Raterink R-J, Cunningham F, et al. Testing tuberculosis drug efficacy in a zebrafish high-throughput translational medicine screen. Antimicrob Agents Chemother. 2015;59(2):753-762.
43. Mesens N, Crawford AD, Menke A, et al. Are zebrafish larvae suitable for assessing the hepatotoxicity potential of drug candidates? J Appl Toxicol. 2015;35:1017-1029.
44. Driessen M, Kienhuis AS, Pennings JLA, et al. Exploring the zebrafish embryo as an alternative model for the evaluation of liver toxicity by histopathology and expression profiling. Arch Toxicol. 2013;87:807-823.
45. Danhof M, Alvan G, Dahl SG, et al. Mechanism-based pharmacokinetic-pharmacodynamic modeling — A new classification of biomarkers. Pharm Res. 2005;22(9):1432-1437.
46. Hornby RJ, Starkey Lewis P, Dear J, et al. MicroRNAs as potential circulating biomarkers of drug-induced liver injury: key current and future issues for translation to humans. Expert Rev Clin Pharmacol. 2014;7(3):349-362.
47. Heard K, Green J, Dart R. Serum alanine aminotransferase elevation during 10 days of acetaminophen administration in non-drinkers. Pharmacotherapy. 2010;30(8):818-822.
48. Vliegenthart ADB, Antoine DJ, Dear JW. Target biomarker profile for the clinical management of paracetamol overdose. Br J Clin Pharmacol. 2015;80(3):351-362.
49. Antoine DJ, Dear JW, Lewis PS, et al. Detection of acetaminophen-induced acute liver injury at first presentation to hospital. Hepatology. 2013;58(2):777-787.
50. Vliegenthart ADB, Tucker CS, Pozo J Del, et al. Zebrafish as model organisms for studying drug-induced liver injury. Br J Clin Pharmacol. 2014;78(6):1217-1227.
51. Guo Y, Veneman WJ, Spaink HP, et al. Three-dimensional reconstruction and measurements of zebrafish larvae from high-throughput axial-view in vivo imaging. Biomed Opt Express. 2017;8(5):2611.
52. Tsedensodnom O, Vacaru AM, Howarth DL, et al. Ethanol metabolism and oxidative stress are required for unfolded protein response activation and steatosis in zebrafish with alcoholic liver disease. Dis Model Mech. 2013;6:1213-1226.
53. Chng HT, Ho HK, Yap CW, et al. An investigation of the bioactivation potential and metabolism profile of zebrafish versus human. J Biomol Screen. 2012;17(7):974-986.
54. Liu T-A, Bhuiyan S, Liu M-Y, et al. Zebrafish as a model for the study of the phase II cytosolic sulfotransferases. Curr Drug Metab. 2010;11(6):538-546.
55. Kurogi K, Dillon J, Nasser A, et al. Sulfation of drug compounds by the zebrafish cytosolic Sulfotransferases (SULTs). Drug Metab Lett. 2010;4(2):62-68.
56. Mohammed YI, Kurogi K, Shaban A Al, et al. Identification and characterization of zebrafish SULT1 ST9, SULT3 ST4, and SULT3 ST5. Aquat Toxicol. 2012;112-113:11-18.
57. Coughtrie MWH. Function and organization of the human cytosolic sulfotransferase (SULT) family. Chem Biol Interact. 2016;259(A):2-7.
58. Li C, Wu Q. Adaptive evolution of multiple-variable exons and structural diversity of drug-metabolizing enzymes. BMC Evol Biol. 2007;7:69.
59. Muramatsu S, Shiraishi S, Miyano K, et al. Metabolism of AM404 from acetaminophen at human therapeutic dosages in the rat brain. Anesthesiol pain Med. 2016;6(1):e32873.
60. Gelotte CK, Auiler JF, Lynch JM, et al. Disposition of acetaminophen at 4, 6, and 8 g/day for 3 days in healthy young adults. Clin Pharmacol Ther. 2007;81(6):840-848.

Chapter 3

Outside-in systems pharmacology combines innovative computational methods with high-throughput whole vertebrate studies

Pascal Schulthess*, Rob C. van Wijk*, Elke H.J. Krekels, James W.T. Yates, Herman P. Spaink, Piet H. van der Graaf

CPT: Pharmacometrics & Systems Pharmacology 7(5): 285-287 (2018)

* authors contributed equally

3.1 Introduction

To advance the systems approach in pharmacology, experimental models and computational methods need to be integrated from early drug discovery onwards. Here, we propose outside-in model development, a model identification technique to understand and predict the dynamics of a system without requiring prior biological and/or pharmacological knowledge. The advanced data required could be obtained by whole vertebrate, high-throughput dose-exposure-effect experimentation with the zebrafish larva. Combination of these innovative techniques could improve early drug discovery.

3.2 Outside-in model development

Systems biology has developed into a research field elucidating biological pathways and networks in great detail. These efforts are not only fuelled by the advanced genetic toolbox in combination with increasingly sensitive and innovative measurement techniques, but especially by combining these experimental approaches with an "inside-out" modelling strategy[1]. Inside-out modelling aims to understand an external behaviour (e.g. cellular apoptosis) by describing the internal processes (e.g. signal transduction pathways) as detailed as possible. The resulting model structures are closely aligned to the underlying processes, while the extensive amount of experimental data required serves to estimate the unknown parameters of the model. Similarly, semi-mechanistic pharmacometric and systems pharmacology models adhere to this modelling paradigm, shifting focus from target-based to systems-, or phenotypic-based drug development[2,3]. In our current understanding of healthy and diseased organisms as complex systems, a single drug selective for a single target within the network would rarely be fully effective.

"Outside-in" model development, on the other hand, is an approach still mainly used in engineering and there known as black box system identification. It does not require prior knowledge of the system of interest, but allows the precise system structure and thus the dynamics of the system to be exposed by only observing its response to well-controlled stimuli (Figure 3.1 A). More specifically, within such identification approaches, the system of interest is excited with oscillating stimuli of different frequencies in order to measure the time resolved response of the system (Figure 3.1 B). For each input frequency, the amplitude of input and output as well as the phase shift between input and output are collected and plotted in a Bode plot (Figure 3.1 C). This visual frequency domain representation of the dynamics of the system can be transformed into a formula by fitting a so-called transfer function which is a representation of a set of linear differential equations that (in matrix notation) contain the state matrix $\boldsymbol{A}$, the input matrix $\boldsymbol{b}$, the output matrix $\boldsymbol{c}^{\boldsymbol{T}}$, and the feedthrough matrix $\boldsymbol{d}$ (for systems with one input and one output $\boldsymbol{d}$ being a scalar). These matrices can then be used to construct the model structure of the identified mathematical model (Figure 3.1 D). Thus, the relationship between input and output of a system can be reconstructed if its complete frequency response is known[4].

One of the advantages of this outside-in approach, the fact that it does not require prior information on the structure or the components of the model, makes this analysis method especially suitable for studying poorly understood (patho)physiological systems, pathways, diseases, or drug effects. Mettetal and colleagues, for example, exposed yeast cells to oscillating NaCl levels of different frequencies and measured a fluorescently labelled protein as biomarker. Application of the outside-in approach lead them to identify the dominant dynamics in the osmo-adaptation system in yeast, without considering all known and unknown reactions[5].

In early drug discovery, similarly little may be known about target pathways or drug effects, making this systems identification method of value. Once outside-in modelling uncovers the system structure and its dynamics, new experiments can be designed to inform the systems model and its detailed components which then allows prediction and interspecies translation of drug effects. Outside-in modelling is therefore an opportunity for close collaboration between experimentalist and modeller. Even though

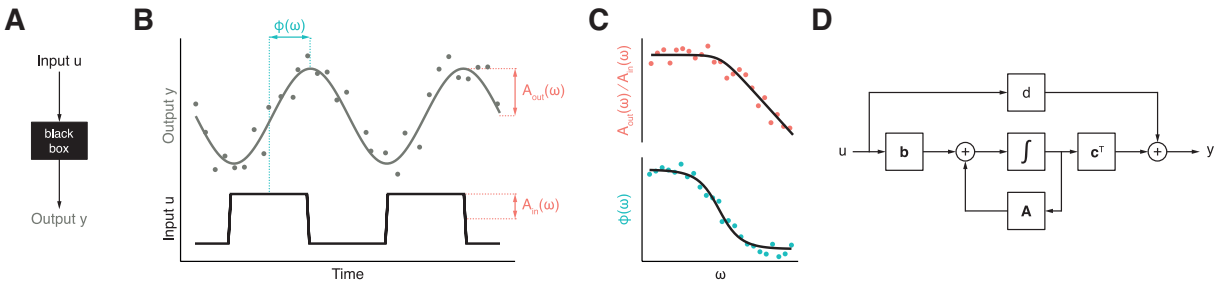

Figure 3.1 Outside-in model identification in the frequency domain. (A) Black box model is excited with input *u* and responds with output *y*. (B) Square wave input with amplitude $A_{in}(\omega)$ (black), output measurements (grey dots), and fitted sinusoid with amplitude $A_{out}(\omega)$ and phase shift $\phi(\omega)$ (grey line) are shown. (C) Bode plot of amplitude ratio and phase shift measurements (red and blue dots, respectively) versus the frequency of the oscillations (ω) are used to fit a transfer function (black lines). (D) The model structure is derived from the differential equations which themselves are determined from the transfer function.

meticulous input/output measurements are still required, the outside-in approach does not initially require exhaustive experimentation typical for inside-out systems biology models, thus enabling a fast turnover in testing drug candidates. This method is furthermore not exclusively tailored to identify model structures from the response of a single target to a single stimulus, it also extends to multiple drugs affecting multiple targets or even the whole organism.

Thus, outside-in modelling can initiate the drug discovery and development learn-and-confirm cycle from the systems-perspective.

3.3 High-throughput whole vertebrate experiments in zebrafish larvae

To use the outside-in methodology in systems pharmacology, informative data from dedicated input/output experimentation is needed. As complementary pathways and feedback loops may attenuate the effect of a single drug compound, pharmacological treatment targeting multiple pathways seems more promising. This means experimental data should reflect perturbation of the whole organism as a system, with all intended and unintended targets available (Figure 3.2 right-hand quarters). Additionally, as little time and resources are available in early drug discovery, performing the required stimulations at different frequencies is preferably performed in a high-throughput set-up (Figure 3.2 upper quarters). These types of high-throughput whole-organism experiments are usually performed in invertebrate organisms like yeast (*Saccharomyces cerevisae*), round worms (*Caenorhabditis elegans*), or fruit flies (*Drosophila melanogaster*), but are unpractical and unethical for commonly-used vertebrate organisms like rodents. However, high-throughput whole vertebrate experiments are now possible in a relatively new model organism; the zebrafish larva (*Danio rerio*).

The zebrafish is an appealing alternative model organism to rodents[6]. They are easily genetically modified, enabling the creation of fluorescent reporter lines, as well as disease models[7]. The zebrafish develops quickly, with all major organ systems present within 72 hours after fertilization, which allows for faster experimentation cycles as compared to traditional vertebrates like rodents. Moreover, the larvae are transparent, making (fluorescence) microscopy highly feasible. Lastly, their small size and litter sizes of 100-200 eggs per breeding couple every 2 weeks, makes this experimental organism very cost effective. Therefore, zebrafish larvae are very suitable for experiments required for outside-in system identification in early drug discovery and development.

Innovative experimental methods in the zebrafish have been developed since the turn of the millennium, especially with the zebrafish larvae. Recently, the first pharmacokinetic model in zebrafish larvae has been developed, an important step for this organism towards serving as model organism for systems pharmacology[8]. Additionally, experimental devices are designed to automatically load and position larvae in different chambers under the flow of for example drug containing medium. These microfluidic

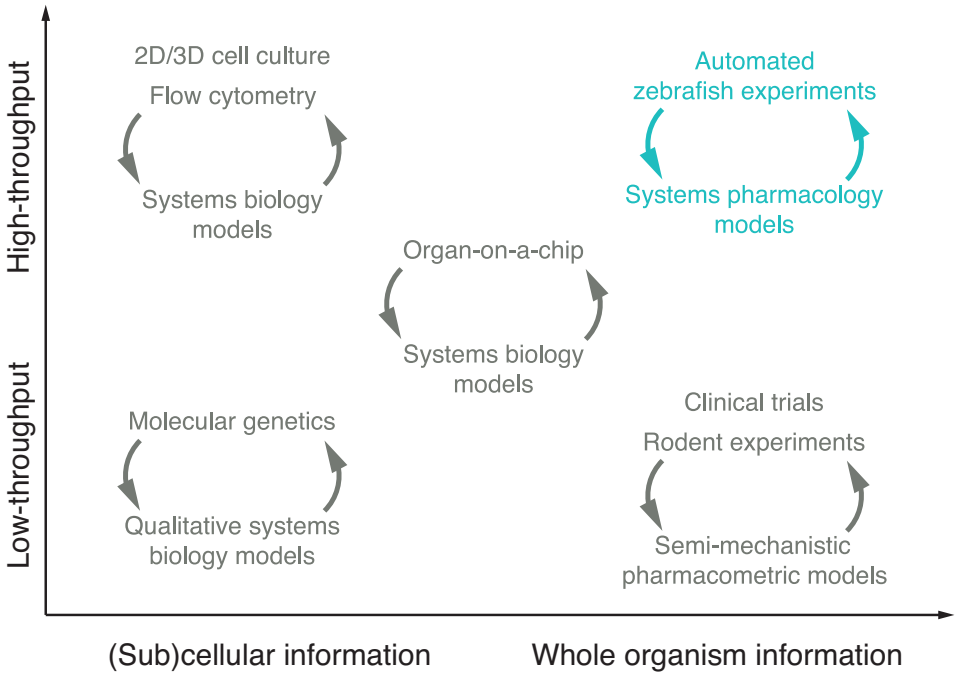

Figure 3.2 Distribution of current experimental methods and corresponding systems modelling approaches. Models to describe aspects of a physiological system in general can be developed at different levels, from subcellular and cellular to tissue-, organ-based, and whole organisms. At subcellular and cellular level, molecular genetics and biomedical experiments have unravelled detailed pathways within cells, and cellular environments in tissues or organs (lower left quarter). Fluorescence labelling, either chemically or genetically, enables high-throughput screening and sorting at cellular level (upper left quarter). Moving towards higher hierarchical levels, organ-on-a-chip informs on organoid processes and interactions (middle). For drug development, the perturbation of the whole organism system by a drug and quantifying the dynamics of the perturbation is very relevant, especially when considering multi-target drugs or combination therapy. Traditionally, from preclinical rodent and clinical patient data, pharmacometric models are used to quantify these effects (lower right quarter). Here, we propose the zebrafish larva as high-throughput whole vertebrate organism for outside-in model informed systems pharmacology, to fill the gap of high-throughput studies in whole organisms (upper right quarter).

devices enable precisely controlled dynamic flow of exposure solution and wash medium, required for the oscillating stimulus of the outside-in systems identification[9]. Integrating such devices with automated fluorescence microscopy could lead to a closed experimental set-up delivering systems pharmacology data in an automated high-throughput fashion[10].

The availability of these methodologies welcomes experimentalists and modellers to combine forces, aimed to tailor experimental data to a systems pharmacology model, and vice versa, continuing the learn-and-confirm iterative approach. Indeed, as the first outside-in data analysis without prior knowledge on system or target pathways will result in information on important features of the system and identify promising candidates, more detailed experiments and subsequent analyses can be designed and executed to elucidate underlying physiological mechanisms. When a comprehensive understanding of the studied system and the perturbing drug candidates has been developed, this knowledge should advance in the development pipeline. Knowledge of the system- and drug-specific parameters will then enable reliable interspecies translation and extrapolation, first from zebrafish larvae to rodent studies, and finally towards the clinic.

3.4 Conclusion

Systems pharmacology models inform drug discovery and development decisions. The models should be fit for purpose, combining the best of systems biology's mechanistic understanding and pharmacometrics' quantification of drug perturbations on a system. Although a system can be studied

on all biological levels, from subcellular to whole organism, the latter is more in line with the current paradigm of pharmaceutical research. Here, we propose the use of systems pharmacology in drug discovery and development firstly by outside-in model identification, where the prominent factors between drug input and biological output are modelled without prior knowledge on the pathways or extensive understanding of the involved processes. Indeed, only the relevant rate-limiting elements will be considered. In early drug discovery, less resources and time are available, so experimentation should provide enough information on these elements within a short timeframe. In other words, high-throughput experiments are preferred, while retaining information on the drug dose-exposure-response relationship. Such high-throughput experiments with the possibility of well-controlled oscillating stimuli and non-invasive detection of response by fluorescence, are possible in zebrafish larva contained in a microfluidics device. These precisely defined input and output data can in turn be used for black box outside-in model identification, unravelling the most relevant features in a target pathway and informing on promising candidates affecting these pathways. Our approach is characterized by close interaction between experimentalists and modellers, and constant iteration of experiments and computational analysis, improving each other. When the understanding of the targets, pathways, and system increases with outside-in modelling, new experiments and subsequent computational analysis can be planned. Towards candidate selection, the understanding of the system- and drug-specific properties of the developed model can be used to extrapolate drug effects and design rodent studies, continuing the iteration. This cost effective and fast approach facilitates the learn-and-confirm cycle, potentially improving the development of systems pharmacology models and candidate selection, and eventually possibly drug discovery and development itself.

3.5 References

1. Malleshaiah M & Gunawardena J. Cybernetics, Redux: An outside-in strategy for unraveling cellular function. Developmental Cell. 2016;36:2–4.
2. Moffat JG, Vincent F, Lee JA, et al. Opportunities and challenges in phenotypic drug discovery: an industry perspective. Nat Rev Drug Discov. 2017;16:531–543.
3. Danhof M. Systems pharmacology- towards the modeling of network interactions. Eur J Pharm Sci. 2016;94:4–14.
4. Schulthess P, Post TM, Yates J, et al. Frequency-domain response analysis for quantitative systems pharmacology models. CPT Pharmacometrics Syst Pharmacol. 2017;6:418.
5. Mettetal JT, Muzzey D, Gómez-Uribe C, et al. The frequency dependence of osmo-adaptation in Saccharomyces cerevisiae. Science. 2008;319:482–484.
6. Van Wijk RC, Krekels EHJ, Hankemeier T, et al. Systems pharmacology of hepatic metabolism in zebrafish larvae. Drug Discovery Today: Disease Models. 2016;22:27–34.
7. Howe DG et al. The zebrafish model organism database: New support for human disease models, mutation details, gene expression phenotypes and searching. Nucleic Acids Research. 2017;45:D758–D768.
8. Kantae V, Krekels EHJ, Ordas A, et al. Pharmacokinetic modeling of paracetamol uptake and clearance in zebrafish larvae: Expanding the allometric scale in vertebrates with five orders of magnitude. Zebrafish. 2016;13(6):504-510.
9. Fuad NM, Kaslin J & Wlodkowic D. Development of chorion-less zebrafish embryos in millifluidic living embryo arrays. Biomicrofluidics. 2017;11:051101.
10. Veneman WJ, Marín-Juez R, De Sonneville J, et al. Establishment and optimization of a high throughput setup to study Staphylococcus epidermidis and Mycobacterium marinum infection as a model for drug discovery. J Vis Exp. 2014;88:e51649.

Chapter 4

Multi-modal 3D reconstruction and measurements of zebrafish larvae and its organs using axial-view microscopy

Yuanhao Guo, Rob C. van Wijk, Elke H.J. Krekels, Herman P. Spaink, Piet H. van der Graaf, Fons J. Verbeek

IEEE International Conference on Image Processing (ICIP), Beijing, 2194-2198 (2017)

4.1 Abstract

In life sciences, light microscopy is used to study specimens. On the organism-level a bright-field representation presents an overview for the whole shape of a specimen; the organ-level fluorescent staining reprsentation supports in the interpretation of the detailed intrinsic structures. We present light microscopy axial-view imaging based on the Vertebrate Automated Screening Technology to acquire axial-view images for the organism and organs of zebrafish larvae. We obtain multi-model 3D reconstruction using a profile-based method, from which we can derive the 3D measurements of volume and surface area. In this method, we employ a microscope camera calibration using voxel residual volume maximization algorithm. We intuitively align and fuse the obtained multi-models. Experimental results show natural visualization both for the whole organism and organ of zebrafish larvae; subsequently accurate 3D measurements are obtained. This method is very suitable for high-throughput research in which knowledge on size and shape is relevant to the understanding of development, effects of compounds or drugs.

4.2 Introduction

In modern life-sciences research, e.g. developmental biology, (patho)physiology, toxicology, and pharmacology, light microscopy is commonly used to produce 2D colour representations of biological phenomena. The zebrafish is a popular vertebrate model organism in biomedical research because of its many advantages, among which is optical transparency at early life stages[1,2]. The organs of the transparent larvae can be studied *in vivo* through microscopy. Transgenic lines are available that express a fluorescent reporter gene in specific organs, tissues, or cell types[3]. In this way, organ development of the genetically engineered zebrafish can be visualized and monitored over time by fluorescence microscopy. This makes the zebrafish very suitable for large scale screening experiments with light microscopy. For the screening of large libraries of compounds for organ toxicity, like hepatotoxicity[4], quantitative endpoints like organ size or growth retardation are required. In order to accurately evaluate the shape and size of an organ like the liver, 3D modelling of both the liver and the whole organism are required. Compared with 2D imaging, 3D measurements, e.g. size, volume and surface area, are more reliable. The organism-level imaging is an overview of the shape of the object, serving as shape reference to normalize the 3D measurements of the liver into unit metrics. Our aim is to develop a method for 3D reconstruction and measurements of zebrafish larvae and its organs with axial-view microscopy.

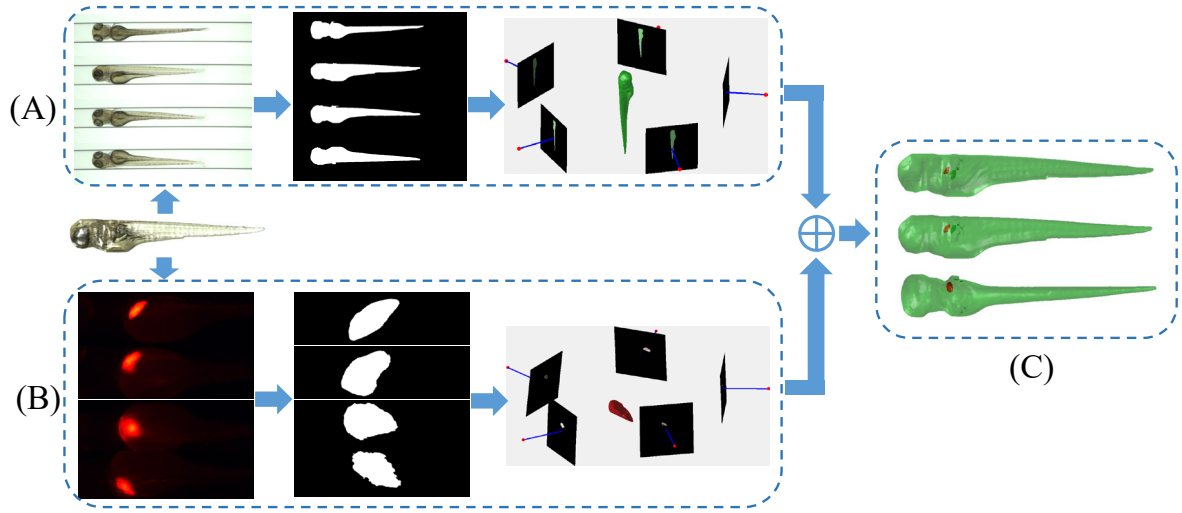

Figure 4.1 A schema of the proposed method. One zebrafish larva presents in the two imaging pipelines. (A) The organism-level 3D reconstruction. (B) The organ-level 3D reconstruction. (C) The multi-modal 3D reconstruction fusion and visualization. In (A) and (B), the first columns show the original axial-view images; the second columns illustrates the 2D binary shapes; the third columns denote the camera system calibration and profile-based 3D reconstruction.

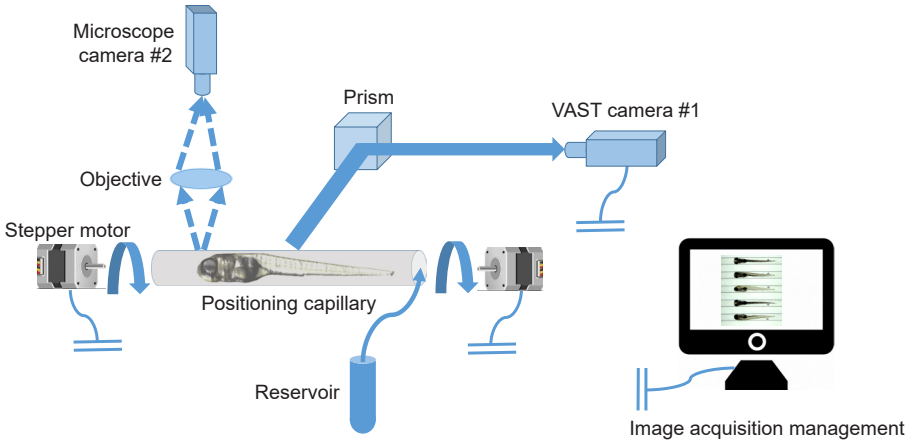

Figure 4.2 An architecture for light microscopy axial-view imaging. The VAST-BioImager delivers a specimen from its reservoir into a capillary. A set of stepper motors hold and manipulate the capillary so that it can rotate in a full revolution; this is synchronized with acquistion so that axial-view images of the specimen can be obtained. The VAST camera #1 detects the presence of a specimen and generates the axial-view images capturing the whole organism in bright-field. The microscope camera #2 captures the organ-level axial-view images in fluorescence.

In stereo vision, a 3D scene can be recovered by matching correlated multi-view images[5]. This is implemented by pixel-level searching[6] or salient point detection and matching[7]. However, these methods are challenged for our typical application at hand, the zebrafish. Here, partial transparency of the zebrafish complicates straightforward application of these methods as it is difficult to match the implicit surface points on the object. Based on the concept of visual hull[8], the space carving algorithm reconstructs the 3D shape from a range of 2D binary shapes[9], which is also referred to as the silhouette-based 3D reconstruction[10,11]. In a sample population of zebrafish a rather large colour variation exists; this holds both for bright-field and fluorescence. Therefore, we propose to use 2D binary representations. Accordingly, we have developed the profile-based 3D zebrafish reconstruction method based on a series of 2D axial-view shapes of the object, obtaining precise 3D representation and accurate 3D measurements for the zebrafish in various larval stages[12].

For this work, we have implemented light microscopy axial-view imaging modality based on the Vertebrate Automated Screening Technology (VAST BioImager)[13,14]. Using the axial-view images acquired from this multi-modal imaging modality, we propose a multi-modal 3D reconstruction method as framed in Figure 4.1. A zebrafish larva with fluorescent marker expressed in the liver is captured in two imaging modes. The VAST camera enables the organism-level imaging and a microscope camera facilitates the organ-level imaging. From the axial-view images, 2D binary shapes are obtained through modern segmentation algorithms[15,16]. We estimate the camera projection geometry for the two camera systems using the voxel residual volume maximization algorithm. We produce the multi-model 3D reconstruction for the organism (zebrafish) and organ (liver) using the profile-based 3D reconstruction method; we use heuristics to fuse the two models acquired from different imaging modalities. From the obtained 3D models, 3D measurements, e.g. volume and surface area, are derived.

4.3 Our approach

In this section, we present multi-modal microscopy axial-view imaging. A dataset containing the zebrafish on both organism- and organ-level imaging is obtained. We introduce the microscope camera calibration and elaborate profile-based 3D reconstruction. We present an interactive method to align and fuse the multi-modal 3D reconstruction.

4.3.1 Light microscopy axial-view imaging

For VAST imaging, zebrafish are positioned along their longitudinal axis. This facilitates easy manipulation of the specimen and the most important features of the specimen can be observed well from the

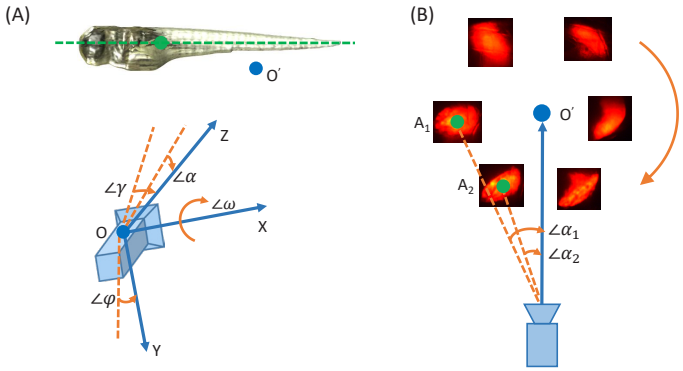

Figure 4.3 (A) The VAST camera pose is modelled as the 3D transformation from the camera centre O to the object centre (green circle). The green line denotes the profile-axis along which the object revolves. $\angle\omega$, $\angle\varphi$ and $\angle\gamma$ represent the 3D rotation angles of the camera along the X, Y and Z directions, respectively. $\angle\alpha$ is modelled as the "translation angle". (B) The centre of the zebrafish liver is not aligned with the zebrafish centre which results in its rotation and revolution with respect to the zebrafish centre, such that the "translation angle" $\angle\alpha$ of the microscope camera is specified for each view.

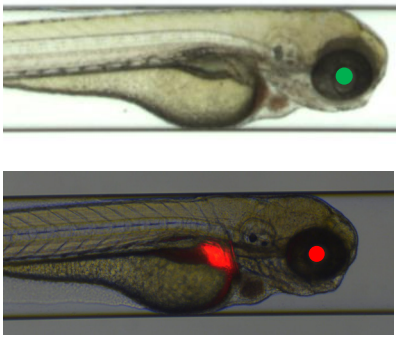

Figure 4.4 The alignment of the multi-modal 3D reconstruction is implemented according to the iris centre of the zebrafish. Top image shows a bright-field image of organism-level imaging. We crop this image to fit the space. Bottom image is a bright-field image overlaid with a fluorescent image of organ-level imaging.

axial-view. The VAST BioImager is developed for zebrafish high-throughput applications[17]. We use this device for our axial-view imaging and thereby generate new functionality of the device. In Figure 4.2, a schematic representation is shown depicting the imaging architecture. The positioning module of the VAST BioImager consists of a capillary and a pair of stepper motors facilitating the rotation of the specimen. A standard CCD camera referred to as the VAST camera #1 is mounted with the device and used to detect the location and orientation of the specimen. We use the VAST camera #1 to acquire the bright-field axial-view images on organism-level. The VAST-unit is mounted on a microscope. We use the microscope camera #2 equipped with a 4x/0.12NA objective to acquire the fluorescent images for the liver on organ-level. This imaging technique is applied to collect a dataset of 7 zebrafish samples, staged as three days post fertilization (3 dpf). A zebrafish transgenic line Tg(lfabp:dsRed; elaA:EGFP) with 2 fluorescent colours for liver and pancreas (2CLIP) is used. The eggs were kept in 60 µg/mL Instant Ocean Sea Salts (Sera Marin, Heinsberg, Germany) in demineralized water and treated with 0.003% 1-phenyl-2-thiourea (PTU, Sigma-Aldrich, Zwijndrecht, The Netherlands) to prevent pigmentation. We evenly sampled 25 axial-views for each zebrafish in both channels in a full revolution. This means the step between adjacent views is approximately 14.4° (due to mechanical drift this is not precise).

4.3.2 Profile-based 3D reconstruction

Given a range of axial-view images **I**, we first obtain the 2D profiles **S** for the object (zebrafish and liver) from image segmentation. We interpret the 3D space in discrete voxel units. Given a voxel centred at a 3D point $\mathrm{X} \in \mathcal{R}^3$, we can find its pixel location $\mathrm{x} \in \mathcal{R}^2$ in a 2D profile according to the camera projection model $\mathrm{x} = \mathrm{PX}$. The profile-based 3D reconstruction projects all the voxels onto all the 2D profiles. According to the visibility of a voxel with respect to the profiles, we assign a confidence score to that voxel. The 3D reconstruction is accomplished by extracting the voxels given a threshold for a confidence score (usually taken as the total number of the axial-views). One can also estimate an enclosed 3D surface from the voxels. For more details of the profile-based 3D reconstruction, we refer to our previous work[12,18].

4.3.3 Light microscope camera system calibration

For a good profile-based 3D reconstruction, we need an accurate camera projection model which can be obtained from a camera calibration. We decompose the camera projection matrix as **P = K R [I|T]**. The **K** denotes the camera intrinsic configuration defined as:

$$\mathrm{K} = \begin{bmatrix} f * k_x & 0 & c_x \\ 0 & f * k_y & c_y \\ 0 & 0 & 1 \end{bmatrix}$$

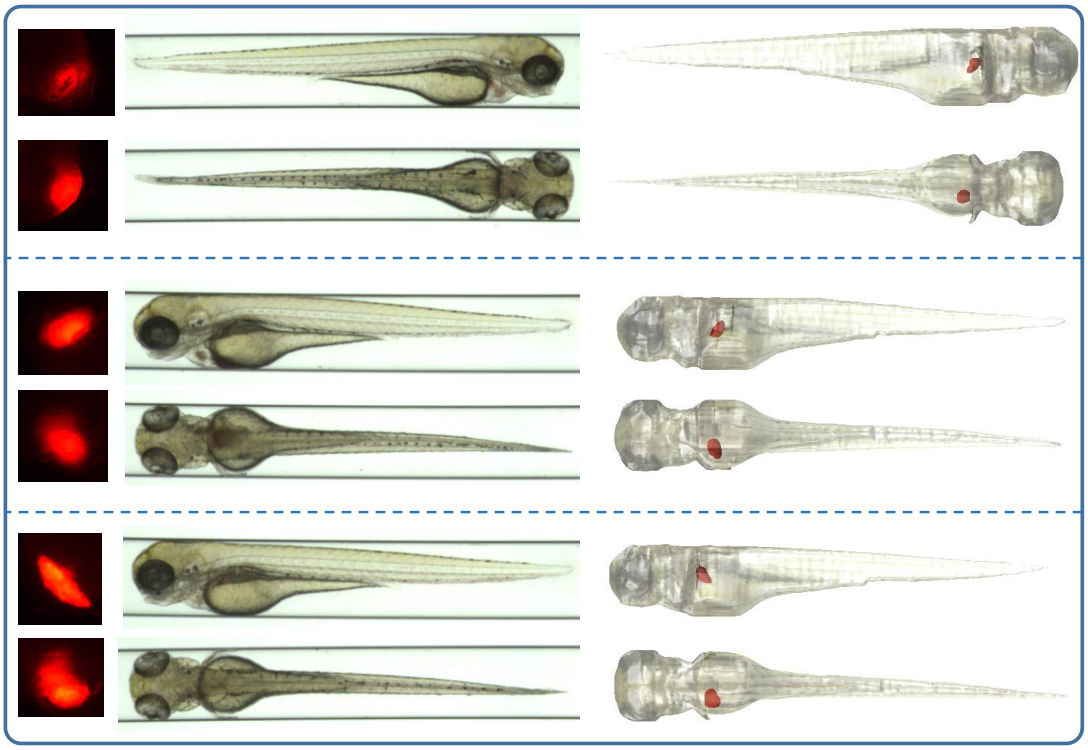

Figure 4.5 Multi-modal 3D reconstruction visualization. We selected three examples from our dataset and for each example we visualize two typical views (lateral and dorsal). The first column represents fluorescent liver images. The middle columns is the zebrafish image in bright-field. The last column visualizes the fusion of the multi-modal 3D reconstruction.

where $\boldsymbol{f}$ is the camera focal length; ($\boldsymbol{k_x}$,$\boldsymbol{k_y}$) denotes the scaling factor and ($\boldsymbol{c_x}$,$\boldsymbol{c_y}$) represents the image centre. In the decomposition of the camera projection model, the $\mathbf{R}_{3x3}$ and $\mathbf{T}_{3x1}$ are the 3D rotation and translation from the camera centre to the object centre, which are also referred to as the camera motion. In practice, the camera remains static and only the specimen rotates. For a better visualization, we arranged the camera as moving around the object as shown in Figure 4.1.

In Figure 4.3 A, we show the VAST camera motion with respect the zebrafish centre. The zebrafish revolves along a fixed profile-axis which is aligned with the object centre, such that the VAST cameras share the rotation angles $\boldsymbol{\varphi}$ and $\boldsymbol{\gamma}$ and the translation angle $\boldsymbol{\alpha}$[19]. The camera rotation angle along the X-axis is specified for each view. So, the whole camera configuration is structured as $\boldsymbol{\psi}$=[$\boldsymbol{f}$,$\boldsymbol{k_x}$,$\boldsymbol{k_y}$,$\boldsymbol{c_x}$,$\boldsymbol{c_y}$,$\boldsymbol{\alpha}$,$\boldsymbol{\varphi}$,$\boldsymbol{\gamma}$,$\boldsymbol{\omega}_{1:N}$], where $\boldsymbol{N}$ is the number of the axial-views. For the microscope cameras, the rotation centre of the zebrafish liver is not aligned with its own centre as shown in Figure 4.3 B, so the translation angle should be specified for each view. We improve the parameterization for microscope camera configuration as $\boldsymbol{\psi}$=[$\boldsymbol{f}$,$\boldsymbol{k_x}$,$\boldsymbol{k_y}$,$\boldsymbol{c_x}$,$\boldsymbol{c_y}$,$\boldsymbol{\alpha}_{1:N}$,$\boldsymbol{\varphi}$,$\boldsymbol{\gamma}$,$\boldsymbol{\omega}_{1:N}$]. The method of voxel residual volume maximization (VRV) is used to estimate accurate camera configuration. The objective is defined as $\mathcal{L}(\psi) = |\mathcal{X}^*|$, where $\mathcal{X}^* = \{\mathrm{X}|\mathcal{S}(\mathrm{P}(\psi)\mathrm{X}) \neq 0, \mathrm{X} \in \mathcal{X}\}$ and $|\mathcal{X}^*|$ are the voxel residual and the volume. The objective maximization is implemented by Nelder-Mead simplex method[20].

4.3.4 Multi-model 3D reconstruction alignment and fusion

The 3D models are obtained from different imaging modes. So, we need to align the resulting multi-modal 3D reconstruction as part of the fusion operation. During the organ-level imaging, we acquired bright-field images in register with the fluorescent images. These images only partially depict the object but provide a good reference for the alignment. We have obtained the camera poses for both models from camera calibration. So, we choose the same axial-view for the zebrafish and localize the iris centre as shown in Figure 4.4. We use the organ-level 3D model as a template. The organism-level 3D model is scaled, rotated and shifted to align with the former according to the camera pose and the position of the iris centre. Finally, we map the multi-models into the same space to obtain the fusion result.

4.4 Experiments

In this section, we apply our method on the zebrafish dataset for performance evaluation. We first visualize some examples of the multi-modal 3D reconstruction in paragraph 4.4.1, and subsequently report on the 3D measurements of volume and surface area for the zebrafish larva and its liver in paragraph 4.4.2.

4.4.1 Results visualization

From our dataset, we select three examples for visualization as shown in Figure 4.5. Two typical axial-views are shown, i.e. lateral and dorsal, and each example is separated by blue lines. The first column shows the original organ-level fluorescent images. Those images depict the natural shape of the zebrafish liver. One can observe a variation in image quality from the different examples. This is caused by strength of the fluorescent marker. The middle column shows the organism-level bright-field images. The zebrafish are partially transparent but retain explicit contours for the shape. The last column visualizes the fusion of the 3D models. For a natural appearance, we map the texture from the zebrafish to the 3D model. One can clearly observe the shape of both the zebrafish and its liver. The visual and spatial discernibility of the models are emphasized from the multi-model fusion. It is interesting that, although the liver is not completely visible in all views (the first view of the first example), our method still recovers a good 3D shape by imposing a threshold to the confidence score to estimate a 3D model allowing a range of errors.

4.4.2 3D measurements for multi-modal 3D reconstruction

From the multi-modal 3D reconstruction, we derive the 3D measurements, i.e. volume and surface area. The volume is obtained by the integration over all the voxels included in the object. A set of surface points is generated from the voxels by the marching cubes algorithm[21], from which a triangulated mesh can be produced. The obtained 3D surface is further refined[22]. Subsequently, the surface area is obtained by the integration of all the facets in the triangulated mesh using Heron's formula[23]. In Table 4.1 we report on the computed 3D measurements of volume and surface area for both the zebrafish and its liver.

In our previous work[12], we have reported accurate 3D measurements for the 3 dpf zebrafish, from which we obtained the volume statistics as 2.53±0.11($\times 10^8$ μm^3) and the surface area as 3.20±0.15($\times 10^6$ μm^2). In this experiment, the statistics of the 3D measurements for the zebrafish are 2.72±0.14($\times 10^8$ μm^3) for the volume and 3.33±0.12($\times 10^6$ μm^2) for the surface area. The phenomenon that the specimens in this experiment are larger compared to our reference set is due to the fact that we did not accurately time the development for this experiment. We also computed the statistics of the 3D measurements for the liver as 9.06±3.33($\times 10^5$ μm^3) for the volume and 5.09±1.10($\times 10^4$ μm^2) for the surface area. The shape variation of the zebrafish liver is large for different individuals, but we can observe that a larger zebrafish tends to have a larger liver[24].

Table 4.1 3D measurements of the 3D reconstructed models for the zebrafish and its liver.

	Volume		**Surface area**	
	Zebrafish ($x10^8$ μm^3)	Liver ($x10^5$ μm^3)	Zebrafish ($x10^6$ μm^2)	Liver ($x10^4$ μm^2)
#1	2.74	7.70	3.33	4.67
#2	2.59	5.38	3.24	3.61
#3	2.50	8.01	3.13	4.91
#4	2.91	9.06	3.44	5.20
#5	2.67	11.60	3.31	6.07
#6	2.80	15.15	3.47	6.89
#7	2.80	6.55	3.41	4.28

We implement our method using Matlab programming on a desktop with an Intel i7 CPU and a 16G RAM. We evaluate the efficiency as runtime for the 3D reconstruction of the zebrafish and its liver separately as 22.0±0.4 (s) and 26.3±1.3 (s). The results of this experiment can be directly used for establishing physiological values of a healthy liver of a 3 dpf zebrafish. This method can be more generically used to assess all observable effects of any compound on the shape and size of an organ.

4.5 Conclusion and future work

In this paper, we have presented a method for multi-model 3D reconstruction and fusion on both organism- and organ-level through light microscopy axial-view imaging. We have implemented the imaging architecture using the VAST BioImager and applied our method to zebrafish larvae. Within the reconstructed 3D models, we observe an overview shape for the object on the organism-level and the detailed structure on the organ-level. The former provides a good shape reference to normalize and evaluate the organ development in phenotypical research. The experimental results show natural visualization of the multi-modal fusion images. Additionally, accurate 3D measurements are obtained, which can be directly used for the evaluation of the biological system with compound screening. This method can be further developed to determine size and shape of other fluorescently labelled organs and objects, like pathogens or tumour cells. In order to further improve this work, a larger sample size of our subjects should be considered to get better statistics for the 3D measurements. High-throughput imaging would be a good approach for this.

4.6 Data availability statement

Animated visualizations of our results can be found at http://bio-imaging.liacs.nl/galleries/VAST-3Dorgan/

4.7 References

1. Van Wijk RC, Krekels EHJ, Hankemeier T, et al. Systems pharmacology of hepatic metabolism in zebrafish larvae. Drug Discov Today Dis Model. 2016;22:27-34.
2. Rennekamp AJ, Peterson RT. 15 years of zebrafish chemical screening. Curr Opin Chem Biol. 2015;24:58-70.
3. Moro E, Vettori A, Porazzi P, et al. Generation and application of signaling pathway reporter lines in zebrafish. Mol Genet Genomics. 2013;288:231-242.
4. McGrath P and Li C. Zebrafish: a predictive model for assessing drug-induced toxicity. Drug Discov. Today. 2008;13:394–401.
5. Hartley R and Zisserman A. Multiple view geometry in computer vision, Cambridge university press, 2003.
6. Yoon K and Kweon IS. Adaptive support-weight approach for correspondence search. IEEE Trans Pattern Anal Mach Intell. 2006;4:650–656.
7. Brown M and Lowe DG. Automatic panoramic image stitching using invariant features. Int J Comput Vis. 2007;74(1):59-73.
8. Laurentini A. The visual hull concept for silhouette based image understanding. IEEE Trans Pattern Anal Mach Intell. 1994;16(2):150-162.
9. Furukawa Y and Ponce J. Carved visual hulls for image-based modeling. Int J Comput Vis. 2009;81(1):,53–67.
10. Cremers D and Kolev K. Multiview stereo and silhouette consistency via convex functionals over convex domains. IEEE Trans Pattern Anal Mach Intell. 2011;33(6):1161–1174.
11. Kolev K, Brox T, and Cremers D. Fast joint estimation of silhouettes and dense 3D geometry from multiple images. IEEE Trans Pattern Anal Mach Intell. 2012;34(3):493–505.
12. Guo Y, Veneman WJ, Spaink HP, et al. Three-dimensional reconstruction and measurements of zebrafish

larvae from high-throughput axial-view in vivo imaging. Biomed Opt Express. 2017;8(5):2611-2634.
13. Pardo-Martin C, Chang T, Koo BK, et al. High-throughput in vivo vertebrate screening. Nat Methods. 2010;7(8):634–636.
14. Pulak R. Tools for automating the imaging of zebrafish larvae. Methods. 2016;96:118-126.
15. Caselles V, Kimmel R, and Sapiro G. Geodesic active contours. Int J Comput Vis. 1997;22(1):61–79.
16. Comaniciu D and Meer P. Mean shift: A robust approach toward feature space analysis. IEEE Trans Pattern Anal Mach Intell. 2002;24(5):603–619.
17. Veneman WJ, Marín-Juez R, De Sonneville J, et al. Establishment and optimization of a high throughput setup to study Staphylococcus epidermidis and Mycobacterium marinum infection as a model for drug discovery. J Vis Exp. 2014;88:e51649.
18. Guo Y, Veneman WJ, Spaink HP, et al. Silhouette-based 3D model for zebrafish high-throughput imaging. IEEE Int Conf Image Process Theory, Tools Appl. 2015; 403–408.
19. Hernandez C, Schmitt F, and Cipolla R. Silhouette coherence for camera calibration under circular motion. IEEE Trans Pattern Anal Mach Intell. 2007;29(2):343–349.
20. Lagarias JC, Reeds JA, Wright ME, et al. Convergence properties of the nelder–mead simplex method in low dimensions. SIAM J Optim. 1998;9(1):112–147.
21. Lorensen WE and Cline HE. Marching cubes: A high resolution 3D surface construction algorithm. ACM Siggraph Comput Graph. 1987;21:163–169.
22. Desbrun M, Meyer M, Schröder P, et al. Implicit fairing of irregular meshes using diffusion and curvature flow. Proc 26th Annu Conf Comput Graph Interact Tech. 1999; 317–324.
23. Cao L and Verbeek FJ. Evaluation of algorithms for point cloud surface reconstruction through the analysis of shape parameters, IS&T/SPIE Electronic Imaging. International Society for Optics and Photonics. 2012; 82900G.
24. Field HA, Ober EA, Roeser T, et al. Formation of the digestive system in zebrafish. I. Liver morphogenesis. Dev Biol. 2003;253:279-290.

Section II. Quantification of internal exposure over time

Chapter 5

Pharmacokinetic modelling of paracetamol uptake and clearance in zebrafish larvae: Expanding the allometric scale in vertebrates with five orders of magnitude

Vasudev Kantae*, Elke H.J. Krekels*, Anita Ordas*, Oskar González, Rob C. van Wijk, Amy C. Harms, Peter I. Racz, Piet H. van der Graaf^, Herman P. Spaink^, Thomas Hankemeier^

Zebrafish 13(6): 504-510 (2016)

* authors contributed equally, ^ authors contributed equally

5.1 Abstract

Zebrafish larvae (*Danio rerio*) are increasingly used to translate findings regarding drug efficacy and safety from *in vitro* based assays to vertebrate species, including humans. However, the limited understanding of drug exposure in this species hampers its implementation in translational research. Using paracetamol as a paradigm compound, we present a novel method to characterize pharmacokinetic processes in zebrafish larvae, by combining sensitive bioanalytical methods and non-linear mixed effects modelling. The developed method allowed quantification of paracetamol and its two major metabolites, paracetamol-sulfate and paracetamol-glucuronide in pooled samples of five lysed zebrafish larvae of 3 days post fertilization. Paracetamol drug uptake was quantified to be 0.289 pmole/min and paracetamol clearance was quantified to be 1.7% of the total value of the larvae. With an average volume determined to be 0.290 µl, this yields an absolute clearance of 2.96 x 10^{-7} L/h, which scales reasonably well with clearance rates in higher vertebrates. The developed methodology will improve the success rate of drug screens in zebrafish larvae and the translation potential of findings, by allowing the establishment of accurate exposure profiles and thereby also the establishment of concentration-effect relationships.

5.2 Introduction

Zebrafish and zebrafish larvae (*Danio rerio*) are increasingly used as a complementary vertebrate model at various stages of drug discovery and development, ranging from disease modelling and target validation, to drug safety, toxicology, and efficacy screenings[1–6]. This is due to 1) their similarity to humans in terms of morphological, molecular, genetic, and pathological features; 2) their small size; 3) their easy and inexpensive maintenance; 4) the availability of a large set of genetic tools; 5) the limited ethical issues involved; and 6) the rapid development of optically transparent larvae, allowing high-throughput imaging-based phenotypic screening.

Although the zebrafish larva is a well-established vertebrate model for toxicity and safety purposes, its utilization has been limited due to the gaps in our understanding of basic pharmacokinetic (PK) processes like absorption, distribution, and clearance, that drive the exposure to drugs and drug metabolites[1,3]. Although, expression patterns of enzymes that drive drug metabolism have been characterized in zebrafish[7–10], to date metabolism and excretion of drug or drug metabolites have never been quantified in zebrafish larvae.

The aim of this study was to develop a new methodology to characterize drug elimination processes in 3-day-old zebrafish larvae, using paracetamol, also known as acetaminophen, as a paradigm compound. A highly sensitive liquid chromatography-mass spectrometry (LC-MS/MS)-based method was developed to accurately measure concentrations of paracetamol and its metabolites in zebrafish larvae. The obtained data were subsequently analysed with non-linear mixed effects modelling techniques.

5.3 Materials and Methods

5.3.1 Study design

To characterize the PK of paracetamol in zebrafish larvae, two experiments were performed. At day 3 post fertilization (dpf), hatched larvae were transferred to 24-well plates, with each well containing five larvae in 2 mL of embryo medium (pH = 7.9) with 1 mM paracetamol. In experiment 1, 150 zebrafish larvae were used to determine the absorption of paracetamol by continuous drug exposure and in experiment 2, 60 zebrafish larvae were used to study the elimination of paracetamol after the larvae were transferred from drug-containing to drug-free medium. All measurements in the experiments were carried out in triplicates, and the measured drug and drug metabolite amounts are expressed per larva, but represent mean values obtained from 5 larvae simultaneously.

Zebrafish larvae were handled in compliance with the local animal welfare regulations and maintained according to standard protocols (zfin.org). Embryos were collected from family crosses of AB/TL wild-type strain and grown at 28°C in embryo medium (60 µg/mL Instant Ocean sea salts; Sera Marin) in the dark.

5.3.2 Experiment 1

Zebrafish larvae were exposed to the drug-containing medium for 10, 20, 30, 40, 50, 60, 80, 100, 120, or 180 min. At the time of the measurement three replicates of five larvae were collected, and washed twice with 80/20 (v/v) water/methanol solution, after which excessive medium was removed. The samples were subsequently prepared for analysis as described below. Additionally, samples from the incubation medium were collected to study the excreted amounts of the metabolites. Larvae in control groups were exposed to the drug solution for a few seconds and to determine drug adherence to the skin[11].

5.3.3 Experiment 2

Larvae were exposed to the drug-containing medium for 1 h, washed with fresh medium to remove the residual drug solution, and then transferred to a drug-free medium. After 0, 1, 2 and 3 h of incubation, three replicates of five larvae were collected and washed twice in 80/20 (v/v) water/methanol solution after which excessive medium was removed and the samples were subsequently prepared for analysis as described below. Samples from the incubation medium were also collected at each time point.

This experiment was repeated a second time with three washing steps before transferal to drug-free medium, as the first time unchanged drug and metabolites appeared to have been transferred to the fresh medium. The second time, the duration of this experiment was also extended with sample collection up to 4 h after transfer to the drug-free medium. Data on paracetamol, paracetamol-sulfate, and paracetamol-glucuronide concentrations in the incubation medium from the first time the experiment was performed were excluded from the analysis as contamination was suspected.

5.3.4 Sample preparation

The five zebrafish larvae of 3 dpf from a single well were added to 100 µL lysis buffer containing 90/10 (v/v) methanol/water solution with 45 ng/mL paracetamol-D4 internal standard (Sigma-Aldrich Chemie B.V., Zwijndrecht, Netherlands). Lysis was performed by snap-freezing each sample in liquid nitrogen followed by 2-3 min sonication. This procedure was repeated until all larvae were lysed and the sample was homogenous. The lysed samples were centrifuged for 10 min at 16,000 g at 4°C. 90 µL of supernatant was collected in a microcentrifuge tube, after which 72 µL water was added, yielding a sample of 50/50 methanol/water solution which was injected to the LC-MS/MS system directly. The medium samples (2 mL) from each well were collected in new eppendorf tubes and concentrated by speedvac. After reconstitution in 150 µL of 50/50 methanol/water solution, samples were injected to the LC-MS/MS system directly.

5.3.5 Calibration curve

Paracetamol, paracetamol-sulfate, and paracetamol-glucuronide were purchased from Sigma-Aldrich. Individual stock solutions at 1 mg/mL were prepared using methanol. Standard working solutions of 1,000 ng/mL were prepared for these three compounds as well as for the paracetamol-D4 internal standard. On the day of analysis, the standard working solutions were further diluted to five additional calibration points and mixed with the internal standard solution to final concentrations of 9, 18, 45, 90, 180, and 270 ng/mL for paracetamol and its metabolites and 45 ng/mL for the internal standard. All calibration points were prepared in a composition similar to the lysis buffer (90/10 methanol/water). For constructing a matrix-matched calibration curve, 100 µL of each calibration point was spiked into a sample of five zebrafish larvae of 3 dpf and followed similar extraction procedure as described for the sample preparation above.

5.3.6 Quantification of paracetamol and metabolites

Analyses were performed on an ultra performance liquid chromatography (UPLC) system (Acquity, Waters, Milford, MA, USA) coupled to a quadrupole-time of flight (QTOF) mass spectrometer (MS) (Synapt G2S, Waters, Wilmslow, UK) with an electrospray ionization (ESI) source. Positive ionization mode was used for the analysis of paracetamol and negative mode for the analysis of the paracetamol-sulfate and paracetamol-glucuronide metabolites.

Chromatography was performed at 40°C on a Waters Acquity UPLC HSS T3 column (1.8 µm, 2.1 x 50 mm) using as aqueous mobile phase a 0.01% formic acid solution (A) and acetonitrile (B) as organic modifier at a flow rate of 0.4 mL/min. The run time was 5 min, with the gradient at 100% A for the first 0.3 min, then B was linearly increased to 100% for the next 3 min and held for 0.5 min and finally the system was equilibrated to the initial conditions for 1.2 min. Injection volume was 5 µL and autosampler temperature was set to 10°C.

The MS method operated in both positive and negative polarities with separate injections in each polarity includes a MS scan function with a scan time of 0.2 s operated at a trap cell collision energy of 4 eV and a transfer cell collision energy of 2 eV. ESI voltage was set at 0.9 kV both for positive and negative modes. Cone voltage was set at 30 V and source offset at 80 V. The source temperature was set at 150°C with desolvation temperature at 500°C. Nitrogen was used for the cone, desolvation and nebulizer gases with settings of 50 L/h, 1,000 L/h and 6 bar, respectively. Data was collected in continuum mode with a scan range of 50-850 m/z using the QTOF detector in high-resolution mode (~20,000 full width at half maximum). About 0.1 mg/L Leucine enkephalin solution (acetonitrile/water 50/50 with 0.1% v/v formic acid) infused at a constant flow of 10 µL/min was used as the lock mass, a single point scan was collected every 10 s and averaged over three scans to perform mass correction (556.2771 m/z). The instrument was calibrated for both positive and negative polarities before analysis using sodium formate.

Masslynx 4.1 SCN916 (Waters) was used to acquire all the data and Targetlynx application to perform the quantitative analysis. The quantification of paracetamol and its metabolites was achieved by correcting the peak area response of paracetamol and its metabolites by the peak area response of the internal standard. The quantified values are expressed in terms of amount/larva. The developed method was sensitive with limits of quantification as low as 0.02 pmole/larva for paracetamol, 0.008 pmole/larva for paracetamol-sulfate, and 0.05 pmole/larva for paracetamol-glucuronide.

5.3.7 Non-linear mixed effects modelling

The non-linear mixed effects modelling of paracetamol was performed using NONMEM 7.3 software (ICON Development Solutions, Ellicott City, MD, USA)[12], facilitated with Pirana[13] and PsN[14,15]. The First Order Conditional Estimation method was used in NONMEM. R 3.0.0 was used for graphical analysis and model diagnostics.

In a pooled analysis of the paracetamol concentrations in the larvae, a zero order absorption rate was estimated to quantify the uptake of paracetamol from the incubation medium. A first order clearance rate was estimated to quantify the elimination of paracetamol from the larvae. Both one- and two-compartment models were tested to describe the distribution of paracetamol within the larvae. For both distribution models, the total distribution volume was fixed to 1, which meant for the two-compartment model that both compartments were expressed as fraction of the total volume of one larva. To quantify the residual variability an additive and a proportional error were tested, and a combination of both. Due to the destructive nature of the measurements, inter-individual variability in the PK processes could not be quantified.

The likelihood ratio test, based on the objective function value (OFV) in NONMEM was used for model selection. Assuming a χ^2-distribution, a decrease in OFV of more than 3.84 points, corresponding to a

significance level of $p < 0.05$ with one degree of freedom, was considered to be statistically significant. Precision of parameter estimates was evaluated based on standard errors obtained from the NONMEM output tables. Furthermore the model fit was assessed by visual inspection of goodness-of-fit plots, these included plots of predicted versus observed paracetamol amounts in the zebrafish larvae, and of conditional weighted residuals[16] versus time after start of the experiment and conditional weighted residuals versus predicted paracetamol amounts.

5.3.8 Volume of zebrafish larvae

To enable the expression of paracetamol clearance in zebrafish larvae in absolute rather than relative terms, the average volume of the larvae was determined. For this, samples of 10, 20, 30, 40, 50, 100 larvae at 3 dpf were placed onto parafilm M(R) (Bemis, Oshkosh, Wisconsin, USA) with a transfer pipette after which the excessive water was removed with variable volume pipettes and filter paper. Subsequently the weight of each sample was measured with a Mettler AE240 analytical balance. The average wet weight of the zebrafish larvae was determined using linear regression. To derive the average volume of the larvae, their density was assumed to be equal to the density of water at 25°C (0.997 g/mL).

5.3.9 Comparing paracetamol clearance in vertebrate species

A search was performed in PUBMED using 'paracetamol' OR 'acetaminophen' AND 'clearance'. Total paracetamol clearance (CL) values reported over the past 10 years in various vertebrate species were collected together with mean bodyweights (BW) of the individuals included in a study. When detailed information on BW was not provided, average BW values from the species were obtained from literature. Data from disease models, combined drug formulation, or obese individuals were excluded. Distinctions were made between data collected in mature or immature individuals of a species.

All obtained clearance values were plotted versus bodyweight on a double log scale. A linear model was fitted through the logarithm of the CL versus the logarithm of the BW in R (version 3.3.1) to obtain the parameters in the allometric equation below that describes the relationship between BW and paracetamol CL (Equation 1).

$$\mathrm{CL} = \mathrm{a} \cdot \mathrm{BW}^{\mathrm{exp}} \tag{1}$$

The fit was based only on CL from the higher vertebrates, excluding the zebrafish larvae.

5.4 Results

5.4.1 Quantification of paracetamol and metabolites

Figure 5.1 A shows the time-course of the amount of paracetamol and its two major metabolites in the zebrafish larvae at 3 dpf, obtained after continuous exposure for various durations in medium with 1 mM paracetamol. The amount of paracetamol in the zebrafish larvae reached a plateau within 2 h, indicating that after 2 h the amount of paracetamol taken up by the larvae and the amounts metabolized and excreted by the larvae are in equilibrium. Paracetamol-sulfate and paracetamol-glucuronide amounts in zebrafish larvae could be detected after 10 and 30 min, respectively. These metabolites reached equilibrium between formation and excretion within 2 h as well.

Figure 5.1 B describes amounts of paracetamol and its major metabolites in the zebrafish larvae at 3 dpf following transfer to drug-free medium after 1 h incubation in drug-containing medium. After transfer to drug-free medium, paracetamol amounts in the zebrafish larvae decreased over time. The amounts of the paracetamol metabolites in the larvae increased initially, indicating that per time unit larger amounts are formed than excreted. After 2 h in drug-free medium the elimination of the metabolites started to exceed the formation, resulting in peak amounts followed by a decline.

In both experiments, the amount of excreted paracetamol-glucuronide in the incubation medium was

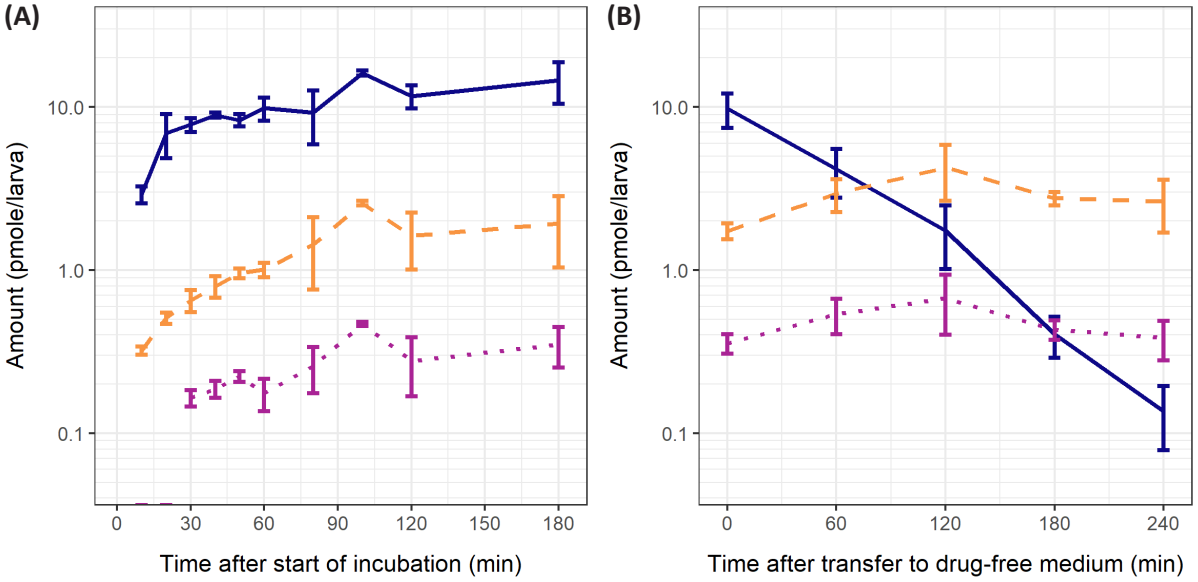

Figure 5.1 Time course of amounts of paracetamol and its major metabolites in zebrafish larvae. Depicted are mean values ±1 standard deviation of paracetamol (blue, solid line), paracetamol-sulfate (orange, dashed line), and paracetamol-glucuronide (magenta, dotted line) amounts, after (A) continuous incubation in medium with 1 mM paracetamol (experiment 1), and (B) 1 h incubation in medium with 1 mM paracetamol and subsequent transfer to drug-free medium (experiment 2).

below the lower limit of quantification (0.5 pmole excreted per larva) throughout the experiment. In the first experiment, excreted sulfate metabolite was detected after 3 h of continuous exposure, but the level remained close to the limit of quantification (0.4 pmole excreted per larva). For the second experiment, excreted amounts of the sulfate metabolite that were close to the limit of quantification were detected in the medium 3 h after the larvae were transferred from the drug-containing medium, to the drug-free medium. The excreted amounts are relatively low compared to the total amount of paracetamol and metabolites measured in the larvae, from which it can be concluded that a significant portion of the elimination of paracetamol is covered by measuring the sulfate and glucuronide metabolite in the larvae. Moreover, control experiments confirmed that paracetamol does not adhere to the skin of the zebrafish larvae, ratifying that paracetamol amounts quantified in the zebrafish larvae samples at 3 dpf indeed represent drug amounts taken up by the larvae.

5.4.2 Non-linear mixed effects model

The time-course of paracetamol amounts in zebrafish larvae at 3 dpf was best described by a standard one-compartment distribution model, with zero order absorption, and linear first order elimination. It was found that the zebrafish larvae in a medium with a 1 mM paracetamol concentration take up 0.289 pmole paracetamol per minute. Every minute, the amount of paracetamol in 1.70% of the volume of the zebrafish larvae was cleared; this includes both metabolism and excretion of the unchanged drug. The obtained parameter values including the relative standard error of these estimates are provided in Table 5.1.

Table 5.1 Pharmacokinetic model parameter estimates including their relative standard errors (RSE) obtained with the non-linear mixed effects pharmacokinetic model.

Parameter	Unit	Parameter value	RSE (%)
Absorption rate constant (ka)	pmole/min	0.289	5.0
Distribution volume (V)	larva	1 FIX	-
Clearance (CL)	proportion of larva volume/min	0.017	5.0
Residual error (variance)		9.73	19

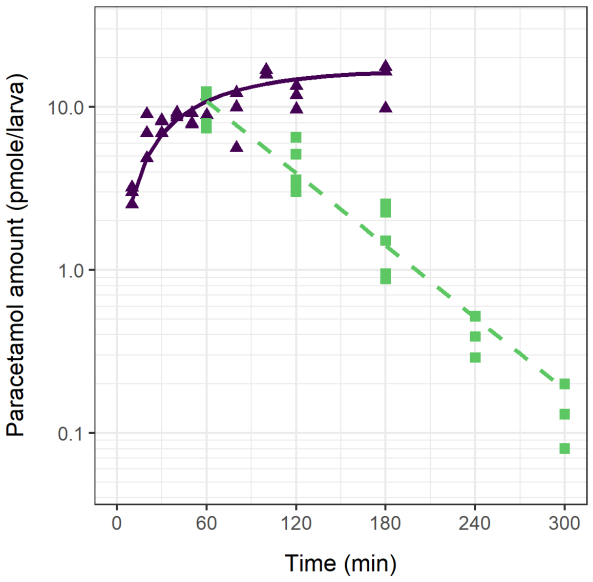

Figure 5.2 Observed and model predicted paracetamol amounts in zebrafish larvae. Observed (symbols) and model predicted (lines) paracetamol amounts in zebrafish larvae over time after continuous incubation in medium with 1 mM paracetamol (experiment 1, purple solid line and triangles) and after 1 h incubation in medium with 1 mM paracetamol and subsequent transfer to drug-free medium (experiment 2, green dashed line and squares).

The relative standard errors in the obtained model parameter estimates were below 20%, indicating good precision of the parameter estimates. Figure 5.2 shows how paracetamol amounts change over time in experiments 1 and 2 according to the obtained non-linear mixed effects PK model, and the amounts that were observed during the experiments. Goodness-of-fit plots are provided in the Supplementary Figure S5.1.

5.4.3 Paracetamol clearance in zebrafish larvae

The average wet weight of the zebrafish larvae at 3 dpf was found to be 0.291 mg, and from this an average volume of 0.290 µL was derived. This yields absolute paracetamol clearance in zebrafish larvae at 3 dpf of 2.96 x 10^{-7} L/h.

5.4.4 Comparing paracetamol clearance in vertebrate species

Paracetamol clearance values reported over the past 10 year in vertebrate species, including humans of different ages, were obtained from literature. Supplementary Table S5.1, provides an overview of the obtained values. Figure 5.3 shows a plot of these clearance versus the bodyweight of each species.

The allometric equation that was fit to the data of mature individuals of the different species had an estimated exponent of 0.781 (R^2=0.902). The obtained relationship is depicted in Figure 5.3 as well, including 95% confidence and prediction intervals and shows an overprediction of the paracetamol clearance of the zebrafish larvae of 3 dpf. Interestingly, however, this relationship also overpredicts the reported paracetamol clearances in human newborns and children. When including both the mature and the immature individuals of all species except the zebrafish larvae, the exponent was estimated to be 0.838 (R^2=0.835). Supplementary Figure S5.2 depicts this relationship and shows that the clearance value for paracetamol in zebrafish larvae obtained in this study does fall within the 95% confidence and prediction interval of this fit.

5.5 Discussion

Analytical methods that can accurately measure concentrations of paracetamol and its metabolites in low volumes are a prerequisite for characterizing the PK of this drug in zebrafish larvae. We have developed an analytical method based on UPLC followed by mass spectrometric detection to separate and reliably quantify paracetamol and its major metabolite concentrations in samples of lysed zebrafish larvae at 3 dpf. The data obtained with this technique enabled the quantification of PK processes in this species with a non-linear mixed effects modelling approach, proving for the first time the feasibility of studies on drug PK and metabolism in zebrafish larvae.

Quantification of PK processes in zebrafish larvae will be invaluable for drug screening procedures in drug discovery and early drug development. This is because it has been recognized in higher species and humans that drug concentrations rather than drug doses, are driving drug effects, but screening studies in zebrafish larvae generally ignore drug PK, or if these aspects are considered, drug concentrations are measured at a single time point, ignoring the full time course of drug and/or metabolite exposure[3,17].

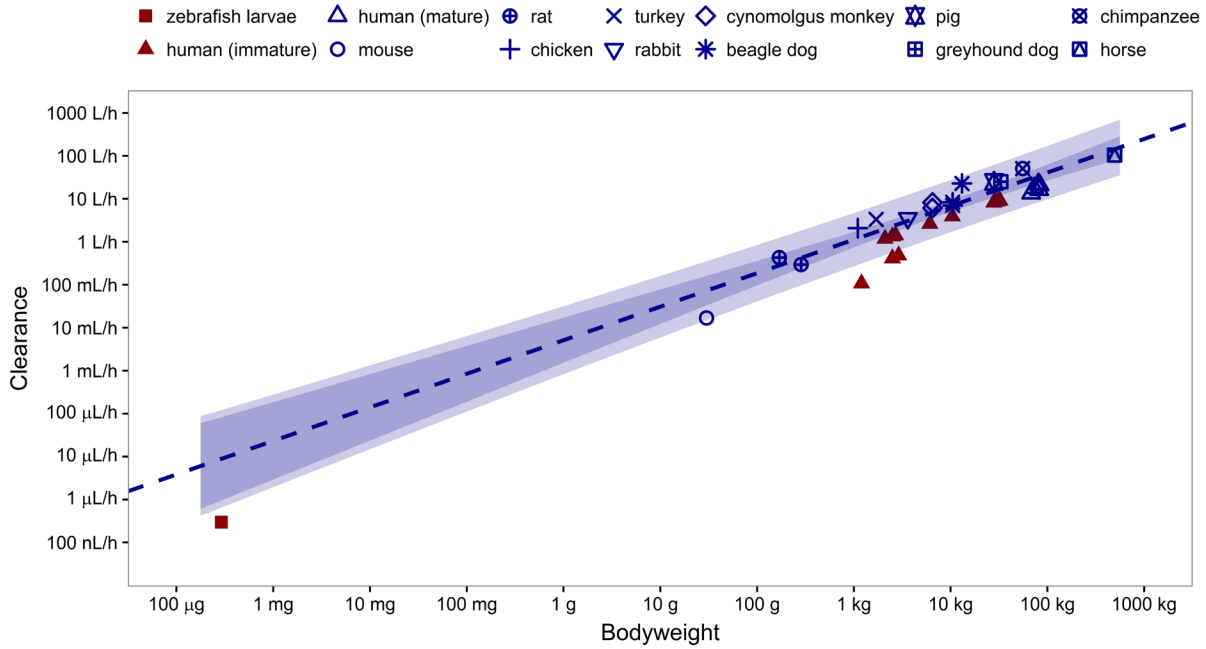

Figure 5.3 Paracetamol clearance across vertebrate species. Reported paracetamol clearances (symbols) and estimated allometric relationship (dashed line) between paracetamol clearance and bodyweight for mature individuals of various vertebrate species, including its 95% confidence (darker shaded) and prediction (lighter shaded) interval. Data from mature individuals of species are depicted in blue, from immature including the zebrafish larvae in red.

Combining information on full PK profiles with information on drug effects, is absolutely essential for the establishment of concentration-effect relationships, which are needed in translational pharmacology to scale drug effects between (vertebrate) species. Given that 70% of human genes have at least one obvious zebrafish orthologue[18] the potential for a strong resemblance between humans and zebrafish larvae regarding disease manifestation and drug response is high. The zebrafish larvae has for instance already been proven useful in studying drug effects in diseases like tuberculosis[17] and cancer[2].

In addition to improving the translation potential of drug effects from zebrafish larvae to higher vertebrate species, it was investigated to what extent PK studies in zebrafish larvae could serve as a convenient translational platform for studies on drug metabolism as well. The comparison of our findings on paracetamol clearance in zebrafish larvae at 3 dpf and reported clearance values in higher vertebrates in Figure 5.3, shows that the clearance of paracetamol in the zebrafish larvae is lower than can be expected based on clearance values obtained in mature individuals of higher vertebrates, but that this value correlates well to values obtained in higher vertebrates when also values of immature individual are considered.

Zebrafish expresses phase II metabolizing genes similar to mammalian uridine glucuronosyltransferases (UGTs) and sulfotransferases (SULTs) isoforms throughout early development[19–21]. Previous studies using different probes in zebrafish larvae, also suggest quantitative similarities in metabolite formation between zebrafish larvae and humans[22–24]. Our quantitative results on the metabolism of paracetamol in zebrafish larvae at 3 dpf do, however, not closely resemble observed metabolic profiles in adult humans. As the graphs in Figure 5.1 show, paracetamol-sulfate concentrations are about five to six times higher than the concentrations of the glucuronide metabolite, which is contrary to findings in humans, in which the glucuronide is the predominantly formed metabolite for paracetamol. This could possibly be attributed to the immaturity of the enzymes in zebrafish larvae at 3 dpf. In human newborns, glucuronidation capacity is, for instance, known to be limited, resulting in an increased relative contribution of sulfation in the metabolism of paracetamol, causing the sulfate metabolite to be formed 3.5 to 8 times more than the glucuronide metabolites in this immature human population[25–27]. Our experiments in the zebrafish larvae of 3 dpf were also performed before maturity in this species is reached. Although the dissimilarities

in metabolic profiles between human adults and zebrafish larvae do not limit the applicability of our developed methodology in characterizing drug PK and determining accurate drug exposure in these larvae, it would be of interest to investigate if older larvae resemble metabolic profiles of human adults more closely. This is part of future investigations, as well as investigations on the clearance rates of other compounds in the zebrafish larvae.

In conclusion, we have successfully developed a feasible methodology for PK studies in zebrafish larvae at 3 dpf. The quantification of PK processes in these larvae by using a combination of ultra-sensitive LC-MS/MS-based analytical methods and non-linear mixed effects modelling, will allow the extraction of more information from experiments in zebrafish larvae during drug discovery and early drug development, which may yield advantages regarding the inter-species translation potential of findings on drug effects in these experiments.

5.6 Acknowledgements

This study was financially supported by the VIRGO consortium, which is funded by the Netherlands Genomics Initiative and by the Dutch Government (FES0908).

5.7 References

1. Fleming A, Alderton WK. Zebrafish in pharmaceutical industry research: Finding the best fit. Drug Discov Today Dis Model. 2013;10(1):e43-e50.
2. Zon LI, Peterson RT. In vivo drug discovery in the zebrafish. Nat Rev Drug Discov. 2005;4(1):35-44.
3. Diekmann H, Hill A. ADMETox in zebrafish. Drug Discov Today Dis Model. 2013;10(1):e31-e35.
4. Barros TP, Alderton WK, Reynolds HM, et al. Zebrafish: An emerging technology for in vivo pharmacological assessment to identify potential safety liabilities in early drug discovery. Br J Pharmacol. 2008;154(7):1400-1413.
5. Lieschke GJ, Currie PD. Animal models of human disease: Zebrafish swim into view. Nat Rev Genet. 2007;8(5):353-367.
6. MacRae CA, Peterson RT. Zebrafish as tools for drug discovery. Nat Rev Drug Discov. 2015;14(10):721-731.
7. Vliegenthart ADB, Tucker CS, Pozo J Del, et al. Zebrafish as model organisms for studying drug-induced liver injury. Br J Clin Pharmacol. 2014;78(6):1217-1227.
8. Goldstone J V, McArthur AG, Kubota A, et al. Identification and developmental expression of the full complement of cytochrome P450 genes in zebrafish. BMC Genomics. 2010;11(1):643.
9. Alderton W, Berghmans S, Butler P, et al. Accumulation and metabolism of drugs and CYP probe substrates in zebrafish larvae. Xenobiotica. 2010;40(8):547-557.
10. Santoro MM. Zebrafish as a model to explore cell metabolism. Trends Endocrinol Metab. 2014;25(10):546-554.
11. Raterink RJ, Van der Kloet FM, Li J, et al. Rapid metabolic screening of early zebrafish embryogenesis based on direct infusion-nanoESI-FTMS. Metabolomics. 2013;9(4):864-873.
12. Beal SL, Sheiner LB BAJ. NONMEM users guide (1989–2006). (Beal S, Sheiner L BA, ed.). Ellicott City, MD: ICON Development Solutions,
13. Keizer R, Van Benten M, Beijnen J, et al. Pirana and PCluster: A modeling environment and cluster infrastructure for NONMEM. Comput Methods Programs Biomed. 2011;101(1):72-79.
14. Lindbom L, Pihlgren P, Jonsson E. PsNtoolkit — a collection of computer intensive statistical methods for non-linear mixed effect modeling using NONMEM. Comput Methods Programs Biomed. 2005;79(3):241-257.
15. Keizer RJ, Karlsson MO, Hooker a. Modeling and simulation workbench for NONMEM: Tutorial on pirana, psn, and xpose. CPT Pharmacometrics Syst Pharmacol. 2013;2(e50).
16. Hooker AC, Staatz CE, Karlsson MO. Conditional weighted residuals (CWRES): A model diagnostic for

the FOCE method. Pharm Res. 2007;24(12):2187-2197.
17. Ordas A, Raterink R-J, Cunningham F, et al. Testing tuberculosis drug efficacy in a zebrafish high-throughput translational medicine screen. Antimicrob Agents Chemother. 2015;59(2):753-762.
18. Howe K, Clark MD, Torroja CF, et al. The zebrafish reference genome sequence and its relationship to the human genome. Nature. 2013;496:498-503.
19. Huang H, Wu Q. Cloning and comparative analyses of the zebrafish UGT repertoire reveal its evolutionary diversity. PLoS One. 2010;5(2):e9144.
20. Yasuda S, Burgess M, Yasuda T, et al. A novel hydroxysteroid-sulfating cytosolic sulfotransferase, SULT3 ST3, from zebrafish: Identification, characterization, and ontogenic study. Drug Metab Lett. 2009;3(4):217-227.
21. Liu T-A, Bhuiyan S, Liu M-Y, et al. Zebrafish as a model for the study of the phase II cytosolic sulfotransferases. Curr Drug Metab. 2010;11(6):538-546.
22. Hu G, Siu SO, Li S, et al. Metabolism of calycosin, an isoflavone from Astragali Radix, in zebrafish larvae. Xenobiotica. 2012;42(3):294-303.
23. Li ZH, Alex D, Siu SO, et al. Combined in vivo imaging and omics approaches reveal metabolism of icaritin and its glycosides in zebrafish larvae. Mol Biosyst. 2011;7(7):2128-2138.
24. Chng HT, Ho HK, Yap CW, et al. An investigation of the bioactivation potential and metabolism profile of zebrafish versus human. J Biomol Screen. 2012;17(7):974-986.
25. Van Lingen RA, Deinum JT, Quak JME, et al. Pharmacokinetics and metabolism of rectally administered paracetamol in preterm neonates. Arch Dis Child Fetal Neonatal Ed. 1999;80(1):F59-F63.
26. Allegaert K, De Hoon J, Verbesselt R, et al. Intra- and interindividual variability of glucuronidation of paracetamol during repeated administration of propacetamol in neonates. Acta Paediatr. 2005;94(9):1273-1279.
27. Krekels EHJ, Van Ham S, Allegaert K, et al. Developmental changes rather than repeated administration drive paracetamol glucuronidation in neonates and infants. Eur J Clin Pharmacol. 2015;71:1075-1082.

5.8 Supplementary material

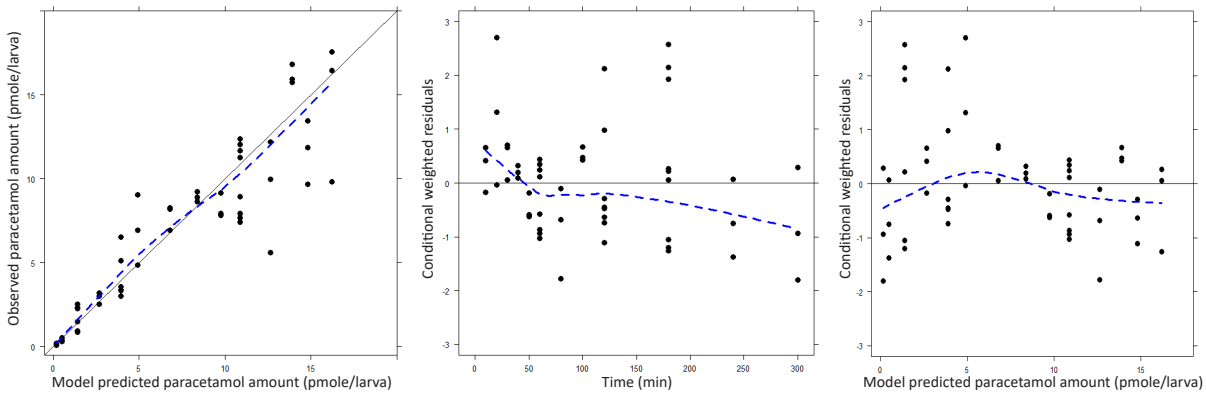

Supplementary Figure S5.1 Basic goodness-of-fit plots with loess curves. Blue dotted lines for the non-linear mixed effects pharmacokinetic model of paracetamol in zebrafish larvae, including observed versus predicted paracetamol amounts (left), conditional weighted residuals versus time (middle), and conditional weighted residuals versus predicted concentration (right).

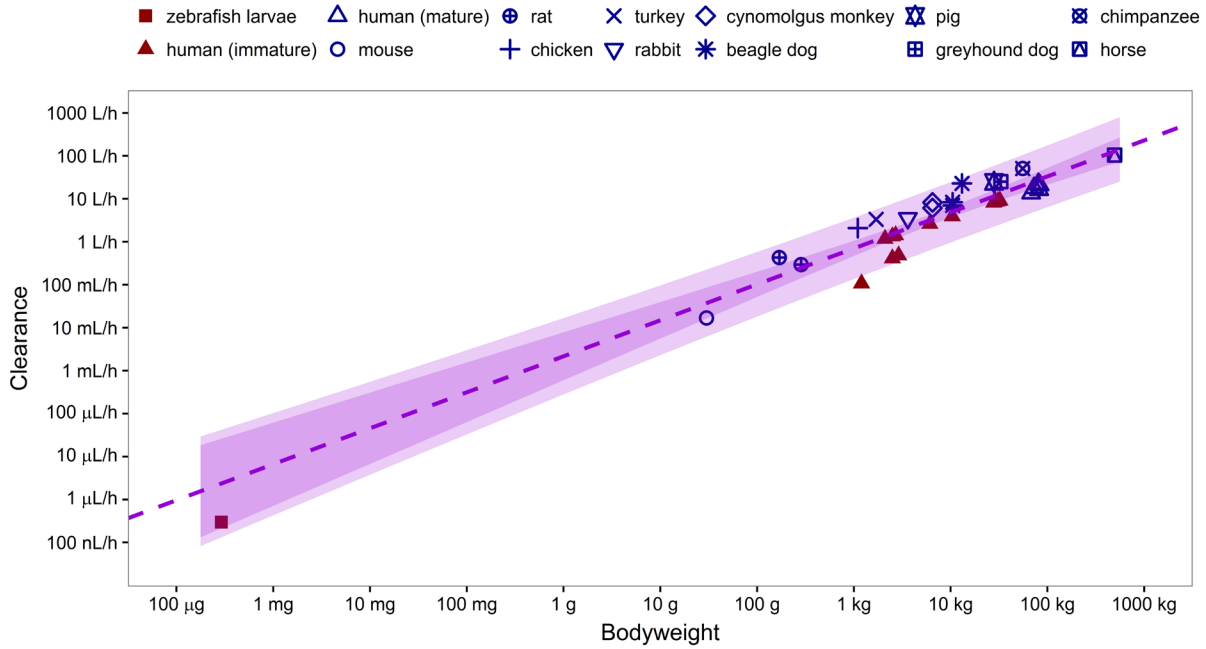

Supplementary Figure S5.2 Paracetamol clearance across mature and immature vertebrate species. Reported paracetamol clearances (symbols) and estimated allometric relationship (dashed line) between paracetamol clearance and bodyweight for both mature and immature individuals of various vertebrate species, including its 95% confidence (darker shaded) and prediction (lighter shaded) interval. Data from mature individuals of species are depicted in blue, from immature including the zebrafish larvae in red.

Supplementary Table S5.1 Overview of paracetamol clearance (CL) values reported over the past 10 years in various higher vertebrates.

Species	Weight (kg)	Reported CL (unit)	CL (L/h)	Reference
Mouse	0.030	0.28 (mL/min)	0.0168	[1,2]
Rat	0.17	2.53 (L/h/kg)	0.430	[2,3]
Rat	0.285	1.03 (L/h/kg)	0.294	[4]
Chicken	1.1	1.89 (L/h/kg)	2.08	[5]
Turkey	1.7	1.95 (L/h/kg)	3.32	[5]
Rabbit	3.61	3.52 (L/h)	3.52	[6]
Cynomolgus monkey	6.5	21.1 (mL/min/kg)	8.23	[7,8]
Cynomolgus monkey	6.5	15.7 (mL/min/kg)	6.12	[7,8]
Beagle dog	13.1	1.74 (L/h/kg)	22.8	[5]
Beagle dog	10.5	13.2 (mL/min/kg)	8.32	[7]
Beagle dog	10.5	11.1 (mL/min/kg)	6.99	[7]
Pig	28.1	0.88 (L/h/kg)	24.7	[5]
Greyhound dog	33	12.7 (mL/min/kg)	25.0	[9]
Greyhound dog	34	17.7 (mL/min/kg)	36.1	[10]
Chimpanzee	55.6	0.91 (L/h/kg)	50.6	[11]
Human (newborn)	1.2	0.0894 (L/h/kg)	0.107	[12]
Human (newborn)	2.1	16.3 (L/h/70 $kg^{0.75}$)	1.17	[13]
Human (newborn)	2.3	0.348 (L/h)	0.348	[14]
Human (newborn)	2.5	5.0 (L/h/70 $kg^{0.75}$)	0.411	[15]
Human (newborn)	2.5	16.3 (L/h/70 $kg^{0.75}$)	1.34	[13]
Human (newborn)	2.7	16.3 (L/h/70 $kg^{0.75}$)	1.42	[13]
Human (newborn)	2.9	5.24 (L/h/70 $kg^{0.75}$)	0.481	[16]
Human (child)	6.1	16.3 (L/h/70 $kg^{0.75}$)	2.61	[13]
Human (child)	10.4	16.3 (L/h/70 $kg^{0.75}$)	3.90	[13]
Human (child)	27.9	16.3 (L/h/70 $kg^{0.75}$)	8.18	[13]
Human (child)	29.3	16.5 (L/h/70 $kg^{0.75}$)	8.59	[17]
Human (child)	30.9	16.3 (L/h/70 $kg^{0.75}$)	8.83	[13]
Human (child)	32.3	16.3 (L/h/70 $kg^{0.75}$)	9.13	[13]
Human (adult)	68	3.3 (mL/min/kg)	13.5	[18]
Human (adult)	73	17.4 (L/h/70 $kg^{0.75}$)	18.0	[19]
Human (adult)	81	4.6 (mL/min/kg)	22.4	[18]
Human (adult)	83	4.2 (mL/min/kg)	20.9	[18]
Human (adult)	83	3.3 (mL/min/kg)	16.2	[18]
Horse	495	0.21 (L/h/kg)	104	[5]

5.9 Supplementary references

1. Saini SPS, Zhang B, Niu Y, et al. Activation of liver X receptor increases acetaminophen clearance and prevents its toxicity in mice. Hepatology. 2011;54:2208-2217
2. Van Zutphen LFM, Baumans VBA. Handboek proefdierkunde, 2nd ed. Elsevier Gezondheidszorg, Maarssen, 2001.
3. Yamasaki I, Uotsu N, Yamaguchi K, et al. Effects of kale ingestion on pharmacokinetics of acetaminophen in rats. Biomed Res. 2011;32(6):357-362.

4. Lee S, An J, Lee H, et al. Evaluation of pharmacokinetic differences of acetaminophen in pseudo germ-free rats. Biopharm Drug Dispos. 2012;33:292-303.
5. Neirinckx E, Vervaet C, Boever S De, et al. Species comparison of oral bioavailability, first-pass metabolism and pharmacokinetics of acetaminophen. Res Vet Sci. 2010;89(1):113-119.
6. Bienert A, Kamiñska A, Olszewski J, et al. Pharmacokinetics and ocular disposition of paracetamol and paracetamol glucuronide in rabbits with diabetes mellitus induced by alloxan. Pharmacol Reports. 2012;64:421-427.
7. Koyanagi T, Yamaura Y, Yano K, et al. Age-related pharmacokinetic changes of acetaminophen, antipyrine, diazepam, diphenhydramine, and ofloxacin in male cynomolgus monkeys and beagle dogs. Xenobiotica. 2014;44(10):893-901.
8. Cawton Lang K. Primate factsheets: Long-tailed macaque (Macaca fascicularis) taxonomy, morphology, & ecology, 2006.
9. KuKanich B. Pharmacokinetics of acetaminophen, codeine, and the codeine metabolites morphine and codeine-6-glucuronide in healthy Greyhound dogs. J Vet Pharmacol Ther. 2010;33(1):15-21.
10. KuKanich B. Pharmacokinetics and pharmacodynamics of oral acetaminophen in combination with codeine in healthy Greyhound dogs. J Vet Pharmacol Ther. 2016;39:514-217.
11. Wong H, Grace JE, Wright MR, et al. Glucuronidation in the chimpanzee (Pan troglodytes): Studies with acetaminophen, oestradiol and morphine. Xenobiotica. 2006;36(12):1178-1190.
12. Van Ganzewinkel C, Derijks L, Anand KJS, et al. Multiple intravenous doses of paracetamol result in a predictable pharmacokinetic profile in very preterm infants. Acta Paediatr Int J Paediatr. 2014;103(6):612-617.
13. Anderson BJ, Pons G, Autret-Leca E, et al. Pediatric intravenous paracetamol (propacetamol) pharmacokinetics: A population analysis. Pediatr Anesth. 2005;15:282-292.
14. Cook SF, Roberts JK, Samiee-Zafarghandy S, et al. Population pharmacokinetics of intravenous paracetamol (acetaminophen) in preterm and term neonates: Model development and external evaluation. Clin Pharmacokinet. 2016;55(1):107-119.
15. Allegaert K, Palmer GM, Anderson BJ. The pharmacokinetics of intravenous paracetamol in neonates : size matters most. 2011:575-580.
16. Palmer GM, Atkins M, Anderson BJ, et al. I.V. acetaminophen pharmacokinetics in neonates after multiple doses. Br J Anaesth. 2008;101(4):523-530.
17. Mohammed BS, Engelhardt T, Cameron GA, et al. Population pharmacokinetics of single-dose intravenous paracetamol in children. 2012;108(March):823-829.
18. Liukas A, Kuusniemi K, Aantaa R, et al. Pharmacokinetics of intravenous paracetamol in elderly patients. Clin Pharmacokinet. 2011;50(2):121-129.
19. Allegaert K, Olkkola KT, Owens KH, et al. Covariates of intravenous paracetamol pharmacokinetics in adults. BMC Anesthisiology. 2014;14(77).

Chapter 6

Impact of post-hatching maturation on the pharmacokinetics of paracetamol in zebrafish larvae

Rob C. van Wijk, Elke H.J. Krekels, Vasudev Kantae, Amy C. Harms, Thomas Hankemeier, Piet H. van der Graaf, Herman P. Spaink

Scientific Reports 9: 2149 (2019)

6.1 Abstract

Zebrafish larvae are increasingly used in pharmacological and toxicological studies, but it is often overlooked that internal exposure to exogenous compounds, rather than the incubation medium concentration, is driving observed effects. Moreover, as the zebrafish larva is a developing organism, continuous physiological changes impact pharmacokinetic or toxicokinetic processes like the absorption and elimination of exogenous compounds, influencing the interpretation of observations and conclusions drawn from experiments at different larval ages. Here, using paracetamol as paradigm compound, mathematical modelling is used to quantify absorption and elimination rates from internal exposure over time profiles after waterborne treatment, as well as changes in these parameters in post-hatching larvae of 3, 4, and 5 days post fertilization (dpf). An increase of 106% in absorption rate was observed between 3 and 4 dpf, but no further increase at 5 dpf, and an increase of 17.5% in elimination rate for each dpf. Paracetamol clearance, determined from elimination rate constants and reported total larval volumes of 253, 263, and 300 nL at 3, 4, and 5 dpf respectively, correlates best with higher vertebrates at 5 dpf. This suggests that when studying direct effects of exogenous compounds, experiments with zebrafish larvae are best performed at 5 dpf.

6.2 Introduction

The zebrafish (*Danio rerio*), especially the zebrafish larva, is increasingly used in drug discovery and early drug development, and toxicological screens[1,2]. It is a data and resource efficient vertebrate model organism[3], that shows 70% genetic homology with humans[4]. Its many advantages include high fecundity and small larval size which is ideal for high-throughput experiments[5]. Additionally, transparency in early life stages enables optical imaging to study *in vivo* effects of exogenous compounds observable by brightfield or fluorescence microscopy. Moreover, it is ethically preferable to perform *in vivo* experiments in the lowest vertebrate, like for example the zebrafish. Additionally, no ethical approval is necessary for studies on larvae before they start independent feeding[6,7]. Experiments in zebrafish larvae bridge the gap between *in vitro* research and *in vivo* preclinical mammal studies as they combine experimental efficiency of cell cultures and organoids with the opportunity to study whole vertebrate organism, including all on- and off-target effects, which will improve extrapolation of observations to higher vertebrates.

In pharmacological and toxicological research with aquatic species, the studied compounds are usually dissolved in the incubation medium (i.e. waterborne treatment). The relationship between the medium concentration of the exogenous compound and its internal exposure is essential for reliable interpretation of the observed results[8–12], since it is the internal concentration that drives pharmacological and toxicological effects. Because target engagement, which is responsible for the response to exogenous compounds, depends on the pharmacokinetics or toxicokinetics of internal exposure over time, longitudinal data of exposure over time is needed for reliable interpretation of observed effects[13–15]. It is well documented that ignoring this critical issue leads to poor outcomes in drug discovery research[16].

To derive internal exposure based on the external concentration of the compounds, for example based on physicochemical properties, has been shown to be very challenging[17–19]. Measuring this essential internal exposure is also a challenge due to the small size of zebrafish larvae and the subsequently required very sensitive quantification methods. Recently however, we demonstrated the technical feasibility of measuring pharmacokinetics in zebrafish by developing a profile of internal amount over time for zebrafish of 3 days post fertilization (dpf), using paracetamol (acetaminophen) as paradigm compound[20]. In this analysis, mathematical modelling was used to describe the pharmacokinetics by quantifying the absorption rate constant, and elimination rate constant which reflects both metabolism and excretion, processes that in addition to the distribution drive the internal exposure.

Although experiments with larva have many advantages, studying an organism during its development will require understanding of the effect of maturation on the studied feature. Zebrafish development is rapid, showing embryogenesis within 3 dpf[21], liver budding from 1 dpf and growth from 2 dpf[22], development of a functional renal system after 2 dpf[23], and presence of a gastro-intestinal (GI) tract from 1-4 dpf[24], reaching adulthood in 3 months[25]. These developmental and maturation processes in the first days post fertilization are expected to have an impact on the absorption and elimination of compounds. As most experiments in the field of pharmacology and toxicology are performed during these first days[1], it is essential to understand and quantify the impact of development, and to know what difference a single experimental day makes on the internal exposure of exogenous compounds. This is especially the case when studying direct, short-term effects of exogenous compounds.

Using paracetamol as paradigm compound, our aim is therefore to use mathematical modelling to quantify absorption and elimination rate constants from internal exposure over time profiles after waterborne treatment in post-hatching zebrafish larvae of 3 to 5 dpf, and to characterize the impact of development on these parameters using post fertilization age as marker.

6.3 Methods

6.3.1 Chemicals

Paracetamol and paracetamol-D4 internal standard were purchased from Sigma (Sigma-Aldrich Chemie B.V., Zwijndrecht, The Netherlands). UPLC-MS grade MeOH was purchased from Biosolve (Biosolve B.V., Valkenswaard, The Netherlands). Purified water (H_2O) was retrieved from PURELAB (Veolia Water Technologies B.V., Ede, The Netherlands).

6.3.2 Zebrafish husbandry

All experiments were planned and executed in compliance with European regulation[6]. Handling and maintenance of zebrafish and zebrafish larvae was in accordance with international standard protocols[26]. Adult wild type AB/TL zebrafish were set-up for overnight family cross breeding, separated by sex. Next morning, males and females were combined in breeding tanks with inserts and after 20 minutes eggs were collected. This way, time of fertilization was controlled. Fertilized eggs were kept at 28°C in petri dishes in embryo medium (demineralized containing 60 µg/mL Instant Ocean sea salts; Sera, Heinsberg, Germany) which was refreshed daily.

6.3.3 Experimental design

The experimental design of Kantae et al. performed in larvae of 3 dpf[20], was repeated with larvae of 4 and 5 dpf in samples of n = 5 zebrafish larvae. In short, two experiments were performed, one in which larvae were continuously treated with 1 mM waterborne paracetamol in embryo medium (treatment medium) for 0 – 180 minutes and one in which the larvae were treated with treatment medium for 60 minutes and then washed with embryo medium using Netwell inserts filters (Corning Life Sciences B.V., Amsterdam, The Netherlands) and transferred to drug-free medium for a washout period of 60 – 240 minutes. After the designated constant waterborne treatment or washout period, the larvae were washed with 20/80 MeOH/H_2O (v/v) using Netwell inserts, transferred to Safe-Lock tubes (Eppendorf Nederland B.V., Nijmegen, The Netherlands), excess volume was removed and 100 µL 90/10 MeOH/H_2O with 45 pg/uL paracetamol-D4 internal standard was added. The sample was snap-frozen in liquid nitrogen and stored at -80°C until quantification. Measurements at all time points were performed at least in triplo.

Additionally, to ensure paracetamol concentrations in the treatment medium remained constant throughout the duration of the experiment, treatment medium from a set-up with and without 3, 4, and 5 dpf larvae was sampled at 180 minutes and compared to 1 mM paracetamol solution in H_2O and to fresh treatment medium, all in triplo. Samples were frozen at-80°C until quantification.

6.3.4 Measurements of internal exposure

The method to quantify internal paracetamol exposure were described earlier by Kantae et al.[20]. In short, samples were lysed by iterations of snap freezing the solution with the larvae in liquid nitrogen and submerging the sample in a sonication bath until a homogeneous suspension was obtained. These suspensions were centrifuged at 16,000 g for 10 minutes and 90 µL supernatant was added to 72 µL H_2O to reach 50/50 MeOH/H_2O (v/v) to be injected into the ultra-performance liquid chromatography (UPLC) system (Acquity, Waters Chromatography B.V., Etten-Leur, The Netherlands) linked to a quadrupole-ion trap MS/MS (QTRAP-6500, AB Sciex B.V., Nieuwerkerk aan den IJssel, The Netherlands) with an electrospray ionisation source in positive mode. Development criteria were 90-100% accuracy and relative standard deviations less than 10% as measure of precision. Paracetamol concentrations were determined through a calibration curve in matrix ranging from 0.09 to 180 pg/uL, and calculated to total paracetamol amount in pmole per zebrafish larva. Treatment medium samples were diluted with H_2O to fall within the academic calibration range from 0.05 to 100 pg/uL with a final internal standard concentration of 25 pg/uL paracetamol-D4.

6.3.5 Pharmacokinetic modelling

To quantify the physiological processes driving the internal exposure of paracetamol, a mathematical model was developed using non-linear mixed effects (NLME) modelling, which combines the quantification of non-random trends in the data called fixed effects as well as random variability known as random effects. NLME modelling was performed using the First Order Conditional Estimation (FOCE) algorithm in NONMEM (v.7.3)[27], which was operated through the interfaces Pirana (v.2.9.6)[28] and PsN (v.4.7.0)[29]. Graphical output was generated using R (v.3.4.2)[30] running through the RStudio (v.1.1.383, RStudio Inc, Boston, Massachusetts, USA) interface.

A one and two compartment model was tested. In case of the two compartment model, the sum of the amounts in both compartments were fitted to the observed total amounts, while elimination was only limited to one compartment. Absorption of paracetamol was estimated as a zero-order process, assuming the paracetamol concentration in the incubation medium to remain constant over time. For the elimination estimation both first-order linear and saturable non-linear Michaelis Menten processes were tested.

Quantification of the residual error was tested as additive, proportional, and a combination of additive and proportional error. As the larvae were lysed to quantify internal exposure, only single observations were obtained from a larval sample. As a result inter-individual variability in internal exposure caused by individual variability in model parameters could not be distinguished from residual variability caused by experimental or analytical error.

Quantification of the correlation between model parameters and larval age, was tested with both continuous (Equations 1 and 2) and discrete (Equation 3) functions:

$$\mathrm{P} = \mathrm{P}_{\mathrm{base}} \cdot \left(1 + \mathrm{slope} \cdot (\mathrm{age} - \mathrm{ref})\right) \tag{1}$$

$$\mathrm{P} = \mathrm{P}_{\mathrm{base}} \cdot (1 + \mathrm{slope})^{\mathrm{age}-\mathrm{ref}} \tag{2}$$

$$\mathrm{P} = \begin{cases} \mathrm{P}_1 & \mathrm{age} = 3\ \mathrm{dpf} \\ \mathrm{P}_2 & \mathrm{age} = 4\ \mathrm{dpf} \\ \mathrm{P}_3 & \mathrm{age} = 5\ \mathrm{dpf} \end{cases} \tag{3}$$

where P is the parameter of interest, P_{base} is the base value at the reference age ref, and P_1, P_2 and P_3 are different functions or estimates of the parameter of interest for their respective conditions.

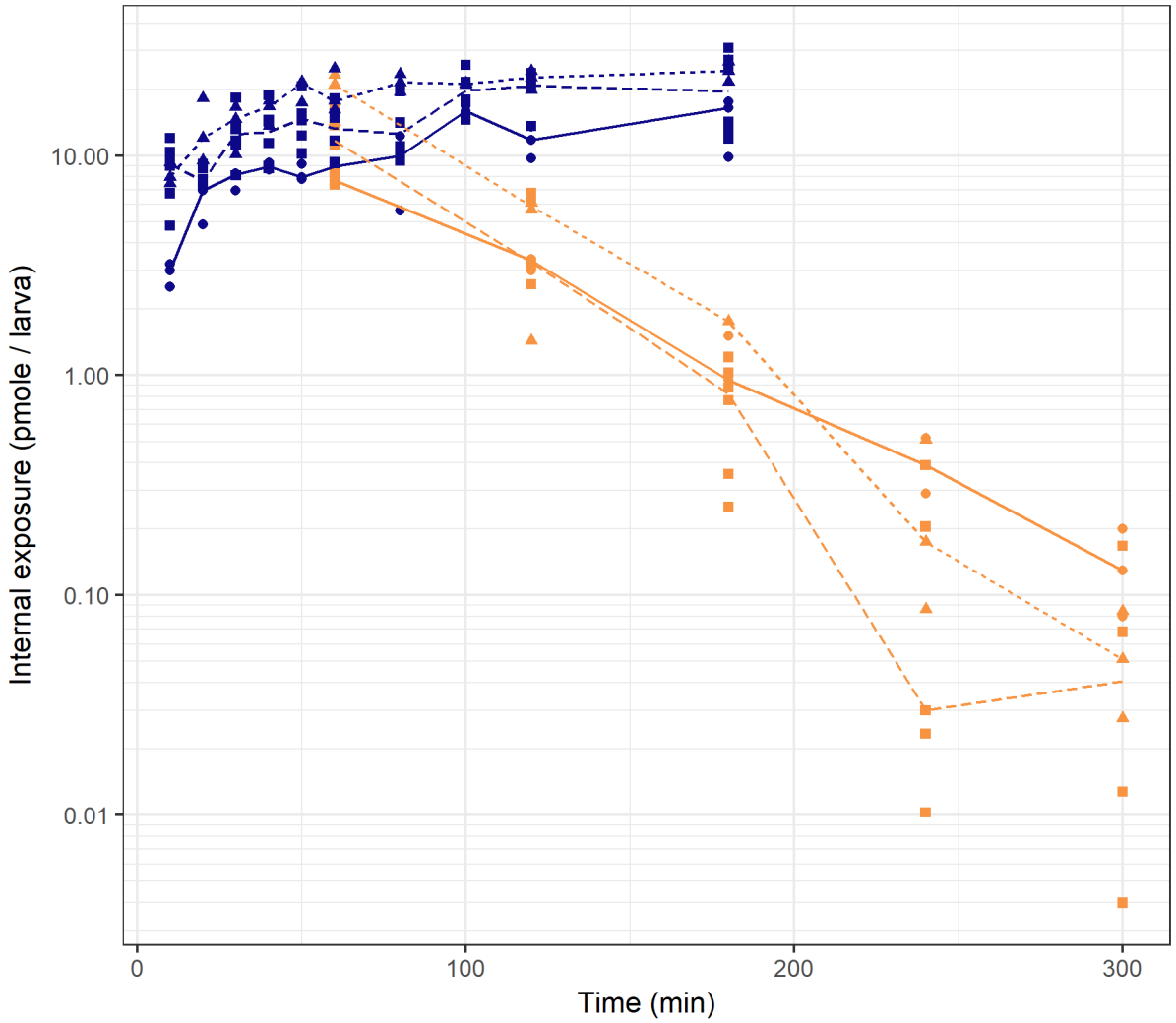

Figure 6.1 Raw data of internal exposure of paracetamol amountsn over time for zebrafish larvae of 3 dpf (solid line, closed circles), 4 dpf (dotted line, closed triangles), and 5 dpf (dashed line, closed squares) for both constant waterborne drug treatment experiment (blue) or washout experiment (orange). Datapoints are total amount per larva from a pooled sample with n = 5. The lines are connecting the median values at each time point.

For the continuous relationship, a linear function (Equation 1) or power function (Equation 2) was tested to describe the relationship between age and parameter values. In the discrete function (Equation 3) different parameter values were estimated for larvae older and/or younger than a specified reference age.

For model selection, the likelihood ratio test was used between nested models[31], assuming a χ^2 distribution and using a significance level of $p < 0.01$. Additional selection criteria were successful minimisation, estimates of parameter values with 3 or more significant digits and relative standard errors below 50%, and biologically plausibility of the parameter estimates. Graphically, model accuracy was assessed using goodness-of-fit plots, consisting of observed versus predicted plots and conditional weighted residuals (CWRES) versus time or predicted paracetamol amounts, which should show no bias over time or predicted paracetamol amounts[32]. Stability of paracetamol concentrations in treatment medium in the control experiment were normalized to H_2O control and tested by non-parametric Kruskall-Wallis test, as the data were not normally distributed, with level of significance of 0.05.

6.3.6 Comparison of paracetamol clearance to higher vertebrates

The degree of correlation between paracetamol clearance in zebrafish larvae with higher vertebrates

was assessed by calculating paracetamol clearance values in the larvae by multiplying the obtained elimination rate constants with previously reported total larval volumes at corresponding ages[33] that are provided in Table 6.1. This assumes the distribution volume to be equal to the total volume of the larva and a homogenous distribution of the compound throughout the whole larva. The paracetamol clearance values in the larvae at different ages, were graphically compared to reported paracetamol clearance values in higher vertebrates[20], in a plot of clearance values versus bodyweight of the species. The bodyweight of the larvae was derived from their volume, assuming a density of 0.997 g/mL[20]. A linear least squares regression with 95% confidence interval of the log transformed clearance and log transformed bodyweight was calculated in R, based on clearance values obtained in mature individuals of the different species included in the graph.

6.4 Results

6.4.1 Measurements of internal exposure

The observed internal exposure of paracetamol expressed as total amount per larva over time is shown in Figure 6.1 for larvae of 3, 4, and 5 dpf for both the constant waterborne treatment and the washout experiment. It can be seen that steady state of internal paracetamol exposure is reached between 100 and 120 minutes of constant waterborne treatment, meaning an equilibrium between paracetamol amounts absorbed and eliminated per time unit has been reached. Steady state exposure in the constant waterborne treatment experiment increased in larvae between 3 and 4 dpf, while it remained relatively constant in larvae between 4 and 5 dpf. The washout experiment showed a mono-exponential decline of the paracetamol amount per larva after the larvae were transferred to paracetamol-free medium. The steepness of this curve, reflecting the elimination rate, increases in larvae with increasing age. The dataset is available through the DDMoRe Respository, Model ID DDMODEL00000294. The stability of the paracetamol concentration in the treatment medium was not impacted by the experimental set-up (Supplementary Figure S6.1).

6.4.2 Pharmacokinetic modelling

Based on the selection criteria, a one compartment model with zero-order absorption and first-order elimination best fitted the observed profiles of paracetamol amounts in zebrafish larvae over time for both experiments. A combination of additive and proportional error model was found to describe residual variability best, with the variance of the proportional error being 0.109 corresponding to 33% and the variance of the additive residual unexplained error being 0.00844 pmole/larva. A schematic and mathematical representation of this model is provided in Figure 6.2 and Equation 4, respectively. The

Table 6.1 Paracetamol elmination rate constant (), reported total larval volume[33], and derived absolute paracetamol clearance (CL) for 3, 4, and 5 dpf larvae.

Age	k_e (min^{-1})	Total volume (nL)	CL (nL/h)
3 dpf	0.0193	253	292.3
4 dpf	0.0226	263	356.8
5 dpf	0.0266	300	478.1

Figure 6.2 Schematic representation of the final model to describe the total amount of paracetamol in zebrafish larvae over time. k_a = zero-order absorption rate constant, A = amount of paracetamol in one larva, k_e = first-order elimination rate constant.

Table 6.2 Obtained model parameter values and their relative standard error (RSE).

	Parameter value	RSE (%)
Structural parameters		
$k_{a,base}$ (pmole/min)	0.289	4
$factor_a$ (-)	1.06	14
$k_{e,base}$ (min^{-1})	0.0193	5
$slope_e$ (-)	0.175	18
Stochastic parameters		
Variance of proportional residual error (-)	0.109	14
Variance of additive residual error (pmole/larva)	0.00844	48

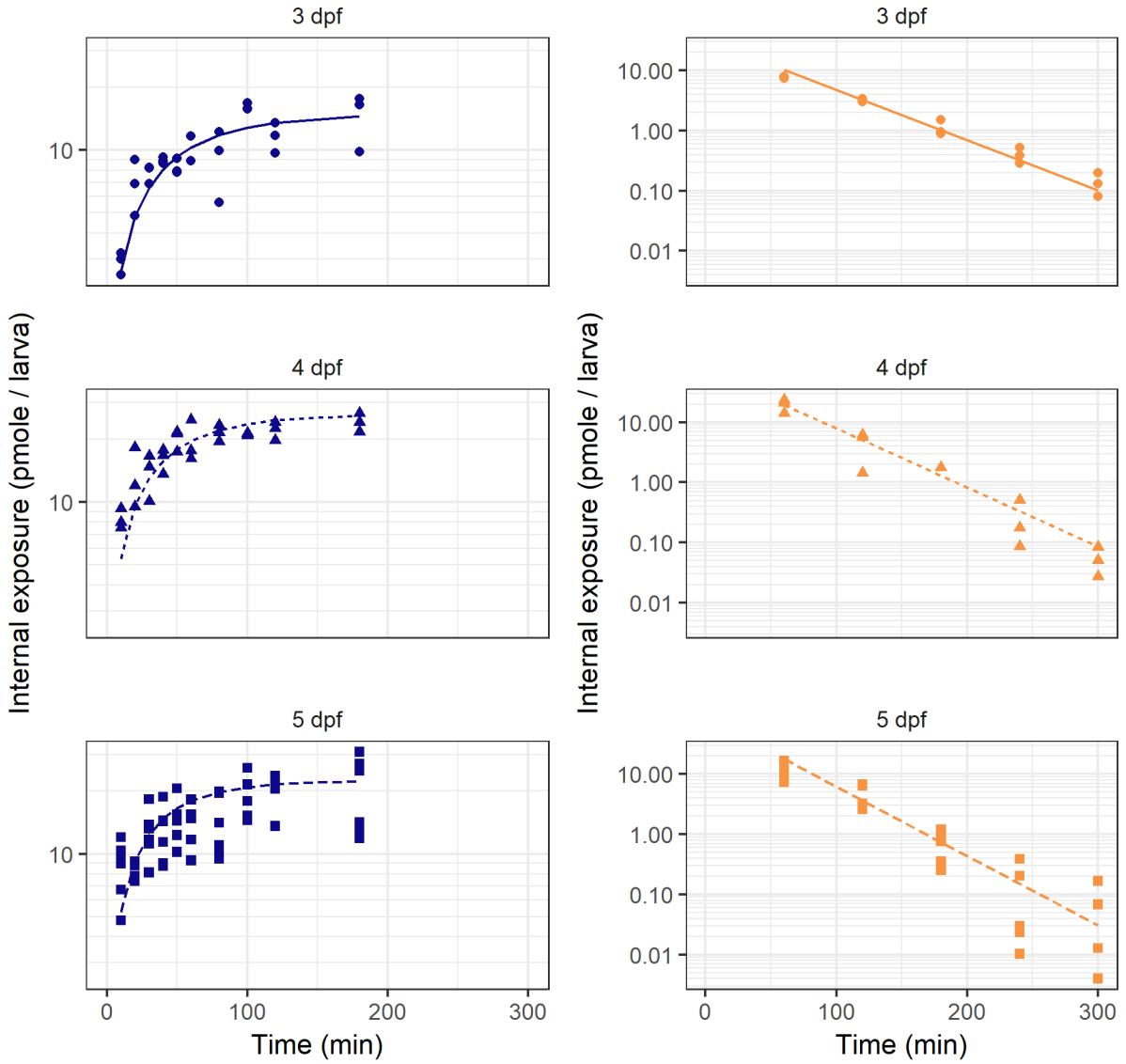

Figure 6.3 Model fit (lines) through observed paracetamol amounts over time (symbols) in larvae of 3 dpf (solid line, closed circles), 4 dpf (dotted line, closed triangles), and 5 dpf (dashed line, closed squares) for both the constant waterborne drug treatment experiment (blue, left panels) and the washout experiment (orange, right panels).

final model included a discrete relationship between age and the absorption rate constant (Equation 5) and a power relationship between age and the elimination rate constant (Equation 6).

$$\frac{dA}{dt} = k_a - k_e \cdot A \tag{4}$$

$$k_a = \begin{cases} k_{a,\,base} & age = 3\ dpf \\ k_{a,base} \cdot (1 + factor_a) & 3\ dpf < age \leq 5\ dpf \end{cases} \tag{5}$$

$$k_e = k_{e,base} \cdot (1 + slope_e)^{age - 3dpf} \tag{6}$$

where A is the paracetamol amount in a single larva, k_a is the zero-order absorption rate constant, $k_{a,base}$ is the base value of the absorption rate constant at the reference age of 3 dpf, and $factor_a$ describes the fractional increase in the absorption rate constant in zebrafish larvae that are older than 3 days, k_e is the first-order elimination rate constant, $k_{e,base}$ is the base value of the elimination rate constant at the

reference age of 3 dpf, and $slope_e$ is the estimated slope in the relationships between the elimination rate constant and age. The obtained parameter values are presented in Table 6.2 and final model code is available through the DDMoRe Respository, Model ID DDMODEL00000294.

According to the obtained results, at 3 dpf the value of the zero-order absorption rate constant of paracetamol is 0.289 pmole/min and the first-order elimination rate constant is 0.0193 min^{-1}. The absorption rate constant was found to be statistically significantly ($p < 1 \times 10^{-10}$) increased between 3 and 4 dpf by 106% in the final model, but the difference in this parameter between larvae of 4 dpf and 5 dpf was found not to be statistically significant (p = 0.46). The elimination rate constant was found to statistically significantly ($p < 1 \times 10^{-6}$) increase between all three ages. In the final model, the elimination rate constant increased by 17.5% per day, resulting in an elimination rate constant of 0.0226 min^{-1} and 0.0266 min^{-1} for larvae of 4 and 5 dpf respectively.

The model predicted concentration-time profile per age and experiment together with the observed concentrations are shown in Figure 6.3, showing good agreement between observed and predicted concentrations. The diagnostic goodness-of-fit plots further confirmed good accuracy of the model predictions (Supplementary Figure S6.2). The relative standard error values of the obtained structural model parameters are well below 20%, indicating good precision of these estimates.

6.4.3 Comparison of paracetamol clearance to higher vertebrates

Paracetamol clearance and previously reported larval volume for 3, 4, and 5 dpf larvae are shown in Table 6.1. Figure 6.4 shows the correlation between paracetamol clearance and bodyweight for 13 species including the zebrafish. This plot has previously been reported including the results of zebrafish larvae of 3 dpf only[20] and now includes also the clearance values for 4 and 5 dpf larvae. It can be seen that the older and heavier larvae show a closer correlation with the higher vertebrates, as they are positioned closer to the 95% confidence interval of the allometric relationship between bodyweight and paracetamol clearance as established based on data from mature individuals only. They do remain below the confidence interval, as do the data points obtained in paediatric human studies (red triangles).

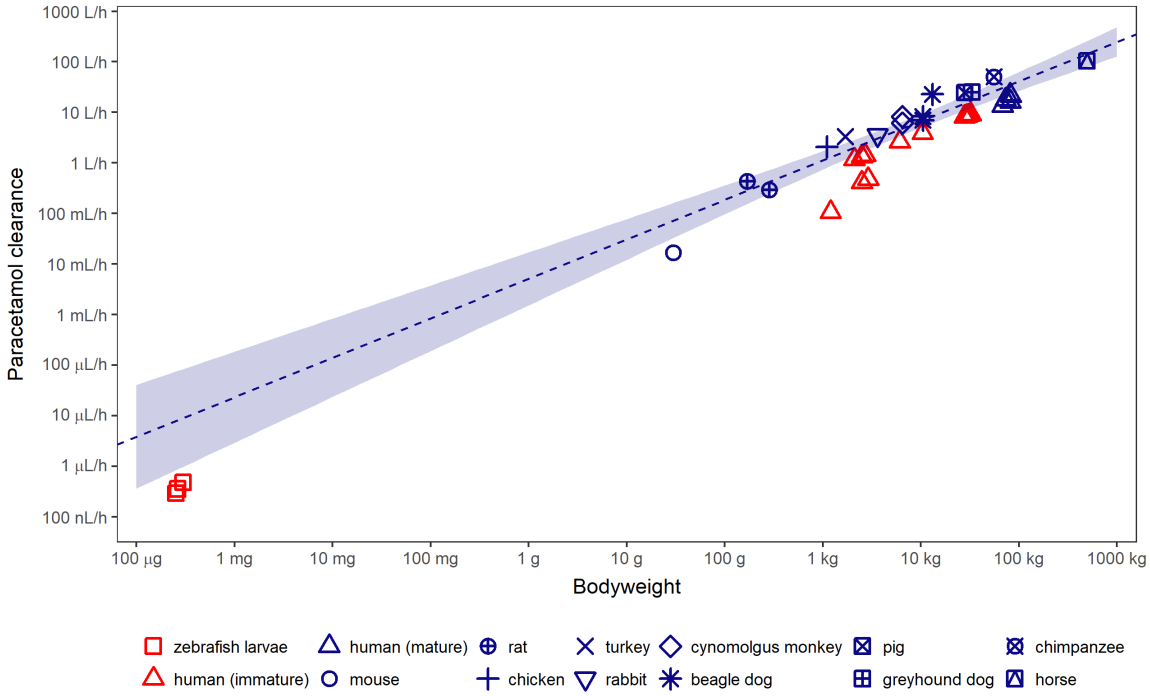

Figure 6.4 Allometric relationship between paracetamol clearance and bodyweight of 13 vertebrate species including the zebrafish larvae at three different ages. Blue and red symbols show mature or immature individuals of the species, respectively. Allometric relationship (dashed blue line) and 95% confidence interval (shaded area) are determined based on data in mature organisms only. Adapted with permission from Kantae et al.[20].

6.5 Discussion

Here the impact of development on the pharmacokinetic or toxicokinetic processes of absorption and elimination through post fertilization age as marker was quantified by mathematical modelling based on the profiles of internal exposure over time after waterborne treatment in post-hatching zebrafish larvae of 3, 4, and 5 dpf. The absorption of paracetamol was shown to increase 106% between 3 and 4 dpf, but not to significantly further increase at 5 dpf, while paracetamol elimination increased 17.5% per day in this 3 to 5 days post fertilization period.

Within the mathematical model, the relationships between age and the absorption and elimination rate constants were parameterized with values for larvae at 3 dpf as reference values. These values are comparable to the values reported previously for zebrafish larvae of 3 dpf alone[20]. The doubling of the absorption rate between 3 and 4 dpf, can be explained by the opening of the GI tract, which is a discrete event completing with the opening of the anus at 4 dpf[7,24]. From that moment, instead of only transdermal or trans-gill absorption, the larvae will also ingest the exogenous compound orally. Recently examined absorption of the antihistamine diphenhydramine between zebrafish embryos and larvae showed an chorion-independent increase in absorption between 2 and 4 dpf and are in concordance with our results here[34]. The absorption rate constant did not increase further between 4 and 5 dpf, suggesting that potential other processes that add to the absorption of paracetamol, do not show maturational changes in the age range studied here.

The 17.5% increase in the elimination rate constant between each of the three post fertilization days is expected to result from the continuous growth of eliminating organs like the liver and kidneys, as well as continuous maturation of enzymatic processes[22]. Indeed, the clearance values of immature organisms of both the zebrafish and human are lower than expected based on bodyweight alone, but these values do move towards the regression line with increasing age (Figure 6.4), with the larval clearance being 35%, 41%, and 49% of the lower bound of the 95% confidence interval of the extrapolated clearance calculated based on the values of higher vertebrates for larvae of 3, 4, and 5 dpf respectively. It has to be kept in mind that for comparison to higher vertebrates, the absolute clearance in the zebrafish larvae was calculated based on total larval volume, assuming a homogenous distribution over the total body of the larvae, because information on the distribution volume of paracetamol in zebrafish is not available in literature. Given that the distribution volume of paracetamol has been reported to range from 0.8-0.9 L/kg[35,36] in humans, this assumption seems to be reasonable, although further research into the distribution of this compound in zebrafish larvae is required. If the true distribution volume is larger, the calculated clearance values would also be proportionally larger and fall within the 95% confidence interval, or vice versa. Another factor that may contribute to deviations of the clearance values in zebrafish larvae from the regression line could be the fact that fish are poikilotherms, for which lower metabolic rates have been reported[37].

From our results it is clear that the age of the larvae during experiments with waterborne treatment influences internal exposure of exogenous compounds, at least for our paradigm compound. Because the internal exposure of the exogenous compound drives its pharmacological or toxicological effect, it can be expected that the age will also impact the observed effects resulting from the treatment. The age of the larvae used to investigate the direct effects of exogenous compounds is therefore an important experimental design consideration. To determine which age to include, three criteria are of importance. Firstly, the internal exposure of the studied compound should be high enough to yield an effect and prevent false negatives. Secondly, the larval metabolic capacity should be large enough to biotransform exogenous compounds to their active metabolites as drug metabolites can also be biologically active. Thirdly, extrapolating observations to higher vertebrates, for instance to improve study design of mammal studies based on translation of clearance, benefits from a direct comparison of the pharmacokinetic processes between species. Based on the results of the paracetamol study presented here, we propose

experiments for the testing of direct effects of exogenous compounds to be performed in zebrafish larvae at 5 dpf, because absorption is highest at 4 and 5 dpf, while the metabolic capacity at 5 dpf is largest and clearance at that time resembles clearance of higher vertebrates most within the age range that still falls within the ethical constraints for experiments in zebrafish larvae[6,7].

6.6 Conclusion

In conclusion, it is of importance to quantify internal exposure over time when testing exogenous compounds by waterborne treatment in zebrafish larvae. The opening of the GI-tract will likely result in increased absorption, which is seen here between 3 and 4 dpf when absorption of paracetamol more than doubles. Continuous growth of eliminating organs as well as maturation of enzymatic processes lead to increased elimination, which is 17.5% daily for paracetamol between 3 and 5 day post fertilization. To increase internal exposure to parent compounds and metabolites in short term exposure studies, we therefore recommend careful consideration of zebrafish age in experimental design when these pharmacokinetic or toxicokinetic processes are of relevance to the research question. Based on our results with paracetamol, using 5 dpf zebrafish larvae may be preferable for studying direct short-term effects of exogenous compounds.

6.7 Acknowledgements

The authors thank Sebastiaan Goulooze for peer-reviewing scripts for data handling and mathematical modelling.

6.8 Data availability statement

The full dataset and model file are available through the DDMoRe Respository, Model ID DDMODEL00000294 (http://repository.ddmore.foundation/model/DDMODEL00000294).

6.9 References

1. Rennekamp AJ, Peterson RT. 15 years of zebrafish chemical screening. Curr Opin Chem Biol. 2015;24:58-70.
2. Peterson RT, Macrae CA. Systematic approaches to toxicology in the zebrafish. Annu Rev Pharmacol Toxicol. 2012;52:433-453.
3. Zon LI, Peterson RT. In vivo drug discovery in the zebrafish. Nat Rev Drug Discov. 2005;4(1):35-44.
4. Howe K, Clark MD, Torroja CF, et al. The zebrafish reference genome sequence and its relationship to the human genome. Nature. 2013;496:498-503.
5. Schulthess P, Van Wijk RC, Krekels EHJ, et al. Outside-in systems pharmacology combines innovative computational methods with high-throughput whole vertebrate studies. CPT Pharmacometrics Syst Pharmacol. 2018;7:285-287.
6. EU. Council Directive 2010/63/EU on the protection of animals used for scientific purposes. Off J Eur Union. 2010;L276/33.
7. Strähle U, Scholz S, Geisler R, et al. Zebrafish embryos as an alternative to animal experiments — A commentary on the definition of the onset of protected life stages in animal welfare regulations. Reprod Toxicol. 2012;33:128-132.
8. Damalas DE, Bletsou AA, Agalou A, et al. Assessment of the acute toxicity, uptake and biotransformation potential of benzotriazoles in zebrafish (Danio rerio) larvae combining HILIC-with RPLC-HRMS for high-throughput identification. Environ Sci Technol. 2018;52:6023-6031.
9. Achenbach JC, Hill J, Hui JPM, et al. Analysis of the uptake, metabolism, and behavioral effects of cannabinoids on zebrafish larvae. Zebrafish. 2018;15(4):349-360.

10. Kühnert A, Vogs C, Altenburger R, et al. The internal concentration of organic substances in fish embryos- a toxicokinetic approach. Environ Toxicol Chem. 2013;32(8):1819-1827.
11. Kühnert A, Vogs C, Aulhorn S, et al. Biotransformation in the zebrafish embryo – temporal gene transcription changes of cytochrome P450 enzymes and internal exposure dynamics of the AhR binding xenobiotic benz[a]anthracene. Environ Pollut. 2017;230:1-11.
12. Brox S, Seiwert B, Küster E, et al. Toxicokinetics of polar chemicals in zebrafish embryo (Danio rerio): Influence of physicochemical properties and of biological processes. Environ Sci Technol. 2016;50(18):10264-10272.
13. Li Y, Wang H, Xia X, et al. Dissolved organic matter affects both bioconcentration kinetics and steady-state concentrations of polycyclic aromatic hydrocarbons in zebrafish (Danio rerio). Sci Total Environ. 2018;639:648-656.
14. Liu H, Ma Z, Zhang T, et al. Pharmacokinetics and effects of tetrabromobisphenol A (TBBPA) to early life stages of zebrafish (Danio rerio). Chemosphere. 2018;190:243-252.
15. Van Wijk RC, Krekels EHJ, Hankemeier T, et al. Systems pharmacology of hepatic metabolism in zebrafish larvae. Drug Discov Today Dis Model. 2016;22:27-34.
16. Morgan P, Van der Graaf PH, Arrowsmith J, et al. Can the flow of medicines be improved? Fundamental pharmacokinetic and pharmacological principles toward improving Phase II survival. Drug Discov Today. 2012;17(9/10):419-424.
17. Geier MC, James Minick D, Truong L, et al. Systematic developmental neurotoxicity assessment of a representative PAH Superfund mixture using zebrafish. Toxicol Appl Pharmacol. 2018;354:115-125.
18. Diekmann H, Hill A. ADMETox in zebrafish. Drug Discov Today Dis Model. 2013;10(1):e31-e35.
19. Ordas A, Raterink R-J, Cunningham F, et al. Testing tuberculosis drug efficacy in a zebrafish high-throughput translational medicine screen. Antimicrob Agents Chemother. 2015;59(2):753-762.
20. Kantae V, Krekels EHJ, Ordas A, et al. Pharmacokinetic modeling of paracetamol uptake and clearance in zebrafish larvae: Expanding the allometric scale in vertebrates with five orders of magnitude. Zebrafish. 2016;13(6):504-510.
21. Kimmel CB, Ballard WW, Kimmel SR, et al. Stages of embryonic development of the zebrafish. Dev Dyn. 1995;203:253-310.
22. Tao T, Peng J. Liver development in zebrafish (Danio rerio). J Genet Genomics. 2009;36:325-334.
23. Gehrig J, Pandey G, Westhoff JH. Zebrafish as a model for drug screening in genetic kidney diseases. Front Pediatr. 2018;6:183.
24. Ng ANY, De Jong-Curtain TA, Mawdsley DJ, et al. Formation of the digestive system in zebrafish: III. Intestinal epithelium morphogenesis. Dev Biol. 2005;286(1):114-135.
25. Parichy DM, Elizondo MR, Mills MG, et al. Normal table of post-embryonic zebrafish development: staging by externally visible anatomy of the living fish. Dev Dyn. 2009;238(12):2975-3015.
26. Westerfield M. The zebrafish book. A Guide for the Laboratory Use of Zebrafish (Danio Rerio). 4th ed. Eugene, OR, USA: University of Oregon Press; 2000.
27. Beal S, Sheiner L, Boeckmann A, et al. NONMEM 7.3.0 users guides. (1989-2013). ICON Development Solutions, Hanover, MD, USA.
28. Keizer R, Van Benten M, Beijnen J, et al. Pirana and PCluster: A modeling environment and cluster infrastructure for NONMEM. Comput Methods Programs Biomed. 2011;101(1):72-79.
29. Lindbom L, Pihlgren P, Jonsson E. PsNtoolkit — a collection of computer intensive statistical methods for non-linear mixed effect modeling using NONMEM. Comput Methods Programs Biomed. 2005;79(3):241-257.
30. R Core Team. R: A language and environment for statistical computing. R Found Stat Comput Vienna, Austria. 2014.
31. Mould DR, Upton RN. Basic concepts in population modeling, simulation, and model-based drug development-part 2: Introduction to pharmacokinetic modeling methods. CPT pharmacometrics Syst Pharmacol. 2013;2(April):e38.
32. Nguyen THT, Mouksassi M-S, Holford N, et al. Model evaluation of continuous data pharmacometric models: metrics and graphics. CPT Pharmacometrics Syst Pharmacol. 2017;6:87-109.

33. Guo Y, Veneman WJ, Spaink HP, et al. Three-dimensional reconstruction and measurements of zebrafish larvae from high-throughput axial-view in vivo imaging. Biomed Opt Express. 2017;8(5):2611-2634.
34. Kristofco LA, Haddad SP, Chambliss CK, et al. Differential uptake of and sensitivity to diphenhydramine in embryonic and larval zebrafish. Environ Toxicol Chem. 2017;37(4):1175-1181.
35. Reith D, Medlicott NJ, Kumara De Silva R, et al. Simultaneous modelling of the Michaelis-Menten kinetics of paracetamol sulphation and glucuronidation. Clin Exp Pharmacol Physiol. 2009;36(1):35-42.
36. Prescott LF. Kinetics and metabolism of paracetamol and phenacetin. Br J Clin Pharmacol. 1980;10:291-298.
37. White CR, Phillips NF, Seymour RS. The scaling and temperature dependence of vertebrate metabolism. Biol Lett. 2006;2(1):125-127.

6.10 Supplementary material

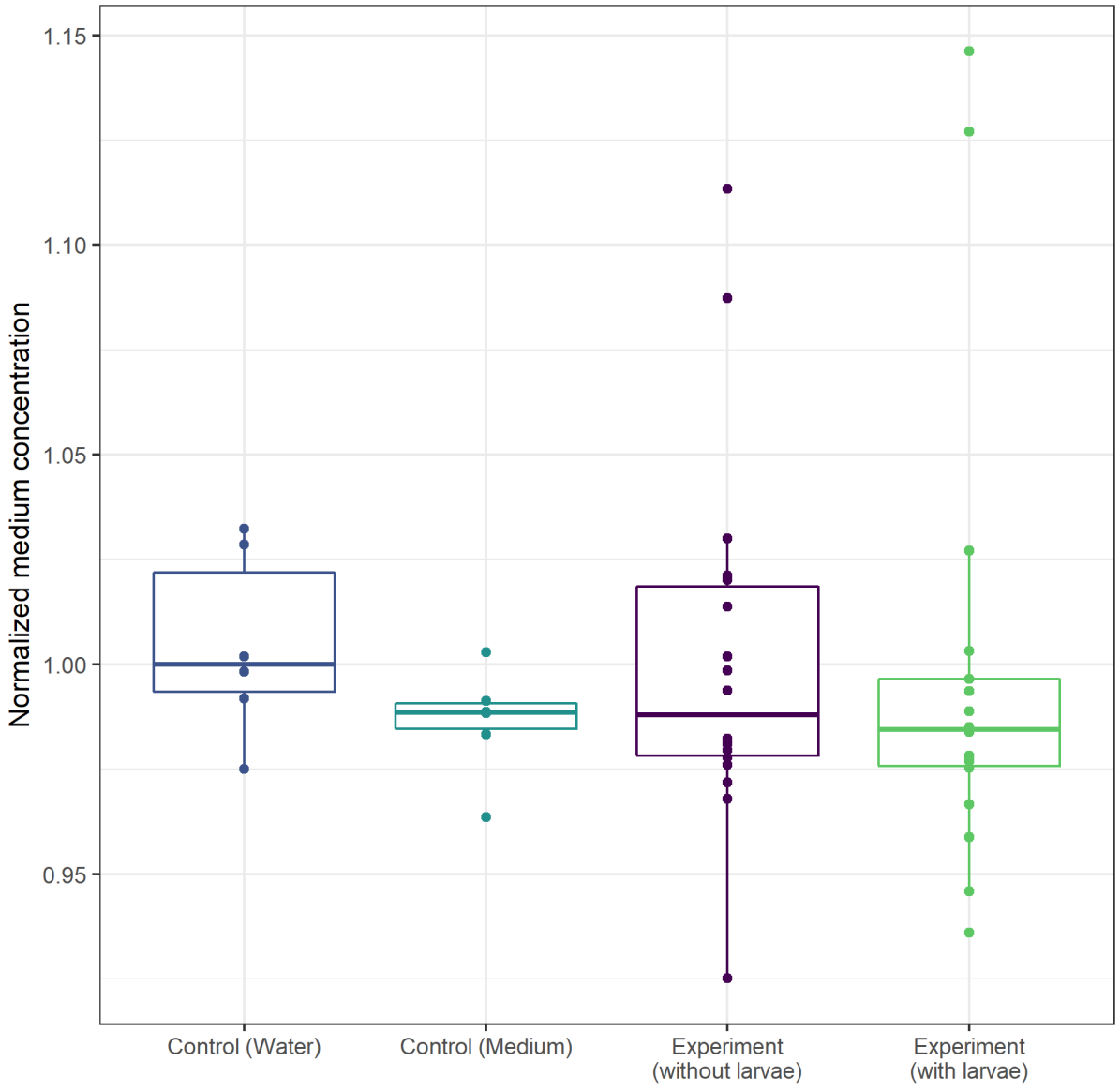

Supplementary Figure S6.1 Control experiment of stability of treatment medium concentration. No statistically significant difference between groups was observed.

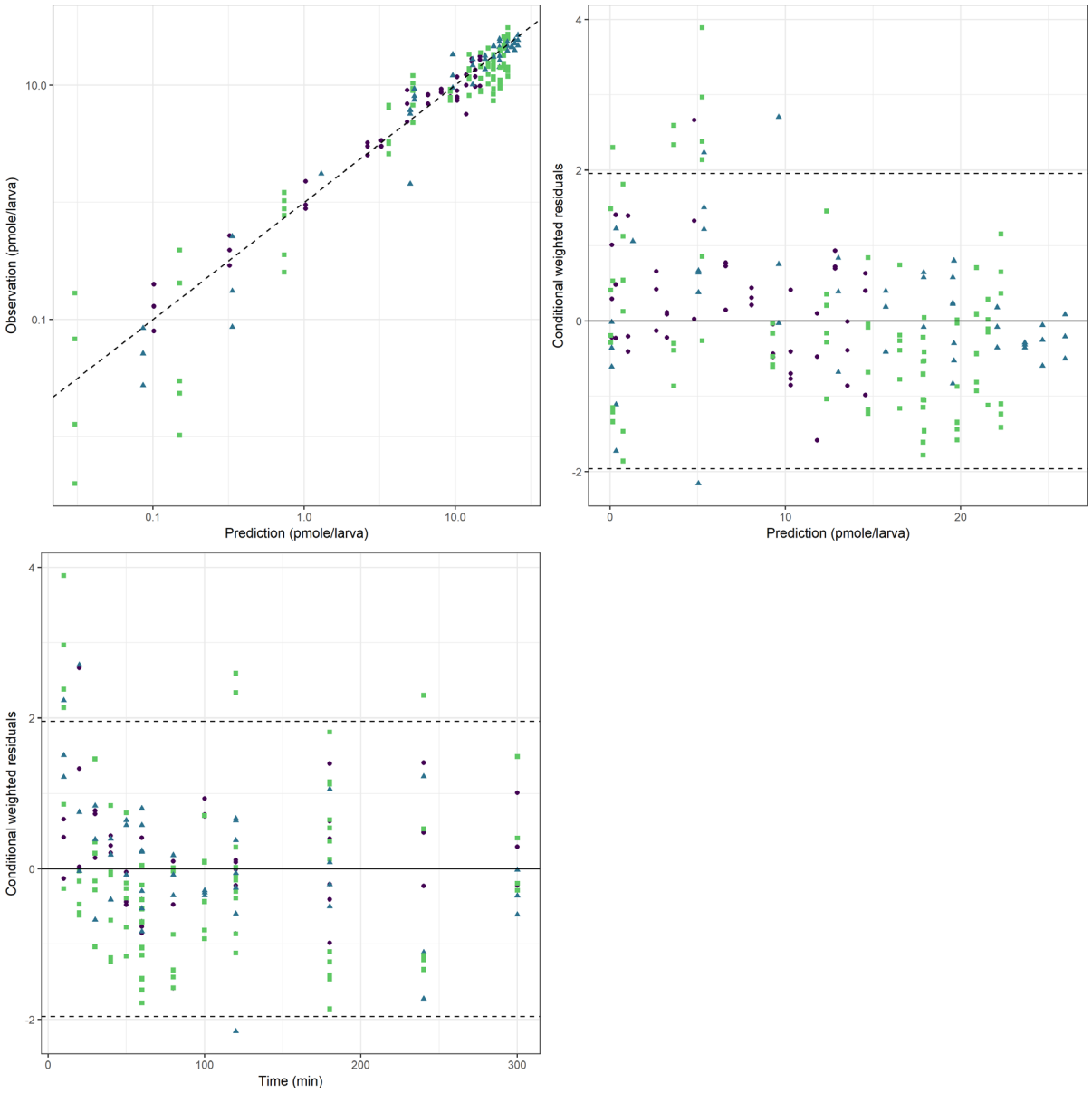

Supplementary Figure S6.2 Goodness-of-fit plots for paracetamol amounts in zebrafish larvae of 3 dpf (purple circles), 4 dpf (blue triangles), and 5 dpf (green squares). Top left: observed versus predicted paracetamol amounts, black dashed line shows the unity line. Top right: Conditional weighted residuals versus predicted paracetamol amounts, black lines show the line y = 0 (solid) as well as ±1.96 (dashed). Bottom left: Conditional weighted residuals versus time, black lines show the line y = 0 (solid) as well as ±1.96 (dashed).

6.11 NONMEM model code

```
$PROBLEM PK
$INPUT   ID TIME AMT DV EVID MDV CMT BQL AGE
$DATA    Impact-of-maturation_dataset_paracetamol_zebrafish_345dpf.csv
IGNORE=@ IGNORE=(BQL.EQ.1)

; units
; TIME = min
; DV   = pmole / larva
; CL   = central volume / min (V = fixed)
; V    = total larval volume
; kA   = pmole / min

$SUBROUTINE ADVAN13 TOL=9
$MODEL
COMP ; CMT 1 dosing compartment
COMP ; CMT 2 central paracetamol in larva

$PK
TVK12 = THETA(2)                                  ;0-order absorption
IF(AGE.GT.3) TVK12 = THETA(2) * (1 + THETA(3)) ;age-dependent absorption
TVK25 = THETA(1) * EXP(ETA(1))                    ;1-order elimination

K12 = TVK12
K25 = TVK25 * ((1 + THETA(4)) ** (AGE - 3))    ;age-dependent rate of elim-
ination

;base parameters
K25_BASE = THETA(1)
K12_BASE = THETA(2)
;covariate parameters
K12_COVAGE = THETA(3)
K25_COVAGE = THETA(4)

$DES
DADT(1) = 0 ;constant infusion
DADT(2) = K12 * A(1) - K25 * A(2)

$ERROR
IPRED = F
Y = IPRED * (1 + EPS(1)) + EPS(2) ; prop and add error
IRES = DV - IPRED

$THETA (0,0.0192529); K25
$THETA (0,0.289485) ; K12
$THETA (0,1.06385)  ; AGE_K12
$THETA (0,0.174529) ; AGE_K25

$OMEGA  0  FIX      ; IIV K25, undistinguishable from residual variability
due to destructive sampling

$SIGMA  0.10906  ; prop error
$SIGMA 0.0084383  ;  add error

$ESTIMATION METHOD=1 MAXEVAL=2000 NOABORT PRINT=5 SIG=3 POSTHOC
$COVARIANCE PRINT=E

$TABLE      ID TIME DV IPRED PRED CWRES NOAPPEND NOPRINT ONEHEADER
            FILE=sdtab001
$TABLE      ID K25 K12 K12_COVAGE K25_COVAGE K12_BASE K25_BASE AGE
            NOPRINT NOAPPEND ONEHEADER FILE=patab001
```

Chapter 7

Mechanistic and quantitative understanding of pharmacokinetics in zebrafish larvae through nanoscale blood sampling and metabolite modelling of paracetamol

Rob C. van Wijk, Elke H.J. Krekels, Vasudev Kantae, Anita Ordas, Thijs Kreling, Amy C. Harms, Thomas Hankemeier, Herman P. Spaink, Piet H. van der Graaf

Journal of Pharmacology and Experimental Therapeutics 371:15-24 (2019)

7.1 Significance statement

In early phases of drug development, new compounds are increasingly screened in zebrafish larvae, but the internal drug exposure is often not taken into consideration. We developed innovative experimental and computational methods, including a blood sampling technique, to measure the paradigm drug paracetamol (acetaminophen) and its major metabolites and quantify pharmacokinetics (absorption, distribution, elimination) in zebrafish larvae of 5 days post fertilization with a total volume of only 300 nL. These parameter values were scaled to higher vertebrates, including humans.

7.2 Abstract

Zebrafish larvae are increasingly used for pharmacological research, but internal drug exposure is often not measured. Understanding pharmacokinetics is necessary for reliable translation of pharmacological results to higher vertebrates, including humans. Quantification of drug clearance and distribution requires measurements of blood concentrations. Additionally, measuring drug metabolites is of importance to understand clearance in this model organism mechanistically. We therefore mechanistically study and quantify pharmacokinetics in zebrafish larvae, and compare this to higher vertebrates, using paracetamol (acetaminophen) as paradigm compound. A method was developed to sample blood from zebrafish larvae five days post fertilization. Blood concentrations of paracetamol and its major metabolites, paracetamol-glucuronide and paracetamol-sulfate, were measured. Blood concentration data were combined with measured amounts in larval homogenates and excreted amounts and simultaneously analysed through non-linear mixed effects modelling, quantifying absolute clearance and distribution volume. Blood sampling from zebrafish larvae was most successful from the posterior cardinal vein with median volume (interquartile range) of 1.12 (0.676-1.66) nL per blood sample. Samples were pooled (n = 15-35) to reach measurable levels. Paracetamol blood concentrations at steady state were only 10% of the external paracetamol concentration. Paracetamol-sulfate was the major metabolite and its formation was quantified using a time-dependent metabolic formation rate. Absolute clearance and distribution volume correlated well to reported values in higher vertebrates, including humans. Based on blood concentrations and advanced data analysis, the mechanistic and quantitative understanding of paracetamol pharmacokinetics in zebrafish larvae has been established. This will improve the translational value of this vertebrate model organism in drug discovery and development.

7.3 Introduction

In drug discovery and development, the zebrafish (*Danio rerio*) larva is a promising vertebrate model organism[1,2]. It has many advantages, including 70% genetic homology to humans[3], the possibility of high-throughput experimentation, easy genetic modification, and imaging of internal processes due to its transparency in early life[4,5]. In experiments with zebrafish larvae it is common practice to expose the larvae to study drugs by waterborne treatment, dissolving the drug of interest in the medium in which the larvae swim. Ignoring the internal exposure as is done in this approach, potentially leads to false positives or negatives[6]. More importantly, translation of pharmacological findings to higher vertebrates is very limited without an internal exposure-response relationship[4,7]. To be able to use zebrafish larvae in pharmacological research to their full potential, a mechanistic understanding of the pharmacokinetic processes in zebrafish larvae is needed together with a framework to quantitatively scale this to higher vertebrates.

Methods to measure internal drug amounts in larval homogenates over time have been established only recently[8–11]. In the case of our paradigm compound paracetamol (acetaminophen), internal paracetamol amounts were subsequently used to quantify the pharmacokinetic processes of absorption and elimination through quantification of the rate of absorption and a clearance relative to total larval volume. Although the clearance derived from relative values in zebrafish larvae scaled quite reasonably

to reported absolute clearance values in higher vertebrates[10,12], accurate scaling of clearance requires absolute clearance values in zebrafish larvae. However, quantification of absolute clearance requires blood concentrations, which will also allow for the estimation of a distribution volume, but blood sampling methods for zebrafish larvae that are only a few hundred microlitres in total volume[13] have not yet been described.

In addition, mechanistic characterisation of metabolic clearance in zebrafish larvae is of importance, as the utility of zebrafish larvae in drug development depends on their drug metabolism being similar to higher vertebrates in a qualitative (similar metabolites) and quantitative (similar rate and extent) manner. This is because drug metabolites can be pharmacologically active or toxic. A first step in assessing mechanistic similarities in drug metabolism between vertebrate species is genetic confirmation that similar enzymatic pathways are present in the zebrafish, through DNA sequencing and gene expression of the enzymes and possible co-factors. For example, our paradigm compound paracetamol, is a substrate for two important metabolic pathways, glucuronidation and sulfation[14–17]. In zebrafish, the enzyme systems for these pathways have been documented based on genetic homology with humans[4,18]. However functional and quantitative confirmation that drug metabolites are actually formed *in vivo* and at what rate they are formed and eliminated is crucial. This is currently lacking for most enzymatic pathways that metabolize drugs in zebrafish larvae.

Here the objective is to mechanistically and quantitatively study pharmacokinetics in zebrafish larvae. To that aim, a method is developed to take nanoscale blood samples to measure paracetamol and its major metabolites. A mechanistic metabolite model is developed, to quantify paracetamol absolute clearance and distribution volume, which are compared to those from higher vertebrates, including humans.

7.4 Materials and Methods

7.4.1 Experimental design

Experiments were performed in zebrafish (*Danio rerio*) larvae of five days post fertilization (dpf), as this age is within the ethically acceptable time frame for larval experiments, and it offers the largest capacity to metabolize paracetamol within that time frame[12]. The investigation was divided into two experiments. In the first experiment, larvae were continuously treated with 1 mM waterborne paracetamol concentration in embryo medium for up to 200 minutes. In the second experiment, larvae were treated with 1 mM waterborne paracetamol concentration for 60 minutes, then washed and transferred to clean wash-out embryo medium, and elimination was studied over 240 minutes.

A new method was developed to sample blood from zebrafish larvae. Blood samples were taken during the first experiment. Observations between 10 and 125 minutes of waterborne treatment consisted of minimal 3 replicates of 15-35 pooled blood samples. These data were combined with data from a previous study, which included 6 replicates of measured paracetamol amounts in whole larval homogenates of 5 zebrafish larvae at 10-180 minutes in the first and 60-300 minutes in the second experiment 12. Additionally, 6 replicates of wash-out medium of the second experiment were sampled at 60-300 minutes to measure excreted paracetamol and metabolites.

Paracetamol and its two major metabolites, paracetamol-glucuronide and paracetamol-sulfate, were measured in blood, medium, and homogenate samples by liquid chromatography-mass spectrometry (LC-MS). Non-linear mixed effects modelling was performed on all data simultaneously to quantify absolute clearance, including metabolic formation and elimination rates, and distribution volume. Finally, obtained parameter values for absolute clearance and distribution volume were compared to published values in higher vertebrates.

7.4.2 Zebrafish larvae husbandry

Maintenance and handling of zebrafish followed international consensus protocols[19], and the planning and execution of all experiments were compliant with European regulation[20]. Adult wild type AB/TL zebrafish were used to fertilize eggs, and kept in glass aquaria (max 6/L, volume 10L, 120x220x490 mm, Fleuren & Nooijen BV, Nederweert, The Netherlands) with circulating water at 27.7°C ±0.1 on a 14h/10h light/dark cycle (lights on at 08:00) and twice daily feeding with artemia or feed particles (Gemma Micro/ Diamond, Skretting, Nutreco NV, Amersfoort, The Netherlands). Water quality was controlled by JUMO Acquis touch S (JUMO GmbH & Co, Weesp, The Netherlands). Fertilized eggs were collected within 20 minutes of fertilization. Eggs and larvae were kept at 28°C in embryo medium which was refreshed daily. Exposure experiments were performed at room temperature.

7.4.3 Blood sampling

To develop a method for blood sampling from zebrafish larvae at 5 dpf, larvae were washed with embryo medium using Netwell insert filters (Corning Life Sciences B.V., Amsterdam, The Netherlands) and transferred to a microscope slide coated with agarose. Larvae were not anaesthetized to prevent decreased blood flow, instead superficial drying with soft lens paper prevented movement.

Sampling was performed using a needle pulled by a micropipette puller (Sutter Instruments, Novato, California, USA) from a 0.75 mm borosilicate glass capillary (Sutter Instruments, Novato, California, USA) without filament, positioned in a micromanipulator (World Precision Instruments, Berlin, Germany), connected to a manual CellTram Vario oil pump (Eppendorf Nederland B.V., Nijmegen, The Netherlands), under 20x magnification (Leica, Amsterdam, The Netherlands). After decapitation or tail cut were found to result in limited yields, direct sampling from the circulation was explored. To identify the most suitable location, sampling from different anatomical locations was tested[21] including the heart, the dorsal aorta, the caudal vein, and the posterior cardinal vein.

An image was taken from each blood sample in the needle to determine the sample volume. The image analysis program Fiji[22] was used to calculate the volume of the blood sample within the needle with the volume formula of a truncated cone (Equation 1).

$$V = \frac{1}{3}\pi \cdot (r_1{}^2 + r_1 r_2 + r_2{}^2) \cdot \frac{h}{\cos 45^\circ} \quad (1)$$

where r_1 and r_2 are the upper and lower radii of the blood sample in the pulled needle and h is the length of the blood sample within the needle taking into account the 45° angle of the needle in respect to the microscope. After the blood sample was imaged, it was injected into a 2 µL droplet of heparin solution (5 IE/mL) under microscope both to prevent coagulation and for sample handling. Sample replicates consisted of blood samples from 15-35 larvae to reach measurable levels, of which the total number depended on experimental and time constraints, and were pooled into a 0.5 mL Eppendorf tube and stored at-80°C.

7.4.4 Measurements of paracetamol and its metabolites

On the day of measurement, blood samples were thawed and 200 µL methanol with paracetamol-D4 internal standard (1.4 pg/µL) was added. Samples were centrifuged (16,000g, 10 minutes) and 180 µL supernatant was transferred to a 0.5 mL Eppendorf tube to be evaporated by vacuum centrifuge (Beun-de Ronde, Abcoude, The Netherlands) until dry. Samples were reconstituted in 10 µL 80/20 (v/v) purified water/methanol and transferred to an LC-MS vial for randomized injection of 7 µL into the ultra-performance liquid chromatography system (Acquity, Waters Chromatography B.V., Etten-Leur, The Netherlands) linked to a quadrupole-ion trap MS-MS (QTRAP-6500, AB Sciex B.V., Nieuwekerk aan den IJssel, The Netherlands). An electrospray ionization source in positive (paracetamol) and negative (paracetamol-glucuronide and paracetamol-sulfate) mode was used as published before[10,12]. Method

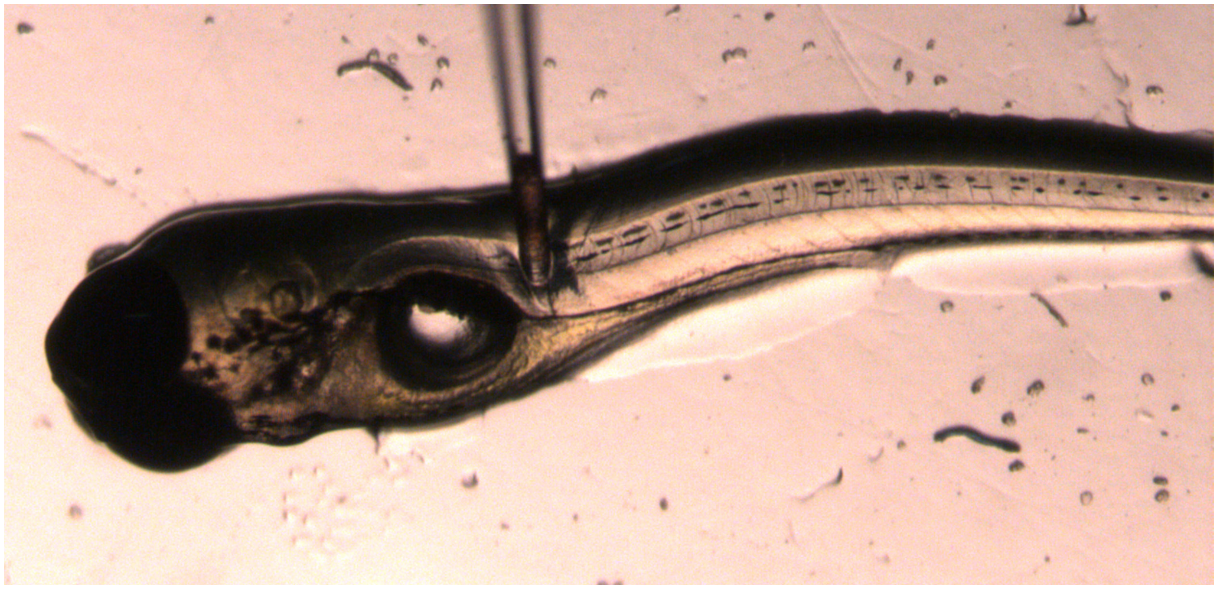

Figure 7.1 Blood sampling from the posterior cardinal vein in a zebrafish larva at 5 days post fertilization using a pulled needle. Blood sample is shown in needle tip. Supplementary Video shows the full procedure.

criteria were 90-100% accuracy and a precision corresponding to a relative standard deviation less than 10%. Lower limit of quantification (LLOQ) in blood samples was 0.05 pg/uL for paracetamol and paracetamol-sulfate, and 5 pg/uL for paracetamol-glucuronide.

The homogenate samples were measured as described before[10,12]. LLOQ in homogenates was 0.09 pg/uL for paracetamol and paracetamol-sulfate, and 9.0 pg/uL for paracetamol-glucuronide. Of the wash-out medium of the second experiment, samples of 1850 µL were collected and stored at-80°C. On the day of measurement, samples were thawed, 10 µL 125 pg/µL paracetamol-D4 internal standard was added and samples were evaporated by vacuum centrifuge until dry. Samples were reconstituted in 50 µL purified water, centrifuged (16,000g, 15 minutes), and 25 µL supernatant was transferred to an LC-MS vial for randomized injection of 5 µL into the LC-MS system as described above. Background measurement of the wash-out medium at t=60 was subtracted from the sample measurements. A calibration curve ranging from 0.05-100 pg/µL was prepared in 50/50 (v/v) methanol/purified water and was used to calculate compound excreted amounts in pmole/larva. LLOQ in wash-out medium was 0.05 pg/uL for paracetamol and paracetamol-sulfate, and 5 pg/uL for paracetamol-glucuronide.

7.4.5 Pharmacokinetic data analysis

A pharmacokinetic model was developed for paracetamol and its metabolites using non-linear mixed effects modelling. NONMEM (version 7.3)[23] was used through interfaces Pirana (version 2.9.6)[24] and PsN (version 4.7.0)[25], and graphical output was created using R (version 3.4.2)[26] through the Rstudio interface (version 1.1.383, RStudio Inc, Boston, Massachusetts, USA). The First Order Conditional Estimation algorithm was used.

A zero-order absorption rate constant was estimated to quantify paracetamol absorption from the surrounding medium, as we have earlier shown that paracetamol concentrations in the treatment medium remain constant during the experiments[12]. One and two compartment models were tested for the distribution of each compound. Linear and non-linear metabolic clearance for paracetamol was tested, including one and two substrate Michaelis Menten kinetics[27], the latter of which was used to account for possible saturation of the sulfation pathway caused by depletion of the sulfate group donor 3'-phosphoadenosine 5'-phosphosulfate (PAPS)[28]. Lastly, time-dependent metabolism using both exponential and sigmoidal relationships were tested[29]. First-order rates of excretion into medium with or without recovery fractions were estimated per compound.

Because of the destructive sampling, inter-individual variability could not be distinguished from residual variability, therefore only the latter was estimated, using an additive, proportional, or a combination of additive and proportional per compound per sample type. Level 2 covariance between the residual error for compounds measured in the same sample was tested[30]. All compounds had less than 10% of data points below the limit of quantification, with the sole exception of paracetamol-glucuronide in blood samples (71%), warranting the M2 method of ignoring these values in the analysis[31].

Model selection was based on the likelihood ratio test between nested models, using a drop in objective function value of 6.63 between nested models to indicate statistical significance, corresponding with $p < 0.01$ assuming a χ^2 distribution. Additionally, physiological plausibility of parameter estimates and goodness-of-fit plots were assessed[32]. Structural parameter precision was considered acceptable when relative standard errors (RSE) were below 50%.

7.4.6 Comparison of absolute clearance and distribution volume of paracetamol to higher vertebrates

The estimate of absolute paracetamol clearance was compared to values reported in higher vertebrates as previously published[10], as was the estimate of the distribution volume. For the latter, similar to the comparison of clearance values, a literature search was performed in PubMed using "distribution volume OR volume of distribution AND paracetamol OR acetaminophen". Only values published in the last 20 years were included. Values obtained from specific disease models, from combination treatment, or from obese patients, and from models with more than one compartment for paracetamol distribution were excluded. A regression through the log transformed parameter values based on log transformed bodyweight was calculated including 95% confidence interval using R (v.3.4.2)[26] through user interface Rstudio (v.1.1.383, RStudio Inc, Boston, Massachusetts, USA). This regression was based on data from mature individuals only, comparable to that of paracetamol clearance. The bodyweight of the larvae was calculated from their previously published volume[13] and an assumed density of 0.997 g/mL, corresponding to that of water[10].

7.4.7 Materials

Paracetamol, paracetamol-glucuronide, paracetamol-sulfate, and paracetamol-D4 internal standard were acquired from Sigma (Sigma-Aldrich Chemie B.V., Zwijndrecht, The Netherlands). Heparin was acquired from Academic Hospital Pharmacy Leiden (LUMC, Leiden, The Netherlands). Embryo medium consisted of demineralized water containing 60 µg/mL Instant Ocean sea salts (Sera, Heinsberg, Germany). Agarose was acquired from Sphaero Q (Gorinchem, The Netherlands). UPLC-MS grade methanol was acquired from Biosolve (Biosolve B.V., Valkenswaard, The Netherlands). PURELAB (Veolia Water Technologies B.V., Ede, The Netherlands) was used to purify water.

7.5 Results

7.5.1 Blood sampling

From the different anatomical locations, the posterior cardinal vein proved most efficient for blood sampling and resulted in a median volume of 1.12 nL per larva with an interquartile range of 0.676-1.66 nL. Figure 7.1 and Supplementary Video show an image of this procedure. The sample volume was determined based on a separately captured image of the blood sample within the needle. Supplementary Table S7.1 lists the number blood samples that were pooled for each sampling time point.

7.5.2 Measurement of paracetamol and metabolites

Paracetamol, paracetamol-glucuronide, and paracetamol-sulfate could be measured in the blood samples, of which representative chromatograms are shown in Supplementary Figure S7.1. The symbols in Figure 7.2 show paracetamol and metabolite concentrations and total amounts in blood samples, and in homogenates and wash-out medium, respectively. Although the data are variable, clear trends can be observed. The paracetamol and metabolite concentrations (top panel) could be measured in

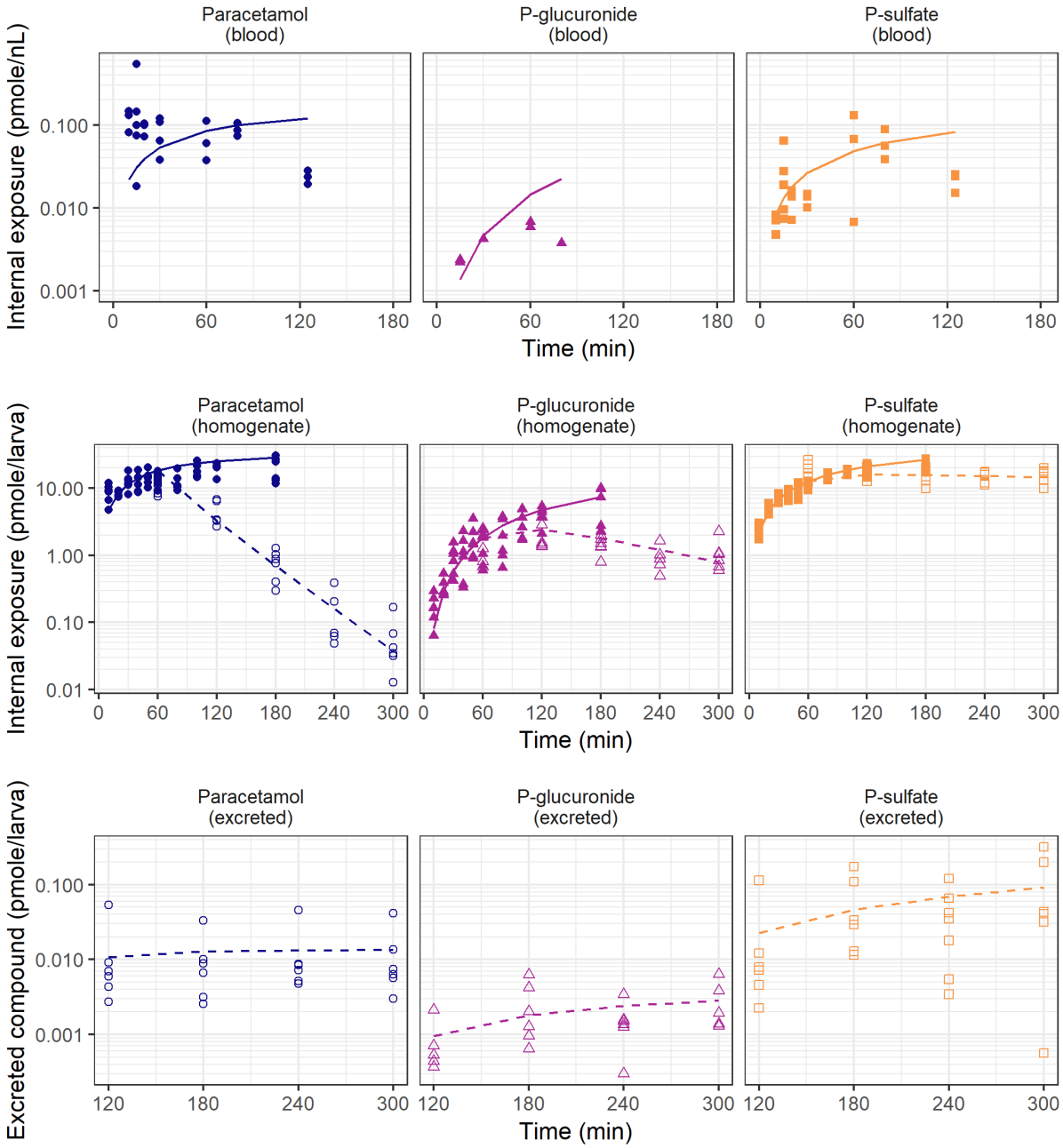

Figure 7.2 Paracetamol (blue circles, left column), paracetamol-glucuronide (magenta triangles, middle column), and paracetamol-sulfate (orange squares, right column) observations in blood samples (top row, concentrations) as well as in homogenates (middle row, amounts), and excreted into medium (bottom row, amounts) after constant waterborne treatment (solid symbols) and wash-out (open symbols) experiments. Blood concentrations are shown in pmole/nL (mM). The model prediction is shown as solid or dotted line for the constant waterborne treatment or wash-out experiment, respectively. The lower number of data points of paracetamol-glucuronide is explained by its LLOQ being higher than that of the other compounds. Paracetamol observations in homogenates have been reported previously[12].

the nanoscale blood samples and show that sulfate metabolite is reaching similar concentrations as the parent, while concentrations of the glucuronide metabolite are about tenfold lower. This is similar to the observations in homogenates (middle panel). Paracetamol concentrations reach a steady state value around 0.1 mM or 15 mg/L, which is 10% of the paracetamol concentration in the treatment medium. The paracetamol amounts in larval homogenate from the wash-out experiment (open symbols) show a mono-exponential decline of paracetamol. For the metabolites, the wash-out experiment shows an increase in internal amounts between 60 and 120 minutes, after which paracetamol-glucuronide decreases to 1 pmole/larva and paracetamol-sulfate stabilizes between 10 and 20 pmole/larva at 300 minutes. The amounts of paracetamol, paracetamol-glucuronide, and paracetamol-sulfate excreted into

the medium during the wash-out experiment are shown in Figure 7.2, bottom panel. These data show low values with high variability, and a minor increase over the wash-out period.

7.5.3 Pharmacokinetic data analysis

Figure 7.3 shows a schematic representation of the developed parent-metabolite model for paracetamol. A model with zero-order absorption and one compartment per compound best fitted the data. The formation of paracetamol-glucuronide was best described with a first-order metabolic formation rate, while the paracetamol sulfation rate could not be captured with a zero- or first-order metabolic formation rate, as both methods lead to under-predictions at earlier time points and over-prediction at later time points. Conventional Michaelis Menten kinetics depending on parent compound concentrations could not be identified for paracetamol-sulfate, neither could a two-substrate Michaelis Menten kinetic model, which represents the potential rate limiting influence of depletion of the sulfate-group donor as well. Regarding functions based on time-related changes in sulfation rate, a sigmoidal function as described by Equation 2 was statistically significantly better than an exponentially declining time-dependent sulfation rate and provided the best fit:

$$k_{PS,f} = k_{PS,f,0} \cdot \left(1 - \frac{t}{t + t_{50}}\right) \quad (2)$$

where $k_{PS,f}$ is the metabolic formation rate for sulfation in min^{-1}, $k_{PS,f,0}$ is the metabolic formation rate for sulfation at time point 0 in min-1, t is the time in min, and t_{50} is the time in min at which the formation rate for the sulfate metabolite is at 50% of its value at time 0.

The excretion of paracetamol and its metabolites was best captured with a first-order rate constant. A recovery fraction on the excreted paracetamol and metabolite amounts was included to prevent overestimation of the excreted compounds, which resulted in a significantly improved fit both graphically and statistically. Figure 7.4 shows the paracetamol clearance over time as sum of the constant metabolic formation rate for glucuronidation, the excretion rate, and the time-dependent metabolic formation rate for sulfation according to the model.

Residual variability for homogenate samples was found to be best described with a combination of additive and proportional error for paracetamol and paracetamol-glucuronide and with a proportional error for paracetamol-sulfate, including covariance between the proportional errors of paracetamol

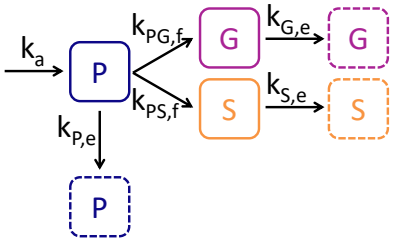

Figure 7.3 Schematic representation of the structural pharmacokinetic model of paracetamol and its metabolites in zebrafish larvae. Compartments depicted with solid lines represent compartments in which both amounts in homogenized larvae or blood concentrations in larvae were available, Compartments indicated with dashed lines represent compartments in which excreted amounts in the medium were available. P = paracetamol, P_G = paracetamol-glucuronide, P_S = paracetamol-sulfate, k_a = absorption rate constant, $k_{PG,f}$ = metabolic formation rate of glucuronidation, $k_{PS,f}$ = metabolic formation rate for sulphation, $k_{P,e}$ = paracetamol excretion rate, $k_{PG,e}$ = paracetamol-glucuronide excretion rate, $k_{PS,e}$ = paracetamol-sulfate excretion rate.

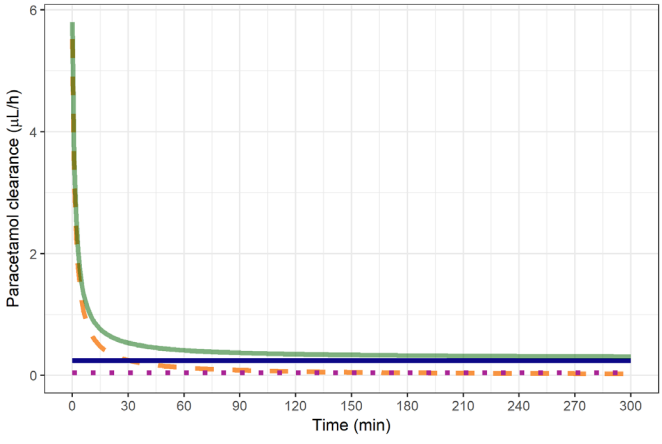

Figure 7.4 Paracetamol clearance over time. Total clearance (transparent green solid line) is the sum of the time-dependent metabolic formation rate for sulphation (orange dashed line), the metabolic formation rate for glucuronidation (magenta dotted line) and the unchanged excretion rate (blue solid line).

and paracetamol-glucuronide, and between the proportional errors of paracetamol-glucuronide and paracetamol-sulfate. Residual variability for blood samples was best described with an additive error for paracetamol, and proportional errors for paracetamol-glucuronide, and for paracetamol-sulfate. The residual variability for medium samples was best described by an additive error for paracetamol, a proportional error for paracetamol-glucuronide, and a combination of additive and proportional for paracetamol-sulfate.

The model predictions (lines) relative to the observed values (symbols) are shown in Figure 7.2 and show

Table 7.1 Parameter estimates for the final model.

	Parameter value	**RSE (%)**
Structural parameters		
k_a (pmole/min)	0.760	6
$k_{PG,f}$ (min^{-1})	0.00327	10
$k_{PS,f,0}$ (min^{-1})	0.422	57
t_{50} (min)	1.42	70
$k_{P,e}$ (min^{-1})	0.0185	10
$k_{G,e}$ (min^{-1})	0.00743	17
$k_{S,e}$ (min^{-1})	0.000664	66
V_P (nL)	218	24
V_G (nL)	125	25
V_S (nL)	262	20
$f_{P,e}$ (%)	0.113	26
$f_{G,e}$ (%)	0.0900	24
$f_{S,e}$ (%)	3.74	71
Stochastic parameters homogenate		
Variance of paracetamol proportional residual error (-)	0.191	17
Variance of paracetamol-glucur. proportional residual error (-)	0.279	17
Variance of paracetamol-sulf. proportional residual error (-)	0.0521	29
Correlation of paracetamol and paracetamol-glucur. proportional error (-)	-0.220	13[a]
Correlation of paracetamol-glucur. and paracetamol-sulf. proportional error (-)	-0.0358	15[a]
Variance of paracetamol additive residual error (pmole/larva)	0.00461	93
Variance of paracetamol-glucur. additive residual error (pmole/larva)	0.0131	71
Stochastic parameters blood		
Variance of paracetamol additive residual error (pmole/nL)	0.0148	70
Variance of paracetamol-glucur. proportional residual error (-)	0.393	50
Variance of paracetamol-sulf. proportional residual error (-)	0.994	33
Stochastic parameters excreted compound		
Variance of paracetamol additive residual error (pmole/larva)	0.000207	41
Variance of paracetamol-glucur. proportional residual error (-)	0.678	23
Variance of paracetamol-sulf. proportional residual error (-)	0.941	47
Variance of paracetamol-sulf. additive residual error (pmole/larva)	0.00113	110

V_P = paracetamol distribution volume, V_G = paracetamol-glucuronide distribution volume, V_S = paracetamol-sulfate distribution volume, $f_{P,e}$ = recovery fraction excreted paracetamol, $f_{G,e}$ = recovery fraction excreted paracetamol-glucuronide, $f_{S,e}$ = recovery fraction excreted paracetamol-sulfate, RSE = relative standard error, see Equation 2 and Figure 7.3 for further details. [a]RSE of the estimate for covariance.

a good description of the data. Table 7.1 contains the parameter estimates including relative standard error as measure of their precision of the final model. Relative standard errors for structural parameters were acceptable. Additional goodness-of-fit-plots, showing good model accuracy, can be found in (Supplementary Figure S7.2-4). The final model code and dataset are available through the DDMoRe Repository, Model ID DDMODEL00000300.

7.5.4 Comparison of absolute clearance and distribution volume of paracetamol to higher vertebrates

A correlation between paracetamol clearance and bodyweight in 12 higher vertebrates, including humans, has been reported before (calculated exponent = 0.78, 95% confidence interval: 0.65-0.91, R^2 = 0.90)[10,12]. Paracetamol clearance estimated from homogenate data alone, assuming homogenous distribution of the drug throughout the whole larvae, fell outside of the 95% confidence interval of this correlation[12]. Here, absolute paracetamol clearance is estimated by simultaneously modelling observed concentrations from blood samples, which could be quantified as the result of the blood sampling method developed here, and observed internal amounts from homogenates. Figure 7.5 shows the estimated absolute paracetamol clearance of the zebrafish larva in relation to that of 12 higher vertebrates. Because of the time-dependent metabolic formation rate for sulfation, the full range from paracetamol clearance at t=0 (solid square) to paracetamol clearance at t=∞ (open square) is shown. This range is partly within the 95% confidence interval. Noticeably, clearance values from higher immature vertebrates are also over-predicted by the correlation based on the values reported for mature organisms.

The literature search resulted in reported values for the distribution volume of paracetamol in 13 higher vertebrates, which are provided with their references in (Supplementary Table S7.2). A correlation between the distribution volume of paracetamol and bodyweight based on data obtained from mature individuals of the higher vertebrates only, is shown in Figure 7.6 (dashed line including 95% confidence interval). The exponent in this relationship was calculated to be 0.94 (95% confidence interval: 0.67-1.2, R^2 = 0.68). Although five orders of magnitude removed from the smallest higher vertebrate, the

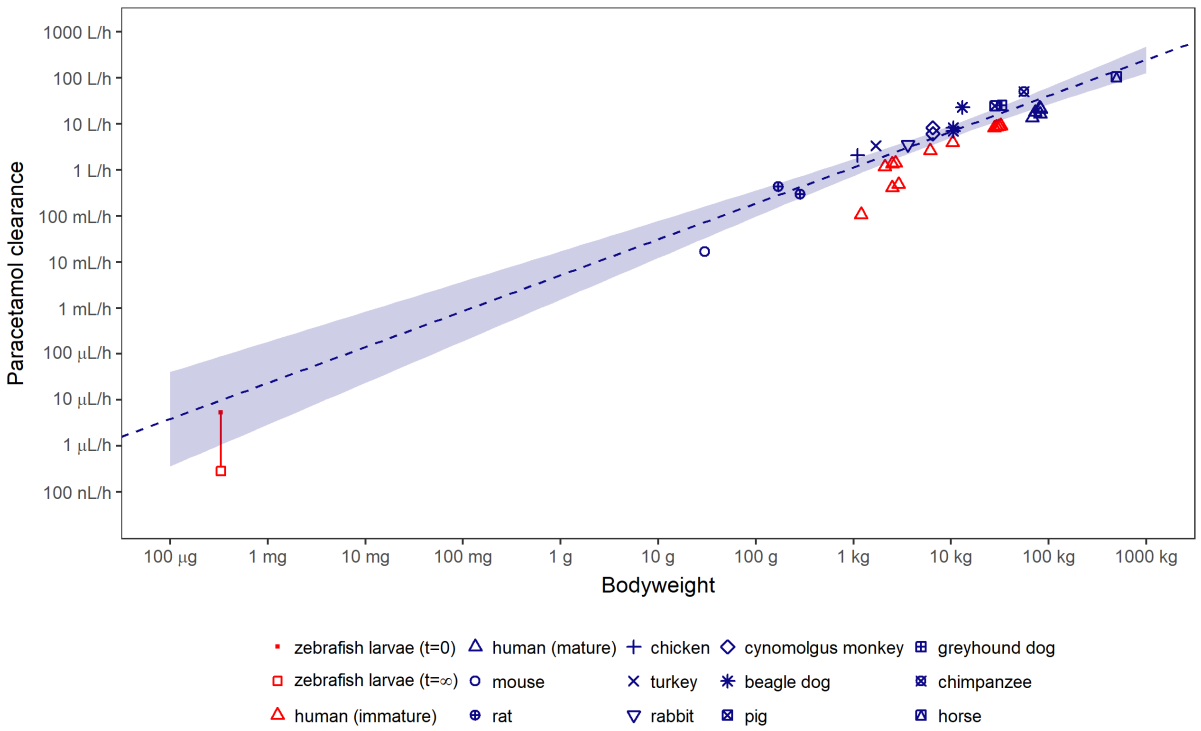

Figure 7.5 Relationship between paracetamol clearance and bodyweight of 13 vertebrate species. Clearance in zebrafish larvae at five days post fertilization is depicted as the clearance value at t=0 (closed square) and t= ∞ (open square), with the vertical line depicting the range in clearance over time. Mature individuals shown in blue, immature individuals in red. The correlation (dashed line, shaded area: 95% confidence interval) is based on values from mature individuals of the higher vertebrates only. Adapted with permission from Kantae et al.[10].

distribution volume of paracetamol in zebrafish larvae lies well within the 95% confidence interval of the correlation between distribution volume and bodyweight. Even though the values from immature organisms are not taken into account for the correlation between the distribution volume of paracetamol and bodyweight, the data points are in agreement with that correlation.

7.6 Discussion

Mechanistic and quantitative characterisation of pharmacokinetics in zebrafish larvae is crucial for this vertebrate model organism to deliver on its promising role in pharmacological research. To date, a method to take blood samples, which are essential to characterize pharmacokinetics, was lacking. The quantification of absolute clearance and also distribution volume in zebrafish larvae, needed for reliable extrapolation of pharmacokinetics between species, required measurements of these blood concentrations in addition to knowing drug amounts in larval homogenates as determinant of the bioavailable dose. This is analogous to the well-known requirement of knowing both blood concentrations and absolute administered drug amounts by intravenous drug administration, to quantify absolute pharmacokinetic parameters of extravascular administered drugs. Additionally, confirmation of functional drug metabolism is of importance, because drug metabolites can be pharmacologically active or toxic.

We report, for the first time, a method for nanoscale blood sampling from zebrafish larvae at 5 dpf, in which not only the paradigm compound paracetamol was measured, but also its two major metabolites. Absolute clearance of paracetamol in zebrafish larvae correlated reasonably well with those reported in higher vertebrates. Results from our study suggest that, in addition to the presence of genetic homology for the enzymatic systems established before[4], also functionally these metabolic pathways behave similarly to higher vertebrates, as both metabolites are present. Quantitatively, the ratio between the two metabolites was different from those reported in mature humans[33]. Paracetamol-sulfate proved to

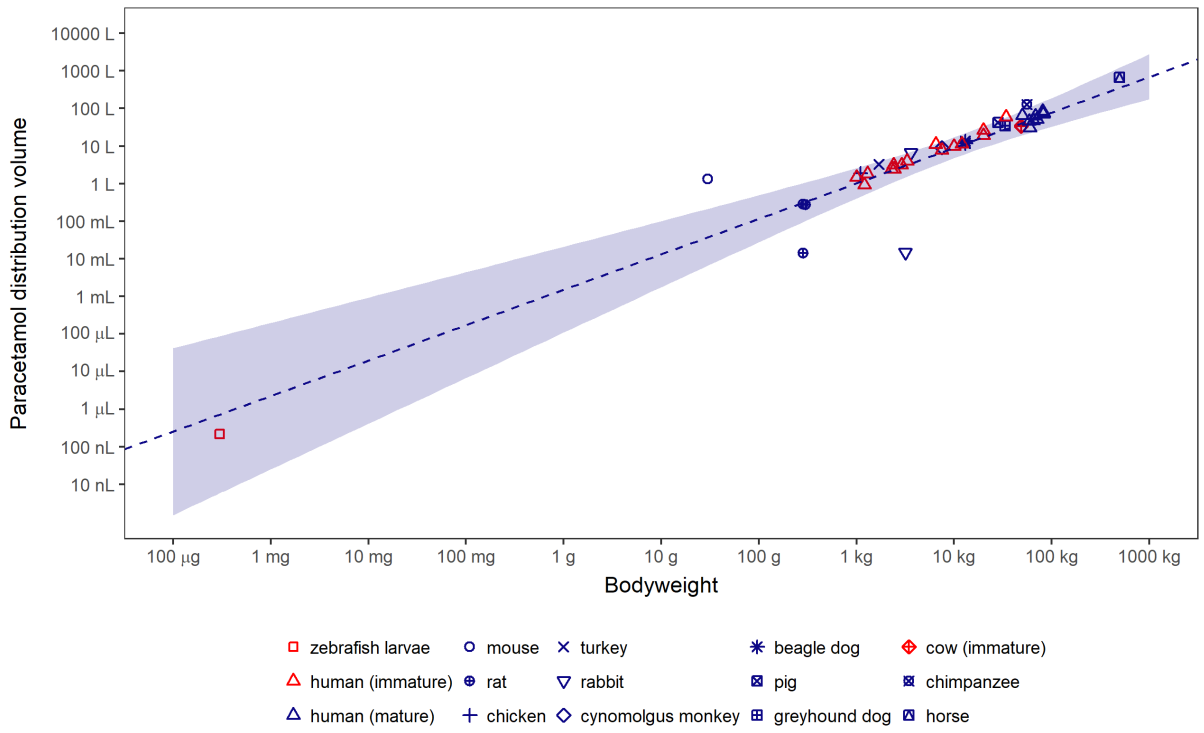

Figure 7.6 Relationship between distribution volume of paracetamol and bodyweight of 14 vertebrate species, including zebrafish larvae at five days post fertilization. Mature individuals shown in blue, immature individuals in red. The correlation (dashed line, shaded area: 95% confidence interval) is based on values from mature individuals in higher vertebrates only. Raw data can be found in (Supplementary Table S7.2).

be the major metabolite at this larval stage with respect to paracetamol-glucuronide. A similar profile, however, has been shown in human newborns and infants, resulting from limited glucuronidation capacity which increases with increasing age[34,35]. This is not unexpected, as zebrafish larvae have also not reached maturity. Consequently, the impact of enzymatic maturation needs to be taken into account when translating results from immature zebrafish larva to mature individuals of higher vertebrates.

Metabolic formation rate for sulfation could not be accurately captured using time-constant parameters. A conventional Michaelis-Menten model could not accurately describe the observed pharmacokinetic profiles. Therefore, a two-substrate Michaelis-Menten kinetic model was tested, accounting for both the concentrations of the substrate paracetamol and a hypothetical donor group, representing the sulfate group donor 3'-phosphoadenosine 5'-phosphosulfate (PAPS) which may limit the biotransformation[28,36,37]. The data however did not allow for reliable and stable estimation of the relevant model parameters. Therefore, an empiric time-dependent function was tested, with a sigmoidal time-dependent metabolic formation rate resulting in the best fit, but with relatively high RSE values of the estimated parameters. Normalization of the metabolic formation rate for sulfation at time point 0, $k_{PS,f,0}$, at a different time point, reduced its RSE value below 50%, indicating no over-parameterization[38]. Supplementary Figure S7.5) shows the paracetamol-sulfate fit of the metabolite model, in which the time-dependent metabolic formation rate for sulfation was replaced by a time-constant first-order rate. The parameters of that model are estimated with acceptable precision (RSE < 50%), but a clear misfit of the paracetamol-sulfate data can be observed. The low t_{50} estimate resulted in a steep decline of sulfation in the first minutes of the experiment (Figure 7.4). We believe this function represents the impact of depletion of the sulfate group donor PAPS on the metabolic formation rate, as the shape of this curve is similar to the shape of simulated PAPS levels from a reported physiological mathematical model at cellular level[28]. As time approached infinity, sulfation nears the asymptote of zero metabolic formation rate. This is unlikely, as for example the sulfate group donor PAPS is expected to be produced by the organism at a constant rate, but this production rate could not be estimated with the current data and timescale[28]. Consequently, interpretation of this model is limited to the time course presented here.

The availability of blood concentrations in addition to absolute internal amounts, allowed for the estimation of absolute values for distribution volume for both the parent and the major metabolites, which is unique. Figure 7.2 shows variable data yielded from extremely small samples and low concentrations, however, this did not limit accurate estimation of distribution volumes as indicated by RSE values being 25% or lower. The estimated distribution volume of paracetamol in zebrafish larvae correlated well with those reported in higher vertebrates. The estimated distribution volume for the glucuronide and sulfate metabolite is 0.6x and 1.2x the distribution volume of paracetamol, respectively. Reported values show large variability and range from 0.2-1.6x that of paracetamol for paracetamol glucuronide, and 0.09-0.9x that of paracetamol for paracetamol-sulfate in humans[17,39–41], and 1.2-2.7x for paracetamol glucuronide, and 0.25-1.5 for paracetamol-sulfate in rats[15,42]. These values are in line with our estimates, but care must be taken when interpreting these data. Determining distribution volume of drug metabolites had to be done in patients which all had specific conditions which also impacted normal physiology. In the zebrafish, the total amounts necessary were readily available for that determination.

The developed method of blood sampling results in blood samples at the nanolitre scale. Multiple blood samples have to be pooled into a single analytical replicate to quantify drug and metabolite concentrations by conventional LC-MS. To improve throughput and efficiency, nano-electrospray ionization mass spectrometry could be considered[43]. This technique directly injects a sample of sub nanolitre volumes together with ionization solvent into an electron spray ionization source and has for instance been used to sample and quantify the anti-cancer drug tamoxifen concentrations in individual cancer cells[44]. Currently, the high-throughput potential in zebrafish larvae for the purpose of obtaining absolute pharmacokinetic parameter values required for interspecies scaling is limited by the practicalities of the blood sampling and by the need for the development of highly sensitive analytical

methods for these samples. We however envision that this step is only performed for promising drug candidates that have been selected for further development. Additionally, microinjection of zebrafish zygotes and embryos has been automated, resulting in higher throughput[45,46]. This technique might in the future also be applicable to sampling.

We have confirmed that the paracetamol metabolites are formed by metabolizing enzymes of the zebrafish larvae and not by metabolizing enzymes of the microbiota, by repeating the experiment with germ-free larvae that lack microbiota (data not shown). To establish whether paracetamol-glucuronide and paracetamol-sulfate were the major metabolites in zebrafish, other metabolites were identified and measured by LC-MS. Two minor metabolites, 3-methoxy-paracetamol and n-acetylcysteine-paracetamol, were detected around or below the limit of quantification resulting in negligible impact on the mass balance.

Low fractions of paracetamol and its metabolites excreted according to the model were recovered in the wash-out experiment, for which an empirical recovery fraction was estimated. This might be due to adhesion of these compounds to the wells. Moreover, the accuracy of the measurements of the excreted amounts may be negatively impacted by measurements being close to the limit of quantification. A sensitivity analysis excluding these measurements showed similar parameter estimates, suggesting negligible impact of these data on the final model outcome.

Limitations in estimating distribution volume and thereby absolute clearance values are overcome by having measurements of both drug concentrations in the blood as well as total amounts in the larvae. It is however not clear whether this approach will also be applicable to study the pharmacokinetics of lipophilic drugs, as these drugs may be more difficult to wash off the larvae due to skin adhesion, which complicates measurements of total internal amounts. However, alternative methods for oral dosing using nanoparticles might provide a solution for this limitation.

In conclusion, an improved understanding of pharmacokinetics in the vertebrate model organism zebrafish larva is presented. Based on the developed method to sample blood from these larvae, absolute clearance resulting from different metabolic routes, as well as distribution could be quantified for the paradigm compound paracetamol. A comparison of the estimated absolute clearance and distribution volume with those reported for higher vertebrates shows a good correlation. This improved confidence in the translational value of the zebrafish can contribute to the role of this small vertebrate in drug discovery and development.

7.7 Acknowledgement

The authors thank Sebastiaan Goulooze for code-review of the R- and NONMEM-scripts, Bjørn Koch for his assistance in the germ-free experiments, and Parth Upadhyay for proofreading the manuscript.

7.8 Data availability statement

Supplementary Video of the nanoscale blood sampling is publicly available through the journal website (http://jpet.aspetjournals.org/content/371/1/15/tab-figures-data).
The full dataset and model file are publicly available through the DDMoRe Repository, Model ID DDMODEL00000300 (http://repository.ddmore.foundation/model/DDMODEL00000300).

7.9 References

1. Zon LI, Peterson RT. In vivo drug discovery in the zebrafish. Nat Rev Drug Discov. 2005;4(1):35-44.
2. MacRae CA, Peterson RT. Zebrafish as tools for drug discovery. Nat Rev Drug Discov. 2015;14(10):721-

731.
3. Howe K, Clark MD, Torroja CF, et al. The zebrafish reference genome sequence and its relationship to the human genome. Nature. 2013;496:498-503.
4. Van Wijk RC, Krekels EHJ, Hankemeier T, et al. Systems pharmacology of hepatic metabolism in zebrafish larvae. Drug Discov Today Dis Model. 2016;22:27-34.
5. Schulthess P, Van Wijk RC, Krekels EHJ, et al. Outside-in systems pharmacology combines innovative computational methods with high-throughput whole vertebrate studies. CPT Pharmacometrics Syst Pharmacol. 2018;7:285-287.
6. Diekmann H, Hill A. ADMETox in zebrafish. Drug Discov Today Dis Model. 2013;10(1):e31-e35.
7. Morgan P, Van der Graaf PH, Arrowsmith J, et al. Can the flow of medicines be improved? Fundamental pharmacokinetic and pharmacological principles toward improving Phase II survival. Drug Discov Today. 2012;17(9/10):419-424.
8. Kühnert A, Vogs C, Altenburger R, et al. The internal concentration of organic substances in fish embryos- a toxicokinetic approach. Environ Toxicol Chem. 2013;32(8):1819-1827.
9. Vogs C, Kühnert A, Hug C, et al. A toxicokinetic study of specifically acting and reactive organic chemicals for the prediction of internal effect concentrations in scenedesmus vacuolatus. Environ Toxicol Chem. 2015;34(1):100-111.
10. Kantae V, Krekels EHJ, Ordas A, et al. Pharmacokinetic modeling of paracetamol uptake and clearance in zebrafish larvae: Expanding the allometric scale in vertebrates with five orders of magnitude. Zebrafish. 2016;13(6):504-510.
11. Kühnert A, Vogs C, Aulhorn S, et al. Biotransformation in the zebrafish embryo – temporal gene transcription changes of cytochrome P450 enzymes and internal exposure dynamics of the AhR binding xenobiotic benz[a]anthracene. Environ Pollut. 2017;230:1-11.
12. Van Wijk RC, Krekels EHJ, Kantae V, et al. Impact of post-hatching maturation on the pharmacokinetics of exogenous compounds in zebrafish larvae. Sci Rep. 2018;9:2149.
13. Guo Y, Veneman WJ, Spaink HP, et al. Three-dimensional reconstruction and measurements of zebrafish larvae from high-throughput axial-view in vivo imaging. Biomed Opt Express. 2017;8(5):2611-2634.
14. Neirinckx E, Vervaet C, Boever S De, et al. Species comparison of oral bioavailability, first-pass metabolism and pharmacokinetics of acetaminophen. Res Vet Sci. 2010;89(1):113-119.
15. Lee S, An J, Lee H, et al. Evaluation of pharmacokinetic differences of acetaminophen in pseudo germ-free rats. Biopharm Drug Dispos. 2012;33:292-303.
16. Janus K, Grochowina B, Antoszek J, et al. The effect of food or water deprivation on paracetamol pharmacokinetics in calves. J Vet Pharmacol Ther. 2003;26(4):291-296.
17. Owens K, Medlicott N, Zacharias M, et al. The pharmacokinetic profile of intravenous paracetamol in adult patients undergoing major abdominal surgery. Ther Drug Monit. 2012;34(6):713-721.
18. Van den Boom J, Heider D, Martin SR, et al. 3′-Phosphoadenosine 5′-phosphosulfate (PAPS) synthases, naturally fragile enzymes specifically stabilized by nucleotide binding. J Biol Chem. 2012;287(21):17645-17655.
19. Westerfield M. The zebrafish book. A guide for the laboratory use of sebrafish (Danio rerio). 4th ed. Eugene, OR, USA: University of Oregon Press; 2000.
20. EU. Council Directive 2010/63/EU on the protection of animals used for scientific purposes. Off J Eur Union. 2010;L276/33.
21. Isogai S, Horiguchi M, Weinstein BM. The vascular anatomy of the developing zebrafish: An atlas of embryonic and early larval development. Dev Biol. 2001;230(2):278-301.
22. Schindelin J, Arganda-Carreras I, Frise E, et al. Fiji: An open-source platform for biological-image analysis. Nat Methods. 2012;9(7):676-682.
23. Beal S, Sheiner L, Boeckmann A, et al. NONMEM 7.3.0 users guides. (1989-2013). ICON Development Solutions, Hanover, MD, USA.
24. Keizer R, Van Benten M, Beijnen J, et al. Pirana and PCluster: A modeling environment and cluster infrastructure for NONMEM. Comput Methods Programs Biomed. 2011;101(1):72-79.
25. Lindbom L, Pihlgren P, Jonsson E. PsNtoolkit — a collection of computer intensive statistical methods

for non-linear mixed effect modeling using NONMEM. Comput Methods Programs Biomed. 2005;79(3):241-257.
26. R Core Team. R: A language and environment for statistical computing. R Found Stat Comput Vienna, Austria. 2014.
27. Ingalls B. Mathematical modelling in systems biology: An introduction. Boston, MA, USA: The MIT Press; 2012.
28. Reddyhoff D, Ward J, Williams D, et al. Timescale analysis of a mathematical model of acetaminophen metabolism and toxicity. J Theor Biol. 2015;386:132-146.
29. Brochot A, Dunne A, Poggesi I, et al. Specifying models with time-dependent pharmacokinetic parameters in NONMEM. PAGE. 2011:Abstr 2176.
30. Karlsson MO, Beal SL, Sheiner LB. Three new residual error models for population PK/PD analyses. J Pharmacokinet Biopharm. 1995;23(6):651-672.
31. Beal SL. Ways to fit a PK model with some data below the quantification limit. J Pharmacokinet Pharmacodyn. 2001;28(5):481-504.
32. Nguyen THT, Mouksassi M-S, Holford N, et al. Model evaluation of continuous data pharmacometric models: metrics and graphics. CPT Pharmacometrics Syst Pharmacol. 2017;6:87-109.
33. Reith D, Medlicott NJ, Kumara De Silva R, et al. Simultaneous modelling of the Michaelis-Menten kinetics of paracetamol sulphation and glucuronidation. Clin Exp Pharmacol Physiol. 2009;36(1):35-42.
34. Krekels EHJ, Van Ham S, Allegaert K, et al. Developmental changes rather than repeated administration drive paracetamol glucuronidation in neonates and infants. Eur J Clin Pharmacol. 2015;71:1075-1082.
35. Anderson BJ, Van Lingen RA, Hansen TG, et al. Acetaminophen developmental pharmacokinetics in premature neonates and infants. Anesthesiology. 2002;96:1336-1345.
36. Slattery JT, Wilson JM, Kalhorn TF, et al. Dose-dependent pharmacokinetics of acetaminophen: Evidence of glutathione depletion in humans. Clin Pharmacol Ther. 1987;41(4):413-418.
37. Liu L, Klaassen CD. Different mechanism of saturation of acetaminophen sulfate conjugation in mice and rats. Toxicol Appl Pharmacol. 1996;139(1):128-134.
38. Goulooze SC, Völler S, Välitalo PAJ, et al. The influence of normalization weight in population pharmacokinetic covariate models. Clin Pharmacokinet. 2019;58(1):131-138.
39. Lowenthal DT, Oie S, Van Stone JC. Pharmacokinetics of acetaminophen elimination by anephric patients. J Pharmacol Exp Ther. 1976;196(3):570-578.
40. Van Rongen A, Välitalo PAJ, Peeters MY, et al. Morbidly obese patients exhibit increased CYP2E1-mediated oxidation of acetaminophen. Clin Pharmacokinet. 2016;55:833-847.
41. Owens K, Murphy P, Medlicott N, et al. Population pharmacokinetics of intravenous acetaminophen and its metabolites in major surgical patients. J Pharmacokinet Pharmacodyn. 2014;41:211-221.
42. Yamasaki I, Uotsu N, Yamaguchi K, et al. Effects of kale ingestion on pharmacokinetics of acetaminophen in rats. Biomed Res. 2011;32(6):357-362.
43. Fujii T, Matsuda S, Tejedor ML, et al. Direct metabolomics for plant cells by live single-cell mass spectrometry. Nat Protoc. 2015;10(9):1445-1456.
44. Ali A, Abouleila Y, Shimizu Y, et al. Single-cell screening of tamoxifen abundance and effect using mass spectrometry and raman-spectroscopy. Anal Chem. 2019;91:2710-2718.
45. Spaink HP, Cui C, Wiweger MI, et al. Robotic injection of zebrafish embryos for high-throughput screening in disease models. Methods. 2013;62(3):246-254.
46. Cordero-Maldonado ML, Perathoner S, Van der Kolk KJ, et al. Deep learning image recognition enables efficient genome editing in zebrafish by automated injections. PLoS One. 2019;14(1):e0202377.

7.10 Supplementary material

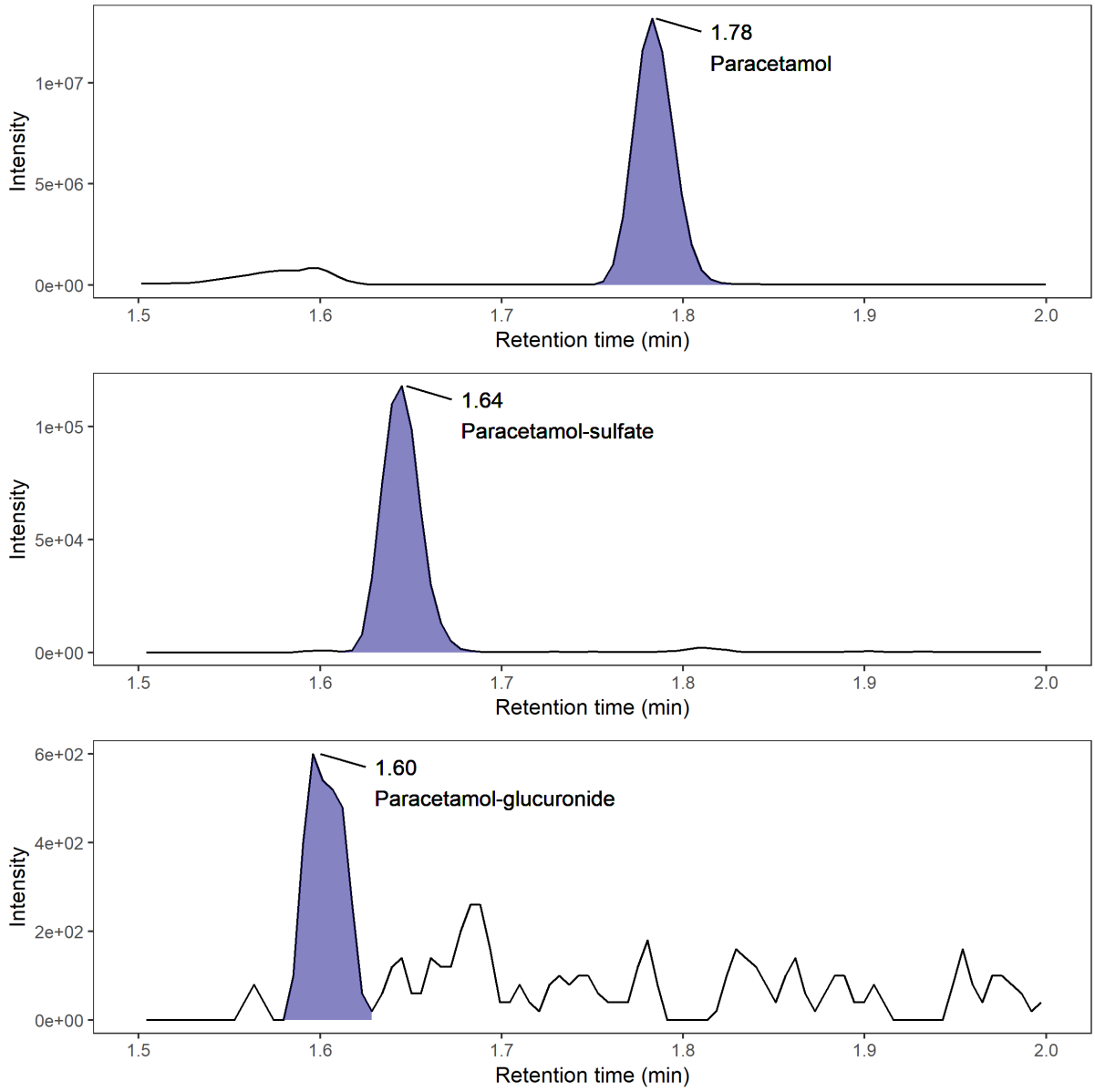

Supplementary Figure S7.1 Representative chromatograms of paracetamol (top), paracetamol-sulfate (middle), and paracetamol-glucuronide (bottom) peaks of a blood sample taken at 80 min. LC-MS separates overlapping peaks by mass difference.

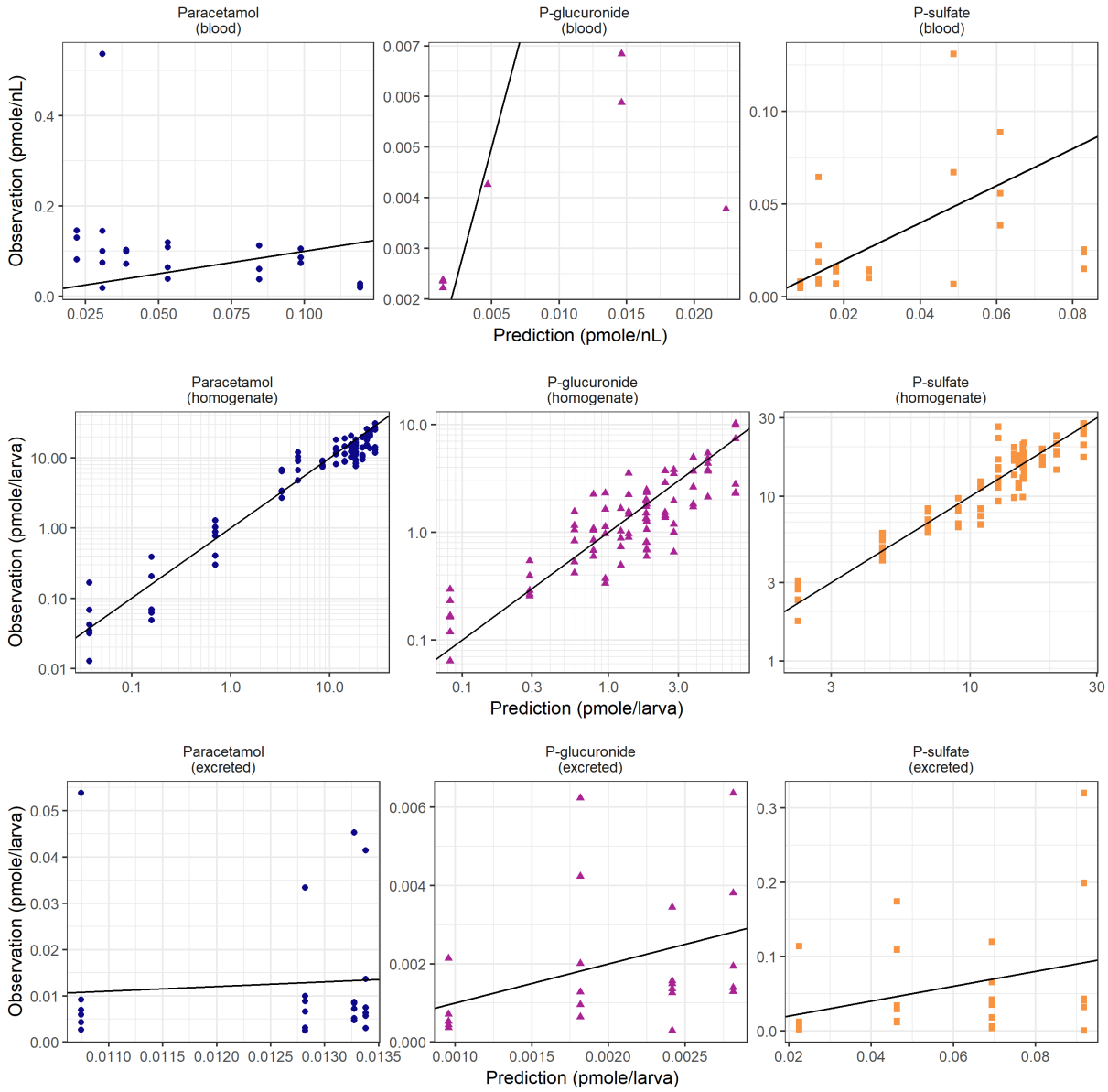

Supplementary Figures S7.2 Observed vs predicted observations for paracetamol (blue circles, left column), paracetamol-glucuronide (magenta triangles, middle column), and paracetamol-sulfate (orange squares, right column). Concentrations in blood samples (top row, concentrations), amounts in homogenates (middle row, amounts), and excreted amounts into medium (bottom row, amounts). The solid black line is line of unity.

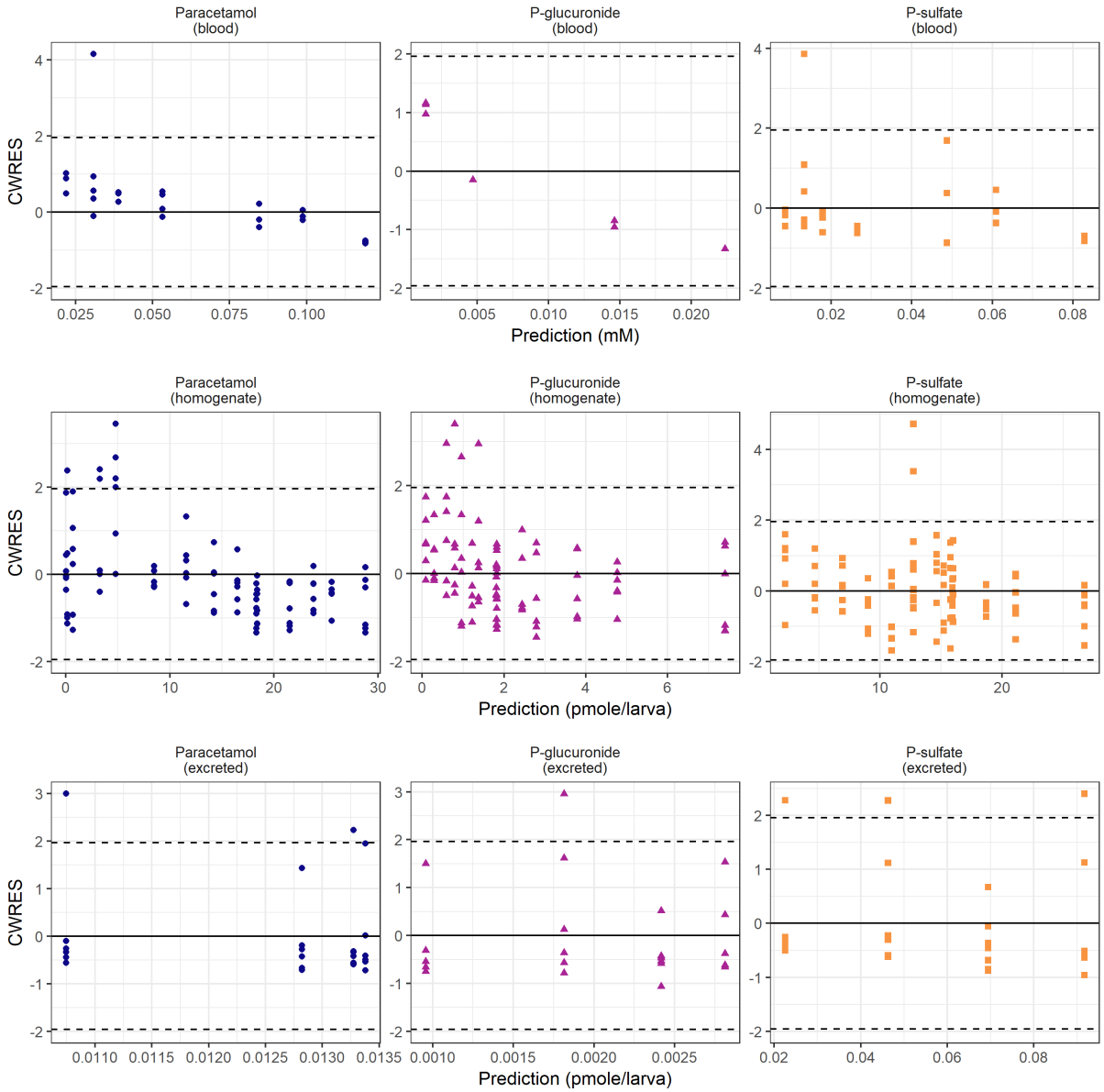

Supplementary Figure S7.3 Conditional weighted residuals (CWRES) vs time for paracetamol (blue circles, left column), paracetamol-glucuronide (magenta triangles, middle column), and paracetamol-sulfate (orange squares, right column).). Concentrations in blood samples (top row, concentrations), amounts in homogenates (middle row, amounts), and excreted amounts into medium (bottom row, amounts). Solid line is zero with dotted lines for ± 1.96 standard deviations (95% confidence interval).

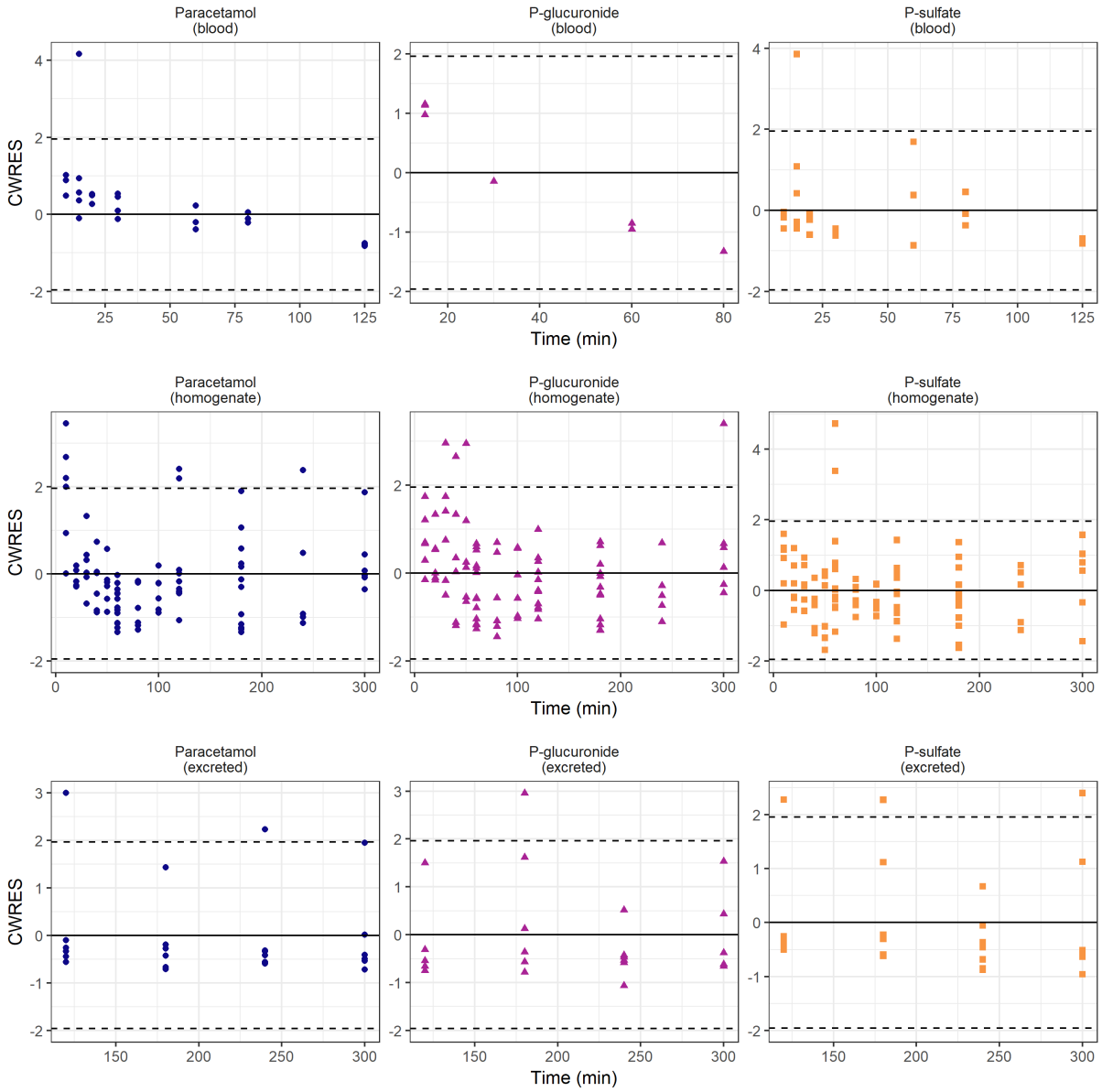

Supplementary Figure S7.4 Conditional weighted residuals (CWRES) vs prediction for paracetamol (blue circles, left column), paracetamol-glucuronide (magenta triangles, middle column), and paracetamol-sulfate (orange squares, right column).). Concentrations in blood samples (top row, concentrations), amounts in homogenates (middle row, amounts), and excreted amounts into medium (bottom row, amounts). Solid line is zero with dotted lines for ± 1.96 standard deviations (95% confidence interval).

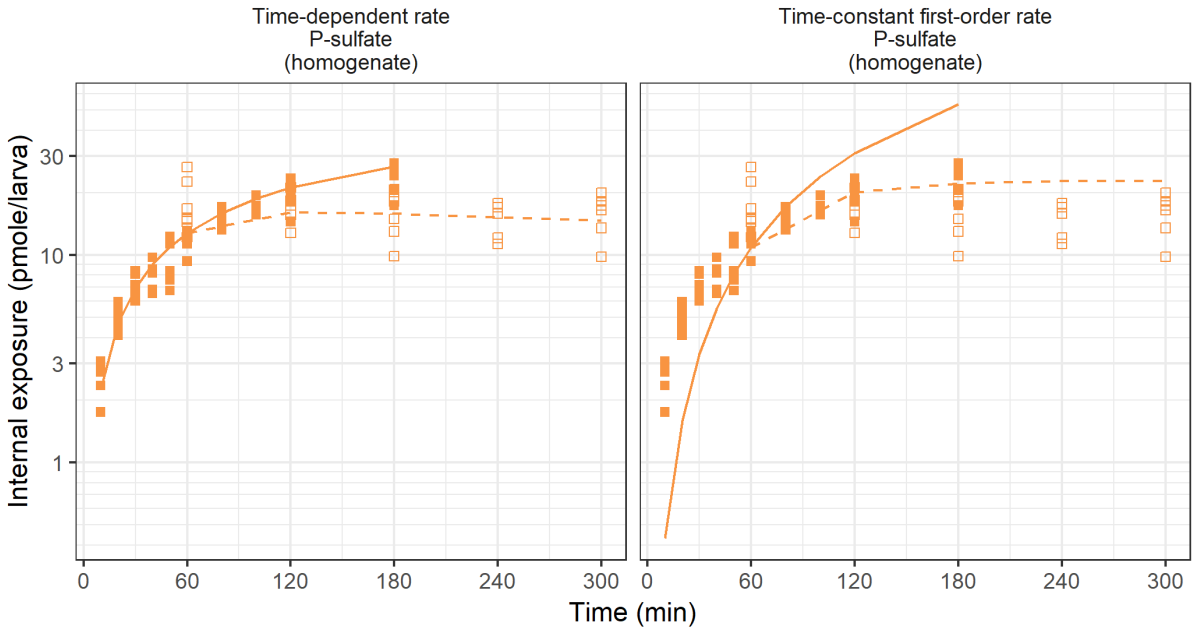

Supplementary Figure S7.5 Paracetamol-sulphate for the final model (left) and alternative metabolite model (right) where the time-dependent metabolic formation rate of sulfation is replaced by a first order metabolic formation rate. Paracetamol-sulfate amounts in homogenates after constant waterborne treatment (solid squares) and wash-out (open squares) experiments. The model prediction is shown as solid or dotted line for the constant waterborne treatment or wash-out experiment, respectively.

Supplementary Table S7.1 Overview of the number of replicates and number of blood samples pooled at each time point.

Time (min)	Number of replicates	Total number of pooled samples*	Total blood volume (nL)*
10	3	31 (30-34)	45.5 (41.5-49.0)
15	5	34 (18-35)	38.7 (26.2-49.8)
20	3	32 (30-34)	61.9 (48.8-83.4)
30	4	26 (18-34)	18.2 (14.8-30.8)
60	3	31 (30-33)	20.9 (14.2-31.8)
80	3	30 (22-32)	54.3 (35.7-61.6)
125	3	15 (15-16)	11.7 (9.78-12.1)

* median and range

Supplementary Table S7.2 Literature values of the distribution volume of paracetamol (V_P) in various vertebrate species.

Species	Weight (kg)	Reported Vp (unit)	Vp (L)	Reference
Mouse	0.03	1.34 (L)	1.34	[1]
Rat	0.285	1.0 (L/kg)	0.285	[2,3]
Rat	0.285	4.96 (ml/kg)	0.014136	[3]
Rat	0.3	0.92 (L/kg)	0.276	[4]
Chicken	1.1	1.70 (L/kg)	1.87	[5]
Turkey	1.7	1.91 (L/kg)	3.247	[5]
Rabbit	3.17	14.67 (mL)	0.01467	[6]
Rabbit	3.61	6.69 (L)	6.69	[7]
Cynomolgus monkey	7.5	1200 (mL/kg)	9	[8,9]
Beagle dog	13.1	0.92 (L/kg)	12.052	[5]
Beagle dog	13.1	900 (mL/kg)	11.79	[5,8]
Beagle dog	13.1	1040 (mL/kg)	13.624	[5,8]
Pig	28.1	1.51 (L/kg)	42.431	[5]
Greyhound dog	33.35	1.05 (L/kg)	35.0175	[10]
Cow (calf)	48.9	0.684 (L/kg)	33.4476	[11]
Cow (calf)	48.9	0.698 (L/kg)	34.1322	[11]
Chimpanzee	55.6	2.29 (L/kg)	127.324	[12]
Human (preterm)	1	1.47 (L/kg)	1.47	[13]
Human (preterm)	1.207	0.764 (L/kg)	0.922148	[14]
Human (preterm)	1.3	1.41 (L/kg)	1.833	[13]
Human (preterm)	2.3	2.46 (L)	2.46	[15]
Human (preterm)	2.4	1.32 (L/kg)	3.168	[13]
Human (preterm)	2.44	70.4 (L/70kg)	2.453942	[16]
Human (neonate)	2.9	76.0 (L/70 kg)	3.148571	[17]
Human (neonate)	3.3	1.21 (L/kg)	3.993	[13]
Human (infant)	6.5	11.1 (L)	11.1	[18]
Human (infant)	7.5	1.04 (L/kg)	7.8	[13]
Human (infant)	10	0.97 (L/kg)	9.7	[13]
Human (infant)	12	0.95 (L/kg)	11.4	[13]
Human (child)	20	0.95 (L/kg)	19	[13]
Human (child)	20	1.32 (L/kg)	26.4	[19]
Human (child)	34	59.8 (L)	59.8	[20]
Human (adult)	50	1.3 (L/kg)	65	[21]
Human (adult)	59	45.9 (L)	45.9	[22]
Human (adult)	60	30.9 (L)	30.9	[23]
Human (adult)	65.3	46.8 (L)	46.8	[22]
Human (adult)	68	0.92 (L/kg)	62.56	[24]
Human (adult)	71	51.3 (L)	51.3	[25]
Human (adult)	81	1.04 (L/kg)	84.24	[24]
Human (adult)	82	0.87 (L/kg)	71.34	[24]
Human (adult)	83	0.9 (L/kg)	74.7	[24]
Horse	495	1.35 (L/kg)	668.25	[5]

7.11 Supplementary references

1. Shankar K, Vaidya VS, Apte UM, et al. Type 1 diabetic mice are protected from acetaminophen hepatotoxicity. Toxicol Sci. 2003;73(2):220-234.
2. Yamasaki I, Uotsu N, Yamaguchi K, et al. Effects of kale ingestion on pharmacokinetics of acetaminophen in rats. Biomed Res. 2011;32(6):357-362.
3. Lee S, An J, Lee H, et al. Evaluation of pharmacokinetic differences of acetaminophen in pseudo germ-free rats. Biopharm Drug Dispos. 2012;33:292-303.
4. Gandia P, Saivin S, Lavit M, et al. Influence of simulated weightlessness on the pharmacokinetics of acetaminophen administered by the oral route: A study in the rat. Fundam Clin Pharmacol. 2004;18(1):57-64.
5. Neirinckx E, Vervaet C, Boever S De, et al. Species comparison of oral bioavailability, first-pass metabolism and pharmacokinetics of acetaminophen. Res Vet Sci. 2010;89(1):113-119.
6. Karbownik A, Szałek E, Sobańska K, et al. The effect of sunitinib on the plasma exposure of intravenous paracetamol and its major metabolite: paracetamol glucuronide. Eur J Drug Metab Pharmacokinet. 2015;40(2):163-170.
7. Bienert A, Kamiñska A, Olszewski J, et al. Pharmacokinetics and ocular disposition of paracetamol and paracetamol glucuronide in rabbits with diabetes mellitus induced by alloxan. Pharmacol Reports. 2012;64:421-427.
8. Koyanagi T, Yamaura Y, Yano K, et al. Age-related pharmacokinetic changes of acetaminophen, antipyrine, diazepam, diphenhydramine, and ofloxacin in male cynomolgus monkeys and beagle dogs. Xenobiotica. 2014;44(10):893-901.
9. Rosso MC, Badino P, Ferrero G, et al. Biologic data of cynomolgus monkeys maintained under laboratory conditions. PLoS One. 2016;11(6):1-17.
10. KuKanich B. Pharmacokinetics of acetaminophen, codeine, and the codeine metabolites morphine and codeine-6-glucuronide in healthy Greyhound dogs. J Vet Pharmacol Ther. 2009;33:15-21.
11. Janus K, Grochowina B, Antoszek J, et al. The effect of food or water deprivation on paracetamol pharmacokinetics in calves. J Vet Pharmacol Ther. 2003;26(4):291-296.
12. Wong H, Grace JE, Wright MR, et al. Glucuronidation in the chimpanzee (Pan troglodytes): Studies with acetaminophen, oestradiol and morphine. Xenobiotica. 2006;36(12):1178-1190.
13. Anderson BJ, Van Lingen RA, Hansen TG, et al. Acetaminophen developmental pharmacokinetics in premature neonates and infants. Anesthesiology. 2002;96:1336-1345.
14. Van Ganzewinkel C, Derijks L, Anand KJS, et al. Multiple intravenous doses of paracetamol result in a predictable pharmacokinetic profile in very preterm infants. Acta Paediatr Int J Paediatr. 2014;103(6):612-617.
15. Cook SF, Roberts JK, Samiee-Zafarghandy S, et al. Population pharmacokinetics of intravenous paracetamol (acetaminophen) in preterm and term neonates: model development and external evaluation. Clin Pharmacokinet. 2016;55(1):107-119.
16. Allegaert K, Anderson BJ, Naulaers G, et al. Intravenous paracetamol (propacetamol) pharmacokinetics in term and preterm neonates. Eur J Clin Pharmacol. 2004;60:191-197.
17. Palmer GM, Atkins M, Anderson BJ, et al. I.V. acetaminophen pharmacokinetics in neonates after multiple doses. Br J Anaesth. 2008;101(4):523-530.
18. Mooij MG, van Duijn E, Knibbe CAJ, et al. Successful use of [14C]paracetamol microdosing to elucidate developmental changes in drug metabolism. Clin Pharmacokinet. 2017;56(10):1185-1195.
19. Hahn TW, Henneberg SW, Holm-Knudsen RJ, et al. Pharmacokinetics of rectal paracetamol after repeated dosing in children. Br J Anaesth. 2000;85(4):512-519.
20. Anderson BJ, Holford NHG, Woollard GA, et al. Perioperative pharmacodyanmics of acetaminophen analgesia in children. Anesthesiology. 1999;90:411-421.
21. Tankanitlert J, Howard TA, Temsakulphong A, et al. A pharmacokinetic study of paracetamol in Thai β-thalassemia/HbE patients. Eur J Clin Pharmacol. 2006;62(9):743-748.
22. Kulo A, van Calsteren K, van de Velde M, et al. Weight, pregnancy and oral contraceptives affect

intravenous paracetamol clearance in young women. Eur Rev Med Pharmacol Sci. 2014;18:599-604.
23. Shinoda S, Aoyama T, Aoyama Y, et al. Pharmacokinetics/pharmacodynamics of acetaminophen analgesia in Japanese patients with chronic pain. Biol Pharm Bull. 2007;30(1):157-161.
24. Liukas A, Kuusniemi K, Aantaa R, et al. Pharmacokinetics of intravenous paracetamol in elderly patients. Clin Pharmacokinet. 2011;50(2):121-129.
25. Rincón JP, Meesters RJW. Evaluation of peripheral blood microsampling techniques in combination with liquid chromatography-high resolution mass spectrometry for the determination of drug pharmacokinetics in clinical studies. Drug Test Anal. 2014;6(6):568-577.

7.12 NONMEM model code

```
$PROBLEM    PK
$INPUT      ID TIME AMT DV EVID MDV CMT XEXP BQL XEXP2 AGE BLOOD
$DATA       Real_Zebrafish_paracetamol_metabolite.csv IGNORE=@ IGNORE=(BQL.
GT.0)

; units
; TIME = min
; DV = pmole / larva or pmole / nL
; V = nL
; kA = pmole / min

$SUBROUTINE ADVAN13 TOL=9
$MODEL      COMP ; CMT 1 dosing compartment
            COMP ; CMT 2 central paracetamol in larva
            COMP ; CMT 3 central paracetamol-glucuronide in larva
            COMP ; CMT 4 central paracetamol-sulfate in larva
            COMP ; CMT 5 excreted paracetamol in medium
            COMP ; CMT 6 excreted paracetamol-glucuronide in medium
            COMP ; CMT 7 excreted paracetamol-sulfate in medium
$PK
TVK25 = THETA(1)
TVK12 = THETA(2)
TVK23 = THETA(3)/1000
TVK24 = THETA(4)
TVK36 = THETA(5)/1000
TVK47 = THETA(6)/1000
TVV2  = THETA(7)
TVV3  = THETA(8)
TVV4  = THETA(9)
TVT50 = THETA(10)
TVF5  = THETA(11)
TVF6  = THETA(12)/1000
TVF7  = THETA(13)

K25 = TVK25 * EXP(ETA(1)) ;first order rate of excretion of paracetamol
K12 = TVK12               ;zero order rate of absorption
K23 = TVK23               ;first order metabolic formation rate for glucuro-
nidation
K24 = TVK24               ;time-dependent metabolic formation rate for sul-
fation
K36 = TVK36               ;first order rate of excretion of paracetamol-glu-
curonide
K47 = TVK47               ;first order rate of excretion of paracetamol-sul-
fate
V2 = TVV2                 ;distribution volume paracetamol
V3 = TVV3                 ;distribution volume paracetamol-glucuronide
V4 = TVV4                 ;distribution volume paracetamol-sulfate
```

```
T50 = TVT50                ;time at which 50% of maximal sulphation is
reached
F5 = TVF5                  ;fraction excreted parent retrieved from medium
sample
F6 = TVF6                  ;fraction excreted glucuronide-metabolite re-
trieved from medium sample
F7 = TVF7                  ;fraction excreted sulfate-metabolite retrieved
from medium sample

ET1 = ETA(1)

S2 = V2
S3 = V3
S4 = V4

$DES
DADT(1) = 0
DADT(2) = K12 * A(1) - K25 * A(2) - K23 * A(2) - K24 * (1 - T/(T50+T)) *
A(2)
DADT(3) = K23 * A(2) - K36 * A(3)
DADT(4) = K24 * (1 - T/(T50+T)) * A(2) - K47 * A(4)
DADT(5) = K25 * A(2) * F5
DADT(6) = K36 * A(3) * F6
DADT(7) = K47 * A(4) * F7

$ERROR
IF(CMT.EQ.2.AND.BLOOD.EQ.0) THEN
IPRED = A(2)
Y = IPRED * (1 + EPS(1)) + EPS(7) ; comb error paracetamol in larva
ENDIF
IF(CMT.EQ.3.AND.BLOOD.EQ.0) THEN
IPRED = A(3)
Y = IPRED * (1 + EPS(2)) + EPS(8) ; comb error paracetamol-glucuronide in
larva
ENDIF
IF(CMT.EQ.4.AND.BLOOD.EQ.0) THEN
IPRED = A(4)
Y = IPRED * (1 + EPS(3)) + EPS(9) ; prop error paracetamol-sulfate in larva
ENDIF

IF(CMT.EQ.2.AND.BLOOD.EQ.1) THEN
IPRED = A(2)/V2
Y = IPRED * (1 + EPS(4)) + EPS(10) ; add error paracetamol in blood
ENDIF
IF(CMT.EQ.3.AND.BLOOD.EQ.1) THEN
IPRED = A(3)/V3
Y = IPRED * (1 + EPS(5)) + EPS(11) ; prop error paracetamol-glucuronide in
blood
ENDIF
IF(CMT.EQ.4.AND.BLOOD.EQ.1) THEN
IPRED = A(4)/V4
Y = IPRED * (1 + EPS(6)) + EPS(12) ; prop error paracetamol-sulfate in
blood
ENDIF

IF(CMT.EQ.5) THEN
IPRED = A(5)
Y = IPRED * (1 + EPS(13)) + EPS(16) ; add error paracetamol in medium
ENDIF
IF(CMT.EQ.6) THEN
IPRED = A(6)
Y = IPRED * (1 + EPS(14)) + EPS(17) ; prop error paracetamol-glucuronide in
```

```
medium
ENDIF
IF(CMT.EQ.7) THEN
IPRED = A(7)
Y = IPRED * (1 + EPS(15)) + EPS(18) ; comb error paracetamol-sulfate in me-
dium
ENDIF

IRES = DV - IPRED

$THETA  (0,0.01142) ; K25
 (0,0.3990)         ; K12
 (0,2.592)          ; K23
 (0,0.09168)        ; K24
 (0,5.838)          ; K36
 (0,0.02447)        ; K47
 (0,103)            ; V2
 (0,240)            ; V3
 (0,262)            ; V4
 (0,5.253)          ; T50
 (0, 0.01, 1)       ; f_Q
 (0, 0.01, 1)       ; f_G
 (0, 0.2, 1)        ; f_S

$OMEGA  0  FIX      ; IIV K25

$SIGMA  BLOCK(3)
 0.1366             ; prop error paracetamol in larva
 -0.1348 0.3150     ; prop error paracetamol-glucuronide in larva
 0 0.03749 0.06675  ; prop error paracetamol-sulfate in larva

$SIGMA
 0 FIX  ; prop error paracetamol in blood
 0.09   ; prop error paracetamol-glucuronide in blood
 0.09   ; prop error paracetamol-sulfate in blood

 0.5    ; add error paracetamol in larva
 0.5    ; add error paracetamol-glucuronide in larva
 0 FIX  ; add error paracetamol-sulfate in larva

 0.05   ; add error paracetamol in blood
 0 FIX  ; add error paracetamol-glucuronide in blood
 0 FIX  ; add error paracetamol-sulfate in blood

 0 FIX  ; prop error paracetamol in medium
 0.09   ; prop error paracetamol-glucuronide in medium
 0.09   ; prop error paracetamol-sulfate in medium
 0.001  ; add error paracetamol in medium
 0 FIX  ; add error paracetamol-glucuronide in medium
 0.05   ; add error paracetamol-sulfate in medium

$ESTIMATION METHOD=1 MAXEVAL=8000 NOABORT PRINT=10 NSIG=3 SIGL=9 POSTHOC
$COVARIANCE PRINT=E
$TABLE ID TIME AMT DV EVID MDV CMT XEXP BQL XEXP2 AGE BLOOD IPRED
CWRES V2 V3 V4 K25 K12 K23 K24 K36 K47 T50 F5 F6 F7 ET1 ONEHEADER
NOPRINT FILE=tab_Zebrafish_paracetamol_metabolite
```

Section III. Linking internal exposure to disease dynamics

Chapter 8

Quantification of internal exposure of isotretinoin and neuroblastoma tumour size over time in the zebrafish disease model

Rob C. van Wijk, Shuning He, Elke H.J. Krekels, Nick Jansen, Maxim Treep, Dirk-Jan van den Berg, Xiaoqin Tang, Gerda Lamers, Fons J. Verbeek, Piet H. van der Graaf, Herman P. Spaink, A. Thomas Look

8.1 Abstract

Drug development is challenging for neuroblastoma, a peripheral sympathetic nervous system (PSNS) tumour that is the most common paediatric non-cranial solid tumour responsible for 15% of paediatric cancer deaths. A strong preclinical rationale is important for the development of novel agents and an innovative disease model for neuroblastoma is the zebrafish. Waterborne treatment with isotretinoin (13-cis-retinoic acid) induces apoptotic cell death and decreases neuroblastoma size within this model organism. However, internal exposure of isotretinoin has not been quantified. Multiple measures of tumour size during treatment time will elucidate onset, intensity, and duration of drug effect. Therefore, we quantified the internal exposure of isotretinoin in zebrafish over a period of 168 hours by sensitive UPLC-MS/MS upon waterborne isotretinoin treatment at doses 0, 1, 1.5, or 2 µM. Tumour size is quantified by two-dimensional fluorescence imaging every 24 hours. Model-based analysis was performed to characterize the internal exposure-time and treatment medium concentration-time profiles simultaneously. Internal exposure was anticipated to reach steady state, but showed a 100-fold drop in initial exposure in the intervals between treatment medium refreshments. Subsequent quantification of treatment medium concentrations showed lower concentrations than nominal dose and a decline over time. No photo-isomerization into 9-cis-retinoic acid or all-trans-retinoic acid, or metabolism accounted for this behaviour. No relationship between drug exposure and tumour size could be quantified, due to low internal isotretinoin exposure and large between-subject variability in tumour size in the treatment groups. Our work underlines the importance of quantification of internal drug exposure in the zebrafish, and of the disease dynamics, through pharmacokinetic-pharmacodynamic analysis. The resulting exposure-response relationship is essential for translational drug development.

8.2 Introduction

Neuroblastoma is a peripheral sympathetic nervous system (PSNS) tumour that is the most common paediatric non-cranial solid tumour, accounting for 15% of cancer mortality in children. Drug development for neuroblastoma is challenging with the ethical constraints inherently linked to the paediatric population and a limited number of agents specifically for this patient population in the pipeline[1]. A preclinical disease model has been developed in MYCN overexpressing zebrafish[2]. This novel disease model is part of a new pragmatic approach of developing drug against neuroblastoma based on strong preclinical rationale, instead of on empirical testing of drugs approved for adult populations[3]. Treatment with isotretinoin of zebrafish with neuroblastoma has shown promising results with reduced growth or even decrease in size of the neuroblastoma tumour after 7 days of waterborne treatment[2]. Isotretinoin, also known as 13-cis-retinoic acid, is a retinoid structurally related to vitamin A, but its mechanism of action in the treatment of neuroblastoma is not fully elucidated[4–6].

Essential for translation of pharmacological findings from zebrafish to higher vertebrates, is the quantification of drug exposure inside the zebrafish, in contrast to the concentration in the water surrounding the zebrafish in which the drug is dissolved which is traditionally used as the exposure measure[7–9]. Indeed, it is the exposure at the target site that drives the pharmacological effect[10]. However, this can be challenging with small sample volumes and low amounts and is therefore often not done in zebrafish, limiting reliable translation of findings to higher vertebrates. Quantification of internal exposure is especially difficult in the case of unstable compounds like isotretinoin, which is subject to photo-isomerization into isomers like 9-cis-retinoic acid or all-trans-retinoic acid when exposed to UV-light[4–6,11].

An important advantage of the zebrafish neuroblastoma disease model is the fluorescent marker expressed within the tumour cells, which enables quantification of disease progression and drug effect through fluorescence imaging[2]. Tumour size and shape can therefore readily be characterized without dissection. Traditional studies on drug effects in zebrafish measure treatment outcome at the end of the

studied treatment period[2]. In the absence of multiple measures of tumour size over a treatment interval, detailed information on the dynamics that determine the onset, intensity, and duration of the drug effect cannot be obtained. Moreover, these studies assume external and internal drug exposure to be constant, but when this is not the case, the absence of exposure measures prevents the quantification of exposure-response relationships within this promising disease model in preclinical drug development.

Here, the internal exposure of isotretinoin has been quantified in the zebrafish neuroblastoma disease model upon 168 hours of waterborne treatment. The detailed dynamics of tumour size over this treatment period were quantified by measures of tumour size every 24 hours. These pharmacokinetic and pharmacodynamic experiments aim to result in an improved understanding of the drug effect of isotretinoin on the neuroblastoma, to enable translation of results between species.

8.3 Methods

8.3.1 Study design

Zebrafish neuroblastoma disease model line with the *nf1a+/+;nf1b+/+;dbh:MYCN;dbh:GFP* genotype was used[2]. At three weeks of age, when neuroblastoma tumours had visibly formed, treatment with isotretinoin commenced for 168 hours at doses 0, 1, 1.5, and 2 µM in the treatment medium. Zebrafish were kept in individual wells of 12-well plates with 3 mL treatment medium. Treatment medium was refreshed after 48 and 96 hours. Quantification of internal exposure and of tumour size were performed in separate studies, all of which were performed with minimal exposure to UV-light to prevent photo-isomerisation of isotretinoin.

Internal exposure was quantified in 4 biological replicates of individual zebrafish per dose for each of 13 time points. Zebrafish were washed and snap-frozen in liquid nitrogen and corresponding treatment medium was sampled as well. Isotretinoin, and its two major isomers 9-cis-retinoic acid and all-trans-retinoic acid, were quantified by LC-MS/MS. Pharmacokinetic modelling was performed to characterize internal exposure over time. All experimental and bioanalytical sample handling was performed with minimal UV-exposure.

Tumour size was quantified in at least 6 biological replicates of individual zebrafish per dose, including negative control, per treatment day. Zebrafish were fixed and stored in PBS at 4°C until fluorescence imaging. All experimental handling and imaging was performed with minimal UV-exposure. Zebrafish husbandry and handling was performed following international standards[12]. Experiments with and maintenance of zebrafish were in accordance with Dana-Farber Cancer Institute IACUC-approved protocol #02–107.

8.3.2 Internal exposure over time

Individual zebrafish (n = 4 per dose per time point) exposed to 0, 1, 1.5, or 2 µM isotretinoin in treatment medium for 1, 3, 6, 12, 24, 47, 49, 72, 95, 97, 120, 144, or 168 hour were collected. Treatment medium was refreshed at 48 and 96 hour after start of treatment. Treatment was determined based on maximal tolerated dose. To obtain samples for internal exposure, zebrafish were anaesthetized using tricaine and washed to prevent contamination of samples with treatment medium. Washing procedures were optimized and 4 washing steps with 20/80 LC-MS grade methanol/demineralized water proved more than sufficient to reach undetectable isotretinoin concentrations in washing solution. Samples, transferred to Safe-Lock tubes (Eppendorf Nederland B.V., Nijmegen, The Netherlands), were snap-frozen in liquid nitrogen and stored at -80°C until bioanalytical quantification. Treatment medium was sampled and stored at-80°C until bioanalytical quantification.

To assess potential external skin adhesion of isotretinoin, unexposed zebrafish were submerged in treatment medium for 1, 5, or 10 seconds, after which they were washed and snap-frozen as described

above. As all of these samples had isotretinoin amounts that were below the lower limit of quantification, skin adhesion of isotretinoin was concluded to be negligible. The influence of experimental material, either plastic or glass, on the stability of isotretinoin during washing or storage was assessed by collecting drug solution in both plastic and glass tubes. No statistically significant difference in isotretinoin concentrations was observed between samples from glass or plastic experimental material (Kruskal-Wallis test, $p = 0.179$).

8.3.3 Quantification of isotretinoin

Zebrafish samples were thawed before 25 µL of isotretinoin internal standard solution (200 ng/mL 13-cis-retinoic acid-d5 in methanol) plus 175 µL of methanol were added to each sample. Samples were homogenized with ~10 mg of 0.5 mm zirconium oxide bullets per Safe-Lock tube, utilizing a bullet blender (Next Advance, Averill Park, New York, USA) for 5 minutes at speed 3 and 5 minutes at speed 5, or until homogenized. Samples were sonicated 5 minutes and 800 µL acetonitrile was added to each sample. After vortexing, the samples were centrifuged for 10 minutes at 20,000 x g. For each sample, the supernatant was transferred to a clean Safe-Lock tube and evaporated to dryness (Labconco vacuum centrifuge, Beun de Ronde, Abcoude, The Netherlands). The residue was reconstituted in 100 µL mobile phase mixture (35/40/25 (v/v) acetonitrile/methanol/water ULC-MS grade) by vortexing and again centrifuged as above. The supernatant was transferred to an amber LC-MS vial with a glass insert and 5 µL was injected into the LC-MS system.

Zebrafish samples were randomized over three bioanalysis runs. Calibration standards in zebrafish matrix for 13-cis-retinoic acid (isotretinoin), 9-cis-retinoic acid, and all-trans-retinoic acid combined, with final concentrations of 0, 2, 5, 10, 25, 50, 100, 150, and 250 ng/mL were freshly prepared for all runs. Individual standards of the isomers at final concentrations of 200 ng/mL were included in all bioanalysis runs to monitor isomerization during sample preparation. Quality control (QC) samples in matrix at final concentrations of 4, 40, and 225 ng/mL were included in all bioanalysis runs.

Treatment medium samples were randomized over two bioanalysis runs. Treatment medium samples were thawed and 25 µL of the sample was diluted into the calibration range by addition of 25 µL of internal standard solution (200 ng/mL 13-cis-retinoic acid-d5) and 50 µL of 30/70 (v/v) methanol/acetonitrile mixture. After centrifugation (10 minutes at 20,000 x g), the supernatant was transferred to an amber LC-MS vial with a glass insert. 5 µL was injected into the LC-MS system. Calibration and QC standard were included as above, without zebrafish matrix.

An LC-MS/MS method was developed and validated following industry guidelines[13]. Bioanalysis was performed on an ultra-high-performance liquid chromatography (UHPLC) system (Shimadzu Nexera X2, 's Hertogenbosch, The Netherlands) with a triple quadrupole mass spectrometry (MS) detector (TSQ Vantage, Thermo Fisher Scientific, Breda, The Netherlands) with Electron Spray Ionization. Chromatographic separation was achieved with a Kinetex EVO C18 1.7 µm (150 x 2.1 mm) column coupled to a 5 mm pre-column with the same packing material (Phenomenex, Utrecht, The Netherlands). The eluent flow was 0.3 mL/min and the column temperature was 45°C. This column was specifically chosen to separate the photo-isomers that were identical in mass and charge and showed similar fragmentation patterns. Two UHPLC pumps were utilized for gradient elution of the aqueous mobile phase consisting of 35/65 methanol/water LC-MS-grade with 0.01% acetic acid and the organic mobile phase of 35/65 methanol/acetonitrile. The gradient started at injection at 47/53 aqueous/organic mobile phases and increased to 38/62 aqueous/organic mobile phases over 15.5 minutes. The column was flushed at a ratio of 10/90 aqueous/organic mobile phases for 3.5 minutes, after which the system was equilibrated at starting conditions for 3 minutes.

Ionization was performed at 3000 V in the negative mode at a capillary temperature of 350°C, sheath gas and auxiliary gas were at 13 and 4 L/min. Multiple Reaction Monitoring was used to quantify 13-cis-

retinoic acid, 9-cis-retinoic acid, and all-trans-retinoic acid (all MH- = 299.2 m/z, fragments 79.1, 119.1, and 255.2 m/z), and internal standard 13-cis-retinoic acid-d5 (MH- = 304.2 m/z, fragments 79.1, 120.1, and 260.3 m/z). Lower limit of quantification was 2 ng/mL for 13-cis-retinoic acid and all-trans-retinoic acid, and 4 ng/mL for 9-cis-retinoic acid. Data acquisition was performed with LC-Quan software (v. 2.7, Thermo Fisher Scientific) in which the compound peak area was corrected by the internal standard peak area and calibration was performed with weighted linear regression using 1/y as weighting factor.

Of the isotretinoin internal exposure measurements, 22.6% were below the lower limit of quantification. 15.5% were above the highest calibration standard, of which the median concentration was 33.7% higher than the highest standard. Of the treatment medium concentrations, 46.5% were below the lower limit of quantification. No oxidative metabolites were detected above quantification level (data not shown).

8.3.4 Model-based characterization of internal isotretinoin exposure

Non-linear mixed effects modelling was performed using NONMEM (version 7.3)[14] through interfaces Pirana (version 2.9.6)[15] and PsN (version 4.7.0)[16], utilizing the Laplacian Estimation method. Data transformation and graphical output was performed with R (version 3.5.0)[17] through the Rstudio interface (version 1.1.383, RStudio Inc, Boston, Massachusetts, USA).

One and two compartment models were tested with a first-order absorption rate constant from the treatment medium. Transit compartments were also tested to describe the absorption phase. For elimination, linear or non-linear saturable excretion back into the treatment medium was tested. Isotretinoin concentrations in the treatment medium were lower than nominal dose, therefore inclusion of an estimate of the fraction of the nominal dose in the treatment medium in the model was tested. Also, a rate of degradation of isotretinoin from the treatment medium was tested. The data showed differences between the refreshments, for example how fast trough levels were reached (Figure 8.1, Supplementary Figure S8.1). To assess the impact on parameters, different parameters were estimated for the three treatment intervals.

Biological variability could not be quantified, because of destructive sampling. To quantify experimental variability, a proportional, additive, and a combination of proportional and additional error model were tested, with separate errors for internal exposure measures and treatment medium measures. Because more than 20% of data points were below the lower limit of quantification, these data points were handled as censored. The M3 method, which maximizes the likelihood that these data points were in fact below the lower limit of quantification, was utilized[18]. Model selection was performed based on the following criteria: successful convergence, biological plausibility of parameter estimates, and acceptable parameter precision with relative standard errors below 50%, as well as absence of bias in goodness-of-fit plots[19]. The likelihood ratio test was utilized between nested models, with a drop in objective function value (OFV) of 3.84 corresponding to $p < 0.05$ in case of a single degree of freedom indicating statistical significance, assuming a χ^2-distribution. Between non-nested models, the Akaike Information Criterion (AIC) was utilized[20].

8.3.5 Tumour size and quantification

In parallel with the pharmacokinetic experiments, individual zebrafish ($n \geq 6$ per dose per day) with established tumours exposed to 0, 1, 1.5, or 2 µM isotretinoin in treatment medium were collected before start of treatment and after 1, 2, 3, 4, 5, 6, and 7 days. Treatment medium was refreshed at 48 and 96 hours. Zebrafish were fixed with 4% paraformaldehyde (PFA) for 24 hours, washed with phosphate buffered saline (PBS) and stored until further analysis. Zebrafish were positioned on a petri dish coated with 2% agarose and imaged by a Fluorescence Stereo Microscope (Leica MZ16FA, Leica Microsystems, Wetzlar, Germany) equipped with a digital colour camera (Leica DFC420 C). Both GFP- and brightfield channels were captured. Images were randomized and tumour area was manually selected and quantified using the image analysis program Fiji[21].

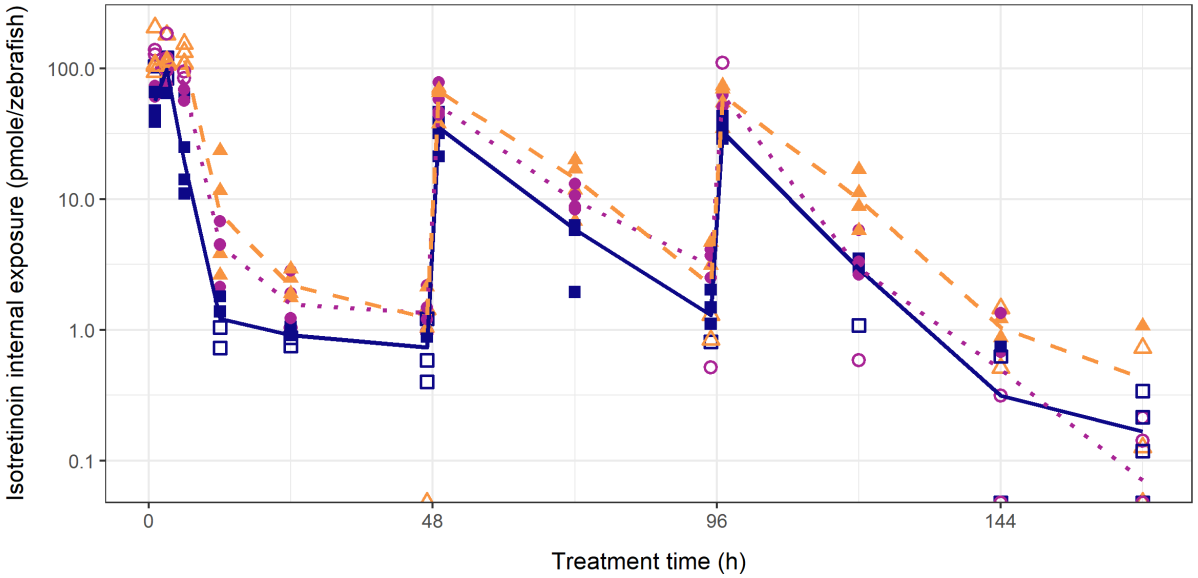

Figure 8.1 Internal exposure of isotretinoin in zebrafish over time. Isotretinoin treatment is for duration of 168 hours at three dose levels, with treatment medium refreshment at 48h and 98h. Closed symbols are measures within the calibration range (1 µM: blue square, 1.5 µM: magenta circle, 2 µM: orange triangle), open symbols are measures below the lower limit of quantification or above the highest calibration standard. Lines (1 µM: blue solid, 1.5 µM: magenta dotted, 2 µM: orange dashed) connect median values.

8.3.6 Chemicals

PFA, PBS, and ethyl 3-aminobenzoate (tricaine) were acquired from Sigma-Aldrich (Sigma-Aldrich Inc, St. Luis, Missouri, USA). Isotretinoin used for treatment was acquired from Selleck Chemicals (Selleck Chemicals, Houston, Texas, USA).

Bioanalytical compounds 13-cis-retinoic acid (isotretinoin), 9-cis-retinoic acid, and all-trans-retinoic acid were acquired from Sigma-Aldrich (Sigma-Aldrich Chemie GmbH, Schnelldorf, Germany), and 13-cis-retinoic acid-D5 from Toronto Research Chemicals (Toronto Research Chemicals, North York, Canada). Acetonitrile ULC-MS-grade and glacial acetic acid were purchased from Biosolve (Biosolve B.V., Valkenswaard, The Netherlands). Unless otherwise stated, methanol was ULC-MS grade (Biosolve B.V.) and nanopure water was utilized from a PURELAB water purification system (Veolia Water Technologies, Ede, The Netherlands). Agarose was acquired from Sphaero Q (Sphaero Q, Gorinchem, The Netherlands).

8.4 Results

8.4.1 Internal exposure over time

Zebrafish were treated with isotretinoin for 168 hours with 0, 1, 1.5, or 2 µM waterborne treatment, which was refreshed at 48 and 96 hours. Figure 8.1 shows the internal isotretinoin exposure over time, quantified as pmole/zebrafish. Given that the concentration of isotretinoin in the treatment medium was expected to remain constant, the internal exposure was anticipated to reach a plateau, yet a 100-fold drop in internal exposure is observed in the 48 hour interval between treatment refreshments.

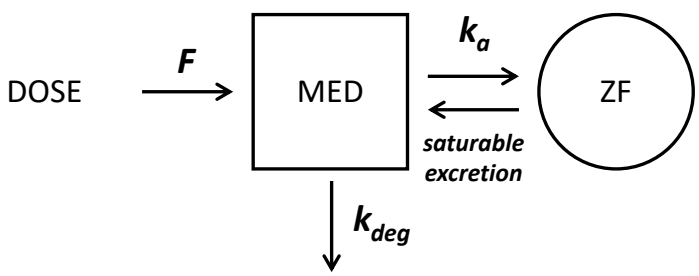

Figure 8.2 Schematic representation of the final pharmacokinetic model. The isotretinoin dose is dissolved in the treatment medium (MED) for which a fraction of nominal dose (F) and a degradation rate constant (k_{deg}) is estimated. A first order absorption rate constant (k_a) from the treatment medium into the zebrafish (ZF) is estimated. Isotretinoin is excreted back into the treatment medium through a saturable process.

Subsequent quantification of the treatment medium concentrations showed that initial concentrations in the treatment wells were lower than the nominal dose and that these concentrations decreased over time (Supplementary Figure S8.1). This was possibly caused by adhesion to experimental materials or instability of isotretinoin. Photo-isomerization was however established to be limited, with less than 10% of isotretinoin being retrieved as isomers. Photo-isomerization within the (transparent) zebrafish was also limited, with on average 16.4% of total internal exposure retrieved as isomer, a third of that as 9-cis-retinoic acid and two-third as all-trans-retinoic acid (Supplementary Figure S8.2).

8.4.2 Model-based characterization of internal isotretinoin exposure

The internal isotretinoin exposure in zebrafish over time was characterized by a quantitative pharmacokinetic model, which analysed internal exposure and treatment medium data simultaneously. Figure 8.2 shows the schematic representation of the model. To account for the lower initial concentration, a fraction (F) of the nominal isotretinoin dose to be available in the prepared solution of the treatment medium, was estimated representing the available dose that was measured in the medium. A first order rate constant (k_{deg}) was estimated to reflect the degradation of isotretinoin observed in the treatment medium over time. A one compartment model representing the zebrafish with first order absorption rate constant (k_a) of isotretinoin from the treatment medium into the zebrafish and saturable excretion of isotretinoin back into the treatment medium, described the internal exposure in the zebrafish best. A separate degradation rate constant for all three treatment intervals was tested and improved the model fit substantially ($p < 0.001$). Residual variability was described by a combination of proportional and additive error for the concentration in the treatment medium and the internal zebrafish exposure.

Parameter estimates of the final pharmacokinetic model are given in Table 8.1. Precision of parameter estimation was good with relative standard errors below 30%. The model predictions of internal isotretinoin exposure in zebrafish is shown in Figure 8.3, model predictions of isotretinoin concentrations in the treatment medium is shown in Supplementary Figure S8.3. Goodness-of-fit plots showed at best small trends, meaning limited bias in the description of isotretinoin concentrations or exposures by the model (Supplementary Figures S8.4-5).

Table 8.1 Parameter estimates including their relative standard errors (RSE) of the final pharmacokinetic model.

	Parameter value	**RSE (%)**
Structural parameters		
F (%)	14.0	7.5
k_{deg} (h^{-1})		
dosing interval 1	0.106	6.4
dosing interval 2	0.0757	5.7
dosing interval 3	0.0964	6.1
k_a (h^{-1})	0.155	17.1
$\text{excretion} = \frac{V_{max} \cdot AMT}{K_m + AMT}$		
V_{max} (pmole/h)	92.2	20.4
K_m (pmole/zebrafish)	33.7	29.6
Stochastic parameters homogenate		
Variance of proportional error treatment medium (-)	0.781	10
Variance of additive error treatment medium (pmole/nL)	0.0326	0.2
Variance of proportional error zebrafish (-)	0.877	8.8
Variance of additive error zebrafish (pmole/zebrafish)	0.958	6.2

F = fraction of nominal dose, k_{deg} = degradation rate constant, k_a = absorption rate constant, AMT = internal exposure, V_{max} = maximal rate of excretion, K_m = internal exposure at which 50% of maximal rate of excretion is reached

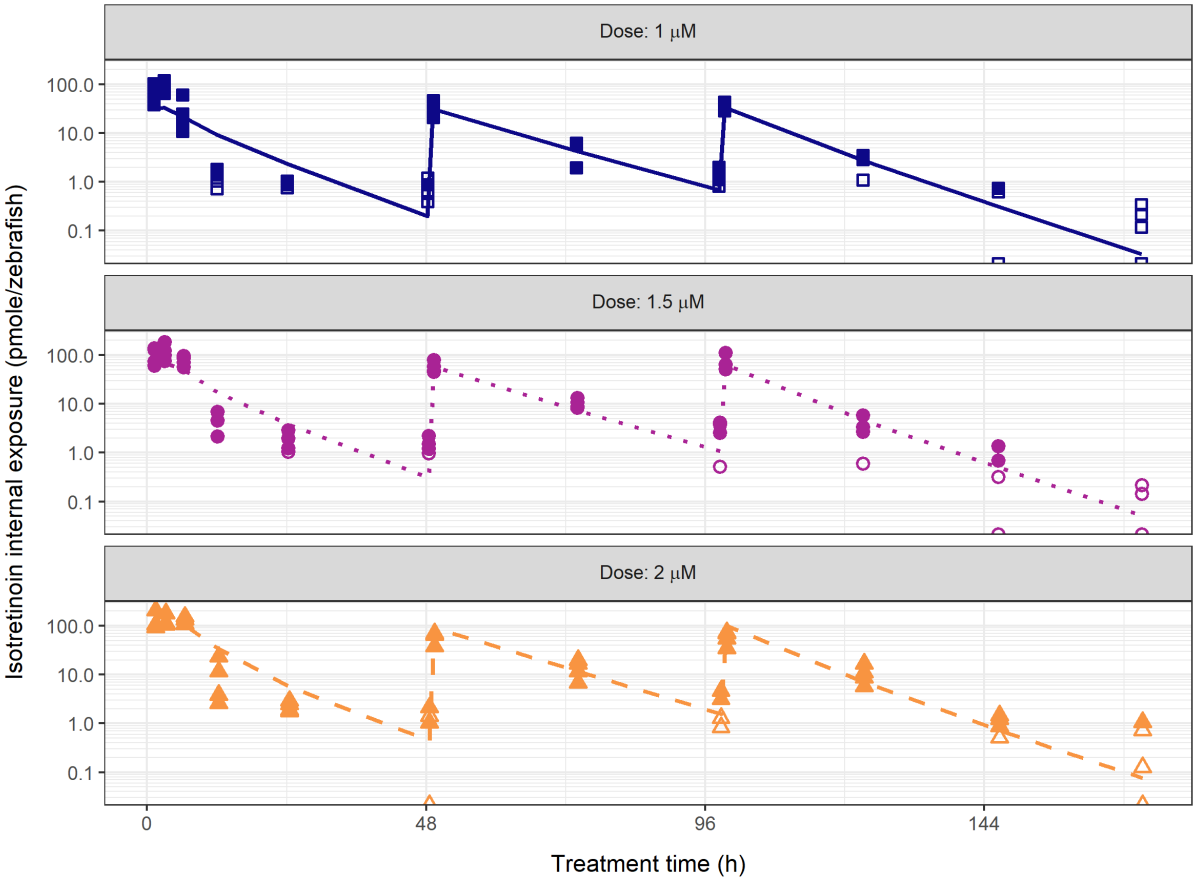

Figure 8.3 Model predicted internal exposure of isotretinoin in zebrafish over time. Isotretinoin treatment is for duration of 168 hours at three dose levels, with treatment medium refreshment at 48h and 98h. Closed symbols are observed internal exposure measures within the calibration range (1 µM: blue square, 1.5 µM: magenta circle, 2 µM: orange triangle), open symbols are measures below the lower limit of quantification or above the highest calibration standard. Lines (1 µM: blue solid, 1.5 µM: magenta dotted, 2 µM: orange dashed) show pharmacokinetic model predictions.

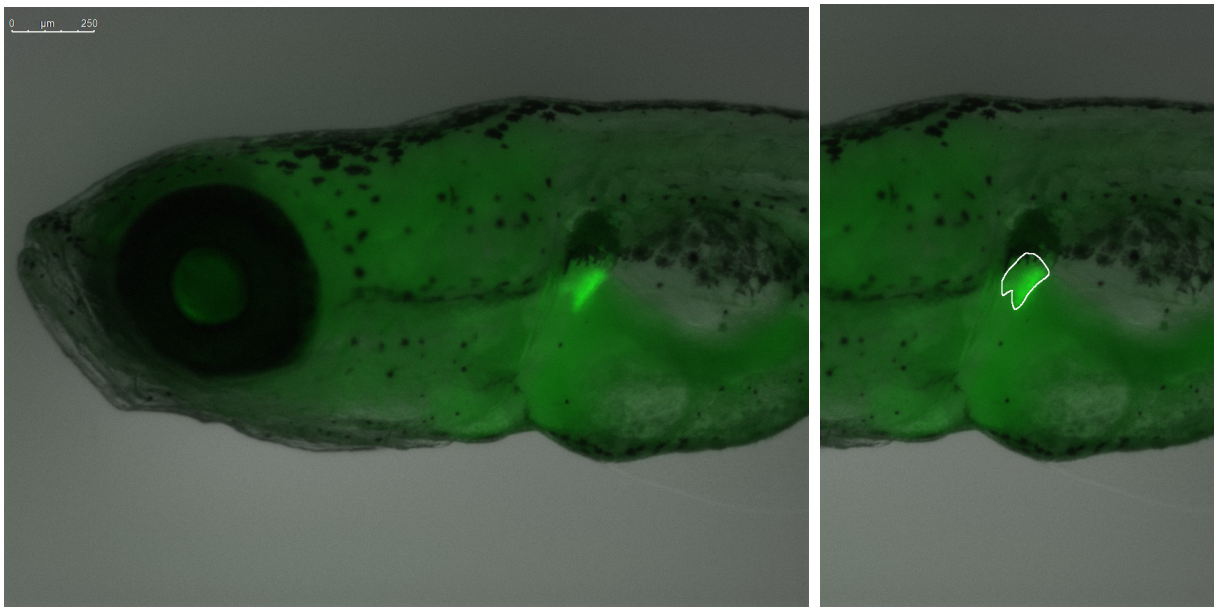

Figure 8.4 Representative image of fluorescent neuroblastoma tumour. Tumour area is manually selected and area is quantified (insert right). Scalebar represents 0.25 mm.

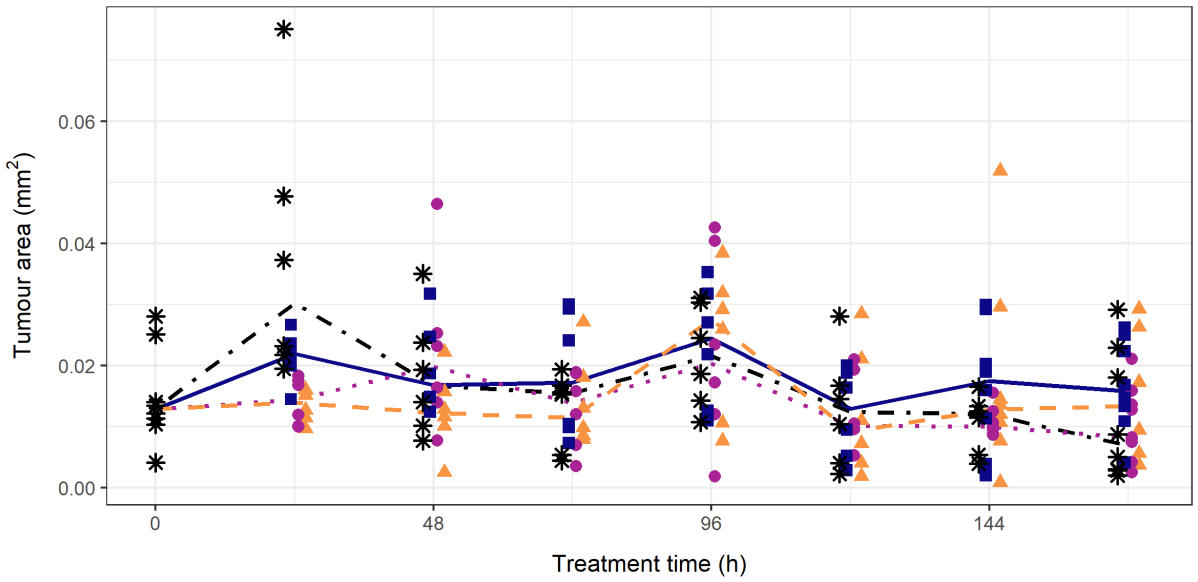

Figure 8.5 Tumour area quantified over time for three doses of isotretinoin in addition to control. Zebrafish with fluorescent neuroblastoma tumours are treated from day 0 onwards. After the indicated treatment interval, the zebrafish were fixated and imaged (n≥6 per dose per day). Symbols (control: black star, 1 µM: blue square, 1.5 µM: magenta circle, 2 µM: orange triangle) show individual tumour area, lines (control: black dot-dashed, 1 µM blue solid, 1.5 µM: magenta dotted, 2 µM: orange dashed) connect median values. No effect of isotretinoin treatment on tumour area is observed.

8.4.3 Tumour measurements over time

Neuroblastoma tumour dynamics over the treatment period were quantified by multiple measurement of neuroblastoma size at 24 hour intervals, to be able to determine onset, intensity, and duration of drug effect. Fluorescence images were captured of the fixed zebrafish (Figure 8.4). Tumour area was quantified two-dimensionally and results are shown in Figure 8.5. No statistically significant effect was observed when testing tumour size against treatment over time (Kruskal-Wallis test, $p > 0.05$). However, after the two treatment medium refreshments at 48 and 96 hours, a small decreasing trend in tumour size could be observed.

8.5 Discussion

Previously, isotretinoin treatment showed reduced growth or even decreased tumour size in the zebrafish neuroblastoma disease model[2]. In biomedical research with zebrafish, it is commonly assumed that drug concentration in the treatment medium is constant and internal exposure will reach a steady state, which we tested here by quantifying isotretinoin exposure inside the zebrafish and isotretinoin concentrations in the treatment medium. Moreover, to study neuroblastoma dynamics in the zebrafish, we have taken multiple measures of tumour size over the treatment period, to determine onset, duration, and intensity of drug effects.

Our analysis showed that internal isotretinoin exposure did not reach steady state in our study. In this case, the general assumption regarding constant external and internal exposure therefore does not hold. Treatment medium concentrations were 14% from nominal concentrations, which was similar to independently quantified drug stock control samples (data not shown). Decline of isotretinoin in treatment medium was described by degradation rate constants, that varied slightly between the dose refreshments. Isomerization was ruled out as the cause of this decline, nor was biotransformation through metabolism by the zebrafish involved, as no 4-oxo-metabolite was observed as major metabolite in the zebrafish or treatment medium (data not shown). Adhesion to experimental material might be the case, although this adhesion needs to be similar for both glass and plastic material which is unlikely. Clearly these studies show that the drug should be refreshed more often than every 48 hours and that

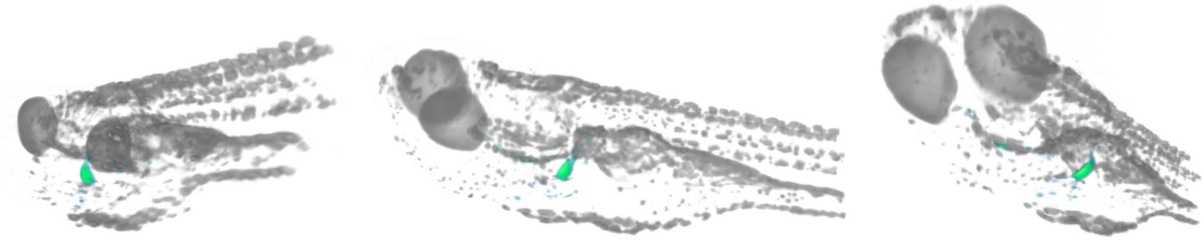

Figure 8.6 Three-dimensional reconstruction of neuroblastoma tumour volume after optical projection tomography. Neuroblastoma tumour shape is depicted in green, zebrafish brightfield signal in grey.

the internal exposure reflects the rapid drop in concentrations of the drug in the treatment medium over the 48 hours dosing interval between refreshing the drug in the treatment medium.

We found no drug effect of isotretinoin on neuroblastoma tumour size. This was in contrast to previous findings, where before and after treatment measurements were taken within the same zebrafish[2]. In that case, repeated measurements within the same subject decrease variability, making distinguishing a drug effect more likely. We suggest to measure individual fish every 24 hours to quantify the change in tumour area in individual fish of each treatment group over time during treatment. This is possible because the fish can be imaged without fixing and sacrificing them for each measurement. Also, the lack of drug effect here is not surprising when considering that internal exposure during the majority of the treatment duration was well below target concentrations of 2-10 µM[6,22–25]. When assuming a homogenous isotretinoin distribution throughout the zebrafish and a volume derived from wet weight[26,27] of 3.5-4 µL, the highest internal isotretinoin concentrations were in the range of 8.4-34 pmole/µL or µM, but declined to subtherapeutic levels within 14-23 hours (Figure 8.3). Another explanation for not observing an isotretinoin effect in the current study could be that photo-isomerization of isotretinoin to 9-cis retinoic acid and all-trans retinoic acid was minimal, as UV-exposure was well-controlled in all experimental procedures performed here (Supplementary Figure S8.2). Because the mechanism of action of isotretinoin therapy is not elucidated and receptor binding to the retinoic acid receptor (RAR) or the retinoid X receptor (RXR) appears to be important, a photo-isomer with different receptor affinity could have been responsible for the drug response on the tumour in previous experiments[6,28].

Additionally, variability in tumour size was large in our study (Figure 8.5), partly because zebrafish were fixed and therefore only one measurement per individual zebrafish could be taken. The tumour size in zebrafish was quantified two-dimensionally, but this technique is not ideal to quantify irregular or asymmetric three-dimensional shapes like tumours. Moreover, in the case of neuroblastoma, a clear lateral view of the tumour can be hindered by the melanocyte umbrella[29], which negatively impacts the accuracy of the tumour area measurement. A recent innovation in fluorescence imaging is three-dimensional reconstruction based on two-dimensional images taken from different angles around an object. This optical projection tomography (OPT)[30] can be used on larger specimen like zebrafish, that surpass the working depth of conventional confocal microscopy. Application of OPT on tumour imaging will result in more precise quantification of shape and therefore the three-dimensional size, and has been explored with representative zebrafish samples, embedded in low melting point agarose, cut into cylindric shapes, and imaged in PBS from 400 angles (Figure 8.6). Further optimization of this technique is warranted, for integration with our current quantitative analysis.

In conclusion, we demonstrated the importance of quantification of internal drug exposure and linking this to tumour dynamics through pharmacokinetic-pharmacodynamic analysis in the zebrafish neuroblastoma model. We propose that this approach should be adopted more widely in pharmacological studies using the zebrafish as disease model.

8.6 Acknowledgements

The authors would like to thank Linda Aulin for code reviewing the R- and NONMEM-scripts.

8.7 References

1. Fletcher JI, Ziegler DS, Trahair TN, et al. Too many targets, not enough patients: Rethinking neuroblastoma clinical trials. Nat Rev Cancer. 2018;18(6):389-400.
2. He S, Mansour MR, Zimmerman MW, et al. Synergy between loss of NF1 and overexpression of MYCN in neuroblastoma is mediated by the GAP-related domain. eLife. 2016;5:e14713.
3. Maris JM. Recent advances in neuroblastoma. N Engl J Med. 2010;362(23):2202-2211.
4. Veal GJ, Errington J, Redfern CPF, et al. Influence of isomerisation on the growth inhibitory effects and cellular activity of 13-cis and all-trans retinoic acid in neuroblastoma cells. Biochem Pharmacol. 2002;63(2):207-215.
5. Nathan Bushue, Wan Y-JY. Retinoid pathway and cancer therapeutics. Adv Drug Deliv Rev. 2010;62(13):1285-1298.
6. Armstrong JL, Redfern CPF, Veal GJ. 13-cis Retinoic acid and isomerisation in paediatric oncology - is changing shape the key to success? Biochem Pharmacol. 2005;69(9):1299-1306.
7. Kantae V, Krekels EHJ, Ordas A, et al. Pharmacokinetic modeling of paracetamol uptake and clearance in zebrafish larvae: Expanding the allometric scale in vertebrates with five orders of magnitude. Zebrafish. 2016;13(6):504-510.
8. Van Wijk RC, Krekels EHJ, Kantae V, et al. Impact of post-hatching maturation on the pharmacokinetics of exogenous compounds in zebrafish larvae. Sci Rep. 2018;9:2149.
9. Van Wijk RC, Krekels EHJ, Kantae V, et al. Mechanistic and quantitative understanding of pharmacokinetics in zebrafish larvae through nanoscale blood sampling and metabolite modelling of paracetamol. J Pharmacol Exp Ther. 2019;371:15-24.
10. Morgan P, Van der Graaf PH, Arrowsmith J, et al. Can the flow of medicines be improved? Fundamental pharmacokinetic and pharmacological principles toward improving Phase II survival. Drug Discov Today. 2012;17(9/10):419-424.
11. Heyman RA, Mangelsdorf DJ, Dyck JA, et al. 9-cis retinoic acid is a high affinity ligand for the retinoid X receptor. Cell. 1992;68(2):397-406.
12. Westerfield M. The zebrafish book. A guide for the laboratory use of zebrafish (Danio rerio). 4th ed. Eugene, OR, USA: University of Oregon Press; 2000.
13. Viswanathan CT, Bansal S, Booth B, et al. Quantitative bioanalytical methods validation and implementation: Best practices for chromatographic and ligand binding assays. Pharm Res. 2007;24(10):1962-1973.
14. Beal S, Sheiner L, Boeckmann A, et al. NONMEM 7.3.0 users guides. (1989-2013). ICON Development Solutions, Hanover, MD, USA.
15. Keizer R, Van Benten M, Beijnen J, et al. Pirana and PCluster: a modeling environment and cluster infrastructure for NONMEM. Comput Methods Programs Biomed. 2011;101(1):72-79.
16. Lindbom L, Pihlgren P, Jonsson E. PsNtoolkit — a collection of computer intensive statistical methods for non-linear mixed effect modeling using NONMEM. Comput Methods Programs Biomed. 2005;79(3):241-257.
17. R Core Team. R: A language and environment for statistical computing. R Found Stat Comput Vienna, Austria. 2014.
18. Beal SL. Ways to fit a PK model with some data below the quantification limit. J Pharmacokinet Pharmacodyn. 2001;28(5):481-504.
19. Nguyen THT, Mouksassi M-S, Holford N, et al. Model evaluation of continuous data pharmacometric models: metrics and graphics. CPT Pharmacometrics Syst Pharmacol. 2017;6:87-109.
20. Ludden TM, Beal SL, Sheiner LB. Comparison of the Akaike Information Criterion, the Schwarz Criterion and the F Test as guides to model selection. Vol 22.; 1994.

21. Schindelin J, Arganda-Carreras I, Frise E, et al. Fiji: An open-source platform for biological-image analysis. Nat Methods. 2012;9(7):676-682.
22. Veal GJ, Errington J, Rowbotham SE, et al. Adaptive dosing approaches to the individualization of 13-cis-retinoic acid (isotretinoin) treatment for children with high-risk neuroblastoma. Clin Cancer Res. 2013;19(2):469-479.
23. Gota V, Chinnaswamy G, Vora T, et al. Pharmacokinetics and pharmacogenetics of 13-cis retinoic acid in Indian high-risk neuroblastoma patients. Cancer Chemother Pharmacol. 2016;78(4):763-768.
24. Matthay KK. Targeted isotretinoin in neuroblastoma: kinetics, genetics, or absorption. Clin Cancer Res . 2013;19(2):311-313.
25. Reynolds CP. Differentiating agents in pediatric malignancies: retinoids in neuroblastoma. Curr Oncol Rep. 2000;2(6):511-518.
26. Von Hertell U, Hörstgen-Schwark G, Langholz HJ, et al. Family studies on genetic variability in growth and reproductive performance between and within test fish populations of the zebrafish, Brachydanio rerio. Aquaculture. 1990;85(1-4):307-315.
27. Avella MA, Place A, Du S, et al. Lactobacillus rhamnosus accelerates zebrafish backbone calcification and gonadal differentiation through effects on the GnRH and IGF systems. PLoS One. 2012;7(9).
28. Sonawane P, Cho HE, Tagde A, et al. Metabolic characteristics of 13-cis-retinoic acid (isotretinoin) and anti-tumour activity of the 13-cis-retinoic acid metabolite 4-oxo-13-cis-retinoic acid in neuroblastoma. Br J Pharmacol. 2014;171(23):5330-5344.
29. Kapp FG, Perlin JR, Hagedorn EJ, et al. Protection from UV light is an evolutionarily conserved feature of the haematopoietic niche. Nature. 2018;558(7710):445-448.
30. Tang X, Van der Zwaan DM, Zammit A, et al. Fast Post-Processing Pipeline for Optical Projection Tomography. IEEE Trans Nanobioscience. 2017;16(5):367-374.

8.8 Supplementary material

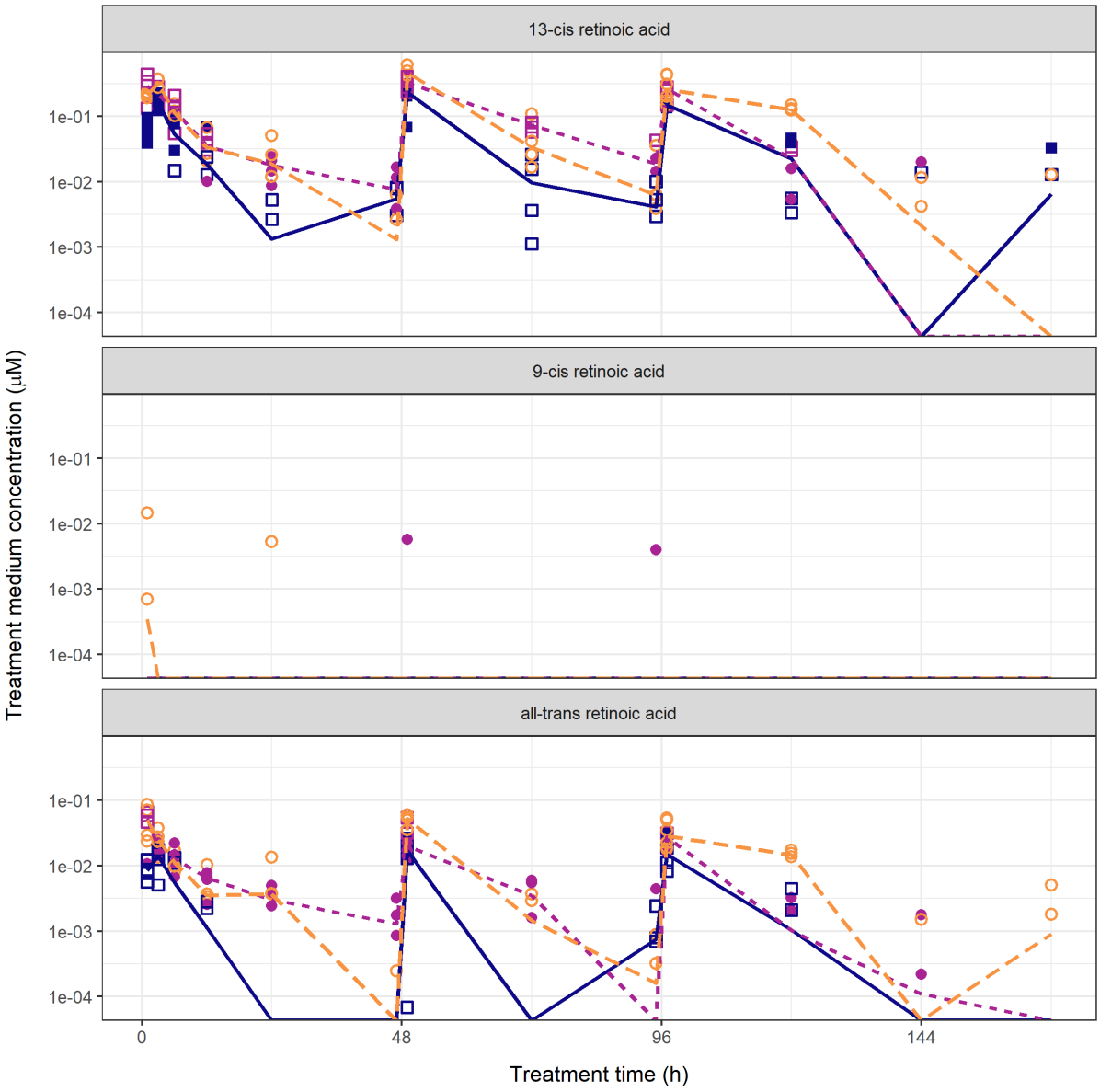

Supplementary Figure S8.1 Concentration of isotretinoin and its photo-isomers in treatment medium over time. Isotretinoin treatment is for duration of 168 hours at three dose levels, with treatment medium refreshment at 48h and 98h. Closed symbols (1 µM: blue square, 1.5 µM: magenta circle, 2 µM: orange triangle) are measures within the calibration range, open symbols are measures below the lower limit of quantification or above the highest calibration standard. Lines (1 µM: blue solid, 1.5 µM: magenta dotted, 2 µM: orange dashed) connect median values. Y-axes are kept to the same scale.

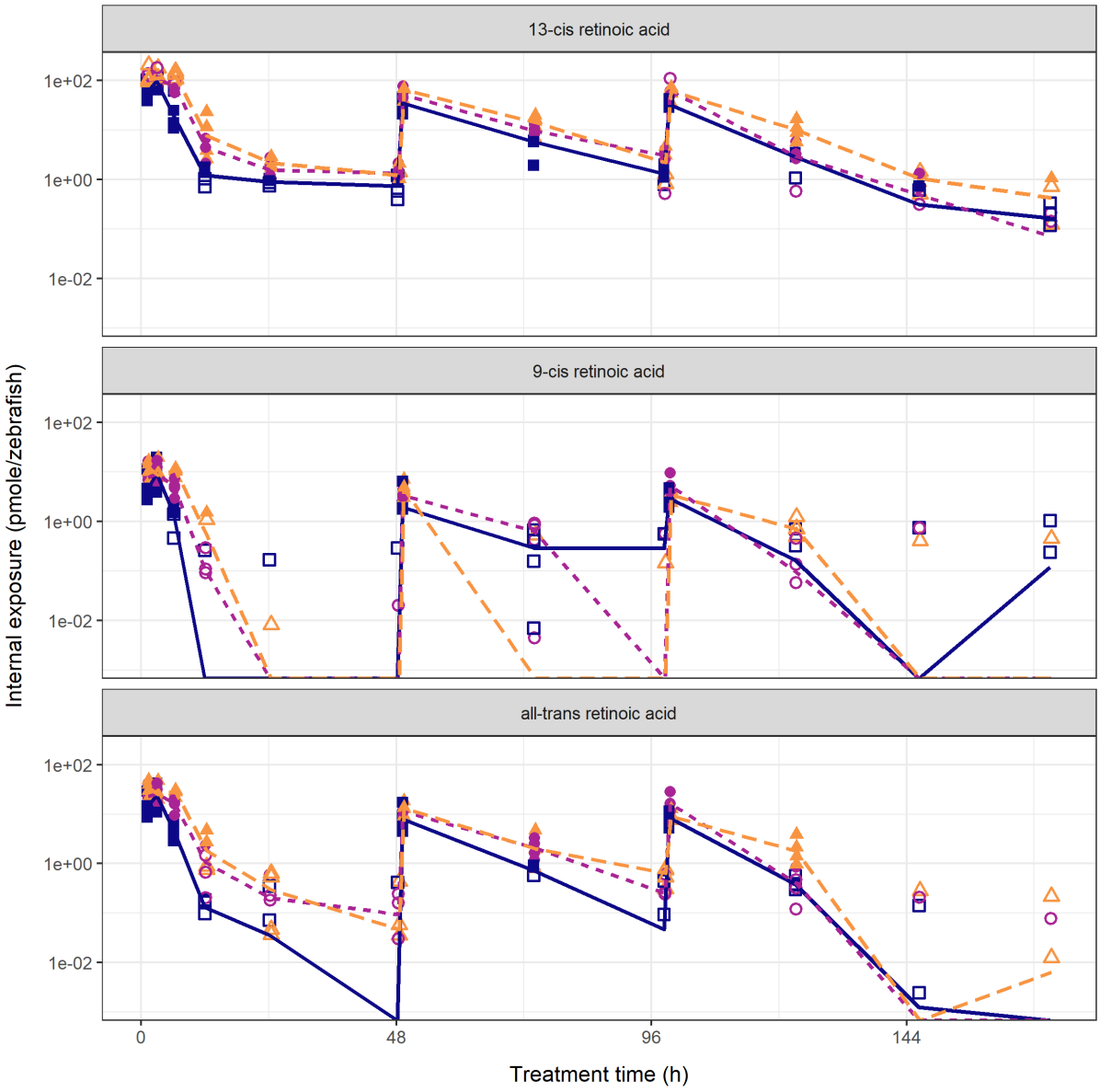

Supplementary Figure S8.2 Internal exposure of isotretinoin and isomers in zebrafish over time. Isotretinoin treatment is for duration of 168 hours at three dose levels, with treatment medium refreshment at 48h and 98h. Closed symbols (1 µM: blue square, 1.5 µM: magenta circle, 2 µM: orange triangle) are measures within the calibration range, open symbols are measures below the lower limit of quantification or above the highest calibration standard. Lines (1 µM: blue solid, 1.5 µM: magenta dotted, 2 µM: orange dashed) connect median values.

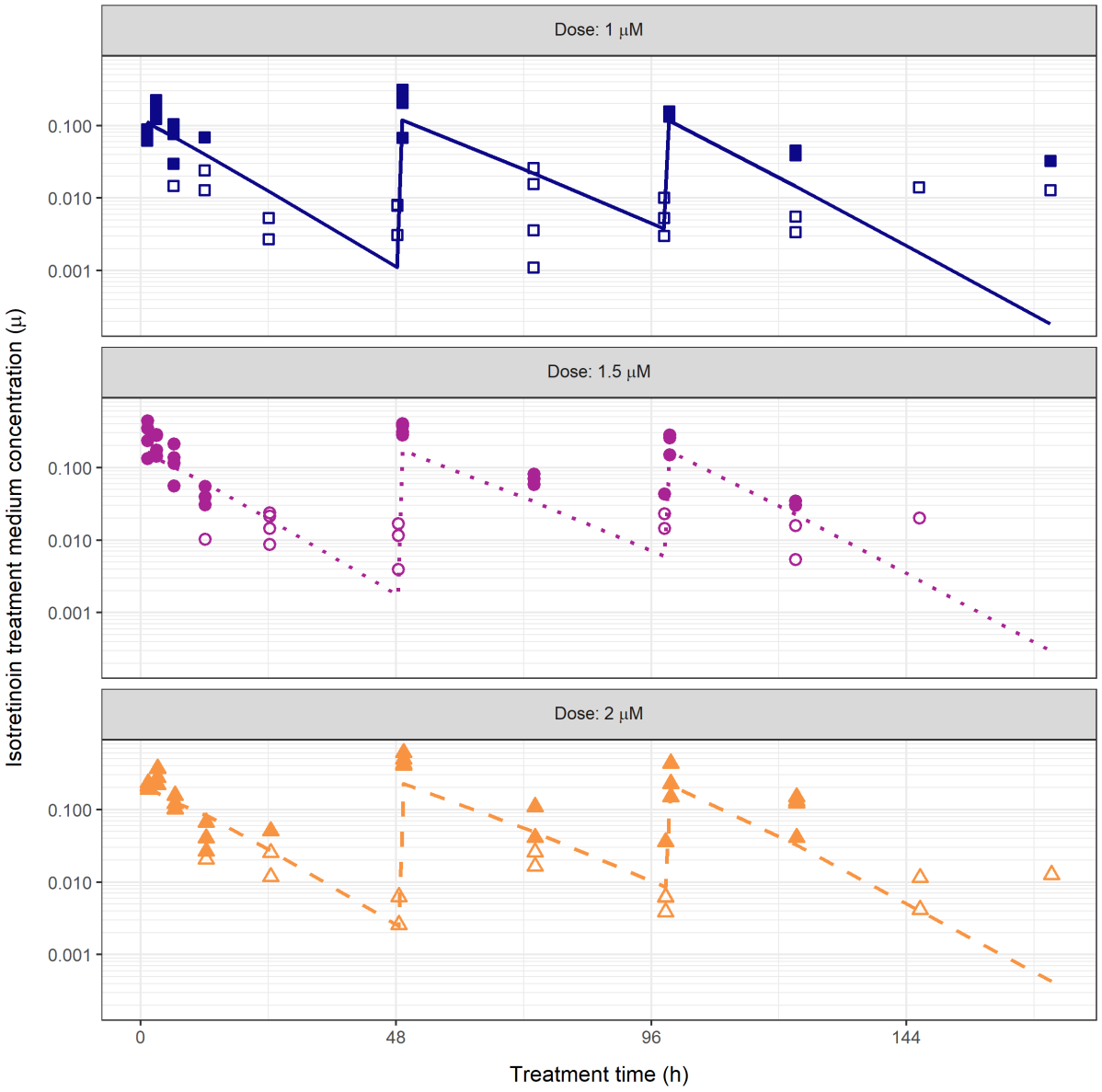

Supplementary Figure 8.3 Model predicted isotretinoin treatment medium concentration over time. Isotretinoin treatment is for duration of 168 hours at three dose levels, with treatment medium refreshment at 48h and 98h. Closed symbols are observed treatment medium concentrations within the calibration range (1 µM: blue square, 1.5 µM: magenta circle, 2 µM: orange triangle), open symbols are measures below the lower limit of quantification or above the highest calibration standard. Lines (1 µM: blue solid, 1.5 µM: magenta dotted, 2 µM: orange dashed) show pharmacokinetic model predictions.

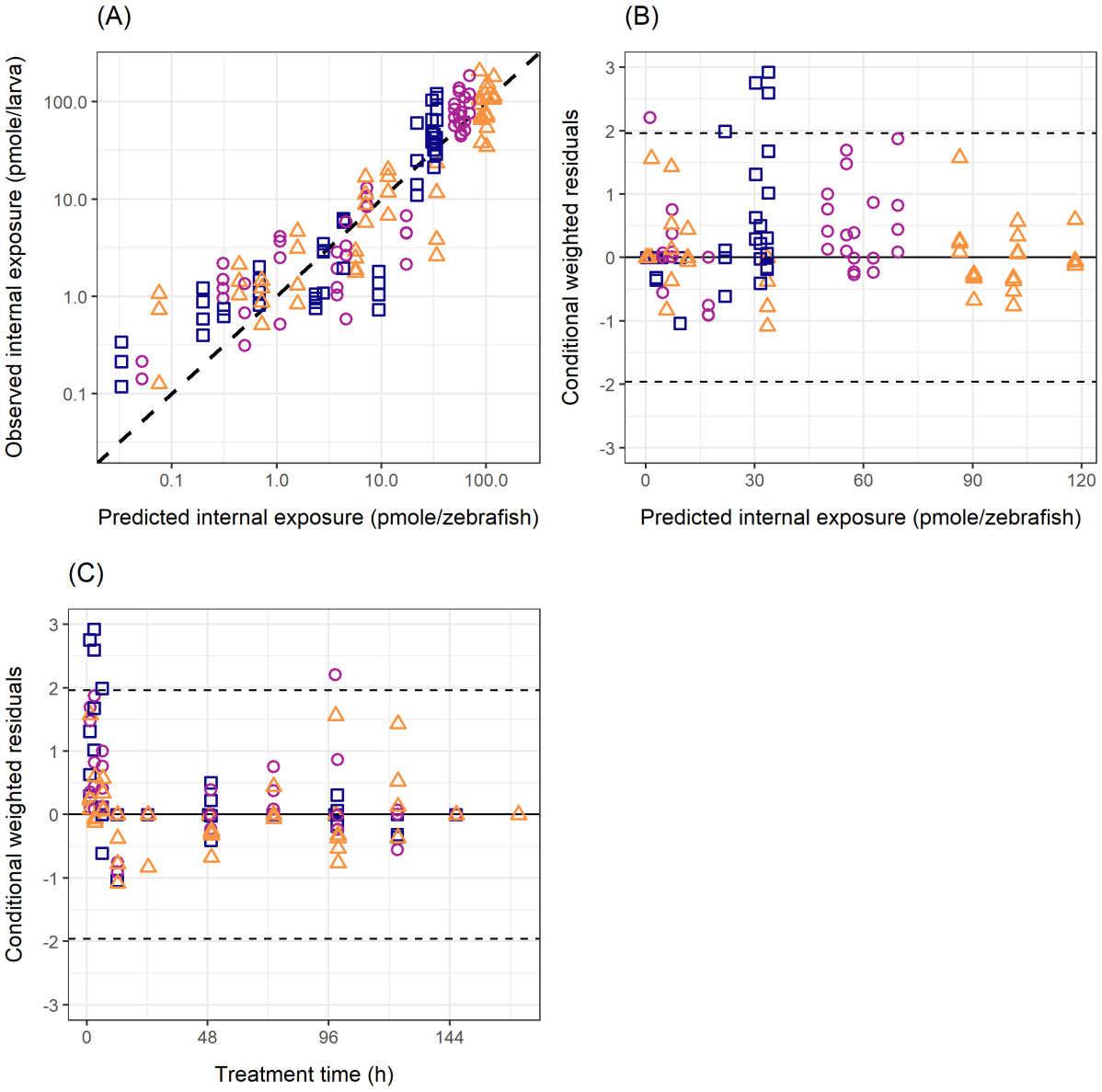

Supplementary Figure 8.4 Goodness-of-fit plots for the isotretinoin internal exposure. (A) Observed vs predicted, dotted line is the line of unity. (B) Conditional weighted residuals vs prediction, solid line represents zero, dashed lines represent 95% interval between ±1.96 standard deviation. (C) Conditional weighted residuals vs time, solid line represents zero, dashed lines represent 95% interval between ±1.96 standard deviation. Symbols represent doses 1 (blue squares), 1.5 (magenta circles), or 2 µM (orange triangles). Limited trends in the goodness-of-fit plots indicates no bias in the description of internal exposure by the final model.

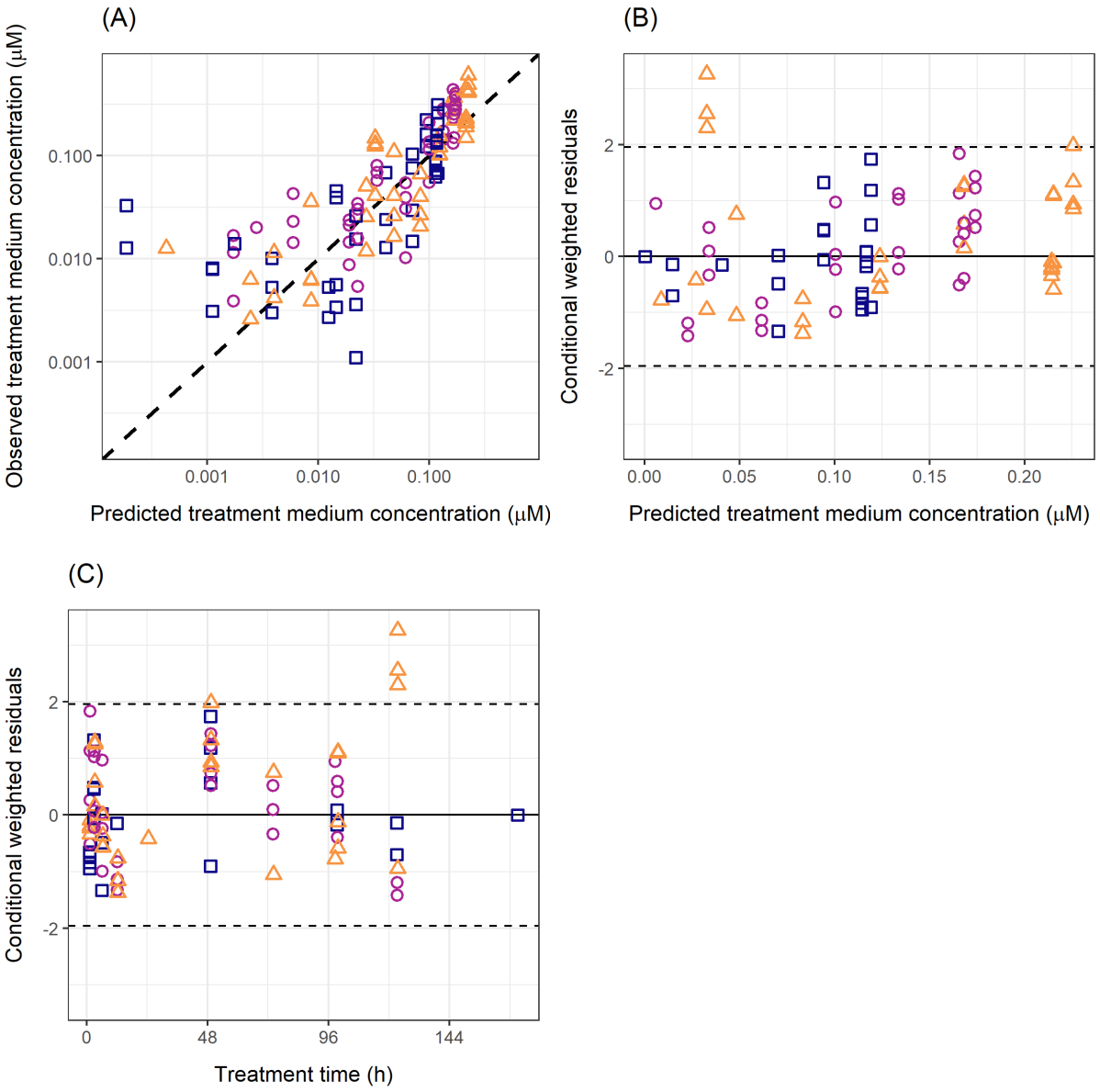

Supplementary Figure S8.5. Goodness-of-fit plots for the isotretinoin treatment medium concentration. (A) Observed vs predicted, dotted line is the line of unity. (B) Conditional weighted residuals vs prediction, solid line represents zero, dashed lines represent 95% interval between ±1.96 standard deviation. (C) Conditional weighted residuals vs time, solid line represents zero, dashed lines represent 95% interval between ±1.96 standard deviation. Symbols represent doses 1 (blue squares), 1.5 (magenta circles), or 2 μM (orange triangles). Limited trends in the goodness-of-fit plots indicates no bias in the description of internal exposure by the final model.

8.9 NONMEM model code

```
$PROBLEM PK
$INPUT ID TIME AMT DV EVID MDV CMT BQL AQL DOSE AREA INJ REFRESH
$DATA ISOTRETINOIN_PK_dataset.csv IGNORE=@

; time in hours of exposure
; DV in pmole/uL or uM (CMT 2) or pmole/zebrafish (CMT 3)

$SUBROUTINE ADVAN13 TOL=9

$MODEL
COMP ;CMT 1 depot (in pmole)
COMP ;CMT 2 treatment medium
COMP ;CMT 3 isotretinoin in zebrafish

$PK

TVKA = THETA(1)      ;depot to treatment medium compartment (fixed to high
value, mathematical solution to be able to estimate F)
TVF1 = THETA(2)      ;fraction of nominal dose quantified in treatment medi-
um
TVKAZF = THETA(3)    ;first order absorption rate constant from treatment
medium  compartment
TVVMAX = THETA(4)    ;maximal rate of excretion (saturable excretion)
TVKM = THETA(5)      ;internal exposure at which half of the maximal rate
of excretion is reached (saturable excretion)

TVKDEG1 = THETA(6)   ;degradation rate constant of isotretinoin from treat-
ment medium, refreshment 1
TVKDEG2 = THETA(7)   ;degradation rate constant of isotretinoin from treat-
ment medium, refreshment 2
TVKDEG3 = THETA(8)   ;degradation rate constant of isotretinoin from treat-
ment medium, refreshment 3

IF(REFRESH.EQ.1) KDEG = TVKDEG1
IF(REFRESH.EQ.2) KDEG = TVKDEG2
IF(REFRESH.EQ.3) KDEG = TVKDEG3

KA = TVKA * EXP(ETA(1))
KAZF = TVKAZF
F1 = TVF1
VMAX = TVVMAX *100   ;multiplied by 100 to bring into same range of parame-
ter estimates
KM = TVKM * 100      ;multiplied by 100 to bring into same range of parame-
ter estimates

$DES
DADT(1) = - KA * A(1)
DADT(2) = KA * A(1) - KDEG * A(2) - KAZF * A(2) + VMAX * A(3) / (KM + A(3))
DADT(3) = KAZF * A(2) - VMAX * A(3) / (KM + A(3))

A1 = A(1)
A2 = A(2)
A3 = A(3)

$ERROR

SIG1 = THETA(9)  ;proportional residual error treatment medium
SIG2 = THETA(10) ;additive residual error treatment medium
SIG3 = THETA(11) ;proportional residual error zebrafish
```

```
SIG4 = THETA(12) ;additive residual error zebrafish

;treatment medium

IF(BQL.EQ.0.AND.CMT.EQ.2) THEN
IPRED = A(2)/3000 ;divide by 3000 which is the volume of the well in uL (3
mL) to get concentration in pmole/uL for treatment medium
F_FLAG = 0
Y = IPRED * (1 + SIG1 * EPS(1)) + SIG2 ; comb error
ENDIF

IF(BQL.EQ.1.AND.CMT.EQ.2) THEN
LOQ = 0.026628 ;pmole/uL
IPRED = A(2)/3000 ;divide by 3000 which is the volume of the well in uL (3
mL) to get concentration in pmole/uL for treatment medium
W = SQRT(IPRED**2 * SIG1**2 + SIG2**2)
DUM = (LOQ - IPRED) / W
CUMD = PHI(DUM)
F_FLAG = 1
Y = CUMD
ENDIF

;zebrafish

IF(BQL.EQ.0.AND.CMT.EQ.3) THEN
IPRED = A(3)
F_FLAG = 0
Y = IPRED * (1 + SIG3 * EPS(1)) + SIG4 ; comb error
ENDIF

;injection 1 has LLOQ 5 ng/mL (or 5 ng/mL * 100 uL / molecular weight =
1.6642)

IF(BQL.EQ.1.AND.CMT.EQ.3.AND.INJ.EQ.1) THEN
LOQ = 1.6642   ;pmole/zebrafish
IPRED = A(3)
W = SQRT(IPRED**2 * SIG3**2 + SIG4**2)
DUM = (LOQ - IPRED) / W
CUMD = PHI(DUM)
F_FLAG = 1
Y = CUMD
ENDIF

;injection 2 and 3 has LLOQ 2 ng/mL (or 2 ng/mL * 100 uL / molecular weight
= 0.66570)

IF(BQL.EQ.1.AND.CMT.EQ.3.AND.INJ.NE.1) THEN
LOQ = 0.66570  ;pmole/zebrafish
IPRED = A(3)
W = SQRT(IPRED**2 * SIG3**2 + SIG4**2)
DUM = (LOQ - IPRED) / W
CUMD = PHI(DUM)
F_FLAG = 1
Y = CUMD
ENDIF

$THETA
(100) FIX   ;1 KA h-1
(0, 0.14)   ;2 F (-)
(0, 0.155)  ;3 KAZF1 h-1
(0, 0.923)  ;4 *100 VMAX pmole/h
(0, 0.337)  ;5 *100 KM pmole/zebrafish
```

```
(0, 0.106)  ;6 KDEG1 h-1
(0, 0.0757) ;7 KDEG2 h-1
(0, 0.0964) ;8 KEDG3 h-1
(0, 0.781)  ;eps1 prop treatment medium (-)
(0, 0.0326) ;eps2 add treatment medium (pmole/uL)
(0, 0.877)  ;eps3 prop zebrafish (-)
(0, 0.958)  ;eps4 add zebrafish (pmole/zebrafish)

$OMEGA
 0 FIX

$SIGMA
 1 FIX

$ESTIMATION METHOD=1 LAPLACIAN NUMERICAL MAXEVAL=8000 NOABORT PRINT=10
NSIG=3 SIGL=9 POSTHOC
$COVARIANCE PRINT=E

$TABLE ID TIME AMT DV EVID MDV CMT BQL AQL DOSE AREA INJ REFRESH
KA F1 KDEG KAZF VMAX KM ETA(1) A1 A2 A3 OBJI IPRED CWRES NOPRINT ONEHEADER
FILE=tab01
```

Section IV. Mechanistic and quantitative translation of exposure-response from zebrafish to higher vertebrates

Chapter 9

Quantification of natural growth of two strains of *Mycobacterium marinum* for translational anti-tuberculosis drug development

Rob C. van Wijk, Astrid M. van der Sar, Elke H.J. Krekels, Theo Verboom, Herman P. Spaink, Ulrika S.H. Simonsson*, Piet H. van der Graaf*

Submitted

* authors contributed equally

9.1 Abstract

9.1.1 Background
The zebrafish infected with *Mycobacterium marinum* is an attractive tuberculosis disease model, which shows similar pathogenesis to that caused by *Mycobacterium tuberculosis* in humans. To translate pharmacological findings from this disease model to higher vertebrates, a quantitative understanding of the natural growth of *M. marinum* in comparison to that of *M. tuberculosis* is essential.

9.1.2 Objectives
To study natural growth of two strains of *M. marinum*, E11 and MUSA, over an extended period using an established model-based approach, the multistate tuberculosis pharmacometric (MTP) model, and compare to that of *M. tuberculosis*.

9.1.3 Methods
Human-derived strain M^{USA} and poikilotherm-derived strain E11 were grown undisturbed for 221 days and viability of cultures (CFU/mL) was determined by plating at different time points. Non-linear mixed effects modelling was performed using the MTP model to quantify the bacterial growth, the transfer between fast-, slow-, and non-multiplying states, and the inoculi.

9.1.4 Results
Both strains showed initial logistic growth, reaching a maximum after 20-25 days for E11 and M^{USA}, respectively, followed by a decrease to a new plateau. Both E11 and M^{USA} were best described with a Gompertz growth function and constant transfer functions. For E11, the inoculum was best described in the slow-multiplying state, for M^{USA} in the fast-multiplying state. The final models described the data well, E11 model parameters were most similar to *M. tuberculosis* results.

9.1.5 Conclusions
Characterization of natural growth of *M. marinum* and quantitative comparison with *M. tuberculosis* brings the zebrafish tuberculosis disease model closer to the quantitative translational pipeline of anti-tuberculosis drug development.

9.2 Introduction

The zebrafish (*Danio rerio*) is an increasingly utilized disease model organism to study tuberculosis pathology and potential novel therapeutic interventions[1,2]. Infections of zebrafish embryos with *Mycobacterium marinum*, a close relative of *Mycobacterium tuberculosis*[3], show similar pathogenesis to that caused by *M. tuberculosis* in humans[4].

Translation of pharmacological findings from zebrafish embryos and larvae to higher vertebrates, including humans, requires a quantitative understanding of similarities and differences in pathophysiology between infecting mycobacteria. This forms the basis for a translational framework in drug development. One proposed model-based drug development approach for tuberculosis is the multistate tuberculosis pharmacometric (MTP) model[5]. This model distinguishes three states of multiplication for mycobacteria and characterizes natural growth in absence of drugs to obtain growth rates and transfer rates between these states. The MTP model has been successfully used in translation from pharmacological findings of *M. tuberculosis* treatment *in vitro*[5], to mice[6] and humans[7]. To include the zebrafish in the translational pipeline for tuberculosis drug development, it is necessary to study the natural growth of *M. marinum* and quantitatively compare this to *M. tuberculosis*.

Here, the natural growth of *M. marinum* was studied over an extended period in two strains, one poikilotherm-derived (E11) and one human-derived (M^{USA}) strain. To facilitate a quantitative comparison

to natural growth of *M. tuberculosis* and assess the translational potential of pharmacological findings between species, the natural growth was characterized using the MTP model[5].

9.3 Material and methods

9.3.1 Natural growth assay

M. marinum sea bass-isolate strain E11[8] and human-derived strain M^{USA} [9], were cultured in DifcoTM Middlebrook 7H9 broth medium (BD Biosciences, Franklin Lakes, USA) containing 0.05% Tween80 (Merck KGaA, Darmstadt, Germany) and 10% BBLTM Middlebrook Albumin Dextrose Catalase (ADC) Enrichment (BD Biosciences) at 30 °C without disturbance for 221 days. Three series of cultures from individually grown colonies each containing at least 24 replicates were included. The start inoculum was set to an OD_{600} of 0.05. At different time points the viability of the cultures, defined as colony forming units (CFU) per millilitre, was determined by plating a series of 10-fold dilutions in triplicate on DifcoTM Middlebrook 7H10 agar (BD Biosciences) containing 5% glycerol (Sigma-Aldrich, St Louis, Missouri, USA) and 10% BBLTM Middlebrook Oleic Albumin Dextrose Catalase (OADC) Enrichment (BD Biosciences).

9.3.2 Model-based quantification of natural growth

Non-linear mixed effects modelling using the First Order Conditional Estimation was performed with NONMEM (version 7.3)[10] through interfaces Pirana (version 2.9.6)[11] and PsN (version 4.7.0)[12]. Data transformations and graphical output were generated with R (version 3.5.0)[13] through interface Rstudio (version 1.1.383, RStudio Inc, Boston, Massachusetts, USA). The previously developed MTP model[5] for *M. tuberculosis* was used to fit the CFU of both *M. marinum* strains. The model structure consisted of three bacterial states for fast-, slow-, and non-multiplying bacteria, where fast- and slow-multiplying bacteria were assumed to yield CFUs:

$$\frac{dF}{dt} = k_g \cdot F + k_{SF} \cdot S - k_{FS} \cdot F - k_{FN} \cdot F \quad (1)$$

$$\frac{dS}{dt} = k_{FS} \cdot F + k_{NS} \cdot N - k_{SF} \cdot S - k_{SN} \cdot S \quad (2)$$

$$\frac{dN}{dt} = k_{FN} \cdot F + k_{SN} \cdot S - k_{NS} \cdot N \quad (3)$$

in which F represented the fast-, S the slow-, and N the non-multiplying state, k_g represents the growth function, k-values represent transfer rates between the first and second state mentioned in the subscript. The transfer rates were fixed to values obtained in the MTP model for *M. tuberculosis*, with the exception of the transfer rate between the fast- and slow-multiplying state, which was estimated. Different functions were tested to quantify the growth rates, as well as the transfer rates between the fast- and slow-multiplying state, and the inoculi. To quantify the growth rate for the *M. marinum* strains, exponential, Gompertz, and logistic functions were tested:

$$k_g = k_{g,e} \quad (4)$$

$$k_g = k_{g,G} \cdot \log\left(\frac{B_{max}}{F + S + N}\right) \quad (5)$$

$$k_g = k_{g,l} \cdot \log\left(B_{max} - (F + S + N)\right) \quad (6)$$

where $k_{g,e}$ is the exponential growth rate, $k_{g,G}$ is the Gompertz growth rate, B_{max} is the maximum capacity of the system, and $k_{g,l}$ is the logistic growth rate.

The transfer rates between the fast- and slow-multiplying state were tested as a constant, or as capacity- or time-dependent function. For the time dependency, linear as well as E_{max} and exponential functions were tested as described previously[5].

The inoculum at t=0 was tested to either be all in the fast-multiplying state (F_0), or all in the slow multiplying state (S_0), or both F_0 and S_0 were estimated independently. No bacteria were assumed to be non-multiplying at the logistic growth phase at start of the experiment, therefore N_0 was fixed to zero. Two levels of variability were tested to distinguish biological from experimental variability. However, biological variability could not be estimated with acceptable precision. Residual error was quantified as a proportional error.

Model selection criteria were biological plausibility of parameter estimates, as well as standard goodness-of-fit plots[14]. The likelihood ratio test was used to test statistical significance between nested models, with p=0.05 at a drop in objective function value (ΔOFV) of 3.84 with a single degree of freedom, assuming the χ^2-distribution. Non-nested models were compared by Akaike Information Criterion (AIC), which penalizes ΔOFV with the number of additional parameters[15].

9.4 Results

9.4.1 Natural growth M. marinum

Both *M. marinum* strains show an initial logistic growth phase as represented by the CFU in Figure 9.1 A and B. This growth phase reaches a maximum for E11 at 1 x 10^9 CFU/mL after 20 days, after which it decreases to a plateau of 1 x 10^7 CFU/mL after 100 days. For M^{USA}, an initial maximum was reached after 25 days at 3 x 10^8 CFU/mL. Its decrease to a plateau similar to E11 was however less clear, due to high variability.

9.4.2 MTP model predictions

For strain E11, the MTP model with a Gompertz growth function, constant transfer rates between the fast- and slow-multiplying states and the inoculum estimated to be exclusively in the slow multiplying state, resulted in the best fit. Both a linear and logistic growth function decreased the fit substantially (ΔAIC = 40.8 and 39.2, respectively). Estimating the inoculum in the fast state (F_0) was statistically significantly worse (ΔOFV = 8.51, $p < 0.005$). Including growth functions on both fast and slow states did not statistically improve the fit.

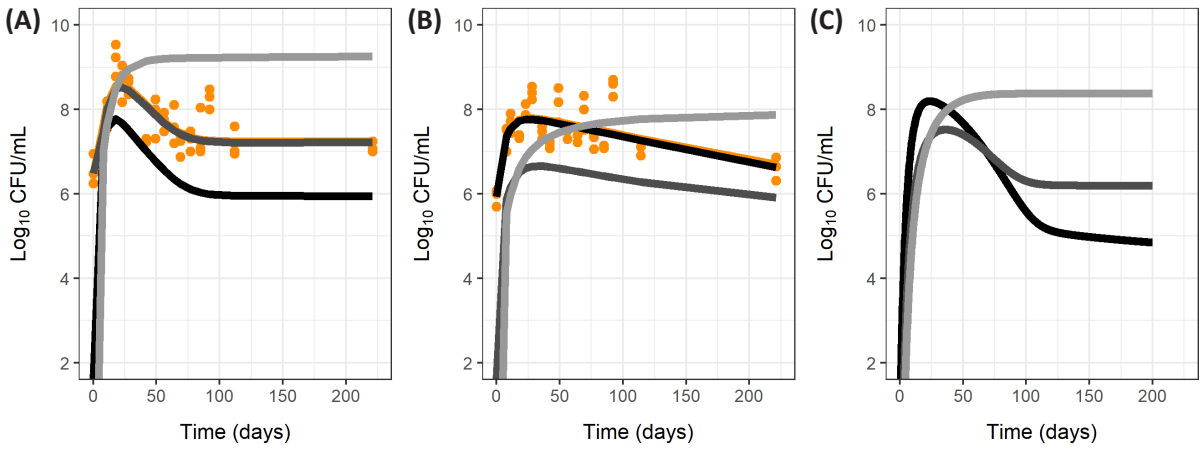

Figure 9.1 Natural growth of *M. marinum* strains E11 and M^{USA} for hypoxic growth during 221 days. (A) Model predictions of bacterial counts in different multiplying states for natural growth in CFU/mL of E11; (B) Model predictions of bacterial counts in different multiplying states for natural growth in CFU/mL of M^{USA}; (C) Model predictions of bacterial counts in different multiplying states for *M. tuberculosis*[5]. Lines: prediction of bacterial counts in fast- (black), slow- (dark grey) and non- (light grey) multiplying states. The sum of fast- and slow-multiplying states (orange line) is assumed to equal the observed CFU/mL (orange symbols).

For strain M^{USA}, the MTP model with Gompertz growth function, constant transfer rates between the fast- and slow-multiplying states, and the inoculum estimated to be exclusively in the fast state resulted in the best fit. Both a linear and logistic growth function decreased the fit substantially (ΔAIC = 23.3 and 34.4, respectively). Model fit was very similar when parameterizing transfer between fast and slow states as capacity- or time-dependent, but based on precision of parameter estimates and parsimony, a constant transfer rate was selected for the final model. All tested approaches for the inoculum resulted in similar fits, based on parameter precision an inoculum in F_0 was selected.

Final model predictions for number of bacteria in all three states are shown in Figure 9.1 A and B, final parameter estimates are given in Table 9.1, diagnostic plots are given in Supplementary Figures S9.1-4. Model prediction of the three states for strain E11 shows relatively quick transfer from F to S and N, while for strain M^{USA} the F state is the major contributor to the natural growth. The growth rate constants of E11 and M^{USA}, 0.188 and 0.169 day^{-1} respectively, were comparable to that of *M. tuberculosis* (0.206 day^{-1})[5]. For *M. tuberculosis*, S_0 contained the majority of the total inoculum[5], which was similar to E11 but not M^{USA}.

9.5 Discussion

To utilize *M. marinum* in the zebrafish tuberculosis disease model, quantification of its natural growth over an extended period is essential to study similarities and differences with *M. tuberculosis*. We made a quantitative comparison between *M. marinum* strains, and with *M. tuberculosis*, using the established MTP model. This modelling and simulation approach is able to use the gained knowledge on these differences when translating effects between species. A more parsimonious model with less compartments or parameters would result in similar predictions of CFU/mL for *M. marinum*, but would as a mere descriptive model lose its translational strength.

Comparison of *M. marinum* to *M. tuberculosis* shows similar growth rates, especially for strain E11 which also shows most similar model prediction for the three states (Figure 9.1 C), suggesting E11 to be preferable when studying tuberculosis pathology in zebrafish. The poikilotherm-derived E11 showed,

Table 9.1 Parameter estimates obtained with the final multistate tuberculosis pharmacometric MTP model for natural growth of *M. marinum* strain E11 and M^{USA} upon undisturbed, hypoxic growth for 221 days. Parameters reported for *M. tuberculosis* with this model[5] are depicted for comparison. Parameters in cursive are fixated to parameters reported for *M. tuberculosis*[5].

Parameter	***M. marinum* E11**		***M. marinum* M^{USA}**		***M. tuberculosis*[5]**
	Value	**RSE (%)**	**Value**	**RSE (%)**	**Value**
k_G (day^{-1})	0.188	4.1	0.169	19.3	0.206
k_{FS} (day^{-1})	1.33[a]	25	0.0157[a]	9.5	0.00166[a]
B_{max} (mL^{-1})	4.99×10^{11}	160	7.91×10^{7}	7.7	242×10^{6}
F_0 (mL^{-1})	0 FIX	-	8.51×10^{5}	21.2	4.1
S_0 (mL^{-1})	3.07×10^{6}	40.1	0 FIX	-	9770
k_{FN} (day^{-1})	*8.97×10^{-7}*	-	*8.97×10^{-7}*	-	*8.97×10^{-7}*
k_{SF} (day^{-1})	*0.0145*	-	*0.0145*	-	*0.0145*
k_{SN} (day^{-1})	*0.186*	-	*0.186*	-	*0.186*
k_{NS} (day^{-1})	*0.00123*	-	*0.00123*	-	*0.00123*
Variance of proportional residual error	0.227	9.5	0.205	9.5	0.407

[a] for *M. marinum*, transfer between fast- and slow-multiplying state was a constant function, for *M. tuberculosis*, transfer between fast- and slow-multiplying state was a time-dependent linear function with unit day^{-2}

B_{max} represents the maximum capacity of the system, F_0 represents the inoculum in the fast-multiplying state, k_g represents the growth function, remaining k-values represent transfer rates between the first state mentioned in the subscript to the state that is mentioned second, and S_0 represents the inoculum in the slow-multiplying state. RSE is the relative standard error.

with the prominence of the slow-multiplying state, a more latent growth behaviour than the human-derived M^{USA}, which remained fast multiplying for an extended period, suggesting more aggressive growth behaviour. These characteristics are consistent with literature[8].

The quantitative MTP approach is essential for the subsequent translation of drug effects. When including drug effects on *M. marinum* in the model, the resulting quantitative description thereof in the zebrafish will enable translation of the observations in this new model organism to higher vertebrates, including humans[16,17], an essential step in anti-tuberculosis drug development.

Transfer rates were fixed to reported values for *M. tuberculosis*. The assumption of similar transfer rates for *M. marinum* and *M. tuberculosis* is biologically reasonable, because both mycobacteria strains share the genetic program for (intracellular) growth[4]. Indeed, genetic functions required for dormant infections are found in both genomes[18].

In conclusion, the natural growth of *M. marinum* was characterized and a quantitative comparison to *M. tuberculosis* was made using an established model-based approach. The improved understanding of the mycobacterial pathogen of the zebrafish tuberculosis disease model brings this promising and versatile model organism one step closer to the quantitative translational pipeline of anti-tuberculosis drug development.

9.6 Acknowledgements

The research leading to these results has received funding from the Innovative Medicines Initiative Joint Undertaking (www.imi.europe.eu) under grant agreement no115337, resources of which are composed of financial contribution from the European Union's Seventh Framework Programme (FP7/2007–2013) and EFPIA companies' in kind contribution.

9.7 References

1. Takaki K, Davis JM, Winglee K, et al. Evaluation of the pathogenesis and treatment of Mycobacterium marinum infection in zebrafish. Nat Protoc. 2013;8(6):1114-1124.
2. Meijer AH, Spaink HP. Host-pathogen interactions made transparent with the zebrafish model. Curr Drug Targets. 2011;12(7):1000-1017.
3. Stinear TP, Seemann T, Harrison PF, et al. Insights from the complete genome sequence of Mycobacterium marinum on the evolution of Mycobacterium tuberculosis. Genome Res. 2008;18(5):729-741.
4. Tobin DM, Ramakrishnan L. Comparative pathogenesis of Mycobacterium marinum and Mycobacterium tuberculosis. Cell Microbiol. 2008;10(5):1027-1039.
5. Clewe O, Aulin L, Hu Y, et al. A multistate tuberculosis pharmacometric model: A framework for studying anti-tubercular drug effects in vitro. J Antimicrob Chemother. 2016;71(4):964-974.
6. Chen C, Ortega F, Rullas J, et al. The multistate tuberculosis pharmacometric model: A semi-mechanistic pharmacokinetic-pharmacodynamic model for studying drug effects in an acute tuberculosis mouse model. J Pharmacokinet Pharmacodyn. 2017;44(2):133-141.
7. Svensson RJ, Simonsson USH. Application of the multistate tuberculosis pharmacometric model in patients with rifampicin-treated pulmonary tuberculosis. CPT Pharmacometrics Syst Pharmacol. 2016;5(5):264-273.
8. Van der Sar AM, Abdallah AM, Sparrius M, et al. Mycobacterium marinum strains can be divided into two distinct types based on genetic diversity and virulence. Infect Immun. 2004;72(11):6306-6312.
9. Abdallah AM, Verboom T, Hannes F, et al. A specific secretion system mediates PPE41 transport in pathogenic mycobacteria. Mol Microbiol. 2006;62(3):667-679.
10. Beal S, Sheiner L, Boeckmann A, et al. NONMEM 7.3.0 users guides. (1989-2013). ICON Development

Solutions, Hanover, MD, USA.
11. Keizer R, Van Benten M, Beijnen J, et al. Pirana and PCluster: A modeling environment and cluster infrastructure for NONMEM. Comput Methods Programs Biomed. 2011;101(1):72-79.
12. Lindbom L, Pihlgren P, Jonsson E. PsNtoolkit — a collection of computer intensive statistical methods for non-linear mixed effect modeling using NONMEM. Comput Methods Programs Biomed. 2005;79(3):241-257.
13. R Core Team. R: A language and environment for statistical computing. R Found Stat Comput Vienna, Austria. 2014.
14. Nguyen THT, Mouksassi M-S, Holford N, et al. Model evaluation of continuous data pharmacometric models: metrics and graphics. CPT Pharmacometrics Syst Pharmacol. 2017;6:87-109.
15. Akaike H. A new look at the statistical model identification. IEEE Trans Automat Contr. 1974;19(6):716-723.
16. Wicha SG, Clewe O, Svensson RJ, et al. Forecasting clinical dose-response from Preclinical studies in tuberculosis research: Translational predictions with rifampicin. Clin Pharmacol Ther. 2018;104(6):1208-1218.
17. Gupta N, Bitton D, Simonsson USH, et al. Transforming translation through quantitative pharmacology for high-impact decision-making in drug discovery and development. CPT Pharmacometrics Syst Pharmacol. 2019:(accepted).
18. Malhotra S, Vedithi SC, Blundell TL. Decoding the similarities and differences among mycobacterial species. PLoS Negl Trop Dis. 2017;11(8):1-18.

9.8 Supplementary material

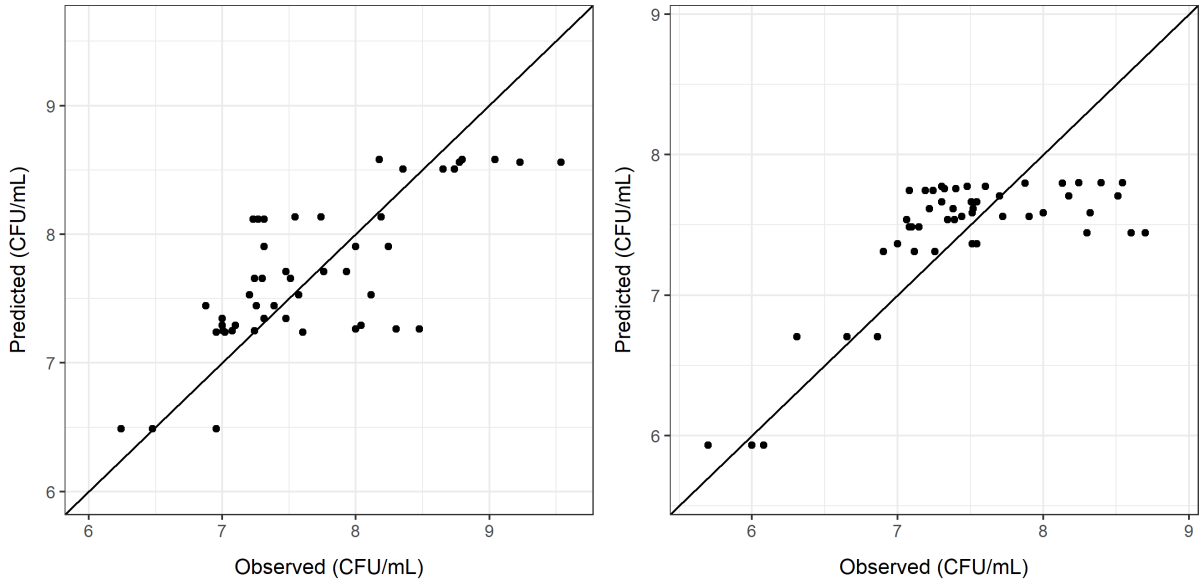

Supplementary Figure S9.1 Observed versus predicted CFU/mL for *M. marinum strain* E11 (left) and M^{USA} (right). The solid line represents the unity line. No systematic bias is observed.

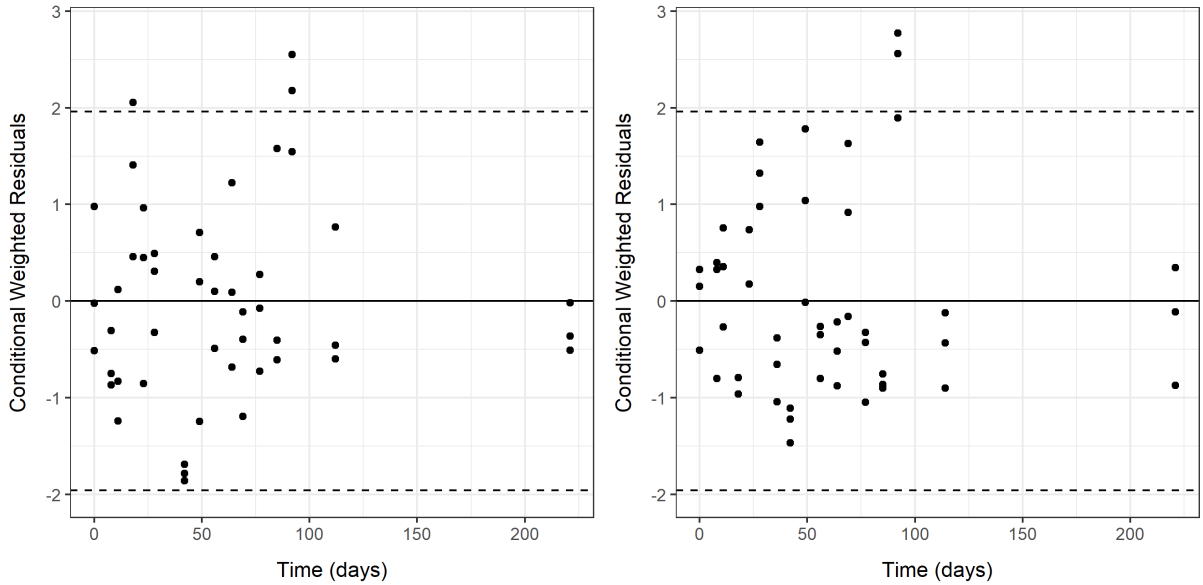

Supplementary Figure S9.2 Conditional weighted residuals versus time for *M. marinum* strain E11 (left) and M^{USA} (right). Solid line shows zero-line, dotted lines show ±1.96 standard deviation which is where 95% are expected to be. This figure indicated that there is no systematic bias in the predicted CFU/mL over time.

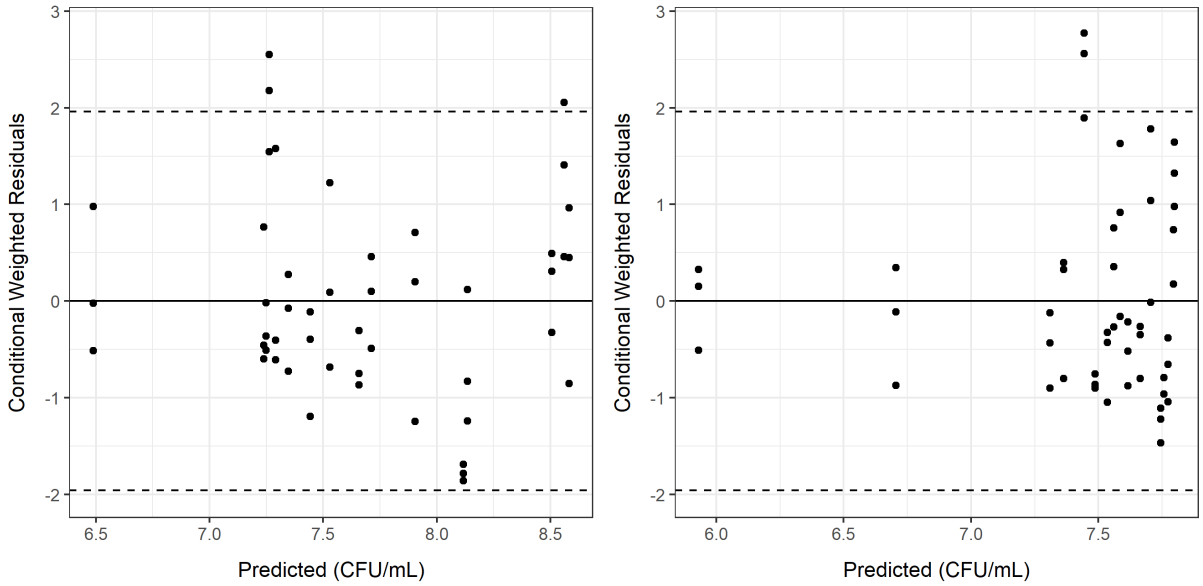

Supplementary Figure S9.3 Conditional weighted residuals versus predicted CFU/mL for *M. marinum* strain E11 (left) and M^{USA} (right). Solid line shows zero-line, dotted lines show ±1.96 standard deviation, which is where 95% are expected to be. This figure indicated that there is no systematic bias in the predicted CFU/mL over time. This figure indicated that there is no systematic bias in the predicted CFU/mL over the predicted range of CFU/mL.

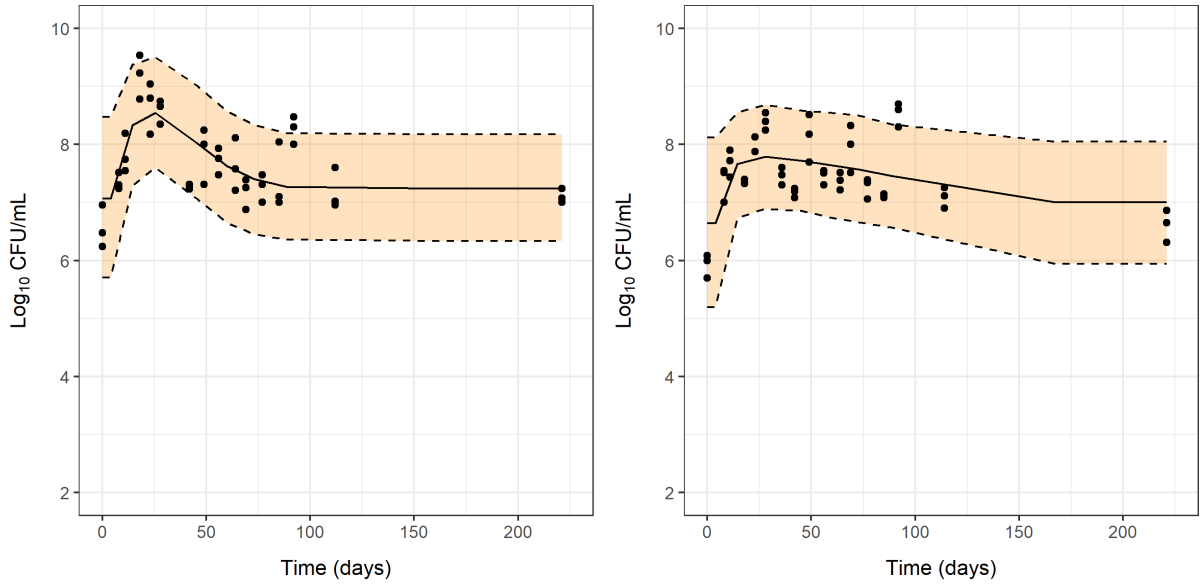

Supplementary Figure S9.4 Visual predictive check of natural growth of *M. marinum* strain E11 (left) and M^{USA} (right). Prediction mean (solid line) and 95% interval (orange shaded area, dashed lines) based on 1,000 simulations of the final model for natural growth of *M. marinum* strain E11 (left) and M^{USA} (right).

Chapter 10

Translational pharmacokinetics-pharmacodynamics of isoniazid in the zebrafish larva tuberculosis disease model

Rob C. van Wijk, Wanbin Hu, Sharka M. Dijkema, Dirk-Jan van den Berg, Jeremy Liu, Rida Bahi, Fons J. Verbeek, Ulrika S.H. Simonsson, Herman P. Spaink, Piet H. van der Graaf, Elke H.J. Krekels

Submitted

10.1 One Sentence Summary

Internal drug exposure and antibacterial response in zebrafish larva as tuberculosis disease model are translated to predict the isoniazid exposure-response relationship in humans using pharmacokinetic-pharmacodynamic modelling.

10.2 Abstract

There is a strong need for innovation in anti-tuberculosis drug development. The zebrafish larva is an attractive disease model in tuberculosis research. However to translate pharmacological findings to higher vertebrates including humans, the internal exposure of drugs commonly dissolved in the external water, needs to be quantified and linked to observed response. We developed experimental methods to quantify internal exposure, including nano-scale blood sampling and to quantify the bacterial burden, using automated fluorescence imaging analysis, with isoniazid as paradigm compound. Internal exposure was only 20% of the external drug concentration. The bacterial burden grew exponentially and an external concentration of 75 mg/L (5x minimum inhibitory concentration) lead to bacteriostasis. We used pharmacokinetic-pharmacodynamic modelling to quantify the exposure-response relationship responsible for the antibiotic response. Based on this quantitative relationship, isoniazid response was translated to humans, which correlated well with observed data. This proof-of-concept confirms the potential of the zebrafish larvae as tuberculosis disease model in translational pharmacology.

10.3 Introduction

Tuberculosis (TB) is the leading cause of death from infectious diseases in adults and *Mycobacterium tuberculosis* is becoming the deadliest pathogens on the planet[1]. The United Nations Sustainable Development Goals aim to eradicate the TB epidemic before 2030[2], but progress is stalling due to ineffectiveness of currently available treatments[3]. Drug development is a challenging, lengthy, and costly process, generally requiring a decade for drugs to reach the market with estimated costs of 1-2.5 billion dollar per approved new drug[4]. Development of anti-TB drugs is especially difficult, with laboratory biosafety issues[5], slow replication rate of *M. tuberculosis*, and long duration of treatment and patient follow-up[6]. As a result, there is a strong need for innovations in the development of new TB treatments[6–8].

Phenotypic- and systems-based drug development both integrate experimental and computational innovation and utilizes whole organisms studies, preferably vertebrates, for quantitative translational purposes to open a new realm of possible discoveries overseen when focusing on single cell-type targets. High-throughput experiments within whole vertebrates may improve efficiency and effectiveness of drug development, and is possible with the zebrafish larva as model organism[9].

The zebrafish (*Danio rerio*) is increasingly used in biomedical research, because of its many advantages which include high fecundity, fast development, transparency throughout the first period of life, easy genetic modification, and limited ethical constraints[9–11]. Zebrafish larvae infected by *M. marinum*, a close

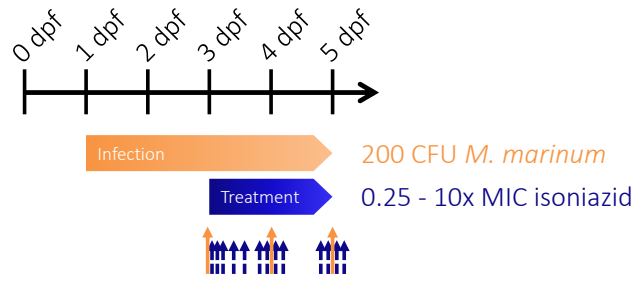

Figure 10.1 Experimental study design. Fertilized eggs at 0 days post fertilization (dpf) were harvested and injected with 200 CFU *M. marinum* at 1 dpf. After two days of establishing the infection, fluorescence imaging was performed (orange arrow, n ≥ 20 larvae per group) and the treatment with isoniazid dissolved in the external treatment medium (0.25-10x MIC, MIC = 15 mg/L, and control) was started. Fluorescence imaging was repeated daily (orange solid arrows). In separate animals groups, destructive homogenate (at least 3 replicates consisting of 5 larvae per dose per time point) and blood samples for internal isoniazid exposure quantification were taken from 0 to 50 hours of treatment (blue dashed arrows).

relative of *M. tuberculosis*, are an established TB disease model to study host-pathogen interaction[12–15] and to screen for novel drugs[16,17], with faster replication times and less biosafety risks than experiments with *M. tuberculosis*[18]. Imaging of zebrafish larvae infected with fluorescent mycobacteria[19,20] allows for repeated longitudinal measurements from individual larvae, which reduces overall noise in data as biological and experimental variability can be quantified separately. This is in contrast to *ex vivo* bacterial burden organ count by colony forming units (CFU) or MGIT liquid media systems currently utilized in preclinical TB research[21–23].

Translation of drug response between species is challenging and considerably limits drug development[24]. Currently, treatment of zebrafish larvae is performed by dissolving drugs into the water in which the larvae swim, without taking into account how much drug is actually taken up by the larvae. Translating pharmacological response between species however requires quantification of the drug exposure at the site of action as a basis for the quantification of the exposure-response relationship[25]. Although challenging because of their small size, we have developed new experimental methods to quantify internal drug exposure based on ultra-sensitive analytical techniques and a novel method for nanoscale blood sampling. Pharmacological model-based approaches can then be used to quantitatively link the internal exposure over time (pharmacokinetics) of anti-TB drugs to bactericidal response in the zebrafish larvae observed by fluorescence microscopy (pharmacodynamics). The exposure-response relationship that is thus obtained is the basis for translational pharmacology to higher vertebrates, including humans.

Here, for the first time, we present an integration of experimental and computational approaches in zebrafish larvae infected with *M. marinum* and treated with increasing waterborne isoniazid doses from 0.25-10x the minimum inhibitor concentration (MIC) (3.75-150 mg/L). The internal exposure is quantified in homogenates and blood samples of the larvae, and the bacterial burden is quantified by automated fluorescence image analysis (Figure 10.1). Pharmacokinetic-pharmacodynamic modelling is performed to quantify the exposure over time and the exposure-response relationship. Isoniazid is chosen because it is known to have the largest early bactericidal activity for single drug treatments among the current standard of care drugs against TB[26]. The quantified exposure-response relationship in the zebrafish larvae together with simulated concentration-time profiles in TB patients is utilized to translate the findings on isoniazid response in the zebrafish larvae to humans. A quantitative comparison with reported observations from patients is made as a proof of concept, to assess translational value of this new disease model in anti-TB drug development.

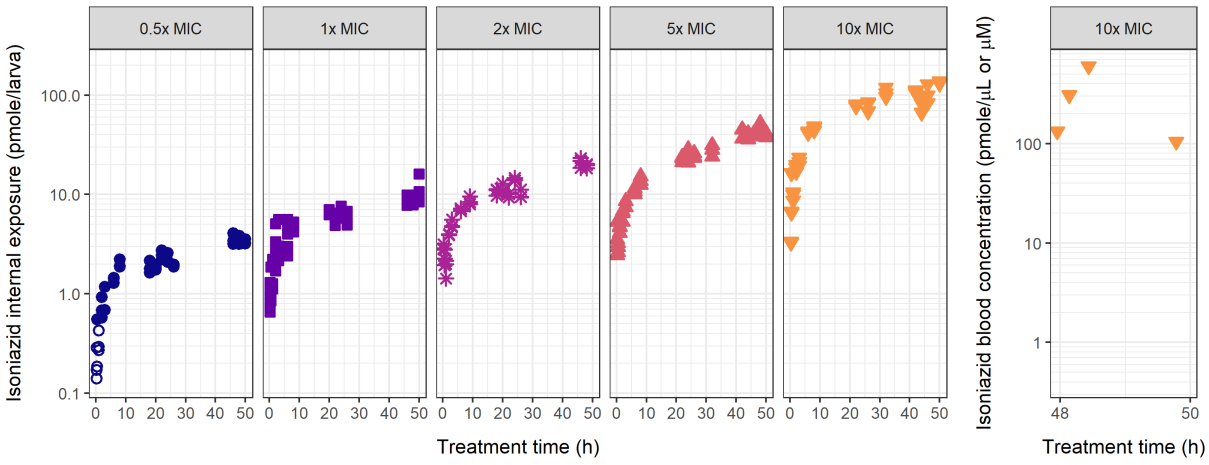

Figure 10.2 Internal isoniazid exposure over time in zebrafish larvae for increasing isoniazid doses. Internal exposure as pmole per larva in homogenate samples (left 5 panels) or as pmole/µL in blood samples (right panel) is shown on a semi-logarithmic scale for waterborne doses in the external treatment medium of 0.5 (blue circles), 1 (purple squares), 2 (lilac stars), 5 (orange upward triangles), and 10 (yellow downward triangles) x MIC (MIC = 15 mg/L) for a constant treatment period of 50 hours. Internal exposure linearly increases with dose, and steady state amounts increase with age, suggesting increased net absorption. Open symbols show observations below lower limit of quantification.

10.4 Results

10.4.1 Internal exposure of isoniazid in zebrafish larvae

Internal exposure of isoniazid in zebrafish larvae after constant treatment between day 3-5 post fertilization (dpf) with increasing doses of 0.5, 1, 2, 5, and 10x MIC (7.5, 15, 30, 75, and 150 mg/L) was quantified. Figure 10.2 showed a clear dose-linearity, where a 10-fold higher dose resulted in a 10-fold higher internal exposure. Internal exposure measured in homogenates reached steady state values within 12 hours and after that increases with age. To quantify the blood concentration in the zebrafish larvae of 5 dpf, an innovative novel blood sampling method was used. Median blood concentration of isoniazid at 48 hour of treatment (5 dpf) with 150 mg/L was 30.3 mg/L (221 µM, range 14.4-82.6 mg/L, Figure 10.2), meaning that the internal exposure to isoniazid was only 20% of the external concentration.

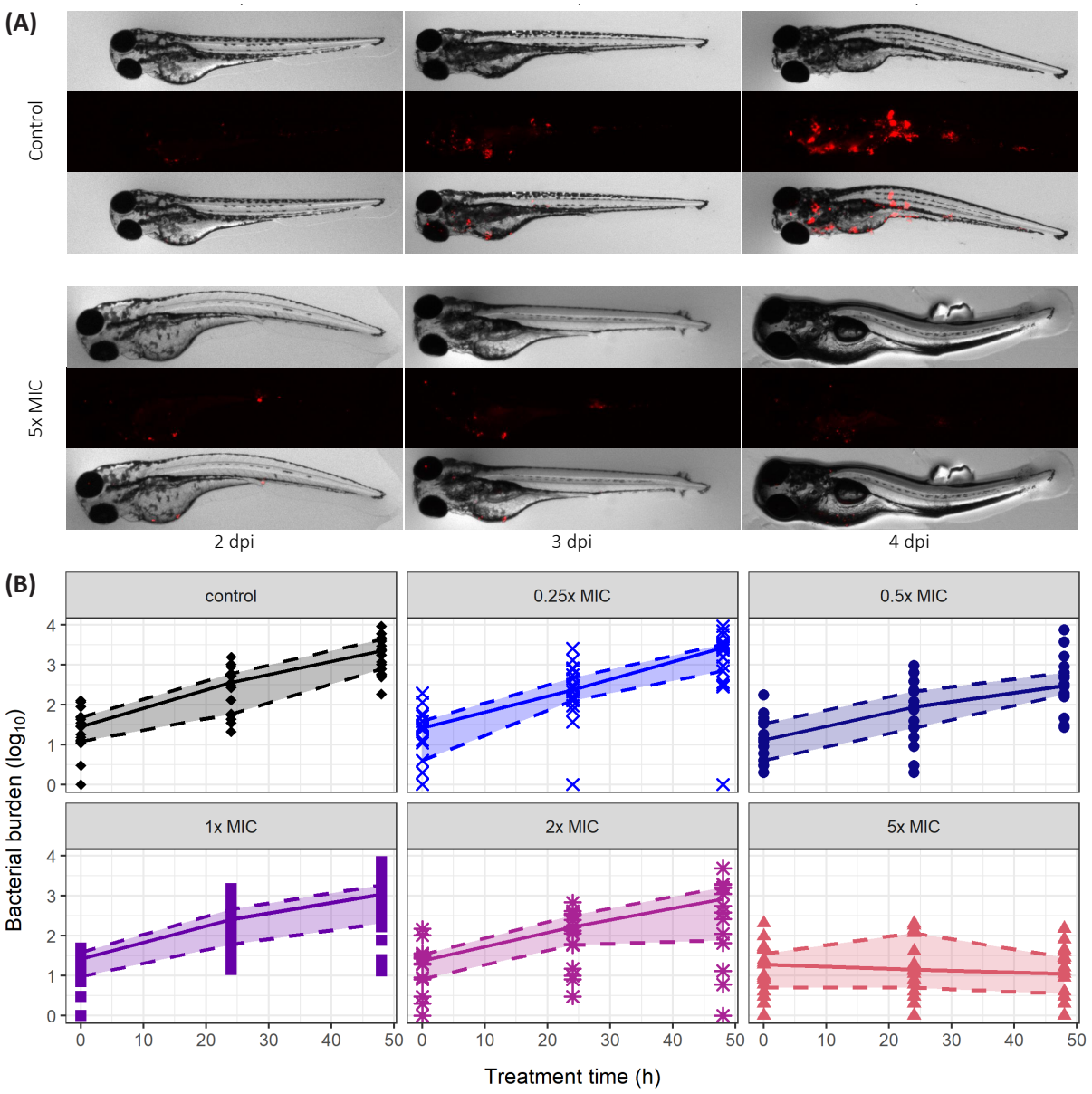

Figure 10.3 Bacterial burden quantified by fluorescence imaging. (A) Representative images (brightfield (top), red fluorescence channel (middle), overlay (bottom)) for control and 5x MIC treatment groups at 2, 3, and 4 dpi (MIC = 15 mg/L). (B) The bacterial burden in fluorescent pixel count quantified by automated image analysis for control and treatment groups with doses 0.25x – 5x MIC selected after feasibility study and taking into account fluorescence detection limit. Symbols represent observations, while lines represent median and quantiles, with the inter-quantile range as shaded area.

10.4.2 M. marinum *bacterial burden in zebrafish larvae upon isoniazid treatment*

The bacterial burden of *M. marinum* was quantified through fluorescence imaging with repeated measurements per individual larva. Doses ranging from 0.25x to 5x MIC were chosen based on a feasibility study, and on the fluorescence detection limit. Figure 10.3 showed representative images of which the fluorescent pixels are quantified by automated image analysis software[19,27], based on pixel counts. The median and inter-quartile range of the bacterial burden clearly showed that bacterial growth is decreasing with increasing doses in comparison to the control. The highest dose of 5x MIC, which corresponded to 1x MIC internal exposure, showed a decline in the bacterial burden over time.

10.4.3 Quantification of the exposure-response relationship for isoniazid in zebrafish larvae

To quantify the exposure-response relationship, a sequential modelling approach was performed. First, the internal exposure over time was quantified in the pharmacokinetic component of the model, after which this was linked to the isoniazid response in the final pharmacokinetic-pharmacodynamic model (Figure 10.4).

A one-compartment model with first order absorption and first order elimination best described the data on internal exposure. Because the larvae are still developing, both absorption and elimination were expected to increase with age[28]. The data showed an increase in the steady state amounts with increasing age, suggesting that absorption rates increase faster than elimination rates. Because the impact of age on absorption and elimination were indistinguishable at steady state, we estimated a net effect as increase on absorption only. Age was included as predictor (covariate) on the absorption rate constant (k_a) in two ways: first, as exponential relationship per hour post fertilization (hpf), and second, based on knowledge on the physiology of the gastro-intestinal (GI) tract which opens between 3 and 4 dpf[29], as discrete increase at 4 dpf (Equation 1).

$$k_a = \begin{cases} k_{a,0} \cdot k_{a,hpf}^{\frac{age}{median(age)}} & age = 3\ dpf \\ k_{a,0} \cdot k_{a,hpf}^{\frac{age}{median(age)}} \cdot \left(1 + k_{a,GI}\right) & age \geq 4\ dpf \end{cases} \quad (1)$$

in which $k_{a,0}$ was the absorption rate constant at the median age of 101 hpf, k_a,hpf was the constant in the exponential covariate relationship, and $k_{a,GI}$ was the discrete factor with which the absorption rate constant increased at 4 dpf. A linear covariate relationship was statistically significantly worse ($p < 0.001$) compared to an exponential relationship, a power relationship was statistically similar ($p > 0.1$), but resulted in worse precision of the parameter estimates.

Precision of all pharmacokinetic parameters in the final model was acceptable (relative standard errors < 36%), with the exception of $k_{a,GI}$ (relative standard error of 51%). Removing the effect of the opening of

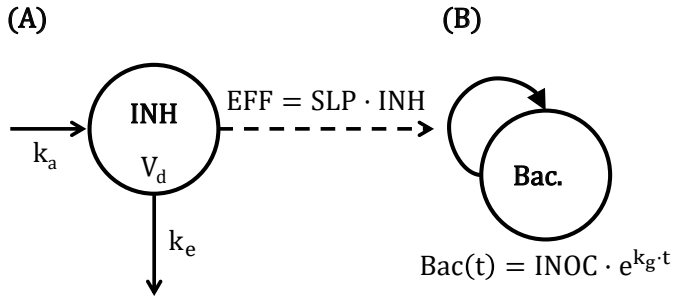

Figure 10.4 Schematic representation of the pharmacokinetic-pharmacodynamic model quantifying the internal exposure of isoniazid and its response on the bacterial burden in zebrafish larvae. Compartments represent drug concentration or number of bacteria inside the larva, solid straight arrows represent mass transfer, curved arrow represent bacterial growth, dashed arrow represents drug response. (A) shows the pharmacokinetic component of the model for isoniazid (INH) with a first order absorption rate constant (k_a) from the external treatment medium on which larval age is included as a covariate (Equation 1), distribution volume (V_d), and first order elimination rate constant (k_e). (B) shows the bacterial burden (Bac.) with exponential growth rate (k_g) as growth function and inoculum (INOC) at time point zero. Exposure-response relationship (EFF) is quantified with a linear model (SLP = slope).

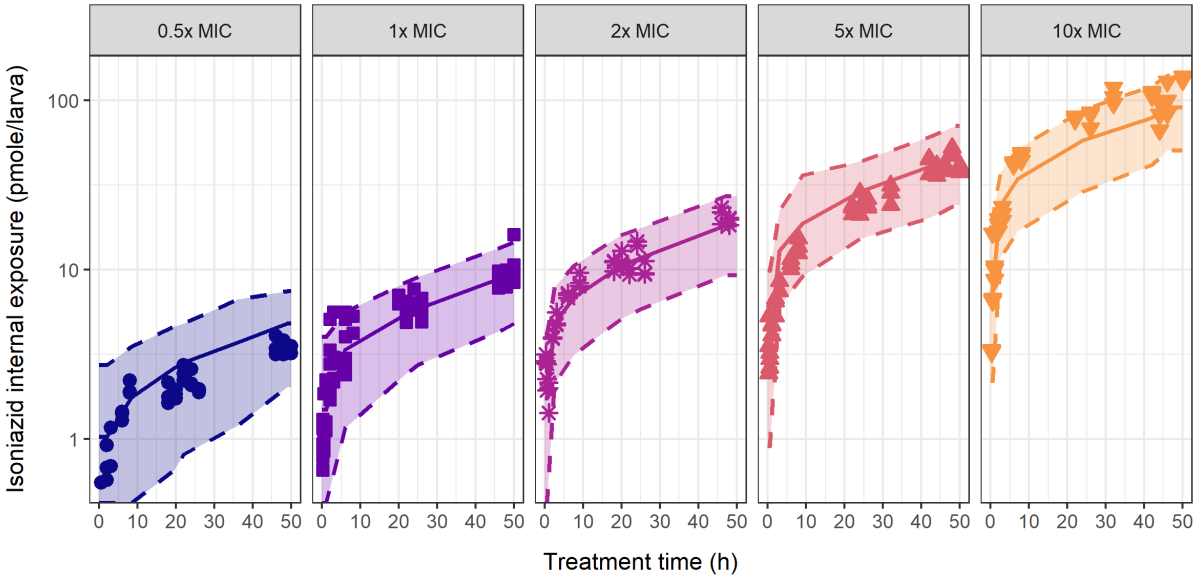

Figure 10.5 Model-based prediction of the internal isoniazid exposure in zebrafish larvae of the final pharmacokinetic-pharmacodynamic model. Median (solid line) and 95% prediction interval (dashed lines, shaded area) from 500 simulations based on the pharmacokinetic component of the final model show good prediction of the observed data (symbols) of internal exposure obtained after constant waterborne isoniazid treatment of 0.5 (blue circles and lines), 1 (purple squares and lines), 2 (lilac stars and lines), 5 (orange upward triangles and lines), and 10 (yellow downward triangles and lines) x MIC (MIC = 15 mg/L).

the GI-tract worsened the fit significantly ($p < 0.05$) and as the opening of the GI-tract was physiologically expected to impact absorption the relationship was retained despite the relative imprecision of the obtained estimate. The precision of the remaining model parameters confirmed that the obtained model and parameter values were supported by the data. Goodness-of-fit plots further confirmed an unbiased fit of the data by the model (Supplementary Figure S10.1). A visual predictive check was provided in Figure 10.5, which showed good prediction of the typical trends and a slight over-prediction of the variability of the observed data by the model.

The bacterial burden data was best described by an exponential growth model (Equation 2). The data did not support separate estimation of growth and decay, thus net growth was estimated. In case of bacterial kill, this net growth will be negative. A linear exposure-response relationship fitted the data best (Equation 6). The biological variability between larvae was quantified by inclusion of inter-individual variability on the inoculum (coefficient of variation 204%) and slope of the drug response (coefficient of variation 50.5%). The experimental variability was very reasonable with a coefficient of variation of 36.3%. The predicted isoniazid response in zebrafish larvae was shown in Figure 10.6 (individual predictions Supplementary Figure S10.2), with a clear increase in antibacterial response by the different doses which was in line with the observations. Goodness-of-fit plots showed unbiased model fit (Supplementary Figure S10.3). Parameter estimates of the final pharmacokinetic-pharmacodynamic model were given in Table 10.1.

10.4.4 Translation of isoniazid response to humans

An exposure-response relationship of a drug can be assumed to be conserved between vertebrates[24,30–32]. As a proof of concept, the response of isoniazid in zebrafish larvae was translated to humans, assuming the isoniazid response on *M. tuberculosis* in humans to be similar to the isoniazid response on its close relative *M. marinum*. Translational factors regarding the difference in sensitivity to isoniazid as reported by MIC, and difference in stage of infection, were taken into account[31]. The exposure-response relationship quantified in the current study was linked to simulated isoniazid concentration-time profiles of patients from a previously published pharmacokinetic model for isoniazid[33]. Simulations with three human doses were performed; a sub- and a super therapeutic dose of 150 and 450 mg, in addition to the

Table 10.1 Parameter estimates including relative standard errors (RSE) of the final pharmacokinetic-pharmacodynamic model (Figure 10.4)

	Parameter value	**RSE (%)**
Pharmacokinetic structural parameters		
$k_{a,0}$ (µL/h^{-1})	0.00349	25
$k_{a,hpf}$ (-)	7.61	17
$k_{a,GI}$ (-)	0.171	51
k_e (h^{-1})	0.580	32
V_d (µL)	0.325	36
Pharmacodynamic structural parameters		
k_g	0.0930	4
Inoculum (Fluorescence)	16.3	13
Slope (µM^{-1})	0.00991	37
Pharmacodynamic inter-individual variability		
Variance of inter-individual variability Inoculum (-)	1.64	18
Variance of inter-individual variability Slope (-)	0.227	93
Pharmacokinetic residual variability		
Variance of proportional error homogenate (-)	0.0609	24
Variance of additive error homogenate (pmole/larva)	0.591	45
Variance of proportional error blood (-)	0.482	49
Pharmacodynamic residual variability		
Variance of proportional error (-)	0.124	17

recommended dose of 300 mg. Reported observations of *M. tuberculosis* bacterial burden quantified in sputum after isoniazid monotherapy of daily 300 mg[34–36] served as quantitative comparison. Figure 10.7 shows the simulated concentration-time profile and the bacterial burden-time profiles for 1,000 virtual patients per dose group, the latter of which for a dose of 300 mg was in good agreement with the observed data. The simulations after sub-therapeutic dose of 150 mg showed limited isoniazid response and hence bacterial growth. The therapeutic dose of 300 mg showed a decline in the bacterial burden. The median translated bacterial burden declined 5-6 $\log_{10}$ CFU/mL during the 7 days treatment period, or 0.7-0.9 $\log_{10}$ CFU/mL/day. The super therapeutic dose of 450 showed a steeper decline of the bacterial burden.

The translated isoniazid response at the therapeutic dose correlated well with the observed data for the first 48 hours which was also the duration of treatment studied in the zebrafish larvae in this work. Extrapolating to later time points showed a slight over-prediction of isoniazid response, while the observations were still within the prediction interval. This proof-of-concept suggests that the zebrafish larva is a promising addition to the quantitative model-based translational pipeline in anti-TB drug development.

10.5 Discussion

There is a strong need for innovation in anti-TB drug development. With its high-throughput potential, its possibility for repeated fluorescence imaging to quantify infection, and its fast, cheap, and relatively safe experimentation, the zebrafish larva tuberculosis disease model combines the advantages of *in vitro* experiments within a whole-organism vertebrate. In this work, we developed an experimental approach to acquire data on the internal exposure, on the bacterial burden, and utilized computational pharmacokinetic-pharmacodynamic modelling to quantify the exposure-response relationship, which

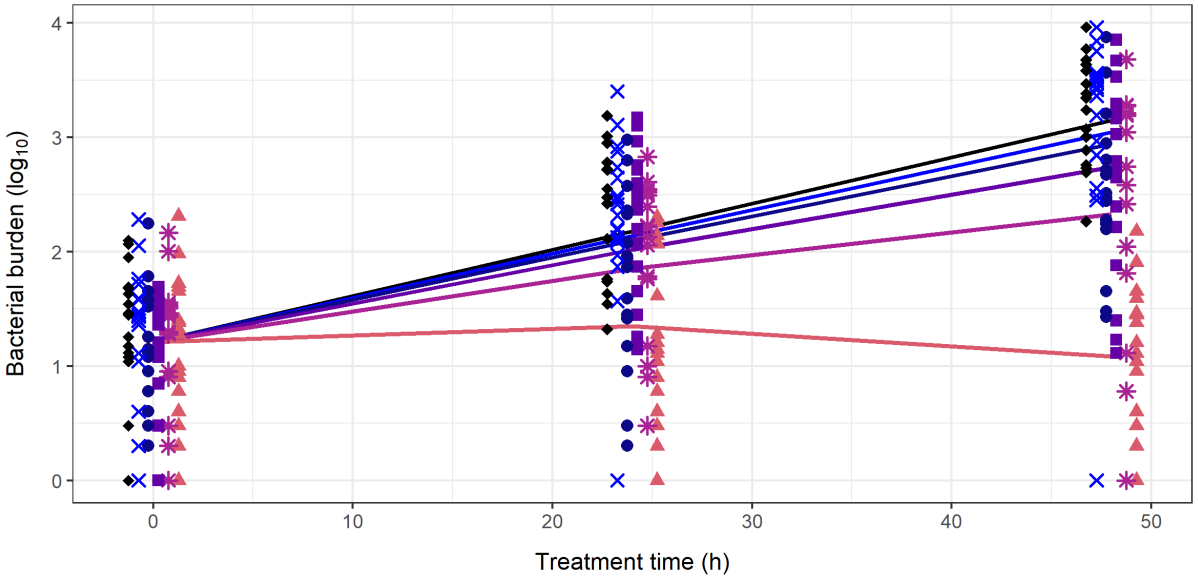

Figure 10.6 Model-based prediction of the bacterial burden after isoniazid treatment in zebrafish larvae infected with *M. marinum*. The bacterial burden as log_{10}-transformed fluorescent pixel count is shown over treatment time of 50 hours at isoniazid doses in the external treatment medium of 0.25 (light blue crosses and line), 0.5 (blue circles and line), 1 (purple squares and line), 2 (lilac stars and line), and 5 (orange upward triangles and line) x MIC (MIC = 15 mg/L), in addition to control (black diamonds and line). Symbols represent observed data, lines represent model prediction. Biological variability as quantified by the model is relatively large in contrast to experimental variability (see for individual predictions Supplementary Figure S10.2).

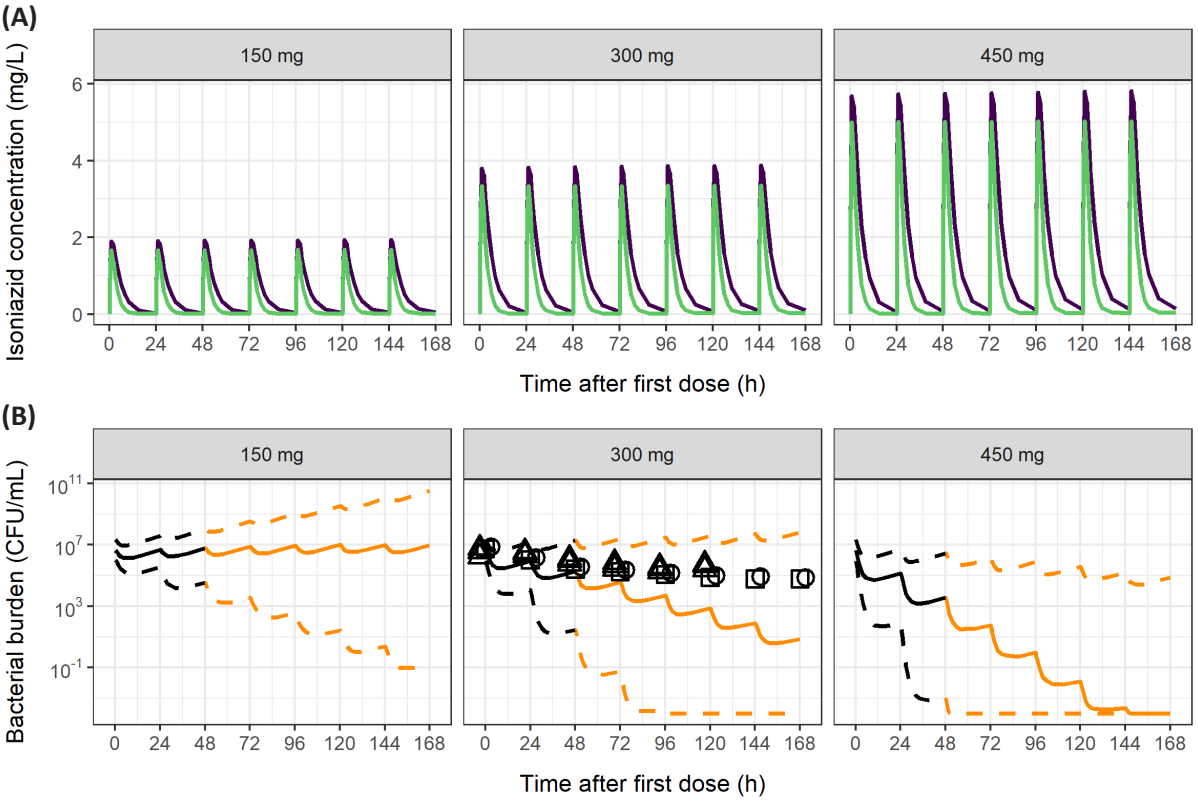

Figure 10.7 Translation of isoniazid response to humans based on final zebrafish pharmacokinetic-pharmacodynamic approach. (A) isoniazid concentration-time profile for a fast (green) and slow (purple) metabolizer typical individual after 7 days of daily isoniazid doses of 150 mg, 300 mg, and 450 mg as simulated from a previously published pharmacokinetic model[33]. (B) Simulated median (solid line) and 10th and 90th percentile (dashed lines) bacterial burden in CFU/mL sputum based on the human isoniazid concentration-time profile for 1,000 individuals per dose group and the exposure-response relationship quantified in zebrafish larvae, and translational factors on isoniazid sensitivity (MIC) and stage of infection (logarithmic vs stationary). Translated response corresponds well to the observed bacterial burden in sputum (circles[34], squares[35], triangles[36]). Orange part of the prediction is extrapolated in time from the 48 hours of treatment studied in the zebrafish, shown in black.

successfully translated to isoniazid response in humans. This translation to human response shows the strengths of quantifying internal exposure-response relationships, crucial for successful translational pharmacology in drug development. Using our workflow, zebrafish studies can bridge the gap between *in vitro* experiments and *in vivo* preclinical drug development, thereby increasing speed and improving quantitative understanding of *in vivo* drug response early in the drug development process. Through this quantitative model based approach, the zebrafish larva becomes a full member of the translational pipeline in drug development.

Quantification of internal exposure in zebrafish larvae after drug treatment is essential for reliable interpretation of drug response, but because of small sample volumes and low amounts this is not straight forward. We have built upon recent work to develop an ultra-sensitive liquid chromatography-mass spectrometry (LC-MS/MS) based quantification method, including derivatization[28,37,38]. This methodology proved sensitive enough to quantify isoniazid in larval homogenates and blood samples of only nanoliters in volume. The latter is especially of importance because blood concentrations are required to scale amounts in homogenates to concentrations, essential for inter-species translation. The state of the art blood sampling method is not yet high-throughput, but automation based on previously developed automated injection systems are under development[39].

Utilizing fluorescence imaging to establish the response of isoniazid on mycobacteria has clear advantages over CFU plating, as the latter has been reported to show large sample-to-sample variability[40]. An important advantage of fluorescence imaging in zebrafish larvae is the possibility of repeated longitudinal measurements of the bacterial burden within a single individual, which is uncommon in preclinical TB research. These repeated measurements not only suppress noise by distinguishing biological from experimental variability, but also reduce the number of subjects needed in an experiment, which is ethically preferable. Additionally, fluorescence imaging of bacteria does not require these bacteria to grow on solid- or in liquid media, and will include both multiplying and non-multiplying, i.e. dormant bacteria. Currently, the medium-throughput imaging set-up used here is restricted by its fluorescence detection limit to clearly quantify mycobacterial kill, which is why the highest dose of 10x MIC was not tested in the bacterial burden study. Imaging systems are continuously being improved, pushing the detection limit to the individual mycobacterium[41].

M. marinum and *M. tuberculosis* are sensitive to isoniazid to a different extent, as MIC against *M. marinum* ranges between 1.6 and 32 mg/L[42–45], in concordance the value obtained in our analysis, which is higher than the MIC against *M. tuberculosis* which ranges from 0.016 to 0.2 mg/L[23,46–49]. This difference in sensitivity was taken into account when predicting human efficacy by scaling the effective concentration with the ratio of MICs as scaling term which has earlier been shown as a method for handling strain differences[31]. The difference in stage of infection between the logarithmic growth of a fresh infection in the zebrafish here, and the stationary infection of patients starting treatment, was taken into account as well which has been shown to be an important translational factor[31].

The pharmacokinetic-pharmacodynamic model developed here was limited by the available data and is currently empirical in nature. The estimation of net absorption and net growth cannot be distinguished from the impact of age on absorption and elimination separately, or on the drug response on growth or kill, respectively. Parameterization as net absorption or growth can impact the interpretation of these parameters, so care must be taken. However, translation based on this empirical model was reasonable, and will further improve with the addition of more physiological or mechanistic details. A multistate tuberculosis pharmacometric (MTP) model has been developed previously for *M. tuberculosis*, quantifying *in vitro* natural growth over 200 days using a fast-, slow-, and non-multiplying subpopulation. The drug responses of isoniazid, rifampicin, and ethambutol have been quantified on these states[50,51] and successfully translated to mice[52,53] and patients[54]. This multistate approach, especially when the *in vitro* natural growth and time-kill is repeated for *M. marinum* as well, can be integrated with our analysis of *M. marinum* to strengthen the translational value of findings in zebrafish to higher vertebrates[55].

The reported bacterial burden in humans after 300 mg isoniazid monotherapy daily fell within the prediction interval obtained from simulated concentration-time profiles in humans and the exposure-response relationship quantified in zebrafish larvae here. The simulated decline in the bacterial burden of 0.7-0.9 $\log_{10}$ CFU/mL/day has been reported in humans before after 2 days of treatment[56]. The large variability in the prediction interval from this work was largely due to the high biological variability in the inoculum, resulting from the establishment of infection during the first two days, and the slope of the linear drug response quantified in zebrafish larva. Care must also be taken when extrapolating a linear exposure-response relationship to exposures outside the studied range, as well as extrapolating the response of treatment after the 48 hours of treatment in zebrafish larvae. The treatment duration was deliberately not extended beyond 48 hours, to remain within the ethically preferable age limit (Figure 10.1)[57].

In conclusion, we have developed a new experimental and computational approach to translate the pharmacokinetic-pharmacodynamic relationship of isoniazid in a zebrafish model of TB to human. We propose that this approach can be used in the search for novel TB regimens.

10.6 Materials and Methods

10.6.1 Study design

Zebrafish embryos of the VUmc wild type strain were dechorionated and infected with *M. marinum* strain E11 at 28 hpf and kept at 28°C throughout the experiment. At 2 days post infection (dpi), the bacterial burden in zebrafish larvae was quantified by fluorescence microscopy and waterborne treatment with isoniazid was commenced at external concentrations of 0, 3.75, 7.5, 15, 30, and 75 mg/L corresponding to 0, 0.25, 0.5, 1, 2, and 5x MIC. Quantification of the bacterial burden was repeated within individual larva at 3 dpi and 4 dpi to assess individual early bactericidal activity. Internal isoniazid exposure was quantified by LC-MS/MS of whole zebrafish larval homogenate samples as well as in larval blood samples in a parallel experiment with uninfected larvae treated with external isoniazid concentrations of 7.5, 15, 30, 75, and 150 mg/L corresponding to 0.5, 1, 2, 5, and 10x MIC. Figure 10.1 shows a schematic overview of the study design.

10.6.2 Chemicals

Isoniazid was acquired from Sigma-Aldrich (Sigma-Aldrich Chemie GmbH, Schnelldorf, Germany) and isoniazid-D4 internal standard from Santa Cruz (Santa Cruz Biotechnology, Santa Cruz, USA). Ethyl 3-aminobenzoate (tricaine) was purchased from Sigma-Aldrich. Cinnamaldehyde was acquired from Sigma-Aldrich. Nanopure water was used from a PURELAB water purification system (Veolia Water Technologies B.V., Ede, The Netherlands) unless otherwise stated. ULC-MS-grade methanol as well as ULC-MS-grade acetonitrile, LC-MS-grade water, and formic acid was acquired from Biosolve (Biosolve B.V., Valkenswaard, The Netherlands). Difco Middlebrook 7H10 agar and 7H9 medium, oleic acid-albumin-dextrose-catalase (OADC), and acid-albumin-dextrose-catalase (ADC) was acquired from BD (BD Biosciences, Sparks, USA). Polyvinylpyrrolidone-40 solution (PVP40) was acquired from Sigma-Aldrich.

10.6.3 Zebrafish husbandry

Zebrafish were maintained and handled following international consensus protocols[58]. Planning and execution of all experiments complied with European regulation[59]. Adult wild type VUmc zebrafish were kept in glass aquaria (max 6/L, volume 10L, 120x220x490 mm, Fleuren & Nooijen BV, Nederweert, The Netherlands) with circulating water (27.7°C ± 0.1 on a 14h/10h light/dark cycle, lights on at 08:00). Adult zebrafish were fed twice daily with artemia or feed particles (Gemma Micro/Diamond, Skretting, Nutreco NV, Amersfoort, The Netherlands). JUMO Acquis touch S (JUMO GmbH & Co, Weesp, The Netherlands) was used to control water quality.

Adult zebrafish were set-up for breeding overnight and in the morning at lights-on, separators between males and females were removed and fertilized eggs were collected within 30 minutes of fertilization.

Eggs, embryos, and larvae were kept in embryo medium (60 µg/mL Instant Ocean sea salts (Sera, Heinsberg, Germany) in demineralized water, daily refreshed) at 28°C, except for the treatment duration, when larvae were kept in treatment solution at 28°C until imaging or sampling.

10.6.4 Internal exposure of isoniazid in zebrafish larvae

Internal exposure of isoniazid in zebrafish larvae was quantified in larval homogenates and blood samples after waterborne treatment with isoniazid concentrations at external concentrations of 0.5, 1, 2, 5, and 10x MIC (7.5, 15, 30, 75, and 150 mg/L).

Homogenate samples were taken with at least three replicates of 5 larvae at time points 0.25, 0.5, 1, 2, 3, 6, 8, 9, 18, 20, 22, 24, 26, 32, 42, 44, 46, 48, and 50 hours after start of treatment. Zebrafish larvae were washed 4 times with 20/80 methanol/water (v/v) using Netwell inserts (Corning Life Sciences B.V., Amsterdam, The Netherlands) and transferred to Safe-Lock tubes (Eppendorf Nederland B.V., Nijmegen, The Netherlands). Excess volume was removed and 50 µL of 200 ng/mL isoniazid-D4 internal standard was added after which the samples were snap-frozen in liquid nitrogen and stored at-80°C until quantification.

Blood samples were taken after 48 hours of treatment at the highest external concentration of 150 mg/L to ascertain quantifiable levels, using a previously published method[38]. In short, zebrafish larvae of 5 dpf were washed 4 times as described above, superficially dried, and transferred to an agarose microscopy slide, after which a pulled needle (0.75 mm borosilicate class capillary without filament, Sutter Instruments, Novato, California, USA) positioned in a micromanipulator (World Precision Instruments, Berlin, Germany) attached to a CellTram Vario oil pump (Eppendorf) was used to sample the blood from the posterior cardinal vein under 20x magnification (Leica, Amsterdam, The Netherlands). An image of each blood sample was captured to calculate blood volume before the sample was injected into a 2 µL heparin droplet (5 International Units/mL) and pooled (19-32 blood samples per replicate) into a 0.5 mL tube (Eppendorf). Blood samples were kept at-80°C until quantification.

10.6.5 Quantification of isoniazid in homogenate and blood samples

Isoniazid was quantified by LC-MS/MS. Derivatization with cinnamaldehyde was performed to achieve adequate retention for LC separation.

Samples of whole zebrafish larva were thawed and 100 µL methanol and 100 µL of 0.5 mm zirconium oxide bullets (NextAdvance, New York, USA) were added. The samples were homogenized using a Bullet Blender (NextAdvance) for at least two rounds of 5 minutes at speed 5. Extraction and derivatization was performed by adding 800 µL acetonitrile, 100 µL 1% cinnamaldehyde in methanol, and 100 µL formic acid and shaking for 20 minutes at 650 rpm (IKA, Staufen im Breisgau, Germany). Samples were centrifuged for 10 minutes at 20,000g, 90% was transferred to a new Safe-Lock tube, and evaporated until dryness in a Labconco vacuum centrifuge (Beun de Ronde, Abcoude, The Netherlands). The residue was reconstituted into 200 µL methanol, centrifuged for 10 minutes at 20,000g and the supernatant was transferred to an LC-MS/MS vial with a glass insert for 5 µL injection into the LC-MS/MS. Quality control (QC) and calibration curve samples were prepared by spiking blank homogenate samples. The QC samples were prepared at the levels of 4, 125, and 225 ng/mL. The calibration curve samples were prepared at the levels of 0, 2, 5, 10, 25, 50, 100, 150, and 250 ng/mL. Blood samples were thawed and briefly centrifuged to concentrate the small sample into the bottom of the tube. 2.5 µL of 200 ng/mL internal standard solution was added. Extraction and derivatization was performed by addition of 200 µL acetonitrile and 50 µL methanol, and 25 µL 1% cinnamaldehyde in methanol and 25 µL formic acid, and samples were shaken for 20 minutes at 650 rpm. Samples were evaporated until dry, reconstituted in 10 µL methanol, and centrifuged for 10 minutes at 20,000 g, after which they were transferred to an LC-MS/MS vial with a glass insert upon 5 µL injection into the LC-MS/MS. An academic calibration curve in methanol was prepared with concentrations 0, 2, 3, 5, 8, 10, 25, 50, 100, 150, and 250 ng/mL.

Quantification of isoniazid was performed on an ultra high-performance liquid chromatography (UHPLC) system (Shimadzu Nexera X2, 's Hertogenbosch, The Netherlands) with a triple quadrupole mass spectrometry (MS) detector (TSQ Vantage, Thermo Fisher Scientific, Breda, The Netherlands). Electron Spray Ionization in positive modes was used to obtain derivative ions.

Chromatography was performed at a flow of 0.4 mL/min on a Luna Omega Polar C18 1.7 µm 100x2.1mm column with a 5 mm guard column with the same packing material (Phenomenex, Utrecht, The Netherlands). The temperature of the column was maintained at 40°C. Gradient elution was performed with two UHPLC pumps using methanol/water mixtures with 0.01% formic acid. The gradient started at the time of injection and increased from a 49/51 methanol/water v/v ratio to a 72/28 methanol/water v/v ratio within 4 minutes. The column was flushed with 95/5 methanol/water v/v ratio starting at 4.1 minutes for 2.4 minutes after which the system was equilibrated to initial conditions.

Within the MS system, the vaporizer temperature was set at 300°C and capillary temperature at 250°C. Sheath gas pressure was 40 psi, Multiple Reaction Monitoring was used to quantify isoniazid-derivative (MH+ = 252.1 m/z) and isoniazid-D4-adduct (MH+ = 256.1 m/z). For isoniazid-derivative, the fragments were 79.01, and 121.01 m/z and for the internal standard-derivative the fragments were 83.10, and 124.96 m/z. The sheath gas pressure was 40 psi, auxiliary gas pressure was 15 psi, S lens RF amplitude was 63 V, capillary pressure was 1.190 mTorr. Detection limit was 0.5 ng/mL, and lower limit of quantification (LLOQ) was 1.75 ng/mL. The LC-MS/MS method was validated according to the US Food and Drug Administration guidelines[60]. LC-Quan software (v. 2.7, Thermo Fisher Scientific) was used for data acquisition where isoniazid peak area was corrected by internal standard peak area, and calibration was performed with weighted linear regression using 1/y as weighting factor. Of the pharmacokinetic data points, 3% was below the LLOQ and 1% was above the highest calibration standard, these samples were excluded from the analysis[61].

10.6.6 Bacterial strain preparation

The bacterial strain *M. marinum* E11 expressing mCherry fluorescent protein[62] was used to induce an infection in zebrafish embryos. *M. marinum* E11 was cultured and harvested as previous described[63]. In short, a colony of *M. marinum* E11 was picked from 7H10 supplemented with 10% OADC, the colony was suspended in 7H9 supplemented with 10% ADC, and cultured overnight at 28°C. The optical density at 600 nm (OD_{600}) of bacteria was measured the next day (Eppendorf Biophotometer 6131, Eppendorf, Hamburg, Germany). The logarithmic phase bacteria were harvested and washed 3 times with sterile phosphate buffer saline (PBS). The infection inoculum was resuspended to a target concentration of 200 CFU/nL in 2% PVP40. The MIC of the used strain had been determined to be 15 mg/L, in line with reported values[42].

10.6.7 M. marinum *bacterial burden in zebrafish larvae upon isoniazid treatment*

The injection procedure was performed as described previously[63]. In short, at 24 hpf zebrafish embryos were dechorionated manually with fine tweezers (F6521-1E Jewelers forceps Dumont No. 5, Sigma-Aldrich). The microinjection needles (BF100-75-10, Sutter Instruments) were prepared with a micropipette puller device (P-97 Flaming/Brown Micropipette Puller, Sutter Instrument). Embryos of 28 hpf were anaesthetized with 200 µg/mL tricaine 10 minutes prior to injection and injected with 1 nL of 200 CFU/nL *M. marinum* E11 using the microinjection system (FemtoJet, Eppendorf, Hamburg, Germany), into the caudal vein at the blood island. After injection, the injected embryos were kept at 28°C. To quantify the established infection at 2 dpi, a Fluorescence Stereo Microscope (Leica MZ16FA, Leica Microsystems, Wetzlar, Germany) equipped with digital camera (Leica DFC420 C, Leica Microsystems) was utilized for fluorescence imaging, after which the larvae were transferred to 96 well plates (655180, Greiner Bio-One, Kremsmünster, Austria) with isoniazid solutions of 0, 3.75, 7.5, 15, 30, or 75 mg/L in embryo medium with at least n = 20 per group. At 3 and 4 dpi, fluorescence imaging of individual larvae was repeated after which they were transferred to a new 96 well plate with fresh isoniazid treatment solution (3 dpi) or sacrificed (4 dpi).

Automated image analysis was performed as reported before[19,27], where count of pixels with fluorescence is assumed to correlate directly with the bacterial burden. Potential differences in the bacterial burden between larvae at the start of treatment were tested by non-parametric Kruskal-Wallis test. 12.7% (16/126) of the larvae were removed from the dataset due to improper injection, developmental defects (e.g. cardiac edema), or death due to mechanical damage from handling or otherwise.

10.6.8 Quantification of the exposure-response relationship for isoniazid in zebrafish larvae

A pharmacokinetic-pharmacodynamic model was developed to quantify the internal exposure-response relationship of isoniazid on bacterial growth. NONMEM (version 7.3)[64] through interfaces Pirana (version 2.9.6)[65] and PsN (version 4.7.0)[66] was used for non-linear mixed effects modelling. R (version 3.5.0)[67] through the Rstudio interface (version 1.1.383, RStudio Inc, Boston, Massachusetts, USA) was used for data transformation and graphical output. The First Order Conditional Estimation (FOCE) algorithm with interaction is used for pharmacokinetic-pharmacodynamic modelling.

In the pharmacokinetic component of the model, the homogenate and blood sample data were fitted simultaneously. The treatment medium was represented as depot compartment from which a first order absorption rate constant into a one compartment model with distribution volume and linear or non-linear (Michaelis-Menten) elimination was estimated. Concentration in the treatment medium was assumed to be constant, as supported by measurements of concentrations (Supplementary Figure S10.4). Age was tested as covariate (predictor) on absorption and elimination rate constants using a linear, power or exponential relationship, in addition to a discrete increase in absorption rate constant between 3 and 4 dpf to reflect the impact of the opening of the gastro-intestinal (GI) tract[28]. Out of additive, proportional, or a combination error models, the residual error, describing biological and experimental error, was best described by a combination of an additive and proportional error model for the isoniazid amounts in homogenates and a proportional error model for isoniazid concentrations in the blood samples. A visual predictive check of the pharmacokinetic component of the model was performed using 500 simulations, stratified per dose.

The pharmacodynamic component of the model was fitted through $\log_{10}$ transformed data of the bacterial burden. Bacterial growth was tested using exponential (Equation 2), Gompertz (Equation 3), or logistic (Equation 4) growth functions.

$$\frac{\mathrm{dBac}}{\mathrm{dt}} = \mathrm{k_g} \cdot \mathrm{Bac} \tag{2}$$

$$\frac{\mathrm{dBac}}{\mathrm{dt}} = \mathrm{k_g} \cdot \log\left(\frac{\mathrm{B_{max}}}{\mathrm{Bac}}\right) \tag{3}$$

$$\frac{\mathrm{dBac}}{\mathrm{dt}} = \mathrm{k_g} \cdot \log(\mathrm{B_{max}} - \mathrm{Bac}) \tag{4}$$

in which Bac represented the bacterial burden, t time (h), k_g the growth rate (h^{-1}), and B_{max} the maximum capacity of the system ($\log_{10}$ fluorescence). Because no ceiling of bacterial growth was observed in the data, the maximum capacity of the system could not be estimated for the Gompertz or logistic growth function. Growth and decay cannot be estimated separately as this is mathematically not identifiable given the data. Therefore a net effect was estimated for growth, with implications on its interpretation, i.e. a negative growth meant decay or kill.

Based on the blood sample and homogenate data at 5 dpf, the distribution volume at this age was estimated. This distribution volume was subsequently scaled to 3 and 4 dpf based on total larval volume[68]. The pharmacokinetic component of the model converts total isoniazid amounts from homogenates to concentrations using these distribution volumes (Equation 5).

$$C_{INH} = \frac{A_{INH}}{V_d} \quad (5)$$

in which C_{INH} is the concentration of isoniazid (pmole/µL or µmole/L (µM)), A_{INH} is the amount of isoniazid (pmole) in the homogenate samples, and V_d is the scaled volume of distribution (µL).
For the exposure-response relationship (EFF), linear (Equation 6), Emax (Equation 7), or sigmoidal Emax (Equation 8) functions were tested.

$$EFF = SLP \cdot C_{INH} \quad (6)$$

$$EFF = \frac{E_{max} \cdot C_{INH}}{EC_{50} + C_{INH}} \quad (7)$$

$$EFF = \frac{E_{max} \cdot C_{INH}^{\gamma}}{EC_{50}^{\gamma} + C_{INH}^{\gamma}} \quad (8)$$

in which SLP represents the slope (μM^{-1}), E_{max} the maximal response (-), EC_{50} the concentration of isoniazid responsible for 50% of the maximal response (µM), and γ the Hill exponent (-).

The exposure-response relationship was linked to the bacterial burden as either inhibition of growth or as kill term as shown for the exponential growth function as example in Equation 9 and Equation 10, respectively.

$$\frac{dBac}{dt} = k_g \cdot Bac \cdot (1 - EFF) \quad (9)$$

$$\frac{dBac}{dt} = k_g \cdot Bac - EFF \cdot Bac \quad (10)$$

Inter-individual variability was tested on the estimate of the inoculum, as well as for the parameters of the exposure-response relationship, and reported as coefficient of variation[69]. Out of an additive, proportional, or a combination of additive and proportional error models, a proportional error model, parameterized as an additive error on the $\log_{10}$ transformed data, best described the residual variability in the bacterial burden.

Model selection was performed based on the likelihood ratio test between nested models, in which a drop in objective function value of 3.84 corresponded to $p < 0.05$ between models with a single degree of freedom difference, assuming a χ^2-distribution. Physiologic plausibility of parameter estimates, as well as visual assessment of goodness-of-fit plots[70] were also used for model selection. Precision of structural parameters was considered to be acceptable when relative standard errors of the structural parameters remained below 50%.

10.6.9 Translation of isoniazid response to humans
To quantitatively compare the findings for isoniazid response in zebrafish infected with *M. marinum* to findings in humans infected with *M. tuberculosis*, the exposure-response relationship obtained in the zebrafish larvae was translated to humans as a proof-of-concept. For this, first the isoniazid concentration-time profile in humans was simulated. The concentration-time profile in humans was simulated from a previously published pharmacokinetic model[33], for a period of 7 days of isoniazid oral dosing at 150, 300, and 450 mg for 1,000 individuals per dose group with a ratio of fast and slow metabolizing of 50:50.

Second, the simulated concentrations for the 1,000 individuals per dose group were linked to the exposure-response relationship for *M. marinum* in zebrafish larvae quantified here, to predict the isoniazid response on the bacterial burden. Two translational factors were utilized[31]. The difference in sensitivity to isoniazid was taken into account by using the ratio of the MIC for *M. marinum* and *M. tuberculosis*[49]. The difference in infection stage between the zebrafish, which is in logarithmic phase, and the patients, which are assumed to be in stationary phase (150 days of infection)[31], was taken into account by scaling the isoniazid drug response as quantified previously[51]. From the multistate tuberculosis pharmacometric model, it is clear that the majority of the mycobacteria are in the fast-multiplying state in the logarithmic phase, while they are in the slow- and non-multiplying state in the stationary phase[50]. The ratio of maximum isoniazid-induced kill rates on the fast- and slow-multiplying state (no effect of isoniazid was observed or quantified on the non-multiplying state) is utilized as translational factor to account for the difference in infection stage[51].

Third, the obtained isoniazid response was quantitatively compared to published bacterial burden data in humans[34–36]. Inoculum of the simulation was set at the mean of the reported inoculi[34–36], and exponential growth rate of the bacterial burden was assumed to be similar irrespective of measurement by fluorescence or CFU/mL.

10.7 Acknowledgments

The authors thank Parth Upadhyay for code-review of the R- and NONMEM-scripts, and Astrid M. van der Sar for sharing the wild type VUmc zebrafish line.

10.8 Data availability statement

Final model codes and datasets are publicly available through the DDMoRe Repository, Model ID DDMODEL00000311 (http://repository.ddmore.foundation/model/DDMODEL00000311).

10.9 References

1. Furin J, Cox H, Pai M. Tuberculosis. Lancet. 2019;393(10181):1642-1656.
2. General Assembly of the United Nations. Transforming our world: The 2030 Agenda for Sustainable Development. Gen Assem 70th Sess. 2015;A/RES/70/1.
3. United Nations. The sustainable development goals report 2019. United Nations Publ issued by Dep Econ Soc Aff. 2019.
4. DiMasi JA, Grabowski HG, Hansen RW. Innovation in the pharmaceutical industry: New estimates of R&D costs. J Health Econ. 2016;47:20-33.
5. World Health Organization. Tuberculosis laboratory biosafety manual. World Heal Organ Publ ISBN 978 92 41504638. 2012:1-60.
6. Ginsberg AM, Spigelman M. Challenges in tuberculosis drug research and development. Nat Med. 2007;13(3):290-294.
7. Lienhardt C, Glaziou P, Uplekar M, et al. Global tuberculosis control: lessons learnt and future prospects. Nat Rev Microbiol. 2012;10:407-416.
8. Koul A, Arnoult E, Lounis N, et al. The challenge of new drug discovery for tuberculosis. Nature. 2011;469:483-490.
9. Schulthess P, Van Wijk RC, Krekels EHJ, et al. Outside-in systems pharmacology combines innovative computational methods with high-throughput whole vertebrate studies. CPT Pharmacometrics Syst Pharmacol. 2018;7:285-287.
10. Rennekamp AJ, Peterson RT. 15 years of zebrafish chemical screening. Curr Opin Chem Biol. 2015;24:58-70.
11. Van Wijk RC, Krekels EHJ, Hankemeier T, et al. Systems pharmacology of hepatic metabolism in

zebrafish larvae. Drug Discov Today Dis Model. 2016;22:27-34.
12. Meijer AH, Spaink HP. Host-pathogen interactions made transparent with the zebrafish model. Curr Drug Targets. 2011;12(7):1000-1017.
13. Meijer AH. Protection and pathology in TB: Learning from the zebrafish model. Semin Immunopathol. 2016;38:261-273.
14. Tobin DM, May RC, Wheeler RT. Zebrafish: A see-through host and a fluorescent toolbox to probe host–pathogen interaction. PLoS Pathog. 2012;8(1):e1002349.
15. Myllymäki H, Bäuerlein CA, Rämet M. The zebrafish breathes new life into the study of tuberculosis. Front Immunol. 2016;7(MAY).
16. Carvalho R, De Sonneville J, Stockhammer OW, et al. A high-throughput screen for tuberculosis progression. PLoS One. 2011;6(2):1-8.
17. Ordas A, Raterink R-J, Cunningham F, et al. Testing tuberculosis drug efficacy in a zebrafish high-throughput translational medicine screen. Antimicrob Agents Chemother. 2015;59(2):753-762.
18. Tobin DM, Ramakrishnan L. Comparative pathogenesis of Mycobacterium marinum and Mycobacterium tuberculosis. Cell Microbiol. 2008;10(5):1027-1039.
19. Stoop EJM, Schipper T, Rosendahl Huber SK, et al. Zebrafish embryo screen for mycobacterial genes involved in the initiation of granuloma formation reveals a newly identified ESX-1 component. Dis Model Mech. 2011;4(4):526-536.
20. Bussi C, Gutierrez MG. Mycobacterium tuberculosis infection of host cells in space and time. FEMS Microbiol Rev. 2019;43:341-361.
21. Kolibab K, Yang A, Parra M, et al. Time to detection of Mycobacterium tuberculosis using the MGIT 320 system correlates with colony counting in preclinical testing of new vaccines. Clin Vaccine Immunol. 2014;21(3):453-455.
22. Kumar N, Vishwas KG, Kumar M, et al. Pharmacokinetics and dose response of anti-TB drugs in rat infection model of tuberculosis. Tuberculosis. 2014;94(3):282-286.
23. Jayaram R, Shandil RK, Gaonkar S, et al. Isoniazid pharmacokinetics-pharmacodynamics in an aerosol infection model of tuberculosis. Antimicrob Agents Chemother. 2004;48(8):2951-2957.
24. Bartelink I, Zhang N, Keizer R, et al. New paradigm for translational modeling to predict long-term tuberculosis treatment response. Clin Transl Sci. 2017;(May):366-379.
25. Morgan P, Van der Graaf PH, Arrowsmith J, et al. Can the flow of medicines be improved? Fundamental pharmacokinetic and pharmacological principles toward improving Phase II survival. Drug Discov Today. 2012;17(9/10):419-424.
26. Jindani A, Aber VR, Edwards EA, et al. The early bactericidal activity of drugs in patients with pulmonary tuberculosis. Am Rev Respir Dis. 1980;121(6):939-949.
27. Nezhinsky A, Verbeek FJ. Pattern recognition for high throughput zebrafish imaging using genetic algorithm optimization. In: Dijkstra T, Tsivtsivadze E, Heskes T, Marchiori E, eds. Lecture Notes in Bioinformatics 6282. Berlin- Heidelberg: Springer-Verlag; 2010:301-312.
28. Van Wijk RC, Krekels EHJ, Kantae V, et al. Impact of post-hatching maturation on the pharmacokinetics of exogenous compounds in zebrafish larvae. Sci Rep. 2018;9:2149.
29. Ng ANY, De Jong-Curtain TA, Mawdsley DJ, et al. Formation of the digestive system in zebrafish: III. Intestinal epithelium morphogenesis. Dev Biol. 2005;286(1):114-135.
30. Musuamba F, Manolis E, Holford N, et al. Advanced methods for dose and regimen finding during drug development: summary of the EMA/EFPIA workshop on dose finding (London 4-5 December 2014). CPT Pharmacometrics Syst Pharmacol. 2017;6:418-429.
31. Wicha SG, Clewe O, Svensson RJ, et al. Forecasting clinical dose-response from preclinical studies in tuberculosis research: translational predictions with rifampicin. Clin Pharmacol Ther. 2018;104(6):1208-1218.
32. De Groote MA, Gilliland JC, Wells CL, et al. Comparative studies evaluating mouse models used for efficacy testing of experimental drugs against Mycobacterium tuberculosis. Antimicrob Agents Chemother. 2011;55(3):1237-1247.
33. Wilkins JJ, Langdon G, McIlleron H, et al. Variability in the population pharmacokinetics of isoniazid

in South African tuberculosis patients. Br J Clin Pharmacol. 2011;72(1):51-62.
34. Li L, Mahan CS, Palaci M, et al. Sputum Mycobacterium tuberculosis mRNA as a marker of bacteriologic clearance in response to antituberculosis therapy. J Clin Microbiol. 2010;48(1):46-51.
35. Johnson JL, Hadad DJ, Boom WH, et al. Early and extended early bactericidal activity of levofloxacin, gatifloxacin and moxifloxacin in pulmonary tuberculosis. Int J Tuberc Lung Dis. 2006;10(6):605-612.
36. Hafner R, Cohn JA, Wright DJ, et al. Early bactericidal activity of isoniazid in pulmonary tuberculosis: Optimization of methodology. Am J Respir Crit Care Med. 1997;156(3 I):918-923.
37. Kantae V, Krekels EHJ, Ordas A, et al. Pharmacokinetic modeling of paracetamol uptake and clearance in zebrafish larvae: Expanding the allometric scale in vertebrates with five orders of magnitude. Zebrafish. 2016;13(6):504-510.
38. Van Wijk RC, Krekels EHJ, Kantae V, et al. Mechanistic and quantitative understanding of pharmacokinetics in zebrafish larvae through nanoscale blood sampling and metabolite modelling of paracetamol. J Pharmacol Exp Ther. 2019;371:15-24.
39. Spaink HP, Cui C, Wiweger MI, et al. Robotic injection of zebrafish embryos for high-throughput screening in disease models. Methods. 2013;62(3):246-254.
40. Gillespie SH, Gosling RD, Charalambous BM. A reitrerative method for calculating the early bactericidal activity of antituberculosis drugs. Am J Respir Crit Care Med. 2002;166(1):31-35.
41. Greenwood DJ, Dos Santos MS, Huang S, et al. Subcellular antibiotic visualization reveals a dynamic drug reservoir in infected macrophages. Science. 2019;364(6447):1279-1282.
42. Aubry A, Jarlier V, Escolano S, et al. Antibiotic susceptibility pattern of Mycobacterium marinum. Antimicrob Agents Chemother. 2000;44(11):3133-3136.
43. Weerakhun S, Hatai K, Murase T, et al. In vitro and in vivo activities of drugs against Mycobacterium marinum in yellowtail Seriola quinqueradiata. Fish Pathol. 2008;43(3):106-111.
44. Boot M, Sparrius M, Jim KK, et al. iniBAC induction is vitamin B12- and MutAB-dependent in mycobacterium marinum. J Biol Chem. 2016;291(38):19800-19812.
45. Boot M, Jim KK, Liu T, et al. A fluorescence-based reporter for monitoring expression of mycobacterial cytochrome bd in response to antibacterials and during infection. Sci Rep. 2017;7(1):1-10.
46. Gumbo T, Louie A, Liu W, et al. Isoniazid bactericidal activity and resistance emergence: Integrating pharmacodynamics and pharmacogenomics to predict efficacy in different ethnic populations. Antimicrob Agents Chemother. 2007;51(7):2329-2336.
47. Budha NR, Lee RB, Hurdle JG, et al. A simple in vitro PK/PD model system to determine time-kill curves of drugs against Mycobacteria. Tuberculosis. 2009;89:378-385.
48. Hemanth Kumar AK, Kannan T, Chandrasekaran V, et al. Pharmacokinetics of thrice-weekly rifampicin, isoniazid and pyrazinamide in adult tuberculosis patients in India. Int J Tuberc Lung Dis. 2016;20(9):1236-1241.
49. Schön T, Juréen P, Giske CG, et al. Evaluation of wild-type MIC distributions as a tool for determination of clinical breakpoints for Mycobacterium tuberculosis. J Antimicrob Chemother. 2009;64(4):786-793.
50. Clewe O, Aulin L, Hu Y, et al. A multistate tuberculosis pharmacometric model: A framework for studying anti-tubercular drug effects in vitro. J Antimicrob Chemother. 2016;71(4):964-974.
51. Clewe O, Wicha SG, de Vogel CP, et al. A model-informed preclinical approach for prediction of clinical pharmacodynamic interactions of anti-TB drug combinations. J Antimicrob Chemother. 2018;73(2):437-447.
52. Chen C, Ortega F, Rullas J, et al. The multistate tuberculosis pharmacometric model: a semi-mechanistic pharmacokinetic-pharmacodynamic model for studying drug effects in an acute tuberculosis mouse model. J Pharmacokinet Pharmacodyn. 2017;44(2):133-141.
53. Chen C, Wicha SG, De Knegt GJ, et al. Assessing pharmacodynamic interactions in mice using the multistate tuberculosis pharmacometric and general pharmacodynamic interaction models. CPT Pharmacometrics Syst Pharmacol. 2017;6(11):787-797.
54. Svensson RJ, Simonsson USH. Application of the multistate tuberculosis pharmacometric model in patients with rifampicin-treated pulmonary tuberculosis. CPT Pharmacometrics Syst Pharmacol.

2016;5(5):264-273.
55. Van Wijk RC, Van der Sar AM, Krekels EHJ, et al. Quantification of natural growth of two strains of Mycobacterium marinum for translational anti-tuberculosis drug development. Submitted. 2019.
56. Jindani A, Doré CJ, Mitchison DA. Bactericidal and sterilizing activities of antituberculosis drugs during the first 14 days. Am J Respir Crit Care Med. 2003;167(10):1348-1354.
57. Strähle U, Scholz S, Geisler R, et al. Zebrafish embryos as an alternative to animal experiments — A commentary on the definition of the onset of protected life stages in animal welfare regulations. Reprod Toxicol. 2012;33:128-132.
58. Westerfield M. The zebrafish book. A guide for the laboratory use of zebrafish (Danio rerio). 4th ed. Eugene, OR, USA: University of Oregon Press; 2000.
59. EU. Council Directive 2010/63/EU on the protection of animals used for scientific purposes. Off J Eur Union. 2010;L276/33.
60. US Food and Drug Administration. Bioanalytical method validation guidance for industry. FDA. 2018:May.
61. Beal SL. Ways to fit a PK model with some data below the quantification limit. J Pharmacokinet Pharmacodyn. 2001;28(5):481-504.
62. Van der Sar AM, Spaink HP, Zakrzewska A, et al. Specificity of the zebrafish host transcriptome response to acute and chronic mycobacterial infection and the role of innate and adaptive immune components. Mol Immunol. 2009;46(11-12):2317-2332.
63. Benard EL, Van der Sar AM, Ellett F, et al. Infection of zebrafish embryos with intracellular bacterial pathogens. J Vis Exp. 2012;61:e3781.
64. Beal S, Sheiner L, Boeckmann A, et al. NONMEM 7.3.0 users guides. (1989-2013). ICON Development Solutions, Hanover, MD, USA.
65. Keizer R, Van Benten M, Beijnen J, et al. Pirana and PCluster: A modeling environment and cluster infrastructure for NONMEM. Comput Methods Programs Biomed. 2011;101(1):72-79.
66. Lindbom L, Pihlgren P, Jonsson E. PsNtoolkit — a collection of computer intensive statistical methods for non-linear mixed effect modeling using NONMEM. Comput Methods Programs Biomed. 2005;79(3):241-257.
67. R Core Team. R: A language and environment for statistical computing. R Found Stat Comput Vienna, Austria. 2014.
68. Guo Y, Veneman WJ, Spaink HP, et al. Three-dimensional reconstruction and measurements of zebrafish larvae from high-throughput axial-view in vivo imaging. Biomed Opt Express. 2017;8(5):2611-2634.
69. Mould DR, Upton RN. Basic concepts in population modeling, simulation, and model-based drug development-part 2: introduction to pharmacokinetic modeling methods. CPT pharmacometrics Syst Pharmacol. 2013;2(April):e38.
70. Nguyen THT, Mouksassi M-S, Holford N, et al. Model evaluation of continuous data pharmacometric models: metrics and graphics. CPT Pharmacometrics Syst Pharmacol. 2017;6:87-109.

10.10 Supplementary material

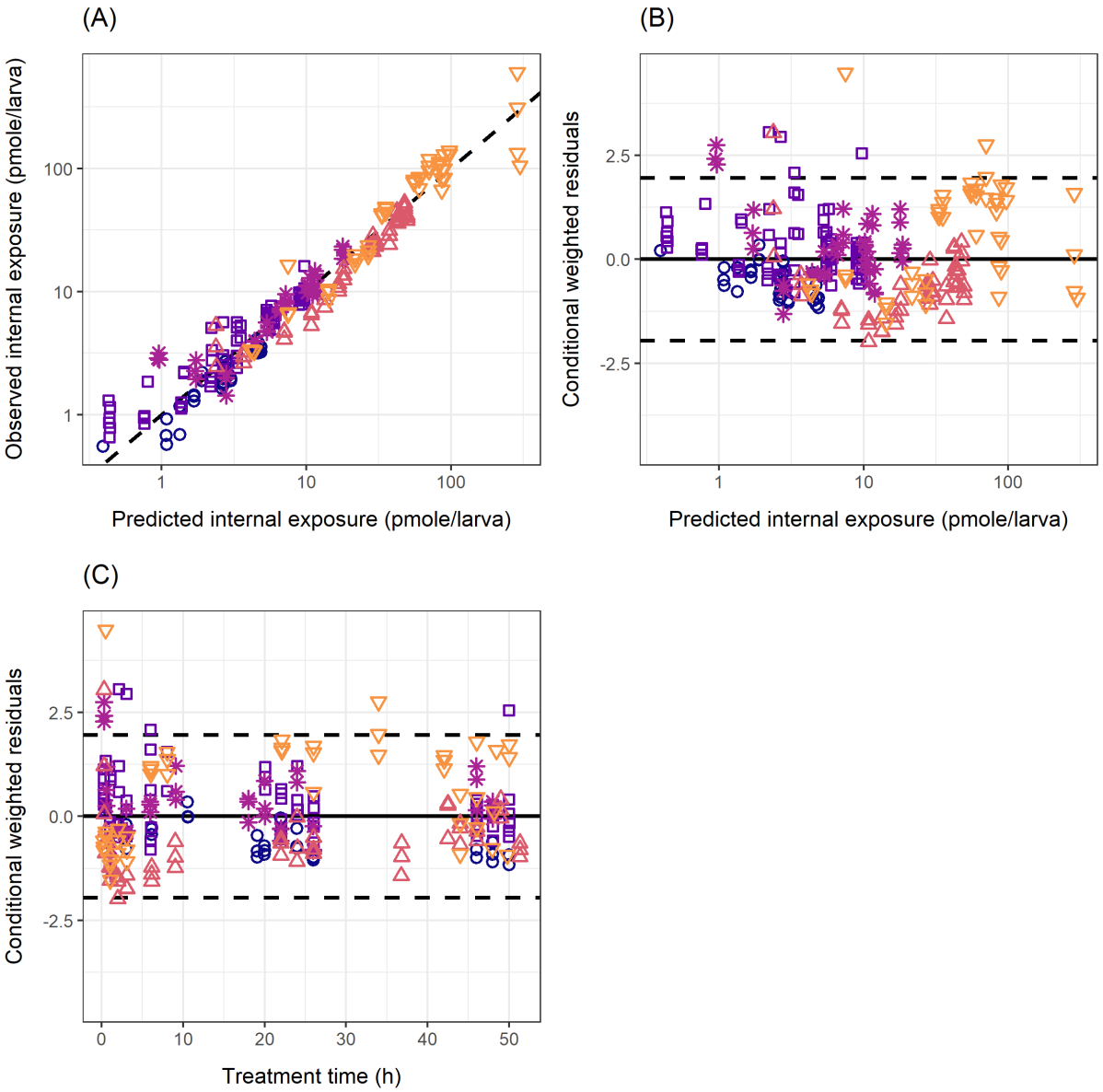

Supplementary Figure S10.1 Goodness-of-fit plots for the pharmacokinetic component of the final pharmacokinetic-pharmacodynamic model in zebrafish larvae. (a) Observed vs predicted, dotted line is the line of unity. (b) Conditional weighted residuals vs prediction, solid line represents zero, dashed lines represent 95% interval between ±1.96 standard deviation. (c) Conditional weighted residuals vs time, solid line represents zero, dashed lines represent 95% interval between ±1.96 standard deviation. Symbols represent waterborne isoniazid doses 0.5 (blue circle), 1 (purple square), 2 (lilac star), 5 (orange upward triangle) and 10 (yellow downward triangle) x MIC (MIC = 15 mg/L). Only small trends for different doses were observed which suggested only limited bias of predicted internal isoniazid amounts by the final model.

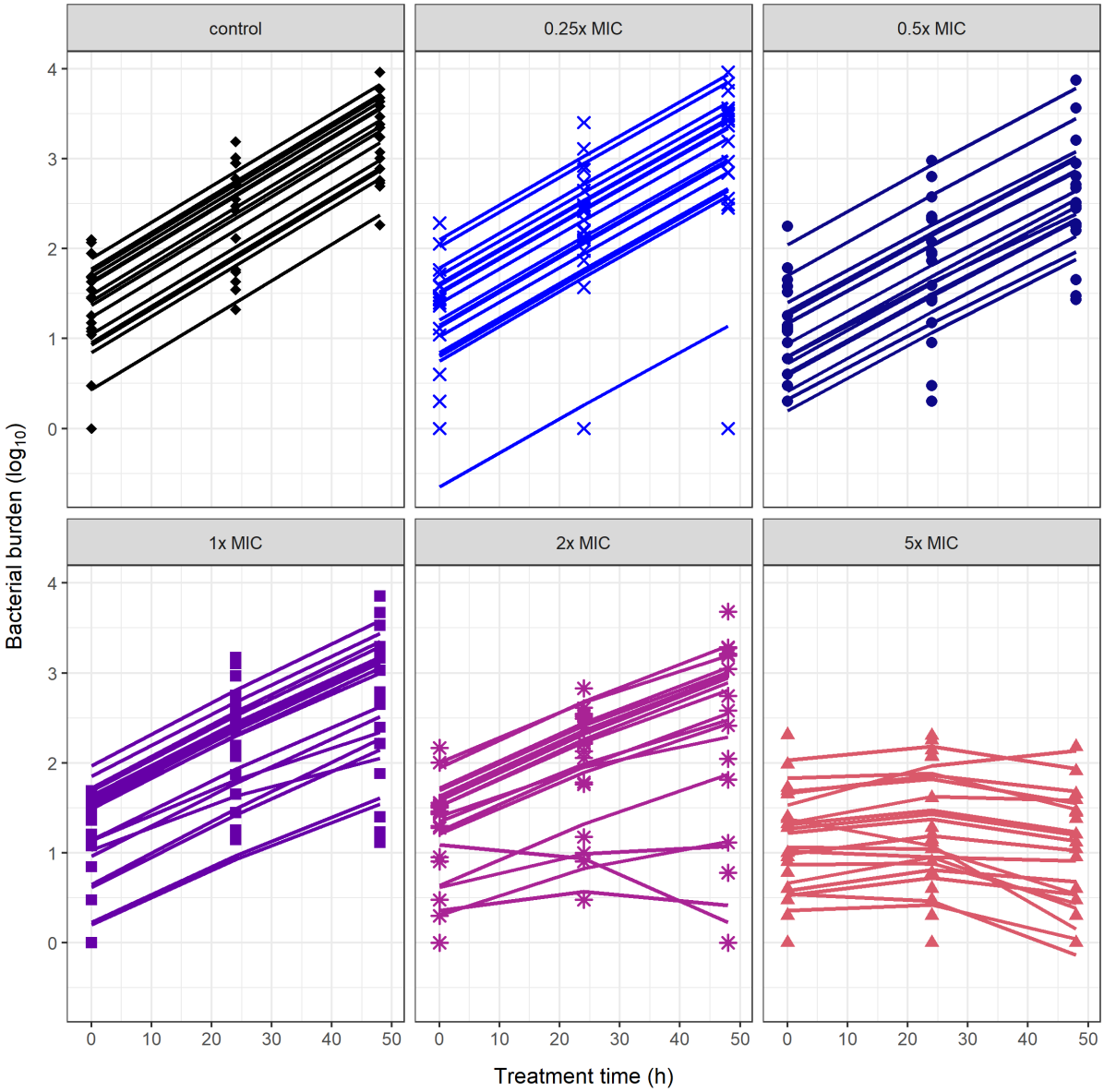

Supplementary Figure S10.2 Model-based individual prediction of the bacterial burden after isoniazid treatment in zebrafish larvae infected with *M. marinum*. The bacterial burden as log_{10}-transformed fluorescent pixel count is shown over treatment time of 50 hours at isoniazid doses in the external treatment medium of 0.25 (light blue crosses and line), 0.5 (blue circles and line), 1 (purple squares and line), 2 (lilac stars and line), and 5 (orange upward triangles and line) x MIC (MIC = 15 mg/L), in addition to control (black diamonds and line). Symbols represent observed data, lines represent model prediction for individual zebrafish.

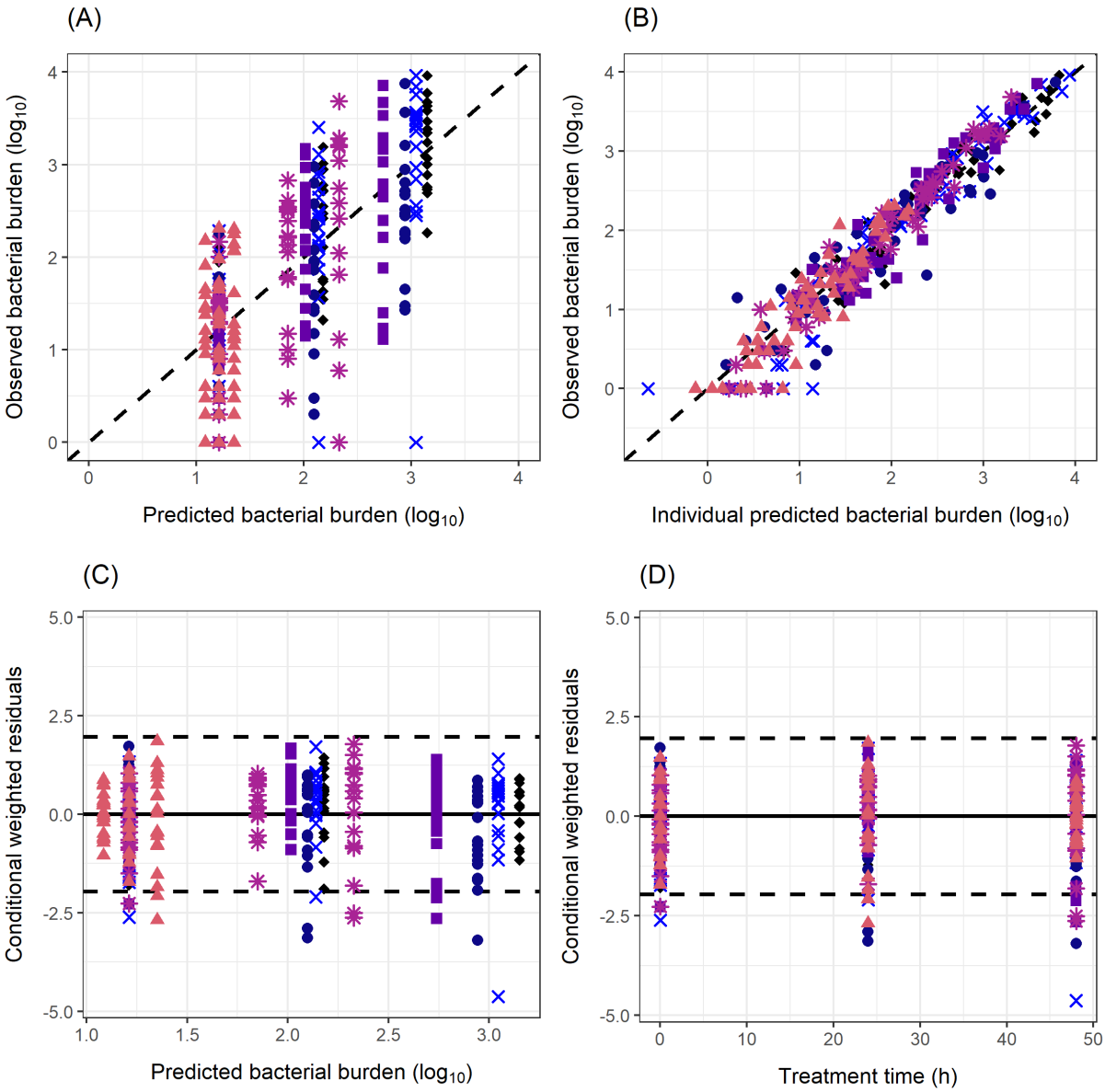

Supplementary Figure S10.3. Goodness-of-fit plots for pharmacodynamic component of the final pharmacokinetic-pharmacodynamic model in zebrafish. (a) Observed vs population predicted, dotted line is the line of unity. (b) Observed vs individual predicted, dotted line is the line of unity. (c) Conditional weighted residuals vs prediction, solid line represents zero, dashed lines represent 95% interval between ±1.96 standard deviation. (d) Conditional weighted residuals vs time, solid line represents zero, dashed lines represent 95% interval between ±1.96 standard deviation. Symbols represent doses 0 (black diamond), 0.25 (light blue cross), 0.5 (blue circle), 1 (purple square), 2 (lilac star), and 5 (orange upward triangle) x MIC (MIC = 15 mg/L). Lack of trends in the goodness-of-fit plots show no bias in the final model.

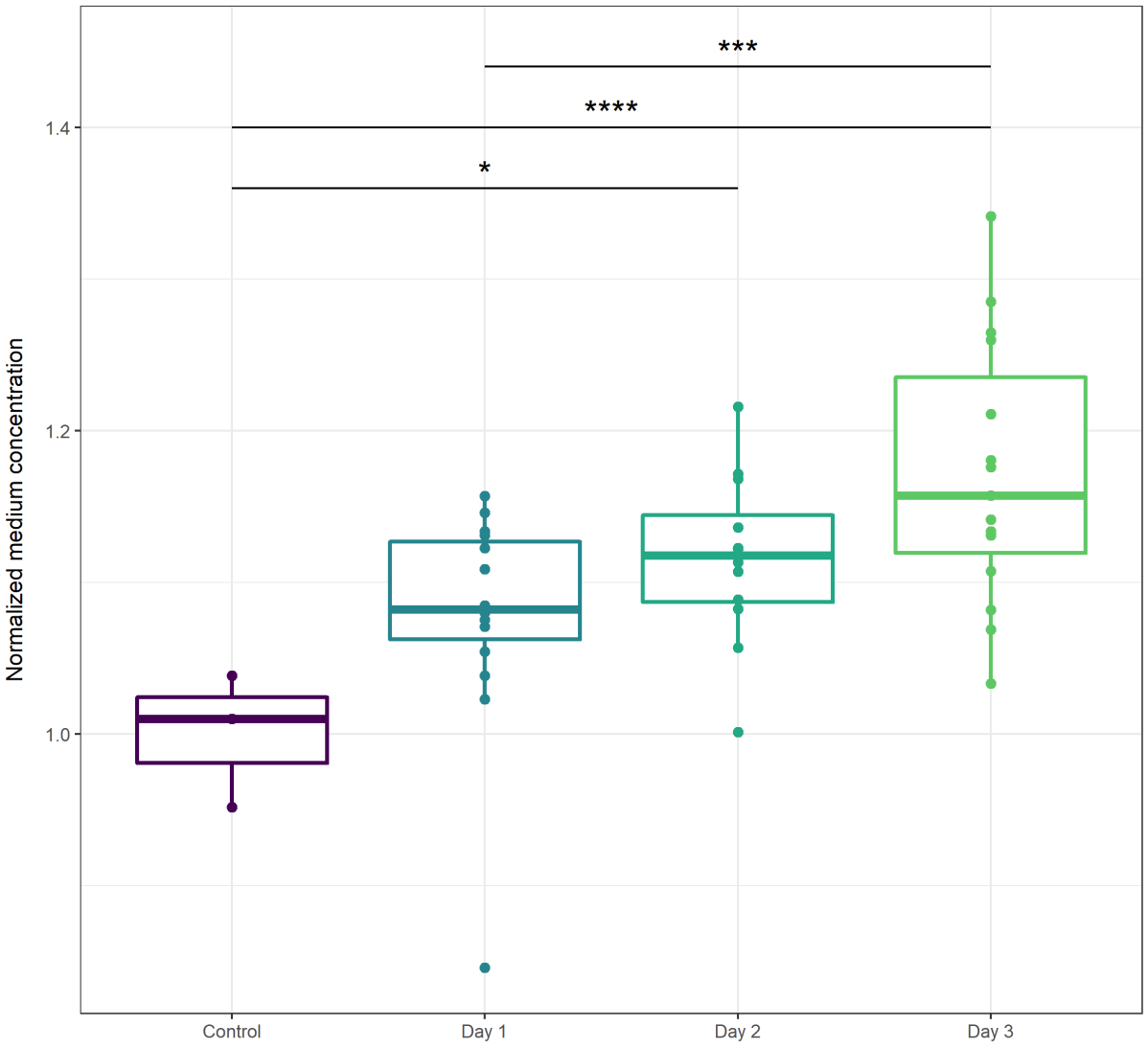

Supplementary Figure 10.4 Stability of waterborne isoniazid over treatment period. Concentrations were normalized to control. An increase of 10-15% was assumed to have negligible impact on the absorption from the treatment medium, which was therefore kept constant in the pharmacokinetic-pharmacodynamic model. Kruskal-Wallis with Dunn post hoc test: * $p < 0.05$, ** $p < 0.01$, *** $p < 0.005$, **** $p < 0.001$

10.11 NONMEM model code final pharmacokinetic-pharmacodynamic model

```
$PROBLEM PKPD
$INPUT ID TIME AMT DV EVID MDV CMT BQL AQL DOSE AGE AGE_H XEXP BLOOD FLAG
$DATA PKPD_dataset.csv IGNORE=@ IGNORE=(BQL.EQ.1) IGNORE=(AQL.EQ.1)

; time in hours of exposure
; amt in uM (concentration)
; DV in pmole / larvae or pmole / uL (uM) / log10(bac burden)
; Vd in uL
; AGE_H age in hpf

$SUBROUTINE ADVAN13 TOL=9

$MODEL
COMP ;CMT 1 dosing
COMP ;CMT 2 isoniazid in larva
COMP ;CMT 3 bacterial burden measured in log10(fluorescence pixels)

$PK

;-----PK-----

TVKE = THETA(1)          ;first order elimination rate
TVV2 = THETA(2)          ;distribution volume in uL/larva
TVKA = THETA(3) / 1e2    ;absorption at start of experiment
KA_GI = THETA(4)         ;effect of GI opening between 3 and 4 dpf on absorp-
tion
KA_HPF = THETA(5)        ;effect of age in hours post fertilization on ab-
sorption

;age effect on KA
KA = TVKA * KA_HPF**(AGE_H / 101)   ;median age is 101 hpf

;GI effect on KA
IF(AGE_H.LE.90) KIN = KA * DOSE
IF(AGE_H.GT.90) KIN = KA * DOSE * (1 + KA_GI)

KE = TVKE
V2 = TVV2

;-----PD-----

KG = THETA(6)                            ;exponential growth rate
INOC = THETA(7) * 1e1                    ;inoculum estimated
SLP = (THETA(8) / 1e2) * EXP(ETA(2))     ;slope (linear drug effect)

A_0(3) = INOC * EXP(ETA(1))              ;inoculum set as compartment ini-
tial value

$DES
DADT(1) = 0                              ;dosing compartment
DADT(2) = KIN - KE * A(2)                ;larva compartment isoniazid

;drug effect

;Distribution volume is estimated based on 5 dpf blood samples, but is ex-
pected to be lower with younger larvae of 3 and 4 dpf.
;It is here assumed that the distribution volume scales with total volume.

IF(AGE.EQ.3) THEN
```

```
V = V2 * 253/300          ;taking total volume into account (DOI: 10.1364/
BOE.8.002611)
ENDIF
IF(AGE.EQ.4) THEN
V = V2 * 263/300          ;taking total volume into account (DOI: 10.1364/
BOE.8.002611)
ENDIF
IF(AGE.EQ.5) THEN
V = V2                    ;taking total volume into account (DOI: 10.1364/
BOE.8.002611)
ENDIF

C = A(2)/V

EFF = 0                   ;for C is zero or NA
IF(C.GT.0) THEN
EFF = SLP * C
ENDIF

DADT(3) = KG * A(3) * (1 - EFF) ;bacterial burden (log10)

$ERROR

;-----PK-----

IF(FLAG.EQ.0.AND.BLOOD.EQ.0) THEN
IPRED = A(2)
Y = IPRED * (1 + EPS(1)) + EPS(2) ; comb error
W = SQRT(IPRED**2*SIGMA(1,1)**2    + SIGMA(2,2)**2)
IRES = DV - IPRED
ENDIF

IF(FLAG.EQ.0.AND.BLOOD.EQ.1) THEN
IPRED = A(2) / V2
Y = IPRED * (1 + EPS(3)) + EPS(4) ; comb error
W = SQRT(IPRED**2*SIGMA(3,3)**2    + SIGMA(4,4)**2)
IRES = DV - IPRED
ENDIF

;-----PD-----

IF(FLAG.EQ.1) THEN
IPRED = LOG10(A(3)+0.00001)
Y = IPRED + W
W = EPS(5)
IRES = DV - IPRED
ENDIF

IF(W.EQ.0)W=1
IWRES = IRES/W

$THETA
(0, 0.58)        ; 1 KE
(0, 0.325)       ; 2 V2
(0, 0.355)       ; 3 KA
(0, 0.178)       ; 4 KA_GI
(1, 7.45)        ; 5 KA_HPF
(0, 0.093)       ; 6 KG
(0, 1.6)         ; 7 *1e1 INOC
(0, 0.991)       ; 8 /1e2 SLP

$OMEGA 1.64      ;IIV INOC
```

```
$OMEGA 0.227    ;IIV SLP

$SIGMA 0.0611   ; 1 prop homogenate INH
$SIGMA 0.59     ; 2 add homogenate INH
$SIGMA 0.485    ; 3 prop blood INH
$SIGMA 0 FIX    ; 4 add blood INH
$SIGMA 0.125    ; 5 prop bacterial burden

$ESTIMATION METHOD=1 INTER MAXEVAL=8000 NOABORT PRINT=10 NSIG=3 SIGL=9
POSTHOC
$COVARIANCE PRINT=E

$TABLE ID TIME KIN KA TVKA KE V2 KA_GI KA_HPF KG INOC SLP C V ETA(1) ETA(2)
DV EVID MDV CMT BQL AQL DOSE AGE AGE_H BLOOD XEXP FLAG IPRED IRES IWRES
CWRES NOPRINT ONEHEADER FILE=tab1
```

10.12 NONMEM model code translation to humans of isoniazid response

```
$PROBLEM TRANSLATION

$INPUT ID TIME AMT DV EVID MDV CMT WT METAB DOSE
$DATA TRANSLATE_dataset.csv IGNORE=@

; time in hours
; amt in mg
; dv in mg/L (--> transform linear slope from zebrafish in uM)
; subjects are all male and HIV negative (no covariates)
; METAB is 1 for fast and 0 for slow metabolizers

$SUBROUTINE ADVAN13 TOL=9

$MODEL

COMP(ABS DEFDOSE)
COMP(CENTRAL DEFOBS)
COMP(PERIPH)
COMP(BAC)

$PK

;PK (simulated from Wilkins et al, Br. J. Clin. Pharmacol. 72, 51–62
(2011))

;typical values
TVKA = THETA(1)      ;typical value absorption rate constant
TVALAG2 = THETA(2)   ;typical value absorption lag time to compartment 2
```

```
TVV2 = THETA(3)      ;typical value distribution volume central compartment
TVV3 = THETA(4)      ;typical value distribution volume peripheral compart-
ment
TVQ = THETA(5)       ;typical value intercompartmental clearance

TVCLS = THETA(6)     ;typical value clearance slow metabolizers
TVCLF = THETA(7)     ;typical value clearance fast metabolizers

;PK parameters

KA = TVKA
ALAG2 = TVALAG2 * EXP(ETA(1))
V2 = TVV2 * (WT/70)**1.00 * EXP(ETA(2))
V3 = TVV3 * (WT/70)**1.00
Q = TVQ * EXP(ETA(3))
CLS = TVCLS * (WT/70)**0.75 * EXP(ETA(4))
CLF = TVCLF * (WT/70)**0.75 * EXP(ETA(4))

;microconstants

KEF = CLF / V2
KES = CLS / V2
KE = KES * (1 - METAB) + KEF * (METAB)  ;distinguish between fast and slow
metabolizer
K23 = Q / V2
K32 = Q / V3

S2 = V2

;PD (from PKPD model of isoniazid in zebrafish)

;estimated exponential growth (kg = 0.093007) is used to backcalculate -48h
from inoculum (inoc = 16.276) which is moment of infection in zebrafish with
200 CFU M marinum
;and subsequently to CFU/mL

FL_start = 16.276 * exp(-48 * 0.093007)
CFU_start = 200
f_FL_CFU = CFU_start/FL_start   ;factor to convert fluorescence to CFU
CFU_INOC = 16.276 * f_FL_CFU
f_INOC_CFU = 4888538/CFU_INOC   ;mean inoculum from digitized papers

TVKG = THETA(8)      ;exponential growth rate
TVINOC = THETA(9)    ;inoculum estimated
TVSLP = THETA(10)    ;slope (linear drug effect)

KG = TVKG
INOC = TVINOC * EXP(ETA(5))
SLP0 = TVSLP * EXP(ETA(6))

A_0(4) = INOC * f_FL_CFU * f_INOC_CFU  ;inoculum in CFU/mL

$DES

DADT(1) = -KA * A(1)
DADT(2) = KA * A(1) - KE * A(2) - K23 * A(2) + K32 * A(3)
DADT(3) = K23 * A(2) - K32 * A(3)

C = A(2)/V2

;translational factors (Wicha et al, Clin. Pharmacol. Ther. 104:6, 1208-
1218 (2018))
```

```
;1. MIC
MIC_fac = 0.2/15         ;correct for MIC of INH for MTB (0.2 mg/L, break-
point MIC from Schön et al, J. Antimicrob. Chemother. 64, 786–793 (2009))
in comparison to MM (15 mg/L) by increasing sensitivity

;2. Stage of infection
INFEC_fac = 22.2/8.55  ;correct for difference in effect on logarithmic (ze-
brafish infection, mostly F) and stationary (clinical infection, mostly S
and N) by taking ratio of maximal kill rate
of isoniazid on F and S state (no isoniazid quantified on N state, Clewe et
al, J. Antimicrob. Chemother. 73, 437–447 (2018))

SLP = SLP0 / MIC_fac / INFEC_fac
EFF = SLP * C

DADT(4) = KG * A(4) * (1 - EFF)

$ERROR

IF(CMT.NE.4) THEN
IPRED = LOG(F + 0.0001)
Y = IPRED + EPS(1)
ENDIF

IF(CMT.EQ.4) THEN
IPRED = LOG10(A(4) + 0.0001)
Y = IPRED + EPS(2)
ENDIF

$THETA
1.85             ;1 KA h-1
0.180            ;2 ALAG2 h
57.7             ;3 V2 L
1730             ;4 V3 L
3.34             ;5 Q L/h
9.70             ;6 CLS L/h slow metabolizer
21.6             ;7 CLF L/h fast metabolizer
0.093007         ;8 KG
16.276           ;9 INOC
0.07227485       ;10 SLP 0.0099117/0.137139 (convert slope from uM to mg/L
by dividing by mol. weight)

$OMEGA
0.781456         ;IIV ALAG2 reported %CV 88.4
0.027225         ;IIV V2 reported %CV 16.5
0.866761         ;IIV Q reported %CV 93.1
0.033856         ;IIV CL reported %CV 18.4
1.64             ;IIV INOC
0.227            ;IIV SLP

$SIGMA
0.042025         ;additive on natural log scale, sd = 0.205 mg/L
0.124            ;additive on natural log scale

$SIMULATION (12345) ONLYSIM SUBPROBLEM=1

$TABLE ID TIME AMT DV EVID MDV CMT WT METAB DOSE
TVKA TVALAG2 TVV2 TVV3 TVQ TVCLS TVCLF TVKG TVINOC TVSLP
KA ALAG2 V2 V3 Q CLS CLF KG INOC SLP SLP0 f_FL_CFU ETA1 ETA2 ETA3 ETA4 ETA5
ETA6 IPRED NOPRINT ONEHEADER FILE=tabsim1
```

Section V. Summary, discussion, and conclusion

Chapter 11

Summary, discussion, and conclusion

11.1 The zebrafish in systems pharmacology

The development of new efficacious and safe drugs is one of the most challenging endeavours in biomedical research. The process includes research on all biomedical scales, from molecular and (sub)cellular scales to whole organisms including different animal species, before reaching the clinical phase. The right target, compound, and dose for treatment of a disease are selected based on prior knowledge and experimental results, for which reliable translation between different experimental contexts and species is essential. Quantitative pharmacology is key in steering that translation into the right direction[1]. Pharmacokinetic parameters – the absorption rate constant, distribution volume, and clearance – describing the dose-exposure relationship over time, can be translated or scaled between species[2]. The same is true for pharmacodynamic parameters that describe the exposure-response relationship, like turnover rates, or drug potency (EC_{50}) or efficacy (E_{max})[3]. The more mechanistic a quantitative pharmacological model is, the more reliable the translation can be expected to be. Integrating quantitative pharmacology with the mechanistic discipline of systems biology – defined as systems pharmacology – therefore instils more confidence in the translation of exposure-response relationships[4]. Systems pharmacology is part of the new systems therapeutics paradigm, which considers all relevant actors in a (patho)physiological system instead of a single interaction between drug and target[5].

Systems pharmacology has the potential to become the standard in drug development to address mechanistic questions on disease and drug pharmacology[6]. It does lean heavily on preclinical data to identify and characterize (patho)physiological processes. However, a lack of dedicated experimental data may hinder successful implementation of systems pharmacology[7]. This is especially the case for data obtained in the full biological context of a whole organism, rather than from isolated *in vitro* assays. Moreover, because of constraints in both resources and time, high-throughput experimentation is preferable. It is unlikely that acquisition of these types and these amounts of experimental data will be feasible in clinical practice or even preclinical mammalian experiments. Conventional *in vitro* experiments are performed at this scale and speed, but lack information on the biological context. Innovative organ-on-a-chip systems, consisting of human cell cultures grown under physiological conditions on microfluidic devices to represent living and functioning organ tissues[8,9], is an improvement in that respect. However, drug targets in different tissue, off-target effects, or physiological signaling between tissues are still not included[10]. Experiments at *in vitro* scale and throughput but within the proper biological context are therefore needed.

The zebrafish (*Danio rerio*) has become an established vertebrate model organism in biomedical research[11]. Especially in its larval stage it is often used, because of its many advantages including optical transparency for non-invasive observations of cells, tissues, or organs. Of all human genes, 71% has an orthologue in the zebrafish, of the human genes involved in disease this is 82%[12]. For comparison, the mouse, a conventional preclinical mammalian species, has an orthologue of 83% of all human genes[12]. However, experimental studies including development of disease models using mice are longer in duration and more expensive than in zebrafish. Because of its external fertilization, genetically modification in zebrafish is much easier compared to higher vertebrates, to create models for human disease[13]. To create a model for human disease for example in the mouse, genetic modification of murine embryos is required which subsequently need to be implanted in a carrier mouse and carried until term[14]. Moreover, the advantages of small size, large litter size, and fast development, make the zebrafish larva an ideal model organism for high-throughput experimentation[15]. It is also ethically preferable to perform *in vivo* experiments in the least developed organism and no ethical approval is required for experimentation on the larval stage of the zebrafish (i.e. first 5 days post fertilization)[16]. The zebrafish larva therefore combines the experimental efficiency of high-throughput potential with the translational value of result from the biological context of a whole vertebrate organism.

Pharmacological or toxicological experiments with zebrafish and zebrafish larvae are commonly performed by dissolving drugs into the water in which the zebrafish swim. Drug effects, or lack thereof,

are interpreted based on the assumption that the external drug concentration reflects the internal concentration inside the zebrafish or zebrafish larva. This assumption ignores basic pharmacokinetics; absorption, distribution, metabolism, and excretion of drugs by an organism, that causes the internal drug exposure to change over time and potentially reach internal steady state concentrations different from the external concentration. This is important because it is the internal exposure at the target site that drives the drug effect[17]. Therefore, ignoring this concentration, and its changes over time, hinders interpretation of drug effects. For translation of drug effects to higher vertebrates, including humans, it is also important to link the internal exposure (pharmacokinetics) to measures of the drug response (pharmacodynamics), to quantify the exposure-response, or pharmacokinetic-pharmacodynamic relationship. To quantify the drug response, the disease dynamics, and changes therein upon treatment, need to be measured, as well as between-species differences in the underlying (patho)physiological and pharmacological processes. A model-based approach can then correct for these differences with translational factors, for inter-species translation of drug effects.

In this thesis, we have therefore developed and integrated innovative experimental and computational methods for the quantification of:

I) internal drug exposure over time in zebrafish larvae after waterborne drug treatment;
II) disease dynamics and drug-induced changes therein;
III) between-species differences in disease mechanisms and drug effects thereon.

Only with a quantitative understanding of these three elements can pharmacological findings be reliably translated and can the zebrafish become a full member of the preclinical drug development pipeline.

11.2 Introduction to high-throughput experimentation in whole vertebrate

The advantages of pharmacological experiments in zebrafish were introduced in **Section I**. Firstly, the need for quantification of internal exposure over time was introduced. It is important to have a mechanistic and quantitative understanding of drug metabolism by the zebrafish. Drug metabolites resulting from biotransformation in for example the liver, can be pharmacologically active or toxic. We therefore reviewed hepatic metabolism of the zebrafish in the context of systems pharmacology in **Chapter 2**. The metabolising enzymes in zebrafish were compared to their human orthologues, with a focus on oxidative and conjugative metabolism involved in the metabolism of our paradigm compound paracetamol (acetaminophen). Genes related to the most important cytochrome P450 (CYP) enzyme isoforms in humans catalysing oxidative metabolism, CYP3A4 and CYP2E1, are expressed in zebrafish as well. The same holds for sulfotransferases, which catalyse conjugation of drugs with sulfate-groups. The enzymes responsible for glucuronidation in humans, the UDP-glucuronosyltransferases, have paralogues in zebrafish, enzymes with comparable metabolic function. The genetic comparison from this chapter, showing similar enzymes for drug metabolism between zebrafish and humans, suggested that this species could yield meaningful results regarding effects from potential drug metabolites. It is important to quantify the internal drug exposure, including their metabolites, to confirm this suggestion. Internal exposure could subsequently be linked to measures of hepatic dysfunction, like biomarkers or organ size.

An important advantage of the zebrafish for pharmacological experiments is its potential for high-throughput experimentation. In **Chapter 3** we introduced the possibilities of high-throughput zebrafish experiments to support systems pharmacology model development. Systems pharmacology models require large datasets that inform on the behaviour of the (patho)physiological system upon pharmacological perturbation. These datasets should include relevant information on all intended and unintended targets and pathways. Because of constraints in both time and resources, experimental data should be gathered as efficiently as possible. This is possible with high-throughput experimentation. In contrast to conventionally used organisms for high-throughput experiments, like yeast (*Saccharomyces*

cerevisiae), round worms (*Caenorhabditis elegans*), or fruit flies (*Drosophila melanogaster*), the zebrafish is a vertebrate organism with larger anticipated translational power to higher vertebrates used in drug development, than these invertebrate species (**Figure 3.2**). In this chapter, we suggested an innovative analysis method for early drug discovery and development. Outside-in model identification is a technique that uses oscillating stimuli at different frequencies to construct a model structure between input and output without prior knowledge on the system driving the output. Using microfluidic devices specifically designed for zebrafish larvae, waterborne stimuli like drug exposure could be tested at different frequencies and observations of for example fluorescence markers from the zebrafish could subsequently be analysed by outside-in modelling. This approach, characterized by a requirement for close collaboration between experimental and computational researchers, would lead to an understanding of rate-limiting steps in the relevant (patho)physiological pathways early in drug development process.

Zebrafish larvae are transparent which is ideal for optical imaging. A microscopy set-up with high-throughput potential that takes advantage of this, is the Vertebrate Automated Screening Technology (VAST) BioImager. The VAST BioImager consists of a capillary in which zebrafish larvae are automatically loaded from a sampling tube or well plate. The capillary is located under a microscope and rotates to capture images of the larva from all angles. **Chapter 4** introduced the application of this method to zebrafish larvae with a fluorescent marker expressed in the liver. By taking multiple images from a total of 25 different angles, a three-dimensional reconstruction of the full larva and of the liver of the larva can be made. Subsequent quantification of surface area and volume of the whole organism, and the liver therein, results in much more information than two-dimensional imaging. The proof of concept in this chapter utilized only a limited number of larvae to develop the imaging architecture and reconstruction algorithm. This method could in the future be applied to quantify shape and volume of different organs during larval development, to constitute a reference database that can for example be used for physiology-based modelling. Additionally, high-throughput screening could be performed of for example impact of hepatotoxic drugs on liver volume and shape, or other application in which organ size is a measure of efficacy or toxicity. With such automated objective and quantitative measurements of drug effects over time, an exposure-response relationship of the drug can be determined, necessary for translation of drug effects to higher vertebrates.

11.2.1 Methodological innovation

- We developed an imaging method to enable high-throughput data acquisition on fluorescently labelled tissues or organs in zebrafish larvae upon pharmacological perturbation.

11.2.2 Key messages

- Internal exposure of a drug over time is essential for proper interpretation and translation of drug effects and side effects.

- Genetic homology in metabolic enzymes between zebrafish and humans suggests experiments in zebrafish to yield meaningful results regarding metabolite formation.

- Zebrafish larvae are ideal whole-vertebrate experimental subjects for high-throughput experiments in systems pharmacology.

- Close collaboration between experimental and computational scientists is important in systems pharmacology.

11.3 Quantification of internal exposure over time

The concentration of a drug at the target site drives drug effects[17]. It is therefore essential to quantify the internal exposure in zebrafish larvae after waterborne drug treatment when assessing drug effects. **Section II** focussed on the development of experimental, bioanalytical, and computational methods to quantify internal drug exposure over time and characterize the pharmacokinetic processes of absorption, distribution, metabolism, and excretion. Paracetamol was used as paradigm compound. Because of the small larval size of only several hundred nanolitres – quantified previously using the VAST BioImager[18] – and low drug amounts in the larvae, it is recognized to be challenging to measure internal drug exposure[19].

As a proof of concept, in **Chapter 5** the internal exposure over time of paracetamol and its two major metabolites was quantified in zebrafish larvae of 3 days post fertilization (dpf). Two types of experiments were performed. In the first, zebrafish larvae were exposed to a constant concentration of waterborne paracetamol for 180 minutes, while in the second the larvae were transferred to drug-free medium after 60 minutes of waterborne paracetamol treatment, to study elimination for an additional 240 minutes. A liquid chromatography-mass spectrometry (LC-MS/MS) method was developed to quantify the paradigm compound paracetamol and its major metabolites paracetamol-glucuronide and paracetamol-sulfate in homogenate samples. Steady state values of paracetamol amounts were reached within 120 minutes of waterborne treatment. In the elimination experiment, paracetamol amounts showed a mono-exponential decline, while internal amounts of its metabolites increased at first, before declining as well after 120 minutes. The major metabolite of paracetamol in the zebrafish larva at 3 dpf was paracetamol-sulfate, which was more abundant than paracetamol-glucuronide. This is in contrast to the metabolic profile of adult humans, in which paracetamol-glucuronide has been reported to be the major metabolite, accounting for 50% of the dose or more[20–22]. However, studies in human neonates and infants have shown that because of maturation of metabolic pathways, paracetamol-sulfate is more abundant than paracetamol-glucuronide[23–26]. Because zebrafish larvae have also not yet reached maturity, a similar metabolic maturation could explain the ratio between paracetamol-glucuronide and paracetamol-sulfate.

Paracetamol amounts over time from zebrafish homogenates were analysed by non-linear mixed effects modelling. The pharmacokinetic model quantified the absorption rate constant and the elimination rate constant. Distribution of paracetamol was assumed to be homogenous throughout the total larval volume. This assumption was necessary to calculate absolute clearance values from the elimination rate constant, as blood concentrations of paracetamol were lacking. Absolute clearance is of importance because it is required for the inter-species scaling of this important pharmacokinetic parameter. To assess if scaling parameters quantified in zebrafish to higher vertebrates was reliable, absolute paracetamol clearance was compared to reported values in 12 higher vertebrates from literature. This scaling is based on the established allometric theory, which states that bodyweight is a predictor of drug clearance between species[27,28]. Inter-species scaling is always based on assumptions, like those in allometric theory, but also here on paracetamol distribution, or the lack of impact of maturation or temperature on the quantification of the parameter of interest. The strength of our quantitative model-based approach, is that these assumptions can be tested and corrected, which instils confidence in our model-based interspecies translation of pharmacological parameters from zebrafish to higher vertebrates.

The zebrafish larva at 3 dpf showed a metabolic profile of paracetamol similar to neonates and infants, suggesting an impact of immaturity on metabolic clearance, and possibly on other pharmacokinetic parameters as well. Zebrafish development is rapid[29] and adulthood is reached within 3 months[30]. It is therefore of interest to study the impact of age on the pharmacokinetics of paracetamol in zebrafish larvae. In **Chapter 6**, we therefore repeated the experiments from Chapter 5 with zebrafish larvae of 4 and 5 dpf. Internal paracetamol amounts showed an increase in plateau values between 3 and 4

dpf, but not between 4 and 5 dpf. The mono-exponential decline of paracetamol amounts observed in the elimination experiment became steeper with age. However, no change in the ratio between paracetamol-glucuronide and paracetamol-sulfate was found (data not shown). It was concluded that an impact of maturation was clear on absorption and elimination. However, the maturation in both the sulfation and glucuronidation pathways were not observed to impact the metabolite ratio between these two metabolites within the three days studied here.

The data on paracetamol amounts from the two experiments in zebrafish larvae of 3, 4, and 5 dpf were combined and analysed using a pharmacokinetic model with age as covariate on absorption and elimination. The relationship between age and absorption rate was discrete, resulting in an increase of the absorption rate constant of 106% between 3 and 4 dpf. This was attributed to the opening of the gastro-intestinal (GI) tract, which completes at 4 dpf[16,31]. When the GI-tract is fully open, oral absorption, in addition to transdermal absorption, contributes to the internal exposure over time. A similar effect has been reported for the antihistamine diphenhydramine[32]. Age was related to paracetamol elimination following a power function, where the elimination rate constant increased 17.5% per dpf. This increase in elimination as a result of metabolism and excretion, might result from growth of the responsible organs, as well as from maturation of enzyme systems and/or transporters[33]. Absolute clearance was calculated as previously described and showed an increase with age and a shift towards the allometric relationship of paracetamol clearance from the 12 higher vertebrates (**Figure 6.4**). It was clear that age had an impact on the internal exposure over time, at least for our paradigm compound paracetamol. This means that a difference of a single day can influence the internal drug exposure over time and corresponding outcome measures. Because both drugs and their metabolites can be pharmacologically active, we advise to perform short-term drug treatment experiments in zebrafish larvae at 5 dpf, optimizing exposure both to the parent drug, because of increased absorption in comparison to 3 dpf, and to drug metabolites, because of increased anticipated metabolism.

The zebrafish was shown to express the metabolic enzymes responsible for oxidation and conjugation of our paradigm compound paracetamol (Chapter 2). The major metabolites paracetamol-glucuronide and paracetamol-sulfate were observed after waterborne treatment with paracetamol (Chapter 5). In **Chapter 7**, this metabolism was studied in more mechanistic and quantitative detail, using a pharmacokinetic metabolite model. The paracetamol internal exposure data at 5 dpf (Chapter 6) were combined with internal exposure data in these larvae of the paracetamol-glucuronide and paracetamol-sulfate, and amounts of parent and metabolites excreted into the treatment medium. A quantification of the pharmacokinetic processes of distribution and absolute clearance is essential for reliable inter-species extrapolation of these parameters. Quantification thereof requires blood concentrations in addition to total amounts. Although methods had been developed to sample blood from adult zebrafish[34–36], this was not yet possible for zebrafish larvae. We have therefore developed a method to draw blood samples from zebrafish larvae of 5 dpf, based on puncture of the posterior cardinal vein[37] by a needle pulled from a capillary with an original diameter of 0.75 mm. The resulting nanolitre-scale blood samples were pooled together to reach quantifiable levels. In these blood samples, both paracetamol and its major metabolites were measured. Paracetamol concentrations were only 10% of external concentrations, which was also reported elsewhere[38]. The data on blood concentrations, combined with the total paracetamol and metabolite amounts from homogenates and amounts excreted to the treatment medium, were simultaneously analysed using the metabolite model we developed. Both absolute paracetamol clearance and volume of distribution obtained with this method correlated well with those reported in higher vertebrates (**Figure 7.5**, **Figure 7.6**).

The formation, distribution, and excretion of the major metabolites of paracetamol were quantified. It was especially of interest to be able to quantify volume of the distribution for the two metabolites. Normally, assumptions on volume of distribution are needed for a metabolite model to remain mathematically identifiable without data on total metabolite amounts[26,39]. Here however, with data on

both total amounts and blood concentrations for these metabolites available, the distribution volume could be quantified by the model. Biotransformation of paracetamol to paracetamol-sulfate was found to be time-dependent. Within the studied time period, sulfation decreased to a minimum, which could be explained by depletion of the sulfate-group donor necessary for this biotransformation[40–42]. It would be interesting to extend the time period of the experiments to be able to include the production of the sulfate-group donor by the zebrafish larva[43], or measure it directly[44].

We have developed and integrated experimental, bioanalytical and computational methods to quantify internal exposure over time in zebrafish larvae after waterborne drug treatment. Model-based quantification of the pharmacokinetic processes enabled a quantitative understanding of the changes of internal exposure over time and subsequent inter-species extrapolation of drug clearance and volume of distribution. When in conventional fish studies internal exposure is of interest, the bioconcentration factor (BCF) is applied[45]. This ratio of internal to external concentration is more useful than just the external concentration, but ignores the kinetics of concentrations changing over time, and is therefore highly variable and dependent on experimental design[46]. Recently, internal exposure over time was studied in zebrafish for other molecules (metals[47–50] or microplastics[51]) or in other disciplines (environmental sciences[52,53] or toxicology[54–58]), but not analysed to the extent of the quantitative translational model-based approach of this section. It was our focus to quantitatively understand internal exposure over time and to enable translation of pharmacokinetic parameters between species, essential for the role of the zebrafish in drug development.

11.3.1 Methodological innovations

- We developed a nanoscale blood sampling method in zebrafish larvae to enable the quantification of drug concentrations in blood, in addition to drug amounts in homogenates.
- We developed LC-MS/MS methods sensitive enough for zebrafish samples of small volumes, to quantify drug and metabolites internal exposure over time.
- We developed non-linear mixed effects models to quantify distribution volume and absolute drug clearance in zebrafish larvae for the first time, essential for the translation of drug pharmacokinetics to higher vertebrates.

11.3.2 Key messages

- For the first time, the translational potential for scaling pharmacokinetics from zebrafish larvae to higher vertebrates has been substantiated.
- Short-term drug treatment experiments in zebrafish larvae are best performed at 5 dpf
- The immaturity of zebrafish larvae has implications for both pharmacokinetics, and the interpretation of drug effects and inter-species translation thereof.

11.4 Linking internal exposure to disease dynamics

A disease is not static but shows changes over time, as the result of disease progression or drug treatment[59]. It is therefore important to have repeated measures of disease dynamics and to link these to internal drug exposure to quantify the drug effect thereon, which was the focus of **Section III**. As disease model, the recently developed zebrafish model for neuroblastoma was studied. This transgenic

zebrafish line spontaneously develops a neuroblastoma tumour after three weeks, which also expresses a fluorescence marker[60]. By fluorescence microscopy tumour size could be quantified and it was reported that isotretinoin (13-cis-retinoic acid) had an effect on neuroblastoma development after 7 days of waterborne treatment[60]. In **Chapter 8**, we quantified tumour development in juvenile zebrafish by multiple measures of tumour size over the 7 days of treatment with 0, 1, 1.5, and 2 µM of waterborne isotretinoin, and linked these to quantified internal exposure of isotretinoin.

Quantification of isotretinoin proved to be challenging because it is a photo-sensitive compound[61–63]. Exposure to ultraviolet (UV) light results in isomerization of isotretinoin into 9-cis-retinoic acid and all-trans-retinoic acid. A sensitive LC-MS/MS method was developed to distinguish the isomers. Additionally, the UV-exposure was minimized by performing experiments after sunset or in laboratories without windows. This resulted in less than 10% of isomerization in the treatment medium and on average 16.4% within the (transparent) juvenile zebrafish.

It was anticipated that internal exposure would reach a plateau after waterborne treatment for a prolonged period of time, similar to that of paracetamol in the previous section. However, after start of treatment and the two treatment medium refreshments, a peak of isotretinoin amounts was followed by a 100-fold drop in internal exposure. Subsequent quantification of corresponding treatment medium samples showed a concentration lower than the nominal dose at the onset of the experiment and this external concentration also declined over the dosing intervals. Model-based analysis of both the internal exposure in the zebrafish and the external concentration simultaneously, characterized these profiles and the absorption from and excretion into the treatment medium by the juvenile zebrafish.

Every 24 hours, zebrafish were fixated to quantify tumour area by two-dimensional fluorescence microscopy. Unfortunately, no statistically significant difference was observed between the different dose groups and control, so no drug effect on the tumour size could be quantified. The lack of drug effect in our experiments could be explained by the internal exposure profile. The internal exposure of isotretinoin was because of the fast decline upon drug treatment, subtherapeutic for the majority of the dosing interval. This result underlines the importance of quantification of internal drug exposure over time, to enable reliable interpretation of observed drug effects, or lack thereof.

Another reason for the lack of a significant drug effects might be the high variability in tumour size per individual juvenile zebrafish. Because we took single measurements per individual, we could not correct for this inter-individual variability. This was in contrast to previous reports, where measurements before and after treatment within the same zebrafish were taken to quantify drug effect[60]. Tumour size measurements could be more precise when instead of its two-dimensional area, its three-dimensional surface area and volume was quantified. Optical projection tomography (OPT) is a three-dimensional microscopy set-up similar to the VAST BioImager but suitable for samples larger than a capillary, like the juvenile zebrafish[64,65]. The advantage of the transparent zebrafish, in contrast to more opaque OPT samples like murine heart tissue, is no sample clearing is necessary to reveal the fluorescent signal of the tumour[66]. A feasibility study with a representative zebrafish with fluorescent neuroblastoma was performed, which yielded promising results (**Figure 8.6**). Three-dimensionally, the tumour was better distinguishable and not partly hidden by the melanocyte-umbrella[67]. Another improvement to quantify tumour dynamics over time could be the repeated measurements of biomarkers as measure of (patho) physiological changes[68,69].

Alternatively, protein binding of isotretinoin[70] might be of influence as it prevents target binding. However, a major drug binding plasma protein, albumin, is absent in zebrafish and no other proteins of importance to drug binding were reported in plasma[71,72]. Another consideration could be the fact that the mechanism of action of isotretinoin was not fully elucidated and its isomers might be responsible for (part of) the drug effects[63,73]. In that case the observed effects from previous studies might have been

diminished as a result of our endeavours to minimize photo-isomerisation. Application of the integrative experimental and computational methods we developed here could be used to test this hypothesis of active isomers and contribute to the elucidation of the mechanism of action of isotretinoin.

11.4.1 Methodological innovation

- We developed a three-dimensional microscopy method to quantify tumour size in juvenile zebrafish more accurately and precisely in comparison to conventional two-dimensional microscopy.

11.4.2 Key messages

- The common assumption that external and internal drug concentrations are constant upon waterborne drug treatment of zebrafish should always be tested by quantitative measurements of both zebrafish and treatment medium over time.

- Pharmacokinetic and pharmacodynamic experiments, quantifying both internal drug exposure over time, and changes in disease dynamics over time upon drug exposure, should both be performed to interpret and quantify drug effects or lack thereof.

11.5 Mechanistic and quantitative translation of exposure-response from zebrafish to higher vertebrates

An exposure-response relationship, linking internal drug exposure to the disease dynamics, is the fundament of inter-species translation of drug effects. Another important element for this inter-species translation is taking into account between-species differences in disease mechanisms. The (patho) physiological processes might differ between vertebrates, for which a quantitative model-based approach can correct by utilizing translational factors. **Section IV** focussed on quantification of between-species differences in (patho)physiological processes to the benefit of mechanistic and quantitative translation of exposure-response from zebrafish to higher vertebrates. Specific focus was on tuberculosis (TB), of which the pathology and treatment has been studied extensively in the zebrafish[74–79]. Zebrafish larvae infected with the aquatic pathogen *Mycobacterium marinum*, a close relative of the human pathogen *Mycobacterium tuberculosis*, served as disease model[80].

In **Chapter 9**, the natural growth of *M. marinum* was studied and compared to that of *M. tuberculosis*. Two strains, a poikilotherm-derived strain E11[81] and a human-derived strain M^{USA} [82], were grown undisturbed for more than 200 days and viability assessed as colony forming units (CFU) was determined at different timepoints. An established TB-model, the multistate tuberculosis pharmacometric (MTP) model[83,84], was utilized to quantitatively characterize this natural growth. The MTP model distinguishes three states of mycobacteria, a fast-multiplying, a slow-multiplying, and a non-multiplying state. The natural growth of *M. tuberculosis* is characterized in this model by the quantified growth rates and transfer rates between the states. Distinction of mycobacteria in the different multiplying states is of importance, because antibiotic effects on the mycobacteria could differ depending on their growth behaviour. The MTP model was successfully applied to quantify drug treatment of *M. tuberculosis in vitro*[83,85], in mice[86,87], and in patients[88,89]. It was here applied to the natural growth data of the two strains of *M. marinum*, to be able to compare their natural growth to that of *M. tuberculosis*. The E11 strain showed a more latent growth behaviour most similar to that of *M. tuberculosis*, while M^{USA} growth was more aggressive (**Figure 9.1**). These findings were in line with previous results[81]. Because growth rates of E11 and *M. tuberculosis* were also most similar, we suggested that the use of E11 was most preferable when studying TB in zebrafish.

Quantification of the internal exposure-response relationship in the zebrafish infected with *M. marinum* as disease model for TB was the focus of **Chapter 10**, with the aim to assess how reliable a translation of the drug effect to humans would be based on such a quantitative internal exposure-response relationship. The antibiotic isoniazid, which shows largest bactericidal activity of the standard of care drugs currently used against TB in the first days of treatment[90], was chosen as paradigm compound. Zebrafish larvae were infected with E11, per the recommendation of Chapter 9, at 28 hours post fertilization. Waterborne treatment with increasing doses of isoniazid at 0.25-10x minimum inhibitory concentration (MIC) started after the infection had 2 days to establish. Internal exposure was quantified in homogenates and blood samples. Fluorescent *M. marinum* were utilized to enable repeated measurements of bacterial burden within individual larvae by non-invasive fluorescence imaging. Automated fluorescent image analysis[91,92] was applied to these images to quantify bacterial burden based on fluorescent pixel count. Simultaneous pharmacokinetic-pharmacodynamic modelling was performed on the combined data of total drug amounts in homogenates, drug concentrations in blood samples, and bacterial burden from fluorescence imaging. Internal exposure reached steady state within 12 hours, but steady state levels increased with each day post fertilization. An impact of age was quantified on the absorption of isoniazid, similar to Chapter 5. Age was also expected to impact elimination, but because the majority of data was obtained when internal amounts were at steady state when rate of absorption and rate of elimination are equal, a distinctive impact on both absorption and elimination was not mathematically identifiable based on the current data. The age effect on absorption should therefore be interpreted as a net increase with age of absorption relative to that of elimination. Blood concentration of isoniazid was only 20% of external concentrations. The bacterial burden showed exponential growth and a decrease in growth with increasing isoniazid exposure. A dose of 5x MIC in the incubation medium resulted in bacteriostasis, which was expected when taking into account the relationship between internal and external concentrations.

As proof of concept for translation, the quantitative exposure-response relationship of isoniazid was translated to humans. Isoniazid concentration over time in humans was simulated for the therapeutic dose of 300 mg, based on a previously reported pharmacokinetic model[93]. Two translational factors were included for the translation, to correct for between-species differences in disease mechanisms and pharmacological response[89]. First, the difference in sensitivity to isoniazid of *M. marinum* and *M. tuberculosis*, as reported by their respective MICs, was taken into account. Second, the difference in stage of infection was taken into account. The fresh infection in zebrafish showed growth in the logarithmic stage, while clinical infections were expected to be in the stationary stage. As described above, drug effect on mycobacteria will differ between different growth behaviour. The MTP model was previously applied to quantify isoniazid effect on *M. tuberculosis* on the different states[85]. The ratio of maximal kill rate on the different states was assumed to reflect the difference in drug effect between the logarithmic stage and stationary stage of infection. With these translational factors, the translation of the exposure-response relationship of isoniazid quantified in zebrafish, correlated reasonably with observations from literature in humans[94–96] (**Figure 10.7**). This was especially the case for the first two days of treatment, the same time period of our experiments. After two days, the isoniazid drug effect was overestimated, which corresponded to reports that the first two days of isoniazid treatment showed a more rapid decline in bacterial burden than after the first two days[90,97]. This decreased drug effect after two days was not quantifiable in the short experiment within the zebrafish larva.

Based on our results from Chapter 9 and Chapter 10, we are confident that the zebrafish is a reliable addition to the preclinical TB drug development workflow using the MTP model. The MTP model has been used previously to quantify drug effects of the current standard of care against TB *in vitro*[83,85], in mice[86,87], and in humans[88,89]. Its application to new anti-TB drugs is the next step for preclinical drug development. The zebrafish is an attractive model organism to test new drugs after *in vitro* experiments, but before mammalian studies. This will result in more information on drug candidates earlier in anti-TB drug development, and with the predictive power of this mechanistic and quantitative model-based approach, a more reliable translation of anti-TB drug effects from the zebrafish to higher vertebrates.

11.5.1 Methodological innovations

- We applied an established mechanistic TB model to characterize natural growth of *M. marinum* for the first time and quantitatively compare it to natural growth of *M. tuberculosis*.

- We developed a method to quantify individual bacterial burden over time in zebrafish larvae upon treatment, based on repeated measures by non-invasive fluorescence imaging and population modelling.

11.5.2 Key messages

- A quantitative model-based approach can translate drug effects between two species which are seemingly quite different, by utilizing a quantitative exposure-response relationship and translational factors that take into account the between-species differences.

- Antibiotic drug effects quantified in the zebrafish could be translated to humans.

11.6 Remaining challenges of the zebrafish in drug development

In the previous sections, we have developed and integrated experimental, bioanalytical, and computational methods to quantify internal drug exposure to be able to quantitatively link it to disease dynamics with the purpose to translate pharmacological findings to higher vertebrates. Quantification of internal drug exposure after waterborne treatment is a major challenge for the zebrafish in drug discovery and development, but not the only one. We discuss three other current challenges. First, the zebrafish is a lower vertebrate than mammalian experimental animals, and not all diseases relevant in higher vertebrates can be examined. Some mammalian organ systems are different (e.g. no cardiac septation) or absent (e.g. respiratory and reproductive organs)[98]. Because the zebrafish is a poikilothermic animal, for example fever cannot be studied and the lower experimental temperatures might impact growth of pathogens or tumours[98,99]. Second, experiments are preferably performed in the embryonic and larval state, when the zebrafish are small and suitable for multi well plates and high-throughput screens. The corresponding immaturity might impact the translation of pharmacological findings[100], as we have also seen in Chapter 6. Another caveat in this respect is the lack of adaptive immune system in embryos and larvae, which only develops after four weeks[99,101]. Third, experiments in zebrafish remain to be standardized and validated[102]. Zebrafish husbandry differs between laboratories[103–109] and treatment conditions like light, temperature, and water composition vary and are often not (completely) reported[110]. Standardized experiments subsequently must be validated with known positive and negative compounds from experiments in higher vertebrates[98,111].

11.7 Future perspectives

In this thesis, we have developed and integrated experimental, bioanalytical, and computational methods for the zebrafish to live up to its potential in early drug discovery and development. Many more opportunities and promising techniques will become available in the near future to answer pharmacological questions and to improve translation from this model organism to higher vertebrates, including humans.

One of the largest advantages of the zebrafish for pharmacological experiments is its versatility and almost endless experimental possibilities. An important example is the role the zebrafish can play in unravelling the importance of the microbiome in pharmacology. The microbiome is expected to impact

health and disease, and to modulate pharmacokinetics and pharmacodynamics[112]. It is difficult to study the microbiome in mammals, as an intervention of the gut-bacteria requires sterilisation and re-colonisation[113]. Because of the zebrafish' external fertilization and the assumption that the zygote is sterile, zebrafish eggs can be sterilized much easier, and colonization of sterile embryos and larvae can simply be done via the medium[114,115]. We have performed a pilot experiment similar to those in Section II in sterile zebrafish to ensure observed metabolites were not the result of bacteria in the gut of the zebrafish. This can be expanded to quantify the impact of the microbiome on pharmacokinetics and on the pharmacokinetic-pharmacodynamic relationship of drugs.

The experimental toolbox in zebrafish will be further expanded. Methods for oral dosing have been developed for adult zebrafish to overcome both translational and drug delivery challenges, for example to treat zebrafish with drugs that are insoluble in water, drugs that are not absorbed from waterborne treatment, or drugs that adhere to the skin of the zebrafish[116,117]. A similar method for oral dosing in zebrafish larvae based on three-dimensional microprinting a syringe gavage tip is currently under development. Another promising addition to the experimental toolbox is the use of microfluidic devices specifically designed to house and position zebrafish larvae[118–121]. The larvae can then be treated with different drug concentrations or frequencies, by changing the flow rate of the treatment medium and washing medium. Integration of these experimental techniques with automated fluorescence imaging (Chapter 4) will result in a high-throughput workflow with many possibilities for measurement of drug effects. This is further improved by the use of robotic injections. Automated robotic injection at a speed of 2,000 injected embryos per hour has been developed[15,78,122] and deep learning has increased efficiency of injections[123]. Currently, a method is under development using the same set-up to automate blood sampling, which will increase throughput of quantification of internal exposure substantially.

One inherent challenge of the zebrafish larva is its small size and subsequent low drug amounts in samples for bioanalytical quantification. Sensitive LC-MS/MS methods have been developed here to quantify drug and metabolites amounts and concentrations in samples which consisted of pooled homogenates or blood samples. Detection limits for drug and metabolites are decreasing to femtomolar levels[124], which would allow measurements of drugs and metabolites amounts or concentrations in individual larvae. Blood samples currently need to be pooled to reach detectable levels, but novel methods are available to measure drug concentrations in single blood samples. One example is backloading the needle with ionization solution and subsequent direct injection into the MS, using nano-electrospray ionization mass spectrometry for improved throughput and efficiency[125]. It has already been applied to quantify drug concentrations in individual cancer cells[126]. Accurate and precise quantification of drug concentrations in blood samples is essential to quantify internal drug exposure, which linked to measurements of the disease dynamics, yields an exposure-response relationship. Reliable quantification of the internal exposure, and exposure-response, are essential for inter-species translation of drug effects. When MS techniques become sensitive enough, minimal blood sample volumes that are required for quantification of drug concentrations will decrease. As a result, repeated blood samples could be drawn from individual larva at different timepoints, enabling the distinction between biological and experimental variability in blood concentrations and reducing noise within the concentration-time data.

The use of zebrafish in early drug discovery and development should always be seen within the context of translating pharmacological findings towards the clinic. The best example of this thus far is the prostaglandin E2 derivative ProHema (16,16-dimethyl-prostaglandin E2), discovered in a phenotypic screen in zebrafish on haematopoietic stem cell formation[127]. It is now in Phase II clinical trials as part of new treatment for graft-versus-host disease in patients receiving allogeneic hematopoietic cell transplantation[128]. Another example is the otoprotective portfolio of urea-thiophene carboxamides[129]. These compounds are the result from a phenotypic screen aimed to find compounds protective of aminoglycoside-induced hearing loss[130]. Zebrafish larvae expressing fluorescent hair cells were used in that screen to mimic loss of hair cells responsible for hearing in humans. The lead compound is currently

in Phase I clinical trials[131]. Similar to these examples, 4 more compounds discovered in zebrafish are in clinical trials and 4 more underway[128]. We envision these are just the first of many drugs reaching clinical development, that were discovered in pharmacological experiments with zebrafish.

11.8 Conclusions

The zebrafish is a promising vertebrate model organism in early drug discovery and development. Translation of pharmacological findings to higher vertebrates requires quantification of the underlying pharmacological and (patho)physiological processes. In this thesis, we therefore developed and integrated innovative experimental and computational methods for the successful quantification of 1) the internal exposure over time after waterborne drug treatment, 2) disease dynamics and drug-induced changes therein, and 3) between-species differences in disease mechanisms. The state-of-the-art methods that we developed included nanoscale blood sampling, sensitive LC-MS/MS methods for drugs and their isomers and metabolites, and three-dimensional microscopy, integrated with non-linear mixed effects modelling to quantify the pharmacological processes in this small vertebrate. This multidisciplinarity enabled quantification of internal drug exposure-response relationships, contributed to positioning the zebrafish in the preclinical drug development pipeline, and inspired continuous collaborations between experimental and computational scientists.

11.9 References

1. Breimer DD, Danhof M. Relevance of the application of pharmacokinetic-pharmacodynamic modelling concepts in drug development - the wooden shoe paradigm. Clin Pharmacokinet. 1997;32(4):259-267.
2. Huang Q, Riviere JE. The application of allometric scaling principles to predict pharmacokinetic parameters across species. Expert Opin Drug Metab Toxicol. 2014;10(9):1241-1253.
3. Mager DE, Woo S, Jusko WJ. Scaling pharmacodynamics from in vitro and preclinical animal studies to humans. Drug Metab Pharmacokinet. 2009;24(1):16-24.
4. Van der Graaf PH, Benson N. Systems pharmacology: Bridging systems biology and pharmacokinetics-pharmacodynamics (PKPD) in drug discovery and development. Pharm Res. 2011;28:1460-1464.
5. Danhof M, Klein K, Stolk P, et al. The future of drug development: The paradigm shift towards systems therapeutics. Drug Discov Today. 2018;23(12):1990-1995.
6. Bradshaw EL, Spilker ME, Zang R, et al. Applications of quantitative systems pharmacology in model-informed drug discovery: Perspective on impact and opportunities. CPT Pharmacometrics Syst Pharmacol. September 2019.
7. Nijsen MJ, Wu F, Bansal L, et al. Preclinical QSP modeling in the pharmaceutical industry: An IQ consortium survey examining the current landscape. CPT Pharmacometrics Syst Pharmacol. 2018:Accepted article.
8. Esch EW, Bahinski A, Huh D. Organs-on-chips at the frontiers of drug discovery. Nat Rev Drug Discov. 2015;14(4):248-260.
9. Ehrlich A, Duche D, Ouedraogo G, et al. Challenges and opportunities in the design of liver-on-chip microdevices. Annu Rev Biomed Eng. 2019;21(1):219-239.
10. Cyr KJ, Avaldi OM, Wikswo JP. Circadian hormone control in a human-on-a-chip: In vitro biology's ignored component? Exp Biol Med. 2017;242(17):1714-1731.
11. Peterson RT, Fishman MC. Designing zebrafish chemical screens. Vol 105. 3rd ed. Elsevier Inc.; 2011.
12. Howe K, Clark MD, Torroja CF, et al. The zebrafish reference genome sequence and its relationship to the human genome. Nature. 2013;496:498-503.
13. Howe DG, Bradford YM, Eagle A, et al. The zebrafish model organism database: New support for human disease models, mutation details, gene expression phenotypes and searching. Nucleic Acids Res. 2017;45(D1):D758-D768.

14. Cho A, Haruyama N, Kulkarni AB. Generation of transgenic mice. In: Curr Protoc Cell Biol. ; 2009.
15. Spaink HP, Cui C, Wiweger MI, et al. Robotic injection of zebrafish embryos for high-throughput screening in disease models. Methods. 2013;62(3):246-254.
16. Strähle U, Scholz S, Geisler R, et al. Zebrafish embryos as an alternative to animal experiments — A commentary on the definition of the onset of protected life stages in animal welfare regulations. Reprod Toxicol. 2012;33:128-132.
17. Morgan P, Van der Graaf PH, Arrowsmith J, et al. Can the flow of medicines be improved? Fundamental pharmacokinetic and pharmacological principles toward improving Phase II survival. Drug Discov Today. 2012;17(9/10):419-424.
18. Guo Y, Veneman WJ, Spaink HP, et al. Three-dimensional reconstruction and measurements of zebrafish larvae from high-throughput axial-view in vivo imaging. Biomed Opt Express. 2017;8(5):2611-2634.
19. Diekmann H, Hill A. ADMETox in zebrafish. Drug Discov Today Dis Model. 2013;10(1):e31-e35.
20. Critchley JAJH, Critchley LAH, Anderson PJ, et al. Differences in the single-oral-dose pharmacokinetics and urinary excretion of paracetamol and its conjugates between Hong Kong Chinese and Caucasian subjects. J Clin Pharm Ther. 2005;30:179-184.
21. Zhao L, Pickering G. Paracetamol metabolism and related genetic differences. Drug Metab Rev. 2011;43(1):41-52.
22. Clements JA, Critchley JAJH, Prescotf LF. The role of sulphate conjugation in the metabolism and disposition of oral and intravenous paracetamol in man. Br J Clin Pharmacol. 1984;18:481-485.
23. Allegaert K, De Hoon J, Verbesselt R, et al. Intra- and interindividual variability of glucuronidation of paracetamol during repeated administration of propacetamol in neonates. Acta Paediatr. 2005;94(9):1273-1279.
24. Krekels EHJ, Van Ham S, Allegaert K, et al. Developmental changes rather than repeated administration drive paracetamol glucuronidation in neonates and infants. Eur J Clin Pharmacol. 2015;71:1075-1082.
25. Van Lingen RA, Deinum JT, Quak JME, et al. Pharmacokinetics and metabolism of rectally administered paracetamol in preterm neonates. Arch Dis Child Fetal Neonatal Ed. 1999;80(1):F59-F63.
26. Van der Marel CD, Anderson BJ, Van Lingen RA, et al. Paracetamol and metabolite pharmacokinetics in infants. Eur J Clin Pharmacol. 2003;59(3):243-251.
27. Mahmood I. Application of allometric principles for the prediction of pharmacokinetics in human and veterinary drug development. Adv Drug Deliv Rev. 2007;59:1177-1192.
28. Mahmood I. Theoretical versus empirical allometry: Facts behind theories and application to pharmacokinetics. J Pharm Sci. 2010;99(7):2927-2933.
29. Kimmel CB, Ballard WW, Kimmel SR, et al. Stages of embryonic development of the zebrafish. Dev Dyn. 1995;203:253-310.
30. Lee KY, Jang GH, Byun CH, et al. Zebrafish models for functional and toxicological screening of nanoscale drug delivery systems: Promoting preclinical applications. Biosci Rep. 2017;37(3):BSR20170199.
31. Ng ANY, De Jong-Curtain TA, Mawdsley DJ, et al. Formation of the digestive system in zebrafish: III. Intestinal epithelium morphogenesis. Dev Biol. 2005;286(1):114-135.
32. Kristofco LA, Haddad SP, Chambliss CK, et al. Differential uptake of and sensitivity to diphenhydramine in embryonic and larval zebrafish. Environ Toxicol Chem. 2017;37(4):1175-1181.
33. Tao T, Peng J. Liver development in zebrafish (Danio rerio). J Genet Genomics. 2009;36:325-334.
34. Pedroso G, Hammes T, Escobar T, et al. Blood collection for biochemical analysis in adult zebrafish. J Vis Exp. 2012;63:e3865.
35. Eames SC, Philipson LH, Prince VE, et al. Blood sugar measurement in zebrafish reveals dynamics of glucose homeostasis. Zebrafish. 2010;7(2):205-213.
36. Vliegenthart AD, Lewis PS, Tucker CS, et al. Retro-orbital blood acquisition facilitates circulating microRNA measurement in zebrafish. Zebrafish. 2014;11(3):219-226.
37. Isogai S, Horiguchi M, Weinstein BM. The vascular anatomy of the developing zebrafish: An atlas of embryonic and early larval development. Dev Biol. 2001;230(2):278-301.

38. Mourabit S, Fitzgerald JA, Ellis RP, et al. New insights into organ-specific oxidative stress mechanisms using a novel biosensor zebrafish. Environ Int. 2019;133(May):105138.
39. Van Rongen A, Välitalo PAJ, Peeters MY, et al. Morbidly obese patients exhibit increased CYP2E1-mediated oxidation of acetaminophen. Clin Pharmacokinet. 2016;55:833-847.
40. Slattery JT, Wilson JM, Kalhorn TF, et al. Dose-dependent pharmacokinetics of acetaminophen: Evidence of glutathione depletion in humans. Clin Pharmacol Ther. 1987;41(4):413-418.
41. Liu L, Klaassen CD. Different mechanism of saturation of acetaminophen sulfate conjugation in mice and rats. Toxicol Appl Pharmacol. 1996;139(1):128-134.
42. Reddyhoff D, Ward J, Williams D, et al. Timescale analysis of a mathematical model of acetaminophen metabolism and toxicity. J Theor Biol. 2015;386:132-146.
43. Van den Boom J, Heider D, Martin SR, et al. 3′-Phosphoadenosine 5′-phosphosulfate (PAPS) synthases, naturally fragile enzymes specifically stabilized by nucleotide binding. J Biol Chem. 2012;287(21):17645-17655.
44. Xu J, Chen Y, Li L, et al. An improved HPLC method for the quantitation of 3′-phosphoadenosine 5′-phosphate (PAP) to assay sulfotransferase enzyme activity in HepG2 cells. J Pharm Biomed Anal. 2012;62:182-186.
45. Miller TH, Gallidabino MD, MacRae JR, et al. Prediction of bioconcentration factors in fish and invertebrates using machine learning. Sci Total Environ. 2019;648:80-89.
46. Wassenaar PNH, Verbruggen EMJ, Cieraad E, et al. Variability in fish bioconcentration factors: Influences of study design and consequences for regulation. Chemosphere. 2020;239:124731.
47. Gao Y, Zhang Y, Feng J, et al. Toxicokinetic-toxicodynamic modeling of cadmium and lead toxicity to larvae and adult zebrafish. Environ Pollut. 2019;251:221-229.
48. Gao Y, Kang L, Zhang Y, et al. Toxicokinetic and toxicodynamic (TK-TD) modeling to study oxidative stress-dependent toxicity of heavy metals in zebrafish. Chemosphere. 2019;220:774-782.
49. Simon O, Gagnaire B, Camilleri V, et al. Toxicokinetic and toxicodynamic of depleted uranium in the zebrafish, Danio rerio. Aquat Toxicol. 2017.
50. Hu S, Han J, Yang L, et al. Impact of co-exposure to titanium dioxide nanoparticles and Pb on zebrafish embryos. Chemosphere. 2019;233:579-589.
51. Qiao R, Lu K, Deng Y, et al. Combined effects of polystyrene microplastics and natural organic matter on the accumulation and toxicity of copper in zebrafish. Sci Total Environ. 2019;682:128-137.
52. Li Y, Wang H, Xia X, et al. Dissolved organic matter affects both bioconcentration kinetics and steady-state concentrations of polycyclic aromatic hydrocarbons in zebrafish (Danio rerio). Sci Total Environ. 2018;639:648-656.
53. Damalas DE, Bletsou AA, Agalou A, et al. Assessment of the acute toxicity, uptake and biotransformation potential of benzotriazoles in zebrafish (Danio rerio) larvae combining HILIC- with RPLC-HRMS for high-throughput identification. Environ Sci Technol. 2018;52:6023-6031.
54. Kirla KT, Groh KJ, Steuer AE, et al. Zebrafish larvae are insensitive to stimulation by cocaine: importance of exposure route and toxicokinetics. Toxicol Sci. 2016;154(1):183-193.
55. Wu Y, Deng M, Jin Y, et al. Uptake and elimination of emerging polyfluoroalkyl substance F-53B in zebrafish larvae: Response of oxidative stress biomarkers. Chemosphere. 2019;215(182-188).
56. Kühnert A, Vogs C, Aulhorn S, et al. Biotransformation in the zebrafish embryo –temporal gene transcription changes of cytochrome P450 enzymes and internal exposure dynamics of the AhR binding xenobiotic benz[a]anthracene. Environ Pollut. 2017;230:1-11.
57. Brox S, Seiwert B, Küster E, et al. Toxicokinetics of polar chemicals in zebrafish embryo (Danio rerio): Influence of physicochemical properties and of biological processes. Environ Sci Technol. 2016;50(18):10264-10272.
58. Cui J, Wang F, Gao J, et al. Bioaccumulation and metabolism of carbosulfan in zebrafish Danio rerio and toxic effects with its metabolites. J Agric Food Chem. October 2019:(accepted).
59. Post TM, Freijer JI, DeJongh J, et al. Disease system analysis: Basic disease progression models in degenerative disease. Pharm Res. 2005;22(7):1038-1049.

60. He S, Mansour MR, Zimmerman MW, et al. Synergy between loss of NF1 and overexpression of MYCN in neuroblastoma is mediated by the GAP-related domain. eLife. 2016;5:e14713.
61. Veal GJ, Errington J, Redfern CPF, et al. Influence of isomerisation on the growth inhibitory effects and cellular activity of 13-cis and all-trans retinoic acid in neuroblastoma cells. Biochem Pharmacol. 2002;63(2):207-215.
62. Nathan Bushue, Wan Y-JY. Retinoid pathway and cancer therapeutics. Adv Drug Deliv Rev. 2010;62(13):1285-1298.
63. Armstrong JL, Redfern CPF, Veal GJ. 13-cis Retinoic acid and isomerisation in paediatric oncology - is changing shape the key to success? Biochem Pharmacol. 2005;69(9):1299-1306.
64. Tang X, Van der Zwaan DM, Zammit A, et al. Fast post-processing pipeline for optical projection tomography. IEEE Trans Nanobioscience. 2017;16(5):367-374.
65. Lindsey BW, Kaslin J. Optical projection tomography as a novel method to visualize and quantitate whole-brain patterns of cell proliferation in the adult zebrafish brain. Zebrafish. 2017;epub.
66. Kolesová H, Čapek M, Radochová B, et al. Comparison of different tissue clearing methods and 3D imaging techniques for visualization of GFP-expressing mouse embryos and embryonic hearts. Histochem Cell Biol. 2016;146(2):141-152.
67. Kapp FG, Perlin JR, Hagedorn EJ, et al. Protection from UV light is an evolutionarily conserved feature of the haematopoietic niche. Nature. 2018;558(7710):445-448.
68. Danhof M, Alvan G, Dahl SG, et al. Mechanism-based pharmacokinetic-pharmacodynamic modeling — A new classification of biomarkers. Pharm Res. 2005;22(9):1432-1437.
69. Trigg RM, Shaw JA, Turner SD. Opportunities and challenges of circulating biomarkers in neuroblastoma. Open Biol. 2019;9(5).
70. US Food and Drug Administration. Isotretinoin drug label. 2019.
71. Noël ES, Arain Z, Ober EA. Analysis of the Albumin / a -Fetoprotein / Afamin / Group specific component gene family in the context of zebrafish liver differentiation. Gene Expr Patterns. 2010;10:237-243.
72. Li C, Tan XF, Lim TK, et al. Comprehensive and quantitative proteomic analyses of zebrafish plasma reveals conserved protein profiles between genders and between zebrafish and human. Sci Rep. 2016;6(March):1-15.
73. Sonawane P, Cho HE, Tagde A, et al. Metabolic characteristics of 13-cis-retinoic acid (isotretinoin) and anti-tumour activity of the 13-cis-retinoic acid metabolite 4-oxo-13-cis-retinoic acid in neuroblastoma. Br J Pharmacol. 2014;171(23):5330-5344.
74. Meijer AH, Spaink HP. Host-pathogen interactions made transparent with the zebrafish model. Curr Drug Targets. 2011;12(7):1000-1017.
75. Meijer AH. Protection and pathology in TB: Learning from the zebrafish model. Semin Immunopathol. 2016;38:261-273.
76. Tobin DM, May RC, Wheeler RT. Zebrafish: A see-through host and a fluorescent toolbox to probe host–pathogen interaction. PLoS Pathog. 2012;8(1):e1002349.
77. Myllymäki H, Bäuerlein CA, Rämet M. The zebrafish breathes new life into the study of tuberculosis. Front Immunol. 2016;7(MAY):196.
78. Carvalho R, De Sonneville J, Stockhammer OW, et al. A high-throughput screen for tuberculosis progression. PLoS One. 2011;6(2):1-8.
79. Ordas A, Raterink R-J, Cunningham F, et al. Testing tuberculosis drug efficacy in a zebrafish high-throughput translational medicine screen. Antimicrob Agents Chemother. 2015;59(2):753-762.
80. Stinear TP, Seemann T, Harrison PF, et al. Insights from the complete genome sequence of Mycobacterium marinum on the evolution of Mycobacterium tuberculosis. Genome Res. 2008;18(5):729-741.
81. Van der Sar AM, Abdallah AM, Sparrius M, et al. Mycobacterium marinum strains can be divided into two distinct types based on genetic diversity and virulence. Infect Immun. 2004;72(11):6306-6312.
82. Abdallah AM, Verboom T, Hannes F, et al. A specific secretion system mediates PPE41 transport in

pathogenic mycobacteria. Mol Microbiol. 2006;62(3):667-679.
83. Clewe O, Aulin L, Hu Y, et al. A multistate tuberculosis pharmacometric model: A framework for studying anti-tubercular drug effects in vitro. J Antimicrob Chemother. 2016;71(4):964-974.
84. Gupta N, Bitton D, Simonsson USH, et al. Transforming translation through quantitative pharmacology for high-impact decision-making in drug discovery and development. CPT Pharmacometrics Syst Pharmacol. 2019:(accepted).
85. Clewe O, Wicha SG, de Vogel CP, et al. A model-informed preclinical approach for prediction of clinical pharmacodynamic interactions of anti-TB drug combinations. J Antimicrob Chemother. 2018;73(2):437-447.
86. Chen C, Ortega F, Rullas J, et al. The multistate tuberculosis pharmacometric model: A semi-mechanistic pharmacokinetic-pharmacodynamic model for studying drug effects in an acute tuberculosis mouse model. J Pharmacokinet Pharmacodyn. 2017;44(2):133-141.
87. Chen C, Wicha SG, De Knegt GJ, et al. Assessing pharmacodynamic interactions in mice using the multistate tuberculosis pharmacometric and general pharmacodynamic interaction models. CPT Pharmacometrics Syst Pharmacol. 2017;6(11):787-797.
88. Svensson RJ, Simonsson USH. Application of the multistate tuberculosis pharmacometric model in patients with rifampicin-treated pulmonary tuberculosis. CPT Pharmacometrics Syst Pharmacol. 2016;5(5):264-273.
89. Wicha SG, Clewe O, Svensson RJ, et al. Forecasting clinical dose-response from preclinical studies in tuberculosis research: Translational predictions with rifampicin. Clin Pharmacol Ther. 2018;104(6):1208-1218.
90. Jindani A, Aber VR, Edwards EA, et al. The early bactericidal activity of drugs in patients with pulmonary tuberculosis. Am Rev Respir Dis. 1980;121(6):939-949.
91. Stoop EJM, Schipper T, Rosendahl Huber SK, et al. Zebrafish embryo screen for mycobacterial genes involved in the initiation of granuloma formation reveals a newly identified ESX-1 component. Dis Model Mech. 2011;4(4):526-536.
92. Nezhinsky A, Verbeek FJ. Pattern recognition for high throughput zebrafish imaging using genetic algorithm optimization. In: Dijkstra T, Tsivtsivadze E, Heskes T, Marchiori E, eds. Lecture Notes in Bioinformatics 6282. Berlin- Heidelberg: Springer-Verlag; 2010:301-312.
93. Wilkins JJ, Langdon G, McIlleron H, et al. Variability in the population pharmacokinetics of isoniazid in South African tuberculosis patients. Br J Clin Pharmacol. 2011;72(1):51-62.
94. Li L, Mahan CS, Palaci M, et al. Sputum Mycobacterium tuberculosis mRNA as a marker of bacteriologic clearance in response to antituberculosis therapy. J Clin Microbiol. 2010;48(1):46-51.
95. Johnson JL, Hadad DJ, Boom WH, et al. Early and extended early bactericidal activity of levofloxacin, gatifloxacin and moxifloxacin in pulmonary tuberculosis. Int J Tuberc Lung Dis. 2006;10(6):605-612.
96. Hafner R, Cohn JA, Wright DJ, et al. Early bactericidal activity of isoniazid in pulmonary tuberculosis: Optimization of methodology. Am J Respir Crit Care Med. 1997;156(3 I):918-923.
97. Jindani A, Doré CJ, Mitchison DA. Bactericidal and sterilizing activities of antituberculosis drugs during the first 14 days. Am J Respir Crit Care Med. 2003;167(10):1348-1354.
98. Ali S, Champagne DL, Spaink HP, et al. Zebrafish embryos and larvae: A new generation of disease models and drug screens. Birth Defect Res (Part C). 2011;93:115-133.
99. Kirchberger S, Sturtzel C, Pascoal S, et al. Quo natas, Danio?- Recent progress in modeling cancer in zebrafish. Front Oncol. 2017;7(August):186.
100. Rennekamp AJ, Peterson RT. 15 years of zebrafish chemical screening. Curr Opin Chem Biol. 2015;24:58-70.
101. Letrado P, De Miguel I, Lamberto I, et al. Zebrafish: Speeding up the cancer drug discovery process. Cancer Res. 2018;78(21):6048-6058.
102. MacRae CA, Peterson RT. Zebrafish as tools for drug discovery. Nat Rev Drug Discov. 2015;14(10):721-731.
103. Lawrence C, Eisen JS, Varga ZM. Husbandry and health program survey synopsis. Zebrafish. 2016;13:S5-S7.

104. Liu L, Pan L, Li K, et al. Zebrafish health conditions in the china zebrafish resource center and 20 major chinese zebrafish laboratories. Zebrafish. 2016;13:S8-S18.
105. Geisler R, Borel N, Ferg M, et al. Maintenance of zebrafish lines at the European zebrafish resource center. 2016;13:19-24.
106. You MS, Jiang YJ, Yuh CH, et al. A sketch of the Taiwan zebrafish core facility. Zebrafish. 2016;13:S24-S29.
107. Murray KN, Varga ZM, Kent ML. Biosecurity and health monitoring at the zebrafish international resource center. Zebrafish. 2016;13:S30-S38.
108. Barton CL, Johnson EW, Tanguay RL. Facility design and health management program at the Sinnhuber aquatic research laboratory. Zebrafish. 2016;13:S39-S43.
109. Leveque RE, Clark KJ, Ekker SC. Mayo clinic zebrafish facility overview. Zebrafish. 2016;13:S44-S46.
110. Rihel J, Ghosh M. Zebrafish. In: Hock FJ, ed. Drug discovery and evaluation: Pharmacological assay. 4th ed. Springer International Publishing Switzerland; 2016:4071-4155.
111. Cassar S, Adatto I, Freeman JL, et al. Use of zebrafish in drug discovery toxicology. Chem Res Toxicol. 2019.
112. Gurwitz D. The gut microbiome: Insights for personalized medicine. Drug Dev Res. 2013;74:341-343.
113. Zimmermann M, Zimmermann-Kogadeeva M, Wegmann R, et al. Separating host and microbiome contributions to drug pharmacokinetics and toxicity. Science. 2019;363(6427).
114. Pham L, Kanther M, Semova I, et al. Methods for generating and colonizing gnotobotioc zebrafish. Nat Protoc. 2008;3(12):1862-1875.
115. Melancon E, Gomez De La Torre Canny S, Sichel S, et al. Best practices for germ-free derivation and gnotobiotic zebrafish husbandry. Vol 138. Elsevier Ltd; 2017.
116. Kulkarni P, Chaudhari GH, Sripuram V, et al. Oral dosing in adult zebrafish: Proof-of-concept using pharmacokinetics and pharmacological evaluation of carbamazepine. Pharmacol Reports. 2014;66(1):179-183.
117. Zang L, Morikane D, Shimada Y, et al. A novel protocol for the oral administration of test chemicals to adult zebrafish. Zebrafish. 2011;8(4):203-210.
118. Yang F, Gao C, Wang P, et al. Fish-on-a-chip: microfluidics for zebrafish research. Lab Chip. 2016;16(7):1106-1125.
119. Zhu F, Skommer J, Huang Y, et al. Fishing on chips: Up-and-coming technological advances in analysis of zebrafish and Xenopus embryos. Cytom Part A. 2014;85(11):921-932.
120. Akagi J, Hall CJ, Crosier KE, et al. OpenSource Lab-on-a-Chip physiometer for accelerated zebrafish embryo biotests. Curr Protoc Cytom. 2014;(SUPPL.67):1-16.
121. Nady A, Peimani AR, Zoidl G, et al. a microfluidic device for head immobilization, chemical exposure, and behavioral screening of zebrafish larvae. 20th Int Conf Miniaturized Syst Chem Life Sci. 2016;(C):475-476.
122. Veneman WJ, Marín-Juez R, De Sonneville J, et al. Establishment and optimization of a high throughput setup to study Staphylococcus epidermidis and Mycobacterium marinum infection as a model for drug discovery. J Vis Exp. 2014;88:e51649.
123. Cordero-Maldonado ML, Perathoner S, Van der Kolk KJ, et al. Deep learning image recognition enables efficient genome editing in zebrafish by automated injections. PLoS One. 2019;14(1):e0202377.
124. Burhenne J, Halama B, Maurer M, et al. Quantification of femtomolar concentrations of the CYP3A substrate midazolam and its main metabolite 1′-hydroxymidazolam in human plasma using ultra performance liquid chromatography coupled to tandem mass spectrometry. Anal Bioanal Chem. 2012;402(7):2439-2450.
125. Fujii T, Matsuda S, Tejedor ML, et al. Direct metabolomics for plant cells by live single-cell mass spectrometry. Nat Protoc. 2015;10(9):1445-1456.
126. Ali A, Abouleila Y, Shimizu Y, et al. Single-cell screening of tamoxifen abundance and effect using mass spectrometry and raman-spectroscopy. Anal Chem. 2019;91:2710-2718.
127. North TE, Goessling W, Walkley CR, et al. Prostaglandin E2 regulates vertebrate haematopoietic

stem cell homeostasis. Nature. 2007;447(7147):1007-1011.
128. Cully M. Zebrafish earn their drug discovery stripes. Nat Rev Drug Discov. 2019.
129. Chowdhury S, Owens KN, Herr RJ, et al. Phenotypic optimization of urea-thiophene carboxamides to yield potent, well tolerated, and orally active protective agents against aminoglycoside-induced hearing loss. J Med Chem. 2018;61(1):84-97.
130. Owens KN, Santos F, Roberts B, et al. Identification of genetic and chemical modulators of zebrafish mechanosensory hair cell death. PLoS Genet. 2008;4(2):e1000020.
131. Kitcher SR, Kirkwood NK, Camci ED, et al. ORC-13661 protects sensory hair cells from aminoglycoside and cisplatin ototoxicity. JCI Insight. 2019;4(15):e126764.

Hoofdstuk 12

Nederlandse samenvatting

12.1 De zebravis in systeemfarmacologie

De ontwikkeling van nieuwe effectieve en veilige medicijnen is één van de meest uitdagende ondernemingen in biomedisch onderzoek. Het vereist onderzoek op alle biomedische niveaus (van moleculair en (sub)cellulair tot het gehele organisme) en met verschillende diersoorten, voor een medicijn de klinische fase bereikt. Het juiste doelwit, de juiste stof en de juiste dosis voor de behandeling van een ziekte worden geselecteerd op basis van reeds vergaarde kennis en nieuwe experimentele resultaten. Hiervoor is betrouwbare vertaling tussen verschillende experimentele contexten en diersoorten essentieel. Kwantitatieve farmacologie stuurt die vertaling in de juiste richting[1]. Farmacokinetische parameters – absorptiesnelheidsconstante, verdelingsvolume en klaring – beschrijven de relatie tussen dosis en blootstelling over tijd en kunnen vertaald of geschaald worden tussen diersoorten[2]. Hetzelfde geldt voor farmacodynamische parameters die de relatie tussen blootstelling en responsie beschrijven, zoals snelheidsconstanten, medicijnpotentie (EC_{50}) of maximaal bereikbaar effect (E_{max})[3]. Hoe mechanistischer een kwantitatief farmacologisch model is, hoe betrouwbaarder de vertaling naar verwachting is. Integratie van kwantitatieve farmacologie met de mechanistische discipline van systeembiologie – gedefinieerd als systeemfarmacologie – wekt daarom meer vertrouwen in de vertaling van de relatie tussen blootstelling en responsie[4]. Systeemfarmacologie is onderdeel van het nieuwe systeemtherapie-paradigma, dat alle relevante actoren in een (patho)fysiologisch systeem beschouwt in plaats van een afzonderlijke interactie tussen medicijn en doelwit[5].

Systeemfarmacologie heeft de potentie om de standaard te worden in medicijnontwikkeling als het gaat om het beantwoorden van mechanistische vragen over ziekte en farmacologie[6]. Het leunt sterk op preklinische data om (patho)fysiologische processen te identificeren en te karakteriseren. Er is echter een beperkte hoeveelheid experimentele data toegespitst op systeemfarmacologie en dat beperkt mogelijk de succesvolle implementatie daarvan[7]. In het bijzonder zijn data over de volledige biologische context beperkt beschikbaar, in vergelijking met data uit geïsoleerde in-vitro-experimenten. Bovendien hebben experimenten met hoge doorvoercapaciteit (*high-throughput*) de voorkeur vanwege beperkte middelen en tijd. Het is onwaarschijnlijk dat de benodigde hoeveelheid van dit type data verzameld kan worden in de klinische praktijk of zelfs in preklinische experimenten met zoogdieren. Conventionele in-vitro-experimenten kunnen op deze schaal en deze snelheid uitgevoegd worden, maar leveren beperkte informatie over de biologische context. Innovatieve orgaan-op-een-chipsystemen, bestaande uit humane celculturen groeiend bij fysiologische omstandigheden op microfluïdische apparaten om levende en functionerende orgaanweefsels te bestuderen[8,9], zijn wat dat betreft een verbetering. Hierin is een aantal zaken nog niet meegenomen, zoals medicijndoelwitten in verschillende weefsels, effecten door binding aan andere moleculen dan het doelwit met bijvoorbeeld bijwerkingen tot gevolg, of fysiologische signalering tussen weefsels[10]. Experimenten op in-vitroschaal en doorvoercapaciteit, maar binnen de juiste biologische context zijn daarom nodig.

De zebravis (*Danio rerio*) is een gevestigd gewerveld modelorganisme in biomedisch onderzoek geworden[11]. In het bijzonder worden de larven vaak gebruikt, vanwege hun vele voordelen zoals optische transparantie voor niet-invasieve observatie van cellen, weefsels of organen. Van alle humane genen heeft 71% een ortholoog in de zebravis, van alle humane genen betrokken bij ziektes is dit zelfs 82%[12]. Ter vergelijking: de muis als conventioneel preklinisch zoogdier heeft een ortholoog voor 83% van alle humane genen[12]. Muisexperimenten, inclusief de ontwikkeling van ziektemodellen hierin, zijn echter langer en duurder dan zebravisexperimenten. Genetische modificatie om ziektemodellen te maken is bij zebravissen eenvoudiger dan bij hogere gewervelden, vanwege de buitenlichamelijke bevruchting[13]. Om hetzelfde in muizen te doen is genetische modificatie van muizenembryo's nodig, waarna de embryo's worden teruggeplaatst in een draagmoeder tot ze voldragen zijn[14]. Bovendien maken de voordelen van de zebravis, zoals kleine grootte, grote vruchtbaarheid met veel eitjes tot gevolg, en snelle ontwikkeling, dit modelorganisme zeer geschikt voor experimenten met hoge doorvoercapaciteit[15]. Het is ook ethisch gewenster om in-vivo-experimenten uit te voeren in het minst ontwikkelde organisme, en daarbij is er

geen toestemming van een ethische commissie vereist in experimenten met zebravislarven (d.w.z. de eerste vijf dagen na bevruchting)[16]. De zebravislarve combineert daarom de experimentele efficiëntie als gevolg van experimenten met hoge doorvoercapaciteit, met de vertaalbare waarde van resultaten uit de biologische context van een geheel gewerveld organisme.

Farmacologische of toxicologische experimenten met zebravissen en zebravislarven worden over het algemeen uitgevoerd door het medicijn in kwestie op te lossen in het water waarin de zebravis zwemt, ook wel het behandelingsmedium genoemd. Medicijneffecten, of het gebrek daaraan, worden geïnterpreteerd op basis van de aanname dat de externe medicijnconcentratie een reflectie geeft van de interne medicijnconcentratie in de zebravis of zebravislarve. Deze aanname negeert de basale farmacokinetiek: medicijnabsorptie, -verdeling, -metabolisme en -excretie door een organisme. Deze actieve processen hebben tot gevolg dat interne medicijnblootstelling verandert over tijd en potentieel een interne plateauconcentratie bereikt wordt die verschilt van de externe medicijnconcentratie. Dit verschil is van belang, omdat het de interne blootstelling bij het medicijndoelwit is die het effect drijft[17]. Het negeren van de interne concentratie en diens verandering over tijd beperkt daarom de interpretatie van medicijneffecten. Voor de vertaling van medicijneffecten naar hogere gewervelden, inclusief de mens, is het tevens van belang om de interne blootstelling (farmacokinetiek) te linken aan metingen van de medicijnresponsie (farmacodynamiek), om de blootstelling-responsierelatie of farmacokinetische-farmacodynamische relatie te kwantificeren. Om medicijnresponsie te kwantificeren, moeten de ziektedynamiek en veranderingen daarin door de behandeling gemeten worden, net als verschillen tussen diersoorten in de onderliggende (patho)fysiologische en farmacologische processen. Een modelmatige aanpak kan vervolgens voor die verschillen corrigeren met vertalingsfactoren, voor vertaling van medicijneffecten tussen diersoorten.

In dit proefschrift hebben we daarom innovatieve experimentele en computationele methodes ontwikkeld en geïntegreerd, voor de kwantificatie van:

I) interne medicijnblootstelling over tijd in zebravislarven na watergebonden medicijnbehandeling;
II) ziektedynamiek en veranderingen daarin door het medicijn;
III) verschillen tussen diersoorten in ziektemechanismen en medicijneffecten daarop.

Slechts met een kwantitatief begrip van deze drie elementen kan een farmacologische bevinding betrouwbaar worden vertaald, en kan de zebravis een volwaardig lid worden van de preklinische medicijnontwikkelingspijplijn.

12.2 Introductie van experimenten met hoge doorvoercapaciteit in een geheel gewerveld organisme

De voordelen van farmacologische experimenten in zebravissen werden uiteengezet in **Sectie I**. Als eerste is de noodzaak van kwantificatie van interne blootstelling over tijd geïntroduceerd. Het is belangrijk om medicijnmetabolisme in de zebravis mechanistisch en kwantitatief te begrijpen. Medicijnmetabolieten zijn het gevolg van biotransformatie in bijvoorbeeld de lever, en kunnen farmacologisch actief of toxisch zijn. We hebben daarom een literatuurstudie naar hepatisch metabolisme in de zebravis in de systeemfarmacologische context uitgevoerd in **Hoofdstuk 2**. De metabole enzymen in de zebravis werden vergeleken met hun humane orthologen, met een focus op oxidatief en conjugatief metabolisme, relevant voor onze modelstof paracetamol (acetaminophen). Genen gerelateerd aan de belangrijkste cytochrome P450 (CYP) enzymisovormen in mensen verantwoordelijk voor de katalyse van oxidatief metabolisme, CYP3A4 en CYP2E1, komen ook tot expressie in de zebravis. Hetzelfde geldt voor sulfotransferases, die conjugatie van medicijnen met sulfaatgroepen katalyseren. De enzymen verantwoordelijk voor glucuronidering in mensen, de UDP-glucuronosyltransferases, hebben paralogen in de zebravis, enzymen

met een vergelijkbare metabole functie. De genetische vergelijking in dit hoofdstuk laat zien dat enzymen voor medicijnmetabolisme vergelijkbaar zijn tussen zebravis en mens, en suggereert dat de zebravis betekenisvolle resultaten aangaande effecten van potentiele medicijnmetabolieten kan opleveren. Het is van belang de interne medicijnblootstelling te kwantificeren, inclusief de medicijnmetabolieten, om deze suggestie te bevestigen. Interne bloostelling kan vervolgens worden gelinkt aan metingen van bijvoorbeeld hepatische disfunctie, zoals biomarkers of orgaangrootte.

Een belangrijk voordeel van de zebravis voor farmacologische experimenten is de potentie voor experimenten met hoge doorvoercapaciteit. In **Hoofdstuk 3** introduceerden we de mogelijkheden van hogedoorvoercapaciteit-experimenten in de zebravis om systeemfarmacologische modelontwikkeling te ondersteunen. Systeemfarmacologische modellen vereisten grote datasets die informatief zijn over het gedrag van het (patho)fysiologische systeem gedurende farmacologische interventies. Deze datasets moeten alle relevante informatie bevatten over gewenste en ongewenste doelmoleculen en signaalroutes. Vanwege beperkingen in tijd en middelen moeten experimentele data bij voorkeur zo efficiënt mogelijk verzameld worden. Dit is mogelijk met experimenten met hoge doorvoercapaciteit. In tegenstelling tot conventioneel gebruikte organismes voor dit type experimenten, zoals gist (*Saccharomyces cerevisiae*), platworm (*Caenorhabditis elegans*) of fruitvlieg (*Drosophila melanogaster*), is de zebravis een gewerveld organisme. Hierdoor wordt verwacht dat de vertaalbare waarde naar hogere gewervelden in geneesmiddelenonderzoek groter is dan van deze niet-gewervelde soorten. In dit hoofdstuk suggereerden we een innovatieve analysemethode voor vroege geneesmiddelenontdekking en -ontwikkeling. Modelidentificatie van buitenaf naar binnen (*outside-in*) is een techniek die gebruikmaakt van oscillerende stimuli bij verschillende frequenties, om een modelstructuur te construeren tussen input en output, zonder voorkennis van het systeem dat de output drijft. Met microfluïdische apparaten speciaal ontworpen voor zebravislarven, kunnen watergebonden stimuli zoals medicijnblootstelling getest worden bij verschillende frequenties, waarna observaties van bijvoorbeeld fluorescente markers in de zebravis geanalyseerd kunnen worden. Deze aanpak wordt gekarakteriseerd door nauwe samenwerking tussen experimentele en computationele onderzoekers, en kan leiden tot een begrip van de snelheidsbepalende stappen in de relevante (patho)fysiologische routes vroeg in het geneesmiddelontwikkelingsproces.

Zebravislarven zijn transparant en daarmee ideaal voor optische beeldvorming. Een microscopie-opstelling met hoge doorvoercapaciteit die hier gebruik van maakt is de Vertebrate Automated Screening Technology (VAST). De VAST BioImager bestaat uit een capillair waarin de zebravislarve automatisch wordt geladen vanuit een reageerbuis of multititerplaat. De capillair is gemonteerd onder een microscoop en draait rond om beelden van de zebravislarve vanuit alle hoeken vast te leggen. **Hoofdstuk 4** introduceerde de toepassing van deze methode op zebravislarven met een fluorescente marker in de lever. Door verschillende beelden vast te leggen vanuit in totaal 25 hoeken kon een driedimensionale reconstructie van de gehele larve en van de lever worden gemaakt. Kwantificatie van de oppervlakte en het volume van het gehele organisme en de lever daarin resulteert in meer informatie dan tweedimensionale beeldvorming. Dit hoofdstuk had als doel dit concept aan te tonen (*proof of concept*), en beschrijft daarom slechts een beperkt aantal larven om de beeldvormingsarchitectuur en het reconstructiealgoritme te ontwikkelen. De methode kan in de toekomst toegepast worden om vorm en volume van verschillende organen tijdens de larvale ontwikkeling te kwantificeren, om een referentietabel te creëren voor bijvoorbeeld fysiologisch-gebaseerde modelontwikkeling. Bovendien kan deze methode met hoge doorvoercapaciteit gebruikt worden om grote hoeveelheden potentiele medicijnen te testen, bijvoorbeeld naar de impact van hepatotoxische medicijnen op levervolume en -vorm, of andere toepassingen waarbij de orgaangrootte een weergave geeft van effectiviteit en toxiciteit. Met deze geautomatiseerde objectieve en kwantitatieve metingen van medicijneffect over tijd kan de relatie tussen blootstelling en responsie bepaald worden, die vereist is voor de vertaling van medicijneffecten naar hogere gewervelden.

12.2.1 Methodologische innovaties

- We hebben een beeldvormingsmethode met een hoge doorvoercapaciteit ontwikkeld om data van fluorescent gelabelde weefsels of organen in zebravislarven te verzamelen gedurende medicijnbehandeling.

12.2.2 Hoofdboodschappen

- Interne medicijnblootstelling over tijd is essentieel voor de juiste interpretatie en vertaling van medicijneffecten en bijwerkingen.

- Genetische homologie in metabole enzymen tussen zebravissen en mensen suggereert dat experimenten in zebravissen betekenisvolle resultaten over de vorming van medicijnmetabolieten zullen opleveren.

- Zebravislarven zijn ideaal voor systeemfarmacologische experimenten in een geheel organisme met een hoge doorvoercapaciteit.

- Nauwe samenwerking tussen experimentele en computationele onderzoekers is belangrijk in systeemfarmacologie.

12.3 Kwantificatie van interne blootstelling over tijd

De medicijnconcentratie op de locatie van het doelwit drijft diens effect[17]. Het is daarom essentieel voor de interpretatie van medicijneffecten om de interne medicijnblootstelling te kwantificeren in zebravislarven na watergebonden medicijnbehandeling. De focus van **Sectie II** was de ontwikkeling van de experimentele, bioanalytische en computationele methodes om interne medicijnblootstelling over tijd te kwantificeren en de farmacokinetische processen van absorptie, verdeling, metabolisme en excretie te karakteriseren. Paracetamol werd gebruikt als modelstof. Het is echter uitdagend om de interne medicijnblootstelling te kwantificeren[18], omdat larven slechts enkele honderden nanoliters groot zijn[19] – eerder gekwantificeerd door middel van de VAST BioImager – en medicijnhoeveelheden klein zijn.

Hoofdstuk 5 had als doel het concept aan te tonen (*proof of concept*) om de interne blootstelling over tijd van paracetamol en zijn twee belangrijkste metabolieten te kwantificeren in zebravislarven van drie dagen na bevruchting (dpf). Twee type experimenten zijn uitgevoerd. In het eerste experiment werden zebravislarven blootgesteld aan een constante concentratie van watergebonden paracetamol voor 180 minuten. In het tweede experiment werden zebravislarven na 60 minuten watergebonden paracetamolbehandeling overgebracht naar medicijnvrij medium voor nog eens 240 minuten om de eliminatie te bestuderen. Een vloeistofchromatografie-massaspectrometriemethode (LC-MS/MS) werd ontwikkeld om de modelstof paracetamol en zijn belangrijkste metabolieten paracetamol-glucuronide en paracetamol-sulfaat te kwantificeren in homogenaatmonsters. Plateauwaardes van paracetamolhoeveelheden werden bereikt binnen 120 minuten watergebonden behandeling. In het eliminatie-experiment lieten paracetamolhoeveelheden een mono-exponentiele afname zien, terwijl interne hoeveelheden van de twee metabolieten in eerste instantie toenamen, tot ze na 120 minuten ook afnamen. De belangrijkste paracetamolmetaboliet in zebravislarven van 3 dpf was paracetamol-sulfaat, dat meer voorkwam dan paracetamol-glucuronide. Dit is in tegenstelling met het metabole profiel van paracetamol in volwassen mensen, waar paracetamol-glucuronide beschreven is als de belangrijkste metaboliet, verantwoordelijk voor 50% van de dosis of meer[20–22]. In studies met menselijke neonaten en kinderen is echter aangetoond dat vanwege maturatie van de metabole routes, paracetamol-sulfaat meer voorkomt dan paracetamol-glucuronide[23–26]. Omdat zebravislarven ook nog niet volgroeid zijn,

zou een vergelijkbaar metabool profiel de ratio tussen paracetamol-glucuronide en paracetamol-sulfaat kunnen verklaren.

Paracetamolhoeveelheden over tijd in de zebravishomogenaten werden geanalyseerd door middel van niet-lineair gemengd modelleren. Het farmacokinetische model kwantificeerde de absorptiesnelheidsconstante en de eliminatiesnelheidsconstante. Er werd aangenomen dat verdeling van paracetamol homogeen was over het gehele larvale volume. Deze aanname was noodzakelijk om absolute klaring te berekenen op basis van de eliminatiesnelheidsconstante bij gebrek aan bloedconcentraties van paracetamol. Absolute klaring is van belang, omdat het essentieel is voor schaling tussen diersoorten van deze belangrijke farmacokinetische parameter. Om te onderzoeken of farmacokinetische parameters gekwantificeerd in de zebravis betrouwbaar geschaald konden worden naar hogere gewervelden werd absolute paracetamolklaring vergeleken met gerapporteerde waardes in twaalf hogere gewervelden uit de literatuur. Deze schaling is gebaseerd op de allometrische theorie die stelt dat lichaamsgewicht van diersoorten voorspellend is voor medicijnklaring[27,28]. Schaling tussen diersoorten is altijd gebaseerd op aannames, zoals die in de allometrische theorie, maar hier ook over de paracetamolverdeling, of over het gebrek aan impact door maturatie of temperatuur op de kwantificatie van de parameter in kwestie. De kracht van onze kwantitatieve modelmatige aanpak is dat deze aannames getest en gecorrigeerd kunnen worden, hetgeen vertrouwen wekt in onze modelmatige vertaling tussen soorten van farmacologische parameters van de zebravis naar hogere gewervelden.

De zebravislarven van 3 dpf lieten een metabool profiel van paracetamol zien dat vergelijkbaar was met dat van menselijke neonaten en kinderen. Dit suggereert dat er een impact van immaturatie is op de metabole klaring, en mogelijk ook op andere farmacokinetische parameters. Zebravisontwikkeling is snel[29] en volwassenheid wordt binnen 3 maanden bereikt[30]. Het is dus interessant om de impact van leeftijd op de farmacokinetische parameters van paracetamol in de zebravis te bestuderen. In **Hoofdstuk 6** hebben we daarom de experimenten uit Hoofdstuk 5 herhaald met zebravislarven van 4 en 5 dpf. Interne paracetamolhoeveelheden lieten een toename in plateauwaardes zien tussen 3 en 4 dpf, maar niet tussen 4 en 5 dpf. De mono-exponentiele afname van paracetamolhoeveelheden uit het eliminatie-experiment werd steiler met de leeftijd. De ratio tussen paracetamol-glucuronide en paracetamol-sulfaat liet echter geen verandering zien (data niet weergegeven). Er werd geconcludeerd dat er een duidelijke impact van maturatie op absorptie en eliminatie was. De maturatie in zowel sulfatering als glucuronidering had echter geen impact op de metabole ratio tussen deze twee belangrijke metabolieten binnen de bestudeerde periode van drie dagen.

De paracetamolblootstellingsdata van de twee experimenten in zebravislarven van 3, 4 en 5 dpf werden gecombineerd en geanalyseerd met een farmacokinetisch model waarin leeftijd een covariaat was op absorptie en eliminatie. De relatie tussen leeftijd en de absorptiesnelheidsconstante was een discrete, die resulteerde in een toename van de absorptiesnelheidsconstante met 106% tussen 3 en 4 dpf. Dit werd toegewezen aan het openen van het gastro-intestinale (GI) stelsel, dat voltooid is na 4 dpf[16,31]. Wanneer het GI-stelsel volledig geopend is, draagt orale absorptie bij aan de interne medicijnblootstelling over tijd, in aanvulling op transdermale absorptie. Een vergelijkbaar effect is eerder gerapporteerd voor de antihistamine difenhydramine[32]. Leeftijd verhield zich tot paracetamoleliminatie met een machtsfunctie, waarbij de eliminatiesnelheidsconstante 17,5% per dag toenam. Deze toename in eliminatie als gevolg van metabolisme en excretie, zou het gevolg kunnen zijn van groei van de verantwoordelijke organen en maturatie van de enzymsystemen en/of transporteiwitten[33]. Absolute klaring was berekend zoals hierboven beschreven en liet een toename met leeftijd zien en een verschuiving richting de allometrische relatie van paracetamolklaring uit de twaalf hogere gewervelden (**Figuur 6.4**). Leeftijd had een heldere impact op de interne medicijnblootstelling over tijd, in elk geval voor onze modelstof paracetamol. Dit betekent dat het verschil van één dag invloed kan hebben op de interne medicijnblootstelling over tijd, en de bijbehorende gemeten uitkomsten. Omdat zowel het medicijn als diens metabolieten farmacologisch actief kunnen zijn, adviseren we om experimenten naar medicijneffecten op de korte termijn uit te

voeren met zebravislarven van 5 dpf, waarin de blootstelling aan zowel het medicijn (door toegenomen absorptie ten opzichte van 3 dpf) als diens metabolieten (door geanticipeerd toegenomen metabolisme) geoptimaliseerd wordt.

Metabole enzymen verantwoordelijk voor oxidatie en conjugatie van onze modelstof paracetamol komen in de zebravis tot expressie (Hoofdstuk 2). De belangrijkste metabolieten paracetamol-glucuronide en paracetamol-sulfaat zijn geobserveerd na watergebonden paracetamolbehandeling (Hoofdstuk 5). In **Hoofdstuk 7** werd dit metabolisme bestudeerd in mechanistischer en kwantitatiever detail door middel van een farmacokinetisch mechanistisch model. De interne paracetamolblootstellingsdata op 5 dpf (Hoofdstuk 6) werden gecombineerd met interne blootstellingsdata van paracetamol-glucuronide en paracetamol-sulfaat in die larven, en hoeveelheden daarvan uitgescheiden in het medium. Kwantificatie van de farmacokinetische processen van verdeling en absolute klaring is essentieel voor betrouwbare extrapolatie van deze parameters tussen diersoorten, maar vereist bloedconcentraties in aanvulling op totale hoeveelheden uit homogenaatmonsters. Hoewel er methodes voor bloedmonstering zijn ontwikkeld voor volwassen zebravissen[34–36], ontbrak het aan een bloedmonstermethode voor zebravislarven. We hebben daarom een bloedmonstermethode ontwikkeld voor zebravislarven van 5 dpf, door middel van het aanprikken van de posterieure kardinale vene[37] met een naald, getrokken van een capillair met een originele diameter van 0,75 mm. De resulterende nanoliterschaal-bloedmonsters werden bij elkaar gevoegd om gezamenlijk de kwantificatielevels te bereiken. In deze bloedmonsters werden zowel paracetamol als beide metabolieten gemeten. Paracetamolconcentraties waren slechts 10% van de externe paracetamolconcentratie, wat ook elders werd gerapporteerd[38]. De bloedconcentratiedata werden gecombineerd met de data van paracetamolhoeveelheden en metaboliethoeveelheden zowel in de zebravislarven als daardoor uitgescheden in het medium, en gezamenlijk geanalyseerd door middel van het ontwikkelde farmacokinetische metabolietmodel. Zowel de door dit model bepaalde absolute paracetamolklaring als het paracetamolverdelingsvolume correleerden goed met de respectievelijke parameterwaardes gerapporteerd in hogere gewervelden (**Figuur 7.5**, **Figuur 7.6**).

De vorming, verdeling en uitscheiding van de twee belangrijkste paracetamolmetabolieten werden gekwantificeerd. Het was in het bijzonder interessant om de mogelijkheid te hebben het verdelingsvolume van de twee metabolieten te kwantificeren. Normaal gesproken zijn aannames over het metabolietverdelingsvolume nodig voor een wiskundig identificeerbaar metabolietmodel bij gebrek aan data van de totale metaboliethoeveelheden[26,39]. Hier hadden we echter zowel data van de metabolietconcentraties in bloed als de totale metaboliethoeveelheden in homogenaatmonsters, waardoor de verdelingsvolumes met het model gekwantificeerd kunnen worden. Biotransformatie van paracetamol naar paracetamol-sulfaat was tijdsafhankelijk. Binnen de bestudeerde tijdsperiode verminderde sulfatering tot een minimum, hetgeen verklaard kan worden door depletie van de sulfaatgroepdonor vereist voor deze biotransformatie[40–42]. Het zou interessant zijn om de tijdsperiode van dit experiment te verlengen om de productie van deze sulfaatgroepdonor door de zebravislarve in het model te includeren[43], of om deze direct te meten[44].

We hebben experimentele, bioanalytische en computationele methodes ontwikkeld en geïntegreerd om interne medicijnblootstelling in de zebravislarve over tijd te kwantificeren na watergebonden medicijnbehandeling. Modelmatige kwantificatie van de farmacokinetische processen leidde tot een kwantitatief begrip van de interne blootstelling over tijd, en vervolgens tot extrapolatie van medicijnklaring en verdelingsvolume tussen diersoorten. Als in conventionele visstudies de interne blootstelling relevant is, wordt de bioconcentratiefactor (BCF) gebruikt[45]. Deze ratio tussen interne en externe concentratie is bruikbaarder dan alleen de externe concentratie, maar negeert de kinetiek van veranderende concentraties over tijd en is daardoor zeer variabel en afhankelijk van de opzet van het experiment[46]. Recent werd de interne blootstelling over tijd bestudeerd in zebravissen voor andere moleculen (metalen[47–50] of microplastics[51]) of binnen andere disciplines (milieuwetenschappen[52,53] of toxicologie[54–58]), maar niet geanalyseerd volgens onze kwantitatieve vertaalbare modelmatige aanpak.

Het was onze focus om een kwantitatief begrip van de interne blootstelling over tijd te verkrijgen en om daarmee een vertaling van farmacokinetische parameters tussen soorten mogelijk te maken, essentieel voor de rol van de zebravis in geneesmiddelenontwikkeling.

12.3.1 Methodologische innovaties

- We hebben een bloedmonsteringsmethode op nanoschaal in de zebravislarve ontwikkeld, om medicijnconcentraties in het bloed te kwantificeren in aanvulling op medicijnhoeveelheden uit homogenaatmonsters.

- We hebben een LC-MS/MS-methode ontwikkeld die sensitief genoeg was voor zebravismonsters met kleine volumes, om interne medicijn- en metabolietblootstelling over tijd te kwantificeren.

- We hebben niet-lineaire gemengde modellen ontwikkeld om het verdelingsvolume en de absolute klaring van een medicijn in zebravislarven voor het eerst te kwantificeren, essentieel voor de vertaling van de farmacokinetiek naar hogere gewervelden.

12.3.2 Hoofdboodschappen

- Voor de eerste keer is de vertaalbaarheid van farmacokinetische parameters gekwantificeerd in de zebravislarve naar hogere gewervelden verwezenlijkt en onderbouwd.

- Experimenten naar medicijneffecten op de korte termijn kunnen het beste uitgevoerd worden bij 5 dpf.

- De immaturiteit van de zebravislarve heeft implicaties voor zowel de farmacokinetiek, als de interpretatie van medicijneffecten en vertaling daarvan tussen diersoorten.

12.4 Het linken van interne blootstelling aan ziektedynamiek

Een ziekte is niet statisch maar vertoont veranderingen over tijd als gevolg van ziekteprogressie of behandeling[59]. Het is daarom belangrijk om herhaalde metingen van de ziektedynamiek te hebben en die vervolgens te linken aan interne medicijnblootstelling om het medicijneffect daarop te kwantificeren. Dit was de focus van **Sectie III**. Als ziektemodel werd het recent ontwikkelde zebravismodel voor de neuroblastoom bestudeerd. Deze transgene zebravislijn ontwikkelt spontaan neuroblastoomtumoren na drie weken, en laat daarbij een fluorescente marker in de tumor tot expressie komen[60]. Door middel van fluorescentiemicroscopie kon vervolgens de tumorgrootte worden gekwantificeerd. Er werd eerder gevonden dat isotretinoïne (13-cis-retinezuur) een effect had op de neuroblastoomontwikkeling na zeven dagen watergebonden behandeling[60]. In **Hoofdstuk 8** kwantificeerden we de tumorontwikkeling in jonge zebravissen op basis van verschillende metingen van de tumorgrootte gedurende de zevendagenbehandeling met 0, 1, 1.5 en 2 µM watergebonden isotretinoïne, om deze vervolgens aan de gekwantificeerde interne medicijnblootstelling te linken.

Kwantificatie van isotretinoïne bleek uitdagend te zijn omdat het een fotosensitieve stof is[61–63]. Blootstelling aan ultraviolet (UV) licht resulteert in isomerisatie van isotretinoïne in 9-cis-retinezuur en all-trans-retinezuur. Een gevoelige LC-MS/MS-methode is ontwikkeld om de isomeren te onderscheiden. Bovendien werd blootstelling aan UV geminimaliseerd door experimenten na zonsondergang of in raamloze laboratoria uit te voeren. Dit resulteerde in minder dan 10% isomerisatie in het behandelingsmedium en gemiddeld 16,4% isomerisatie in de (transparante) jonge zebravis.

De interne medicijnblootstelling werd verwacht een plateau te bereiken na een langdurige watergebonden behandeling, vergelijkbaar met die van paracetamol in de vorige sectie. Na de start van de behandeling

en de twee verversingen van het behandelingsmedium werd echter een isotretinoïnepiek opgevolgd door een honderdvoudige daling in interne blootstelling. Nadat vervolgens de isotretinoïneconcentratie in het behandelingsmedium werd gekwantificeerd bleek dat de concentratie lager was dan de nominale dosis bij de start van het experiment, en dat deze externe concentraties tevens daalden tijdens de dosisintervallen. De isotretinoïneprofielen in de zebravis en in het behandelingsmedium werden gekarakteriseerd door middel van modelmatige simultane analyse van zowel de interne medicijnblootstelling in de zebravis als de externe medicijnconcentratie, waarmee de absorptie vanuit en excretie naar het behandelingsmedium door de jonge zebravis werden gekwantificeerd.

Elke 24 uur werden zebravissen opgeofferd om de tumorgrootte te kwantificeren met tweedimensionale fluorescentiemicroscopie. Helaas werd geen statistisch significant verschil gevonden tussen de verschillende dosisgroepen en de controlegroep, waardoor geen medicijneffect op de tumorgrootte kon worden gekwantificeerd. Het gebrek aan medicijneffect in onze experimenten zou verklaard kunnen worden door het interne blootstellingsprofiel. De interne isotretinoïneblootstelling was voor het grootste gedeelte van de behandeling subtherapeutisch, vanwege de snelle afname tijdens de dosisintervallen. Dit resultaat onderstreept het belang van de kwantificatie van interne medicijnblootstelling over tijd, om betrouwbare interpretatie van geobserveerde medicijneffecten, of het gebrek daaraan, mogelijk te maken.

Een andere reden voor het gebrek aan een significant medicijneffect zou de hoge variabiliteit in tumorgrootte per individuele jonge zebravis kunnen zijn. Vanwege het feit dat we slechts één meting per individu namen, konden we niet corrigeren voor deze interindividuele variabiliteit. Dit was in tegenstelling tot vorige studies, waar metingen voor en na behandeling in dezelfde zebravis werden genomen om het medicijneffect te kwantificeren[60]. Meting van de tumorgrootte zou preciezer kunnen worden als in plaats van tweedimensionale oppervlakte het driedimensionale volume wordt vastgesteld. Optische projectietomografie (OPT) is een driedimensionale microscopieopstelling vergelijkbaar met de VAST BioImager, maar toepasbaar op materiaal dat niet in de capillair zou passen, zoals de jonge zebravis[64,65]. Het voordeel van de transparante zebravis is dat er, in tegenstelling tot ondoorzichtigere OPT-monsters zoals muizenhartweefsel, geen monsterklaring vereist is om het fluorescente signaal van de tumor op te kunnen vangen[66]. Een eerste studie naar de mogelijkheden van OPT in deze toepassing met representatieve zebravissen met de fluorescente neuroblastoom leidde tot veelbelovende resultaten (**Figuur 8.6**). De driedimensionaal gekwantificeerde tumor was beter te onderscheiden en niet deels verborgen achter de melanocyt-paraplu[67]. Een andere verbetering voor de kwantificatie van tumordynamiek over tijd zou de herhaalde metingen van biomarkers als maat van (patho)fysiologische veranderingen kunnen zijn[68,69].

Eiwitbinding van isotretinoïne[70] zou tevens van invloed kunnen zijn, omdat het binding aan het doelwit voorkomt. Een belangrijk bloedeiwit voor medicijneiwitbinding, albumine, is echter absent in de zebravis en geen andere eiwitten van betekenis werden in plasma gerapporteerd[71,72]. Een andere overweging zou kunnen komen vanuit het feit dat het werkingsmechanisme van isotretinoïne nog niet volledig bekend is, en dat de isomeren mogelijk verantwoordelijk zouden kunnen zijn voor (een gedeelte van) het medicijneffect[63,73]. In dat geval zouden de resultaten uit de vorige studie verminderd kunnen zijn juist omdat we hier de fotoisomerisatie tot een minimum hebben beperkt. Toepassing van de geïntegreerde experimentele en computationele methodes die we hier hebben ontwikkeld kan gebruikt worden om deze hypothese van actieve isomeren te testen, en kan bijdragen aan het ophelderen van het werkingsmechanisme van isotretinoïne.

12.4.1 Methodologische innovatie

- We hebben een driedimensionale microscopiemethode ontwikkeld om accurater en preciezer tumorgrootte te kwantificeren in jonge zebravissen in vergelijking met conventionele tweedimensionale microscopie.

12.4.2 Hoofdboodschappen

- De gebruikelijke aanname dat externe en interne medicijnconcentraties constant zijn gedurende watergebonden behandeling moet altijd getest worden door kwantitatieve metingen over tijd in zowel de zebravis als het behandelingsmedium.

- Farmacokinetische en farmacodynamische experimenten om zowel interne medicijnblootstelling over tijd als veranderingen in ziektedynamiek over tijd tijdens de behandeling te kwantificeren, moeten beiden uitgevoerd worden om medicijneffecten, of het gebrek daaraan, te interpreteren en te kwantificeren.

12.5 Mechanistische en kwantitatieve vertaling van de blootstelling-responsierelatie van een medicijn van de zebravis naar hogere gewervelden

Een blootstelling-responsierelatie waarbij interne medicijnblootstelling wordt gelinkt aan de ziektedynamiek, is het fundament van de vertaling van medicijneffecten tussen diersoorten. Een tweede belangrijk element voor deze vertaling tussen diersoorten is rekening houden met verschillen in ziektemechanismen tussen die diersoorten. De (patho)fysiologische processen kunnen verschillen tussen gewervelden en een kwantitatief modelmatige aanpak kan daarvoor corrigeren door middel van vertalingsfactoren. Het was de focus van **Sectie IV** om verschillen in (patho)fysiologische processen tussen diersoorten te kwantificeren ten bate van een mechanistische en kwantitatieve vertaling van de medicijnblootstelling-responsierelatie van de zebravis naar hogere gewervelden. Specifiek lag de focus op tuberculose (TB), een ziekte waarvan de pathologie en behandeling uitgebreid onderzocht worden in de zebravis[74–79]. Zebravislarven geïnfecteerd met de aquatische pathogeen *Mycobacterium marinum*, nauw verwant aan de humane pathogeen *Mycobacterium tuberculosis*, functioneerden als ziektemodel[80].

In **Hoofdstuk 9** werd de natuurlijke groei van *M. marinum* bestudeerd en vergeleken met die van *M. tuberculosis*. We hebben twee bacteriestammen, één koudbloedig-afgeleide stam E11[81] en één humaan-afgeleide stam M^{USA} [82], ongestoord laten groeien voor meer dan tweehonderd dagen en de levensvatbaarheid op verschillende tijdspunten werd bepaald op basis van kolonievormende eenheden (CFU). Een gevestigd TB-model, het multistaat-tuberculose-farmacometrisch (MTP)-model[83,84], werd gebruikt om deze natuurlijke groei kwantitatief te karakteriseren. Het MTP-model maakt onderscheid tussen drie staten van mycobacterieel groeigedrag: een snel vermenigvuldigende, een langzaam vermenigvuldigende en een niet-vermenigvuldigende staat. De natuurlijke groei van *M. tuberculosis* is eerder al gekarakteriseerd met dit model door middel van het kwantificeren van de groeisnelheden en de overdrachtssnelheden tussen de staten. Het onderscheiden van mycobacteriën in de verschillende vermenigvuldigingsstaten is van belang omdat antibiotica-effecten op de mycobacteriën kunnen verschillen afhankelijk van hun groeigedrag. Het MTP-model was succesvol toegepast om het medicijneffect op *M. tuberculosis* te kwantificeren in-vitro[83,85], in muizen[86,87], en in patiënten[88,89]. Het is hier toegepast op de natuurlijke groeidata van de twee *M. marinum*-stammen om hun natuurlijke groei te vergelijken met die van *M. tuberculosis*. De E11-stam liet een latenter groeigedrag zien, vergelijkbaar met dat van *M. tuberculosis*, terwijl de groei van de M^{USA}-stam juist agressiever was (**Figuur 9.1**). Deze bevindingen waren in lijn met eerder gerapporteerde resultaten[81]. Omdat ook de groeisnelheden van E11 en *M. tuberculosis* vergelijkbaar waren, suggereerden we dat het gebruik van E11 de voorkeur heeft bij het bestuderen van TB in zebravissen.

Het was de focus van **Hoofdstuk 10** om de interne medicijnblootstelling-responsierelatie te kwantificeren in zebravissen geïnfecteerd met *M. marinum* als ziektemodel voor TB, met als doel te onderzoeken hoe betrouwbaar een vertaling van medicijneffecten naar mensen zou zijn op basis van een dergelijke kwantitatieve blootstelling-responsierelatie. Het antibioticum isoniazide werd gekozen als modelstof,

omdat het de grootste bacteriedodende activiteit in de eerste behandelingsdagen laat zien van de antibiotica uit de huidige zorgstandaard voor TB-behandeling[90]. Zebravislarven werden 28 uur na bevruchting geïnfecteerd met E11 volgens de aanbeveling uit Hoofdstuk 9. Na twee dagen vestiging van de infectie werd begonnen met watergebonden behandeling met toenemende isoniazidedoses van 0,25-10x de minimaal remmende concentratie (MIC). Interne isoniazideblootstelling werd gekwantificeerd in homogenaatmonsters en bloedmonsters. Fluorescente *M. marinum* werden gebruikt om herhaalde metingen mogelijk te maken van de bacterielading in individuele zebravislarven door middel van niet-invasieve fluorescentiemicroscopie. Geautomatiseerde fluorescentiebeeldanalyse[91,92] werd toegepast op de vastgelegde beelden om de bacterielading per zebravislarve te kwantificeren op basis van fluorescente pixelaantallen. Simultane farmacokinetische-farmacodynamische modelanalyse werd uitgevoerd op de gecombineerde data van totale medicijnhoeveelheden in homogenaatmonsters, medicijnconcentraties in bloedmonsters, en bacterielading op basis van fluorescentie. Interne blootstelling bereikte plateaulevels binnen twaalf uur, maar de plateaulevels stegen met elke dag na bevruchting. Een invloed van leeftijd op de absorptie van isoniazide werd gekwantificeerd, vergelijkbaar met Hoofdstuk 5. Er was ook verwacht dat leeftijd een impact had op eliminatie, maar omdat de meerderheid van de datapunten verzameld werd tijdens de plateaufase waarin absorptiesnelheid en eliminatiesnelheid hetzelfde zijn, was een uitgesplitste impact van leeftijd op zowel absorptie als eliminatie niet wiskundig identificeerbaar op basis van de huidige data. Het leeftijdseffect op absorptie moet daarom geïnterpreteerd worden als een netto toename van absorptie ten opzichte van die van eliminatie. Bloedconcentraties van isoniazide waren slechts 20% van de externe concentratie. De bacterielading liet een exponentiele groei zien en een afname in groei met toenemende isoniazideblootstelling. Een dosis van 5x MIC in het behandelingsmedium resulteerde in bacteriostase, wat verwacht werd, gezien de relatie tussen interne en externe concentraties.

Om het concept van vertaling aan te tonen (*proof of concept*) werd de kwantitatieve blootstelling-responsierelatie van isoniazide vertaald naar mensen. Isoniazideconcentraties over tijd in de mens werden gesimuleerd voor de therapeutische dosis van 300 mg, gebaseerd op een eerder gepubliceerd farmacokinetisch model[93]. Twee vertalingsfactoren werden geïncludeerd in de vertaling, om te corrigeren voor verschillen in ziektemechanismen tussen diersoorten en de farmacologische responsie[89]. De eerste vertalingsfactor corrigeerde voor het verschil in gevoeligheid voor isoniazide van *M. marinum* en *M. tuberculosis* zoals gerapporteerd in hun respectievelijke MICs. De tweede vertalingsfactor corrigeerde voor het verschil in infectiefase. De verse infectie in zebravissen liet groei zien in de logaritmische infectiefase, terwijl klinische infecties in de stationaire infectiefase verwacht werden. Zoals hierboven beschreven kan het medicijneffect op mycobacteriën verschillen tussen verschillend groeigedrag. Het MTP-model is eerder toegepast om het isoniazide-effect op *M. tuberculosis* in verschillende staten te kwantificeren[85]. De ratio van de maximale dodingssnelheid gerelateerd aan de verschillende staten werd aangenomen om het verschil in medicijneffect tussen de logaritmische en stationaire infectiefase te weerspiegelen. Met deze vertalingsfactoren in beschouwing genomen correleerde de vertaling van de blootstelling-responsierelatie van isoniazide gekwantificeerd in de zebravis redelijk met observaties in mensen zoals gerapporteerd in de literatuur[94–96] (**Figuur 10.7**). Dit gold in het bijzonder voor de eerste twee behandelingsdagen, dezelfde periode als in onze experimenten. Na twee dagen werd het isoniazide-effect overschat, wat correspondeerde met bevindingen in de literatuur dat de eerste twee dagen van de isoniazidebehandeling een snellere afname in bacterielading lieten zien dan daarna[90,97]. Deze afname in medicijneffect na twee dagen was echter niet kwantificeerbaar in het korte experiment in de zebravislarve.

Uitgaande van onze resultaten van Hoofdstuk 9 en Hoofdstuk 10 vertrouwen we erop dat de zebravis een betrouwbare toevoeging is aan de preklinische TB-medicijnontwikkelingspijplijn op basis van het MTP-model. Het MTP-model is eerder gebruikt om medicijneffecten te kwantificeren in de huidige zorgstandaard voor TB-behandeling in-vitro[83,85], in muizen[86,87] en in mensen[88,89]. Analyse van nieuwe medicijnen tegen TB door middel van het MTP-model is de volgende stap in de preklinische

medicijnontwikkeling. De zebravis is een aantrekkelijk modelorganisme om nieuwe medicijnen te testen ná in-vitro-experimenten, maar vóór zoogdierstudies. Dit zal resulteren in meer informatie over nieuwe medicijnkandidaten in een eerder stadium van de medicijnontwikkeling tegen TB, en met de voorspelbare kracht van deze mechanistische en kwantitatieve modelmatige aanpak ook in een betrouwbaardere vertaling van anti-TB-medicijneffecten van de zebravis naar hogere gewervelden.

12.5.1 Methodologische innovaties

- We hebben een gevestigd mechanistisch TB-model toegepast om de natuurlijke groei van *M. marinum* voor de eerste keer te karakteriseren en kwantitatief te vergelijken met de natuurlijke groei van *M. tuberculosis*.

- We hebben een methode ontwikkeld om individuele bacterielading over tijd te kwantificeren in zebravislarven gedurende behandeling, gebaseerd op herhaaldelijke metingen gebruikmakend van niet-invasieve fluorescentiemicroscopie en populatiemodelleren.

12.5.2 Hoofdboodschappen

- Een kwantitatief modelmatige aanpak kan medicijneffecten vertalen tussen twee diersoorten die ogenschijnlijk van elkaar verschillen, door gebruik te maken van een kwantitatieve blootstelling-responsierelatie en vertalingsfactoren die corrigeren voor verschillen tussen diersoorten.

- Antibiotische medicijneffecten gekwantificeerd in de zebravis konden vertaald worden naar de mens.

12.6 Overige uitdagingen voor de zebravis in geneesmiddelenontwikkeling

In Secties II t/m IV hebben we experimentele, bioanalytische en computationele methodes ontwikkeld en geïntegreerd om interne medicijnblootstelling te kwantificeren, om die vervolgens kwantitatief te linken aan ziektedynamiek met als doel om farmacologische bevindingen te vertalen naar hogere gewervelden. Kwantificatie van de interne medicijnblootstelling na watergebonden behandeling is een belangrijke uitdaging voor de zebravis in geneesmiddelenontwikkeling, maar niet de enige. We bespreken drie andere uitdagingen. Allereerst is de zebravis een lagere gewervelde dan de zoogdieren die als proefdier worden gebruikt, en niet alle ziektes relevant voor hogere gewervelden kunnen onderzocht worden. Sommige orgaansystemen van zoogdieren zijn anders (bijv. geen hartseptatie) of absent (bijv. respiratoire en reproductieve organen)[98]. Omdat de zebravis een koudbloedig dier is kan bijvoorbeeld koorts niet onderzocht worden en hebben de lagere experimentele temperaturen mogelijk een impact op de groei van pathogenen of tumoren[98,99]. Ten tweede worden experimenten bij voorkeur uitgevoerd in de embryonale of larvale staat, wanneer de zebravis klein en geschikt is voor multititerplaten en experimenten met hoge doorvoercapaciteit. De bijbehorende immaturiteit heeft mogelijk een impact op de vertaling van farmacologische bevindingen[100], zoals we ook zagen in Hoofdstuk 6. Een andere beperking in dit opzicht is het gebrek aan een verworven immuunsysteem in embryo's en larven, dat zich pas na vier weken ontwikkelt[99,101]. Ten derde dienen experimenten in zebravissen nog gestandaardiseerd en gevalideerd te worden[102]. Zebravisverzorging verschilt tussen laboratoria[103–109] en behandelingsomstandigheden zoals licht, temperatuur en watersamenstelling variëren en worden vaak niet (volledig) gerapporteerd[110]. Gestandaardiseerde experimenten kunnen vervolgens gevalideerd worden met positieve en negatieve teststoffen bekend uit experimenten met hogere gewervelden[98,111].

12.7 Toekomstperspectieven

In dit proefschrift hebben we experimentele, bioanalytische en computationele methodes ontwikkeld en geïntegreerd om de potentie van de zebravis in vroege medicijnontdekking en -ontwikkeling waar

te maken. Vele mogelijkheden en veelbelovende technieken komen binnenkort beschikbaar om farmacologische vragen te beantwoorden en om de vertaling van dit modelorganisme naar hogere gewervelden, inclusief de mens, te verbeteren.

Eén van de grote voordelen van de zebravis voor farmacologische experimenten is zijn veelzijdigheid en schier eindeloze experimentele mogelijkheden. Een belangrijk voorbeeld is de rol die de zebravis kan spelen in het ontrafelen van het belang van het microbioom in de farmacologie. Er wordt verwacht dat het microbioom een impact heeft op ziekte en gezondheid, en de farmacokinetiek en farmacodynamiek beïnvloedt[112]. Het is moeilijk om het microbioom te bestuderen in zoogdieren, omdat voor een interventie van de bacteriën in de ingewanden sterilisatie en vervolgens rekolonisatie vereist is[113]. Omdat de zebravis een buitenlichamelijke bevruchting heeft en er wordt aangenomen dat de zygote steriel is, kunnen zebraviseitjes veel eenvoudiger gesteriliseerd worden, en kolonisatie van steriele embryo's en larven gaat simpelweg via het medium[114,115]. We hebben een haalbaarheidsexperiment uitgevoerd in steriele zebravislarven, vergelijkbaar met de experimenten uit Sectie II, om te verzekeren dat de geobserveerde metabolieten niet het gevolg waren van metabolisme door de bacteriën in de ingewanden van de zebravislarve. Dit kan verder uitgebreid worden om de impact van het microbioom op de farmacokinetiek en op de farmacokinetische-farmacodynamische relatie van medicijnen te kwantificeren.

De experimentele gereedschapskist voor de zebravis zal verder uitgebreid worden. Methodes voor orale dosering zijn reeds ontwikkeld voor volwassen zebravissen om uitdagingen in zowel vertaling als medicijntoediening te overwinnen, bijvoorbeeld door zebravissen te behandelen met medicijnen die onoplosbaar zijn in water, medicijnen die niet geabsorbeerd worden gedurende watergebonden behandeling, of medicijnen die aan de huid van de zebravis plakken[116,117]. Een vergelijkbare methode voor orale dosering in zebravislarven wordt op dit moment ontwikkeld, waarbij gebruik gemaakt wordt van het driedimensionaal microprinten van een opzetstuk voor een injectiespuit. Een andere veelbelovende toevoeging aan de experimentele gereedschapskist is het gebruik van microfluïdische apparaten specifiek ontworpen om zebravislarven te huisvesten en positioneren[118–121]. De larven kunnen vervolgens behandeld worden met verschillende medicijnconcentraties of-frequenties door het aanpassen van de stroomsnelheid van het behandelmedium of het wasmedium door de kanaaltjes. Integratie van deze experimentele technieken met automatische fluorescentiebeeldvorming (Hoofdstuk 4) zal resulteren in een werkopstelling met hoge doorvoercapaciteit met vele mogelijkheden voor metingen van medicijneffecten. Dit wordt verder verbeterd door het gebruik van gerobotiseerde injecties. Automatische gerobotiseerde injectiemethodes met een snelheid van 2.000 geïnjecteerde embryo's per uur zijn reeds ontwikkeld[15,78,122] en diepgaand machinaal leren (*deep learning*) heeft de efficiëntie verder verbeterd[123]. Op dit moment wordt er gewerkt aan een methode om dezelfde opstelling te gebruiken om bloedmonstering te automatiseren, hetgeen de doorvoercapaciteit van experimenten om interne medicijnblootstelling te kwantificeren substantieel zal vergroten.

Een inherente uitdaging van de zebravislarve is de kleine grootte en bijbehorende kleine medicijnhoeveelheden in monsters voor bioanalytische kwantificatie. Gevoelige LC-MS/MS-methodes zijn hier ontwikkeld om medicijn- en metaboliethoeveelheden en-concentraties in monsters bestaande uit samengevoegde homogenaatmonsters of bloedmonsters te kwantificeren. Detectielimieten voor medicijnen en metabolieten zullen afnemen tot femtomol-levels[124], hetgeen metingen van medicijn- en metaboliethoeveelheden of-concentraties in individuele larven mogelijk zal maken. Bloedmonsters moeten op dit moment samengevoegd worden om kwantificeerbare levels te behalen, maar nieuwe methodes zijn beschikbaar om medicijnconcentraties in individuele bloedmonsters te kwantificeren. Eén voorbeeld is het toedienen van ionisatievloeistof achter in de monsternaald om het geheel vervolgens direct te injecteren in de massaspectrometer, gebruikmakend van nanoelectroverstuiving-ionisatiemassaspectrometrie om de doorvoercapaciteit en gevoeligheid te verbeteren[125]. Het is reeds toegepast om medicijnconcentraties in individuele kankercellen te kwantificeren[126]. Accurate en precieze kwantificatie van medicijnconcentraties in bloedmonsters is essentieel voor de kwantificatie van interne

medicijnblootstelling, die gelinkt aan metingen van de ziektedynamiek een blootstelling-responsierelatie opleveren. Betrouwbare kwantificatie van interne blootstelling en van blootstelling-responsie is essentieel voor vertaling van medicijneffecten tussen diersoorten. Wanneer massaspectrometrietechnieken gevoeliger worden, worden bloedvolumes noodzakelijk voor kwantificatie van medicijnconcentraties kleiner. Dit kan leiden tot de mogelijkheid om meer dan één bloedmonster per individuele larve te nemen, waardoor de onderscheiding van biologische en experimentele variabiliteit in bloedconcentraties mogelijk wordt met de bijbehorende afname van ruis in de concentratie-tijddata tot gevolg.

Het gebruik van de zebravis in vroeg geneesmiddelenontdekking en -ontwikkeling moet altijd in de context gezien worden van vertaling van farmacologische bevindingen richting de kliniek. Het beste voorbeeld tot dusver is het prostaglandine E2-derivaat ProHema (16,16-dimethyl-prostaglandine E2), ontdekt in een fenotypisch experiment naar hematopoëtische stamcelvorming in zebravissen[127]. De stof is nu in Fase II klinische experimenten als onderdeel van een nieuwe behandeling voor de transplantaat-tegen-gastheerreactie (*graft-versus-host*) in patiënten die een donorstamceltransplantatie ontvangen[128]. Een ander voorbeeld is het gehoorbeschermend portfolio van ureumthiofeencarbonzuuramiden[129]. Deze stoffen zijn het resultaat van een fenotypisch experiment gericht op het vinden van stoffen die beschermend werken tegen aminoglycoside-geïnduceerde gehoorschade[130]. Zebravislarven met fluorescente haarcellen werden in deze experimenten gebruikt om haarcelverlies, verantwoordelijk voor gehoorschade in de mens, na te bootsten. De hoofdstof is op dit moment in Fase I klinische experimenten[131]. Vergelijkbaar met deze voorbeelden zijn er vier andere stoffen die ontdekt zijn in zebravisexperimenten in klinische experimenten, en nog eens vier in de fase daarvoor[128]. Wij voorzien dat dit slechts de eerste van velen stoffen zijn, ontdekt in farmacologische experimenten in de zebravis, die klinische ontwikkeling bereiken.

12.8 Conclusies

De zebravis is een veelbelovend gewerveld modelorganisme in vroege geneesmiddelenontdekking en -ontwikkeling. Vertaling van farmacologische bevindingen naar hogere gewervelden vereist kwantificatie van de onderliggende farmacologische en (patho)fysiologische processen. In dit proefschrift hebben we daarom innovatieve experimentele en computationele methodes ontwikkeld en geïntegreerd ten bate van de succesvolle kwantificatie van 1) de interne medicijnblootstelling over tijd na watergebonden behandeling, 2) de ziektedynamiek en medicijn-geïnduceerde veranderingen daarin en 3) verschillen in ziektemechanismen tussen diersoorten. De baanbrekende methodes die we hebben ontwikkeld zijn onder andere de bloedmonstermethode op nanoschaal, gevoelige LC-MS/MS-methodes voor medicijnen en hun isomeren en metabolieten, en driedimensionale microscopie, geïntegreerd met niet-lineair gemengd modelleren om de farmacologische processen te kwantificeren in deze kleine gewervelde. Deze multidisciplinariteit maakt kwantificatie van interne medicijnblootstelling-responsierelaties mogelijk, draagt bij aan de positionering van de zebravis in preklinische medicijnontwikkeling, en inspireert continue samenwerking tussen experimentele en computationele onderzoekers.

12.9 References

1. Breimer DD, Danhof M. Relevance of the application of pharmacokinetic-pharmacodynamic modelling concepts in drug development - the wooden shoe paradigm. Clin Pharmacokinet. 1997;32(4):259-267.
2. Huang Q, Riviere JE. The application of allometric scaling principles to predict pharmacokinetic parameters across species. Expert Opin Drug Metab Toxicol. 2014;10(9):1241-1253.
3. Mager DE, Woo S, Jusko WJ. Scaling pharmacodynamics from in vitro and preclinical animal studies to humans. Drug Metab Pharmacokinet. 2009;24(1):16-24.
4. Van der Graaf PH, Benson N. Systems pharmacology: Bridging systems biology and pharmacokinetics-pharmacodynamics (PKPD) in drug discovery and development. Pharm Res. 2011;28:1460-1464.

5. Danhof M, Klein K, Stolk P, et al. The future of drug development: The paradigm shift towards systems therapeutics. Drug Discov Today. 2018;23(12):1990-1995.
6. Bradshaw EL, Spilker ME, Zang R, et al. Applications of quantitative systems pharmacology in model-informed drug discovery: Perspective on impact and opportunities. CPT Pharmacometrics Syst Pharmacol. September 2019.
7. Nijsen MJ, Wu F, Bansal L, et al. Preclinical QSP modeling in the pharmaceutical industry: An IQ consortium survey examining the current landscape. CPT Pharmacometrics Syst Pharmacol. 2018:Accepted article.
8. Esch EW, Bahinski A, Huh D. Organs-on-chips at the frontiers of drug discovery. Nat Rev Drug Discov. 2015;14(4):248-260.
9. Ehrlich A, Duche D, Ouedraogo G, et al. Challenges and opportunities in the design of liver-on-chip microdevices. Annu Rev Biomed Eng. 2019;21(1):219-239.
10. Cyr KJ, Avaldi OM, Wikswo JP. Circadian hormone control in a human-on-a-chip: In vitro biology's ignored component? Exp Biol Med. 2017;242(17):1714-1731.
11. Peterson RT, Fishman MC. Designing zebrafish chemical screens. Vol 105. 3rd ed. Elsevier Inc.; 2011.
12. Howe K, Clark MD, Torroja CF, et al. The zebrafish reference genome sequence and its relationship to the human genome. Nature. 2013;496:498-503.
13. Howe DG, Bradford YM, Eagle A, et al. The zebrafish model organism database: New support for human disease models, mutation details, gene expression phenotypes and searching. Nucleic Acids Res. 2017;45(D1):D758-D768.
14. Cho A, Haruyama N, Kulkarni AB. Generation of transgenic mice. In: Curr Protoc Cell Biol. ; 2009.
15. Spaink HP, Cui C, Wiweger MI, et al. Robotic injection of zebrafish embryos for high-throughput screening in disease models. Methods. 2013;62(3):246-254.
16. Strähle U, Scholz S, Geisler R, et al. Zebrafish embryos as an alternative to animal experiments — A commentary on the definition of the onset of protected life stages in animal welfare regulations. Reprod Toxicol. 2012;33:128-132.
17. Morgan P, Van der Graaf PH, Arrowsmith J, et al. Can the flow of medicines be improved? Fundamental pharmacokinetic and pharmacological principles toward improving Phase II survival. Drug Discov Today. 2012;17(9/10):419-424.
18. Guo Y, Veneman WJ, Spaink HP, et al. Three-dimensional reconstruction and measurements of zebrafish larvae from high-throughput axial-view in vivo imaging. Biomed Opt Express. 2017;8(5):2611-2634.
19. Diekmann H, Hill A. ADMETox in zebrafish. Drug Discov Today Dis Model. 2013;10(1):e31-e35.
20. Critchley JAJH, Critchley LAH, Anderson PJ, et al. Differences in the single-oral-dose pharmacokinetics and urinary excretion of paracetamol and its conjugates between Hong Kong Chinese and Caucasian subjects. J Clin Pharm Ther. 2005;30:179-184.
21. Zhao L, Pickering G. Paracetamol metabolism and related genetic differences. Drug Metab Rev. 2011;43(1):41-52.
22. Clements JA, Critchley JAJH, Prescotf LF. The role of sulphate conjugation in the metabolism and disposition of oral and intravenous paracetamol in man. Br J Clin Pharmacol. 1984;18:481-485.
23. Allegaert K, De Hoon J, Verbesselt R, et al. Intra- and interindividual variability of glucuronidation of paracetamol during repeated administration of propacetamol in neonates. Acta Paediatr. 2005;94(9):1273-1279.
24. Krekels EHJ, Van Ham S, Allegaert K, et al. Developmental changes rather than repeated administration drive paracetamol glucuronidation in neonates and infants. Eur J Clin Pharmacol. 2015;71:1075-1082.
25. Van Lingen RA, Deinum JT, Quak JME, et al. Pharmacokinetics and metabolism of rectally administered paracetamol in preterm neonates. Arch Dis Child Fetal Neonatal Ed. 1999;80(1):F59-F63.
26. Van der Marel CD, Anderson BJ, Van Lingen RA, et al. Paracetamol and metabolite pharmacokinetics in infants. Eur J Clin Pharmacol. 2003;59(3):243-251.

27. Mahmood I. Application of allometric principles for the prediction of pharmacokinetics in human and veterinary drug development. Adv Drug Deliv Rev. 2007;59:1177-1192.
28. Mahmood I. Theoretical versus empirical allometry: Facts behind theories and application to pharmacokinetics. J Pharm Sci. 2010;99(7):2927-2933.
29. Kimmel CB, Ballard WW, Kimmel SR, et al. Stages of embryonic development of the zebrafish. Dev Dyn. 1995;203:253-310.
30. Lee KY, Jang GH, Byun CH, et al. Zebrafish models for functional and toxicological screening of nanoscale drug delivery systems: Promoting preclinical applications. Biosci Rep. 2017;37(3):BSR20170199.
31. Ng ANY, De Jong-Curtain TA, Mawdsley DJ, et al. Formation of the digestive system in zebrafish: III. Intestinal epithelium morphogenesis. Dev Biol. 2005;286(1):114-135.
32. Kristofco LA, Haddad SP, Chambliss CK, et al. Differential uptake of and sensitivity to diphenhydramine in embryonic and larval zebrafish. Environ Toxicol Chem. 2017;37(4):1175-1181.
33. Tao T, Peng J. Liver development in zebrafish (Danio rerio). J Genet Genomics. 2009;36:325-334.
34. Pedroso G, Hammes T, Escobar T, et al. Blood collection for biochemical analysis in adult zebrafish. J Vis Exp. 2012;63:e3865.
35. Eames SC, Philipson LH, Prince VE, et al. Blood sugar measurement in zebrafish reveals dynamics of glucose homeostasis. Zebrafish. 2010;7(2):205-213.
36. Vliegenthart AD, Lewis PS, Tucker CS, et al. Retro-orbital blood acquisition facilitates circulating microRNA measurement in zebrafish. Zebrafish. 2014;11(3):219-226.
37. Isogai S, Horiguchi M, Weinstein BM. The vascular anatomy of the developing zebrafish: An atlas of embryonic and early larval development. Dev Biol. 2001;230(2):278-301.
38. Mourabit S, Fitzgerald JA, Ellis RP, et al. New insights into organ-specific oxidative stress mechanisms using a novel biosensor zebrafish. Environ Int. 2019;133(May):105138.
39. Van Rongen A, Välitalo PAJ, Peeters MY, et al. Morbidly obese patients exhibit increased CYP2E1-mediated oxidation of acetaminophen. Clin Pharmacokinet. 2016;55:833-847.
40. Slattery JT, Wilson JM, Kalhorn TF, et al. Dose-dependent pharmacokinetics of acetaminophen: Evidence of glutathione depletion in humans. Clin Pharmacol Ther. 1987;41(4):413-418.
41. Liu L, Klaassen CD. Different mechanism of saturation of acetaminophen sulfate conjugation in mice and rats. Toxicol Appl Pharmacol. 1996;139(1):128-134.
42. Reddyhoff D, Ward J, Williams D, et al. Timescale analysis of a mathematical model of acetaminophen metabolism and toxicity. J Theor Biol. 2015;386:132-146.
43. Van den Boom J, Heider D, Martin SR, et al. 3′-Phosphoadenosine 5′-phosphosulfate (PAPS) synthases, naturally fragile enzymes specifically stabilized by nucleotide binding. J Biol Chem. 2012;287(21):17645-17655.
44. Xu J, Chen Y, Li L, et al. An improved HPLC method for the quantitation of 3′-phosphoadenosine 5′-phosphate (PAP) to assay sulfotransferase enzyme activity in HepG2 cells. J Pharm Biomed Anal. 2012;62:182-186.
45. Miller TH, Gallidabino MD, MacRae JR, et al. Prediction of bioconcentration factors in fish and invertebrates using machine learning. Sci Total Environ. 2019;648:80-89.
46. Wassenaar PNH, Verbruggen EMJ, Cieraad E, et al. Variability in fish bioconcentration factors: Influences of study design and consequences for regulation. Chemosphere. 2020;239:124731.
47. Gao Y, Zhang Y, Feng J, et al. Toxicokinetic-toxicodynamic modeling of cadmium and lead toxicity to larvae and adult zebrafish. Environ Pollut. 2019;251:221-229.
48. Gao Y, Kang L, Zhang Y, et al. Toxicokinetic and toxicodynamic (TK-TD) modeling to study oxidative stress-dependent toxicity of heavy metals in zebrafish. Chemosphere. 2019;220:774-782.
49. Simon O, Gagnaire B, Camilleri V, et al. Toxicokinetic and toxicodynamic of depleted uranium in the zebrafish, Danio rerio. Aquat Toxicol. 2017.
50. Hu S, Han J, Yang L, et al. Impact of co-exposure to titanium dioxide nanoparticles and Pb on zebrafish embryos. Chemosphere. 2019;233:579-589.
51. Qiao R, Lu K, Deng Y, et al. Combined effects of polystyrene microplastics and natural organic matter on the accumulation and toxicity of copper in zebrafish. Sci Total Environ. 2019;682:128-37.

52. Li Y, Wang H, Xia X, et al. Dissolved organic matter affects both bioconcentration kinetics and steady-state concentrations of polycyclic aromatic hydrocarbons in zebrafish (Danio rerio). Sci Total Environ. 2018;639:648-656.
53. Damalas DE, Bletsou AA, Agalou A, et al. Assessment of the acute toxicity, uptake and biotransformation potential of benzotriazoles in zebrafish (Danio rerio) larvae combining HILIC- with RPLC-HRMS for high-throughput identification. Environ Sci Technol. 2018;52:6023-6031.
54. Kirla KT, Groh KJ, Steuer AE, et al. Zebrafish larvae are insensitive to stimulation by cocaine: importance of exposure route and toxicokinetics. Toxicol Sci. 2016;154(1):183-193.
55. Wu Y, Deng M, Jin Y, et al. Uptake and elimination of emerging polyfluoroalkyl substance F-53B in zebrafish larvae: Response of oxidative stress biomarkers. Chemosphere. 2019;215(182-188).
56. Kühnert A, Vogs C, Aulhorn S, et al. Biotransformation in the zebrafish embryo –temporal gene transcription changes of cytochrome P450 enzymes and internal exposure dynamics of the AhR binding xenobiotic benz[a]anthracene. Environ Pollut. 2017;230:1-11.
57. Brox S, Seiwert B, Küster E, et al. Toxicokinetics of polar chemicals in zebrafish embryo (Danio rerio): Influence of physicochemical properties and of biological processes. Environ Sci Technol. 2016;50(18):10264-10272.
58. Cui J, Wang F, Gao J, et al. Bioaccumulation and metabolism of carbosulfan in zebrafish Danio rerio and toxic effects with its metabolites. J Agric Food Chem. October 2019:(accepted).
59. Post TM, Freijer JI, DeJongh J, et al. Disease system analysis: Basic disease progression models in degenerative disease. Pharm Res. 2005;22(7):1038-1049.
60. He S, Mansour MR, Zimmerman MW, et al. Synergy between loss of NF1 and overexpression of MYCN in neuroblastoma is mediated by the GAP-related domain. eLife. 2016;5:e14713.
61. Veal GJ, Errington J, Redfern CPF, et al. Influence of isomerisation on the growth inhibitory effects and cellular activity of 13-cis and all-trans retinoic acid in neuroblastoma cells. Biochem Pharmacol. 2002;63(2):207-215.
62. Nathan Bushue, Wan Y-JY. Retinoid pathway and cancer therapeutics. Adv Drug Deliv Rev. 2010;62(13):1285-1298.
63. Armstrong JL, Redfern CPF, Veal GJ. 13-cis Retinoic acid and isomerisation in paediatric oncology - is changing shape the key to success? Biochem Pharmacol. 2005;69(9):1299-1306.
64. Tang X, Van der Zwaan DM, Zammit A, et al. Fast post-processing pipeline for optical projection tomography. IEEE Trans Nanobioscience. 2017;16(5):367-374.
65. Lindsey BW, Kaslin J. Optical projection tomography as a novel method to visualize and quantitate whole-brain patterns of cell proliferation in the adult zebrafish brain. Zebrafish. 2017;epub.
66. Kolesová H, Čapek M, Radochová B, et al. Comparison of different tissue clearing methods and 3D imaging techniques for visualization of GFP-expressing mouse embryos and embryonic hearts. Histochem Cell Biol. 2016;146(2):141-152.
67. Kapp FG, Perlin JR, Hagedorn EJ, et al. Protection from UV light is an evolutionarily conserved feature of the haematopoietic niche. Nature. 2018;558(7710):445-448.
68. Danhof M, Alvan G, Dahl SG, et al. Mechanism-based pharmacokinetic-pharmacodynamic modeling — A new classification of biomarkers. Pharm Res. 2005;22(9):1432-1437.
69. Trigg RM, Shaw JA, Turner SD. Opportunities and challenges of circulating biomarkers in neuroblastoma. Open Biol. 2019;9(5).
70. US Food and Drug Administration. Isotretinoin drug label. 2019.
71. Noël ES, Arain Z, Ober EA. Analysis of the Albumin / a -Fetoprotein / Afamin / Group specific component gene family in the context of zebrafish liver differentiation. Gene Expr Patterns. 2010;10:237-243.
72. Li C, Tan XF, Lim TK, et al. Comprehensive and quantitative proteomic analyses of zebrafish plasma reveals conserved protein profiles between genders and between zebrafish and human. Sci Rep. 2016;6(March):1-15.
73. Sonawane P, Cho HE, Tagde A, et al. Metabolic characteristics of 13-cis-retinoic acid (isotretinoin) and anti-tumour activity of the 13-cis-retinoic acid metabolite 4-oxo-13-cis-retinoic acid in

neuroblastoma. Br J Pharmacol. 2014;171(23):5330-5344.
74. Meijer AH, Spaink HP. Host-pathogen interactions made transparent with the zebrafish model. Curr Drug Targets. 2011;12(7):1000-1017.
75. Meijer AH. Protection and pathology in TB: Learning from the zebrafish model. Semin Immunopathol. 2016;38:261-273.
76. Tobin DM, May RC, Wheeler RT. Zebrafish: A see-through host and a fluorescent toolbox to probe host–pathogen interaction. PLoS Pathog. 2012;8(1):e1002349.
77. Myllymäki H, Bäuerlein CA, Rämet M. The zebrafish breathes new life into the study of tuberculosis. Front Immunol. 2016;7(MAY):196.
78. Carvalho R, De Sonneville J, Stockhammer OW, et al. A high-throughput screen for tuberculosis progression. PLoS One. 2011;6(2):1-8.
79. Ordas A, Raterink R-J, Cunningham F, et al. Testing tuberculosis drug efficacy in a zebrafish high-throughput translational medicine screen. Antimicrob Agents Chemother. 2015;59(2):753-762.
80. Stinear TP, Seemann T, Harrison PF, et al. Insights from the complete genome sequence of Mycobacterium marinum on the evolution of Mycobacterium tuberculosis. Genome Res. 2008;18(5):729-741.
81. Van der Sar AM, Abdallah AM, Sparrius M, et al. Mycobacterium marinum strains can be divided into two distinct types based on genetic diversity and virulence. Infect Immun. 2004;72(11):6306-6312.
82. Abdallah AM, Verboom T, Hannes F, et al. A specific secretion system mediates PPE41 transport in pathogenic mycobacteria. Mol Microbiol. 2006;62(3):667-679.
83. Clewe O, Aulin L, Hu Y, et al. A multistate tuberculosis pharmacometric model: A framework for studying anti-tubercular drug effects in vitro. J Antimicrob Chemother. 2016;71(4):964-974.
84. Gupta N, Bitton D, Simonsson USH, et al. Transforming translation through quantitative pharmacology for high-impact decision-making in drug discovery and development. CPT Pharmacometrics Syst Pharmacol. 2019:(accepted).
85. Clewe O, Wicha SG, de Vogel CP, et al. A model-informed preclinical approach for prediction of clinical pharmacodynamic interactions of anti-TB drug combinations. J Antimicrob Chemother. 2018;73(2):437-447.
86. Chen C, Ortega F, Rullas J, et al. The multistate tuberculosis pharmacometric model: A semi-mechanistic pharmacokinetic-pharmacodynamic model for studying drug effects in an acute tuberculosis mouse model. J Pharmacokinet Pharmacodyn. 2017;44(2):133-141.
87. Chen C, Wicha SG, De Knegt GJ, et al. Assessing pharmacodynamic interactions in mice using the multistate tuberculosis pharmacometric and general pharmacodynamic interaction models. CPT Pharmacometrics Syst Pharmacol. 2017;6(11):787-797.
88. Svensson RJ, Simonsson USH. Application of the multistate tuberculosis pharmacometric model in patients with rifampicin-treated pulmonary tuberculosis. CPT Pharmacometrics Syst Pharmacol. 2016;5(5):264-273.
89. Wicha SG, Clewe O, Svensson RJ, et al. Forecasting clinical dose-response from preclinical studies in tuberculosis research: Translational predictions with rifampicin. Clin Pharmacol Ther. 2018;104(6):1208-1218.
90. Jindani A, Aber VR, Edwards EA, et al. The early bactericidal activity of drugs in patients with pulmonary tuberculosis. Am Rev Respir Dis. 1980;121(6):939-949.
91. Stoop EJM, Schipper T, Rosendahl Huber SK, et al. Zebrafish embryo screen for mycobacterial genes involved in the initiation of granuloma formation reveals a newly identified ESX-1 component. Dis Model Mech. 2011;4(4):526-536.
92. Nezhinsky A, Verbeek FJ. Pattern recognition for high throughput zebrafish imaging using genetic algorithm optimization. In: Dijkstra T, Tsivtsivadze E, Heskes T, Marchiori E, eds. Lecture Notes in Bioinformatics 6282. Berlin- Heidelberg: Springer-Verlag; 2010:301-312.
93. Wilkins JJ, Langdon G, McIlleron H, et al. Variability in the population pharmacokinetics of isoniazid in South African tuberculosis patients. Br J Clin Pharmacol. 2011;72(1):51-62.

94. Li L, Mahan CS, Palaci M, et al. Sputum Mycobacterium tuberculosis mRNA as a marker of bacteriologic clearance in response to antituberculosis therapy. J Clin Microbiol. 2010;48(1):46-51.
95. Johnson JL, Hadad DJ, Boom WH, et al. Early and extended early bactericidal activity of levofloxacin, gatifloxacin and moxifloxacin in pulmonary tuberculosis. Int J Tuberc Lung Dis. 2006;10(6):605-612.
96. Hafner R, Cohn JA, Wright DJ, et al. Early bactericidal activity of isoniazid in pulmonary tuberculosis: Optimization of methodology. Am J Respir Crit Care Med. 1997;156(3 I):918-923.
97. Jindani A, Doré CJ, Mitchison DA. Bactericidal and sterilizing activities of antituberculosis drugs during the first 14 days. Am J Respir Crit Care Med. 2003;167(10):1348-1354.
98. Ali S, Champagne DL, Spaink HP, et al. Zebrafish embryos and larvae: A new generation of disease models and drug screens. Birth Defect Res (Part C). 2011;93:115-133.
99. Kirchberger S, Sturtzel C, Pascoal S, et al. Quo natas, Danio?- Recent progress in modeling cancer in zebrafish. Front Oncol. 2017;7(August):186.
100. Rennekamp AJ, Peterson RT. 15 years of zebrafish chemical screening. Curr Opin Chem Biol. 2015;24:58-70.
101. Letrado P, De Miguel I, Lamberto I, et al. Zebrafish: Speeding up the cancer drug discovery process. Cancer Res. 2018;78(21):6048-6058.
102. MacRae CA, Peterson RT. Zebrafish as tools for drug discovery. Nat Rev Drug Discov. 2015;14(10):721-731.
103. Lawrence C, Eisen JS, Varga ZM. Husbandry and health program survey synopsis. Zebrafish. 2016;13:S5-S7.
104. Liu L, Pan L, Li K, et al. Zebrafish health conditions in the china zebrafish resource center and 20 major chinese zebrafish laboratories. Zebrafish. 2016;13:S8-S18.
105. Geisler R, Borel N, Ferg M, et al. Maintenance of zebrafish lines at the European zebrafish resource center. 2016;13:19-24.
106. You MS, Jiang YJ, Yuh CH, et al. A sketch of the Taiwan zebrafish core facility. Zebrafish. 2016;13:S24-S29.
107. Murray KN, Varga ZM, Kent ML. Biosecurity and health monitoring at the zebrafish international resource center. Zebrafish. 2016;13:S30-S38.
108. Barton CL, Johnson EW, Tanguay RL. Facility design and health management program at the Sinnhuber aquatic research laboratory. Zebrafish. 2016;13:S39-S43.
109. Leveque RE, Clark KJ, Ekker SC. Mayo clinic zebrafish facility overview. Zebrafish. 2016;13:S44-S46.
110. Rihel J, Ghosh M. Zebrafish. In: Hock FJ, ed. Drug discovery and evaluation: Pharmacological assay. 4th ed. Springer International Publishing Switzerland; 2016:4071-4155.
111. Cassar S, Adatto I, Freeman JL, et al. Use of zebrafish in drug discovery toxicology. Chem Res Toxicol. 2019.
112. Gurwitz D. The gut microbiome: Insights for personalized medicine. Drug Dev Res. 2013;74:341-343.
113. Zimmermann M, Zimmermann-Kogadeeva M, Wegmann R, et al. Separating host and microbiome contributions to drug pharmacokinetics and toxicity. Science. 2019;363(6427).
114. Pham L, Kanther M, Semova I, et al. Methods for generating and colonizing gnotobotioc zebrafish. Nat Protoc. 2008;3(12):1862-1875.
115. Melancon E, Gomez De La Torre Canny S, Sichel S, et al. Best practices for germ-free derivation and gnotobiotic zebrafish husbandry. Vol 138. Elsevier Ltd; 2017.
116. Kulkarni P, Chaudhari GH, Sripuram V, et al. Oral dosing in adult zebrafish: Proof-of-concept using pharmacokinetics and pharmacological evaluation of carbamazepine. Pharmacol Reports. 2014;66(1):179-183.
117. Zang L, Morikane D, Shimada Y, et al. A novel protocol for the oral administration of test chemicals to adult zebrafish. Zebrafish. 2011;8(4):203-210.
118. Yang F, Gao C, Wang P, et al. Fish-on-a-chip: microfluidics for zebrafish research. Lab Chip. 2016;16(7):1106-1125.
119. Zhu F, Skommer J, Huang Y, et al. Fishing on chips: Up-and-coming technological advances in

analysis of zebrafish and Xenopus embryos. Cytom Part A. 2014;85(11):921-932.
120. Akagi J, Hall CJ, Crosier KE, et al. OpenSource Lab-on-a-Chip physiometer for accelerated zebrafish embryo biotests. Curr Protoc Cytom. 2014;(SUPPL.67):1-16.
121. Nady A, Peimani AR, Zoidl G, et al. a microfluidic device for head immobilization, chemical exposure, and behavioral screening of zebrafish larvae. 20th Int Conf Miniaturized Syst Chem Life Sci. 2016;(C):475-476.
122. Veneman WJ, Marín-Juez R, De Sonneville J, et al. Establishment and optimization of a high throughput setup to study Staphylococcus epidermidis and Mycobacterium marinum infection as a model for drug discovery. J Vis Exp. 2014;88:e51649.
123. Cordero-Maldonado ML, Perathoner S, Van der Kolk KJ, et al. Deep learning image recognition enables efficient genome editing in zebrafish by automated injections. PLoS One. 2019;14(1):e0202377.
124. Burhenne J, Halama B, Maurer M, et al. Quantification of femtomolar concentrations of the CYP3A substrate midazolam and its main metabolite 1′-hydroxymidazolam in human plasma using ultra performance liquid chromatography coupled to tandem mass spectrometry. Anal Bioanal Chem. 2012;402(7):2439-2450.
125. Fujii T, Matsuda S, Tejedor ML, et al. Direct metabolomics for plant cells by live single-cell mass spectrometry. Nat Protoc. 2015;10(9):1445-1456.
126. Ali A, Abouleila Y, Shimizu Y, et al. Single-cell screening of tamoxifen abundance and effect using mass spectrometry and raman-spectroscopy. Anal Chem. 2019;91:2710-2718.
127. North TE, Goessling W, Walkley CR, et al. Prostaglandin E2 regulates vertebrate haematopoietic stem cell homeostasis. Nature. 2007;447(7147):1007-1011.
128. Cully M. Zebrafish earn their drug discovery stripes. Nat Rev Drug Discov. 2019.
129. Chowdhury S, Owens KN, Herr RJ, et al. Phenotypic optimization of urea-thiophene carboxamides to yield potent, well tolerated, and orally active protective agents against aminoglycoside-induced hearing loss. J Med Chem. 2018;61(1):84-97.
130. Owens KN, Santos F, Roberts B, et al. Identification of genetic and chemical modulators of zebrafish mechanosensory hair cell death. PLoS Genet. 2008;4(2):e1000020.
131. Kitcher SR, Kirkwood NK, Camci ED, et al. ORC-13661 protects sensory hair cells from aminoglycoside and cisplatin ototoxicity. JCI Insight. 2019;4(15):e126764.

Section VI. Appendices

Curriculum vitae

Rob Christiaan van Wijk (1991, Zevenaar, The Netherlands) started his academic education in 2009 with the Bachelor of Science programme Bio Pharmaceutical Sciences, and the Bachelor Honours programme Beta and Life Sciences, both at the Faculty of Science, Leiden University. He finished two Bachelor internships, one in toxicology, and one in pharmacology where he was introduced to pharmacometrics. In the academic year 2012-2013, he was assessor (student-member) of the Faculty Board of the Faculty of Science and chair of the Leiden Assessor Board.

Rob started his Master of Science programme Bio Pharmaceutical Sciences with an internship at GlaxoSmithKline in London, UK, under the supervision of Prof. Dr. Oscar Della Pasqua, where he experienced drug development from an industry perspective. His second internship was under the supervision of Dr. Eric Wong and Prof. Dr. Elizabeth de Lange, where he was trained in preclinical animal experiments. Under the supervision of Dr. Francesco Bellanti and Prof. Dr. Oscar Della Pasqua, Rob wrote a literature review on benefit risk assessments. He participated in the Master Honours programme Leiden Leadership Programme, an extracurricular programme combining personal assessment, theory on leadership and motivation, and practical experience in change management within a project team.

In 2015, Rob started his PhD research on translational pharmacology in the zebrafish, a collaboration between the Leiden Academic Centre for Drug Research (LACDR) and the Institute of Biology Leiden (IBL), under the supervision of Prof. Dr. Piet Hein van der Graaf, Prof. Dr. Herman Spaink, and Dr. Elke Krekels. During his PhD, he was involved in teaching of several academic courses, and the supervision of seven bachelor interns, four master interns, and four interns from the University of Applied Sciences. The projects within his PhD research combined multiple disciplines, including pharmacology, biology, analytical chemistry, and computational bio-imaging. A first international collaboration started in June 2016 with Prof. Dr. Ulrika Simonsson at Uppsala University and Dr. Astrid van der Sar at Free University Medical Centre (VUmc) in Amsterdam, to quantify drug effects in zebrafish as disease model for tuberculosis infections. In October 2016, a second international collaboration commenced with Dr. Shuning He and Prof. Dr. Thomas Look at Dana Farber Cancer Institute (DFCI), Harvard Medical School, to quantify drug effects in zebrafish as disease model for neuroblastoma tumours. As part of this collaboration, Rob visited DFCI in Boston in 2019 to perform experiments and present his work.

During his PhD, Rob has visited more than ten international conferences and a summer school, and has been awarded best oral presentation three times, and best poster presentation three times. He received a total of fourteen study or travel grants. Rob is a motivated and enthusiastic speaker and has reached out to present his work to academic audiences, as well as to prospective bachelor and master students, and broader audiences.

After a short postdoc at the Institute of Biology Leiden on nontuberculous mycobacterial infections, Rob will start as a postdoctoral researcher at the Department of Pharmaceutical Biosciences at Uppsala University, Sweden. He will work on translational pharmacology in anti-tuberculosis drug development.

List of publications

Publications related to this thesis

Van Wijk RC, Van der Sar AM, Krekels EHJ, Verboom T, Spaink HP, Simonsson USH, Van der Graaf PH. Quantification of natural growth of two strains of *Mycobacterium marinum* for translational anti-tuberculosis drug development. *Submitted*

Van Wijk RC, Hu W, Dijkema SM, Van den Berg DJ, Liu J, Bahi R, Verbeek FJ Krekels EHJ, Simonsson USH, Spaink HP, Van der Graaf PH, Krekels EHJ. Translational pharmacokinetics-pharmacodynamics of isoniazid in the zebrafish larva tuberculosis disease model. *Submitted*

Van Wijk RC, Krekels EHJ, Kantae V, Ordas A, Kreling T, Harms AC, Hankemeier T, Spaink HP, van der Graaf PH. Mechanistic and quantitative understanding of pharmacokinetics in zebrafish larvae through nanoscale blood sampling and metabolite modelling of paracetamol. *Journal of Pharmacology and Experimental Therapeutics* 2019;371:15-24.

Van Wijk RC, Krekels EHJ, Kantae V, Harms AC, Hankemeier T, Van der Graaf PH, Spaink HP. Impact of post-hatching maturation on the pharmacokinetics of exogenous compounds in zebrafish larvae. *Scientific Reports* 2018;9:2149.

Schulthess P*, **Van Wijk RC***, Krekels EHJ, Yates JWT, Spaink HP, Van der Graaf PH. Outside-in systems pharmacology combines innovative computational methods with high-throughput whole vertebrate studies. *CPT: Pharmacometrics and Systems Pharmacology* 2018;7:285-287.

Guo Y, **Van Wijk RC**, Krekels EHJ, Spaink HP, Van der Graaf PH, Verbeek FJ. Multi-modal 3D reconstruction and measurements of zebrafish larvae and its organs using axial-view microscopy. *IEEE International Conference on Image Processing* 2017.

Van Wijk RC, Krekels EHJ, Hankemeier T, Spaink HP, Van der Graaf PH. Systems pharmacology of hepatic metabolism in zebrafish larvae. *Drug Discovery Today: Disease Models* 2016;22:27-34.

Kantae V, Krekels EHJ, Ordas A, González O, **Van Wijk RC**, Harms AC, Racz PI, Graaf PH Van Der, Spaink HP, Hankemeier T. Pharmacokinetic modeling of paracetamol uptake and clearance in zebrafish larvae: Expanding the allometric scale in vertebrates with five orders of magnitude. *Zebrafish* 2016;13(6):504-510.

Publications unrelated to this thesis

Kantae V, Van Esbroeck ACM, Stevens AF, Lelieveld LT, Van Rooden, EJ, Florea BI, **Van Wijk RC**, Harms AC, Van der Graaf PH, Overkleeft HS, Aerts JMFG, Hankemeier T, Van der Stelt M. Activity-based proteomics and lipidomics of zebrafish larvae as tools in early drug discovery. *Manuscript in preparation*

Wong YC, Ilkova T, **Van Wijk RC**, Hartman R, de Lange ECM. Development of a population pharmacokinetic model to predict brain distribution and dopamine D2 receptor occupancy of raclopride in non-anesthetized rat. *European Journal of Pharmaceutical Sciences* 2018;111:514-525.

Bellanti F, **Van Wijk RC**, Danhof M, Della Pasqua O. Integration of PKPD relationships into benefit-risk analysis. *British Journal of Clinical Pharmacology* 2015;80(5):979-991.

* authors contributed equally

Affiliations of authors

Rida Bahi	*Systems Biomedicine and Pharmacology, Leiden Academic Centre for Drug Research, Leiden University, Leiden, The Netherlands*
Dirk-Jan van den Berg	*Systems Biomedicine and Pharmacology, Leiden Academic Centre for Drug Research, Leiden University, Leiden, The Netherlands*
Sharka M. Dijkema	*Systems Biomedicine and Pharmacology, Leiden Academic Centre for Drug Research, Leiden University, Leiden, The Netherlands*
Oskar González	*Systems Biomedicine and Pharmacology, Leiden Academic Centre for Drug Research, Leiden University, Leiden, The Netherlands*
	Science and Technology Faculty, Analytical Chemistry Department, University of Basque Country/EHU, Bilbao, Spain
Piet H. van der Graaf	*Systems Biomedicine and Pharmacology, Leiden Academic Centre for Drug Research, Leiden University, Leiden, The Netherlands*
	Certara QSP, Canterbury, United Kingdom
Yuanhao Guo	*Imaging and Bioinformatics Group, Leiden Institute of Advanced Computer Sciences, Leiden University, Leiden, The Netherlands*
Thomas Hankemeier	*Systems Biomedicine and Pharmacology, Leiden Academic Centre for Drug Research, Leiden University, Leiden, The Netherlands*
Amy C. Harms	*Systems Biomedicine and Pharmacology, Leiden Academic Centre for Drug Research, Leiden University, Leiden, The Netherlands*
Shuning He	*Department of Pediatric Oncology, Dana-Farber Cancer Institute, Harvard Medical School, Boston, United States*
Wanbin Hu	*Division of Animal Sciences and Health, Institute of Biology Leiden, Leiden University, Leiden, The Netherlands*
Nick Jansen	*Systems Biomedicine and Pharmacology, Leiden Academic Centre for Drug Research, Leiden University, Leiden, The Netherlands*
Vasudev Kantae	*Systems Biomedicine and Pharmacology, Leiden Academic Centre for Drug Research, Leiden University, Leiden, The Netherlands*
Elke H.J. Krekels	*Systems Biomedicine and Pharmacology, Leiden Academic Centre for Drug Research, Leiden University, Leiden, The Netherlands*
Thijs Kreling	*Systems Biomedicine and Pharmacology, Leiden Academic Centre for Drug Research, Leiden University, Leiden, The Netherlands*
Gerda Lamers	*Core facility visualisation, Institute of Biology Leiden (IBL), Leiden University, Leiden, The Netherlands*

Jeremy Liu	*Systems Biomedicine and Pharmacology, Leiden Academic Centre for Drug Research, Leiden University, Leiden, The Netherlands*
A. Thomas Look	*Department of Pediatric Oncology, Dana-Farber Cancer Institute, Harvard Medical School, Boston, United States*
Anita Ordas	*Division of Animal Sciences and Health, Institute of Biology Leiden, Leiden University, Leiden, The Netherlands*
Peter I. Racz	*ZF-screens BV, Leiden, The Netherlands*
Astrid M. van der Sar	*Department of Medical Microbiology and Infection Control, VU University Medical Center, Amsterdam, The Netherlands*
Pascal Schulthess	*Systems Biomedicine and Pharmacology, Leiden Academic Centre for Drug Research, Leiden University, Leiden, The Netherlands*
Ulrika S.H. Simonsson	*Department of Pharmaceutical Biosciences, Uppsala University, Uppsala, Sweden*
Herman P. Spaink	*Division of Animal Sciences and Health, Institute of Biology Leiden, Leiden University, Leiden, The Netherlands*
Xiaoqin Tang	*Imaging and Bioinformatics Group, Leiden Institute of Advanced Computer Sciences, Leiden University, Leiden, The Netherlands*
Maxim Treep	*Systems Biomedicine and Pharmacology, Leiden Academic Centre for Drug Research, Leiden University, Leiden, The Netherlands*
Fons J. Verbeek	*Imaging and Bioinformatics Group, Leiden Institute of Advanced Computer Sciences, Leiden University, Leiden, The Netherlands*
Theo Verboom	*Department of Medical Microbiology and Infection Control, VU University Medical Center, Amsterdam, The Netherlands*
James W.T. Yates	*DMPK, Oncology, Innovative Medicines and Early Development, AstraZeneca, Chesterford Research Park, United Kingdom*

Acknowledgements

Research is a team effort and I would like to acknowledge and thank everyone that supported the completion of this thesis.

Foremost, I thank my promotores Piet Hein van der Graaf and Herman Spaink, for the opportunity and their trust to perform my PhD research at the interface of their respective disciplines. Piet Hein; I could always count on your support and your critical thoughts, and for that I thank you. Herman; you introduced me to the international zebrafish field while remaining very approachable, and for that I thank you.

My copromotor and daily supervisor, Elke Krekels, I would like to thank for all her time and the critical revision of all elements of this thesis. You saw me overly enthusiastic and deeply exhausted and I thank you for your patience.

I thank our international collaborators. I gratefully acknowledge Ulrika Simonsson for her guidance and Astrid van der Sar for her experimental work in the tuberculosis project. Shuning He and Thomas Look were instrumental in the neuroblastoma project and I thank them for their hospitality in Boston. I also thank my external advisor Jeroen den Hertog for his advice.

This thesis is the result of multidisciplinary answers to challenging questions. I thank the experts in analytical chemistry, especially Vasudev Kantae, Amy Harms, Thomas Hankemeier and Dirk-Jan van den Berg. I thank the caretakers, and the experts in zebrafish research, especially Anita Ordas, Bjørn Koch, and Wanbin Hu. I thank the experts in microscopy and three-dimensional reconstructions, especially Yuanhao Guo, Fons Verbeek, Gerda Lamers, and Xiaoqin Tang.

I thankfully acknowledge the funders that enabled me to attend international conferences from Singapore to Washington DC, including the Swaantje Mondt Fund of LUF, and the travel grants from LNPT, ASCPT, ZDM, PAGE, FIGON, and NVF.

I thank my colleagues, especially my desk-mates Bas and Wilbert, and of course Linda, Sînziana, Willem, Michiel, Aline, Mohammed, Tian, Anthony, Lu, Laura, Ilona, Parth, Swantje, Jantine, Elisa, Francesco, Sven, and Pascal, without whom I would not have learnt and grown, nor enjoyed it, so much.

I am grateful for the opportunity to supervise many industrious students, especially Thijs, Sharka, Dani, and the interns from the University of Applied Sciences Maxim, Nick, Jeremy, and Rida.

Finally, I heartily thank my family for their support and encouragement to be curious and communicative, my friends for listening and holding up a mirror when necessary, and those who are a mentor to me.

Thank you.